This is to certify that the

dissertation entitled

Excited State Chemistry and Mechanistic Studies
of Quadruply Bonded Bimetallic Systems

presented by

Tsui-Ling Carolyn Hsu

has been accepted towards fulfillment
of the requirements for

PhD degree in Chemistry

Daniel G Nocera
Professor Daniel G. Nocera
Major professor

Date Sept. 22, 1995

EXCITED STATE CHEMISTRY AND MECHANISTIC STUDIES OF QUADRUPLY BONDED BIMETALLIC SYSTEMS

By

Tsui-Ling Carolyn Hsu

A DISSERTATION

Submitted to
Michigan State University
in partial fulfillment of the requirements
for the degree of

DOCTOR OF PHILOSOPHY

Department of Chemistry
1995

ABSTRACT

EXCITED STATE CHEMISTRY AND MECHANISTIC STUDIES OF QUADRUPLY BONDED BIMETALLIC SYSTEMS

By

Tsui-Ling Carolyn Hsu

Multielectron reactions are fundamental to promoting energy conversion transformations such as the oxidation of water, and the reduction of oxygen and nitrogen. This research effort focuses on using the electronic excited state of specially designed transition metal complexes to harness the energy of a photon to drive oxidation-reduction reactions useful for energy storage. Can excited states directly participate in multielectron reactions initiated by visible light? We address this issue by using quadruply bonded metal-metal compounds ($M\overset{4}{-}M$) as photoreagents. These systems possess low energy excited states localized at a coordinately unsaturated, electron rich core, which is essential for small molecule activation. The lowest energy $^1(\delta^2 \rightarrow \delta\delta^*)$ transition of $M\overset{4}{-}M$ complexes, corresponding to a metal-to-metal charge transfer (MMCT) transition, produces a two-electron mixed-valence excited state (i.e. M^{II}—$M^{II} \rightarrow M^{I}$—M^{III}), which is predisposed for multielectron photochemistry. Two-electron reductions of substrate may be promoted at the M^{I} site whereas oxidation may occur at the M^{III} site.

The quadruply bonded metal-metal systems chosen to study are $Mo_2[O_2P(OC_6H_5)_2]_4$ (D_{4h}), $M_2Cl_4(dppm)_2$ (D_{2h}) and $M_2Cl_4(PR_3)_4$ (D_{2d}), where M_2= Mo_2, W_2; dppm = bis(diphenylphosphino)methane, PR_3 = PMe_3, PMe_2Ph, PBu_3. $Mo_2[O_2P(OC_6H_5)_2]_4$ photoreduces 1,2-dichlorocarbons and produces a

mixed

reveal

are re

monc

substr

edge-s

wavel

photo

reactiv

with d

W_2(II,

consist

excited

virtue

repres

photoc

system

such a

and W

mixed-valence $Mo_2[O_2P(OC_6H_5)_2]_4Cl$. Analysis of the organic photoproducts reveals that dichlorocarbons such as 1,2-dichloroalkanes and 1,2-dichloroalkenes are reduced via an initial chloride atom abstraction to yield olefins and monohalogenated alkenes, respectively, depending on the nature of the substrates. Excitation of $M_2Cl_4(dppm)_2$ in the presence of PhSSPh affords an edge-sharing bioctahedral M_2(III,III) addition product, $M_2Cl_5(dppm)_2(SPh)$. The wavelength dependence of quantum yield studies for the $M_2Cl_4(dppm)_2$ photochemistry and the presence of a long-lived transient suggest that the reactivity is derived from metal-localized excited states. $W_2Cl_4(PR_3)_4$ photoreacts with dihalocarbons upon near-ultraviolet excitation and affords a mixed-valence W_2(II,III) photoproduct, $W_2Cl_5(PR_3)_3$. The photoreaction of the D_{2d} complexes is consistent with LMCT excited state parentage as opposed to the metal-localized excited states of D_{2h} counterparts.

The critical mixed-valence M^{I}—M^{III} excited state may be stabilized by virtue of the asymmetry of the bimetallic core. Heterobimetallic Mo$\overset{4}{-}$W systems represent a straightforward means to further study the multielectron photochemistry. Prior to undertaking photochemical experiments of these systems, their photophysics have been explored. The excited state properties such as energy and lifetime of Mo$\overset{4}{-}$W species fall in the range of their Mo$\overset{4}{-}$Mo and W$\overset{4}{-}$W analogues.

Dedicated to my dearest parents,

Tsang-Sui and Hui-Yuan

whose endless love and support were essential to this accomplishment.

ACKNOWLEDGMENTS

First and foremost, I would like to thank my present group members, especially the metal-metal quadruple bond subgroup, Ann Macintosh, Sara Helvoigt, Dan Engebretson for their numerous helpful discussions and long-term friendship. I am greatly indebted to my former group collaborators I-Jy. Chang, Colleen Partigianoni, Claudia Turró for generously sharing their experience with me during my early years. My other fifteen labmates present and past, too many to be mentioned here, have furnished this research lab with a tremendous family atmosphere, which warmed my heart and got me going through the difficult times over the past several years. It is always a great joy working in Nocera's group.

I wish to express my sincere thanks to all who help me learn the instruments for taking physical measurements, in particular, Dr. Rui Huang, Dr. Zhi-Heng Huang, Professor Doug Gage, and Ms. Bev Chamberlin in Mass Spectrometry Facility for introducing me to the Mass spec field; Dr. Yvonne Gindt, Dr. Kurt Warncke and people in Professor Gerald Babcock's group for training me on EPR spectroscopy; Jim Roberts and Dr. Neils van Dantzig, in my group, for luminescence lifetime measurements, and Dr. Long Le for his expertise in polishing my NMR skills. In the absence of their assistance, the work presented here would be impossible.

The chemistry department at Michigan State has provided me with a very pleasant working environment and I am most grateful to the machine shop, the glass shop, and electronic shop for their friendly technical help. My deepest appreciation goes to my special friends, Stacey Bernstein, Ying Liang, Zoe

Pikran
Wu he

with t
chemi
Kwon
I wish

is my
invalu
once,
enthus
Withou
unders
next st
for che

Pikramenou, J. P. Kirby, Wen Lian Lee, Kuolih Tsai, Hui-Lein Tsai and Chun-Guey Wu here for giving me strength and encouragement during my graduate years.

Other contributions to this work come from many stimulating discussions with the chemistry professors, including Dr. Kim Dunbar on metal-metal bond chemistry, Dr. Peter Wagner on organic photochemistry, Dr. Ned Jackson, Dr. Chi Kwong Chang and Dr. George Leroi for their thoughtful supports in many ways. I wish to show my gratitude to them.

The most memorable person in my graduate life who can not be forgotten is my academic father, Professor Daniel Nocera. Dan's scientific insight and invaluable guidance have lead me to see the big picture of science. More than once, I would like to express my profound appreciations for his patience, enthusiasm and concerns by taking his time to train me as a good scientist. Without his intense criticisms, I would not be able to accomplish this work. His understanding and inspiration have always ensured me to move steadily on to the next step of my academic career. With all my heart, I gratefully acknowledge him for cherishing my scientific growth!

TABLE OF CONTENTS

3.1

3.2

4.1

4.2

4.3

4.4

4.5

5.1

6.1

6.2

LIST OF TABLES

1.1

1.2

1.3

1.4

1.5

1.6

1.7

1.8

1.9

3.1.

LIST OF FIGURES

Page

3.

3.

3.

3.

3.6

3.7.

3.8

3.9

3.10

.1

4.2

4.3

4.4

4.5

4.6

4.7

4.8

4.9

4.1

4.1

5.1

5.2

5.3

5.4

5.5

Page

5.6

5.7

5.8

5.9

5.10

5.11

5.12

5.1

5.1

6.1

6.2

6.3

6.4

6.5

6.6

6.7

6.8

6.9

Page

6.1

6.11

6.1

6.13

6.14

6.15

6.16

6.17

end

natu

phot

the b

of th

of th

Figu

captu

than

fossil

sourc

artific

energ

produ

natur

CHAPTER I

INTRODUCTION

Seeking and developing alternate sources of energy is a necessary endeavor as global needs continue to deplete fossil fuels. The energy resource for nature is photosynthesis. Solar energy provides the driving force in photosynthesis for the continuous cycling of atmospheric CO_2 and O_2 through the biosphere to the high energy fuels, sugar and water, respectively. About 50% of the incident radiation on the earth is used photosynthetically (350 to 700 nm of the entire solar spectral distribution, which ranges from 350 to 2500 nm; see Figure 1.1). Each year at least $3\text{-}6 \times 10^{17}$ kcal of free energy from sunlight is captured by photosynthetic organisms and used for biosynthesis.[1] This is more than ten times the amount of energy derived from the annual global usage of fossil fuels. In addition to its abundance, solar energy is also a pollution-free source of energy. A challenging goal confronting chemists is to develop an artificial photosynthetic system for the conversion of light energy into chemical energy, thereby providing an alternate process for energy storage and production.[2] Accordingly, mimicking the highly efficient initial reactions of natural photosynthesis is a central goal of photochemical research.[3–6]

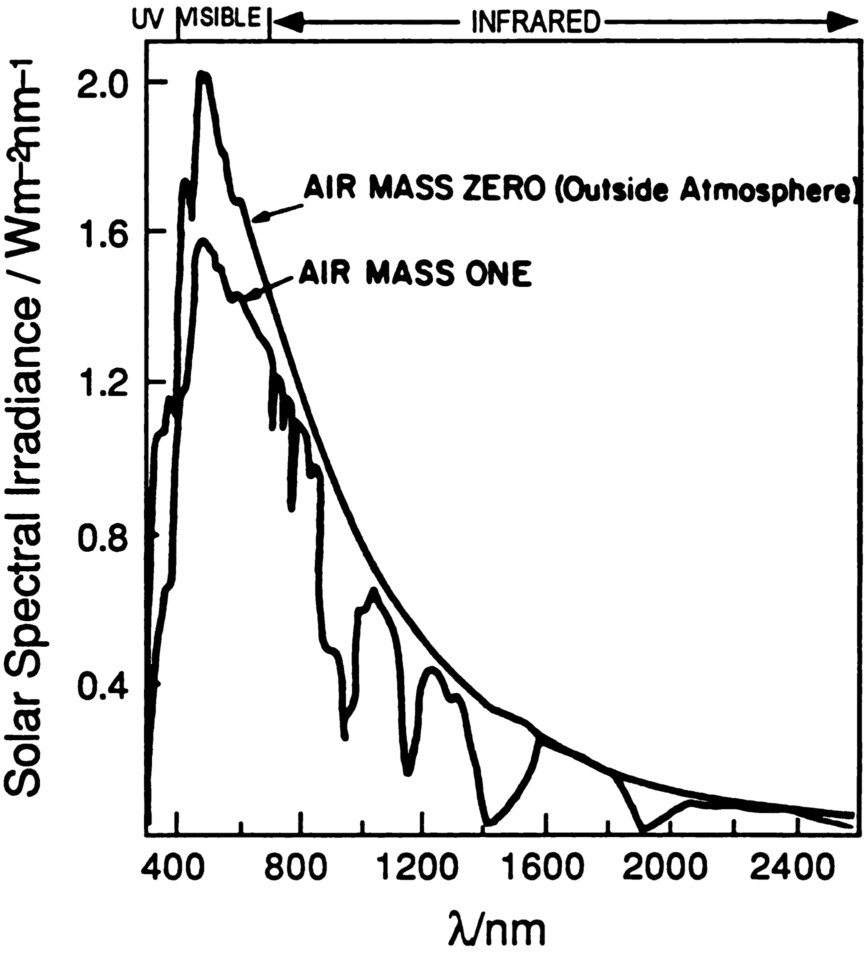

Figure 1.1 Solar spectral distribution outside the Earth's atomsphere (air mass 0) and at normal incidence to the Earth's surface (air mass 1). Shaded area is where is used for photosynthesis. (ref. 26)

I.

stc

ph

lov

Pla

by

can

whe

pyru

invol

wher

phot

name

chlor

phot

excit

separ

I. Photosynthesis

The development of efficient, artificial systems for the conversion and storage of solar energy requires an understanding of the mechanism of photosynthesis. Natural photosynthesis occurs not only in green plants but in lower microorganisms such as algae, cyanobacteria, and green sulfur bacteria. Plants and bacterial photosynthesis are fundamentally similar processes and differ by the hydrogen donors that they employ. The overall reaction of photosynthesis can be written in a general form:

$$2H_2D + CO_2 \xrightarrow[Chl]{h\nu} (CH_2O) + H_2O + 2D \qquad (1.1)$$

where Chl = chlorophyll; $H_2D = H_2O$, H_2S, or lactate; D = oxygen, sulfur, or pyruvate for green plants, green sulfur bacteria and bacteria, respectively.[7]

The reaction that has been most intensively investigated in green plants involves the absorption and transduction of light to chemical energy as follows,

$$2H_2O + A \xrightarrow[Chl]{h\nu} 2H_2A + O_2 \qquad (1.2)$$

where A is the electron acceptor. This process is performed with two photosystems. Each of them contains a photoreaction center working in series, namely P700 in Photosystem I and P680 in Photosystem II (Figure 1.2). The chlorophyll molecule in each of the photochemical reaction centers captures the photon energy with 100% quantum efficiency to yield a high energy electronic excited state. This initial absorption event initiates electron/hole charge separation via a series of electron transfer steps within the reaction center. In

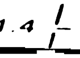
-1.4

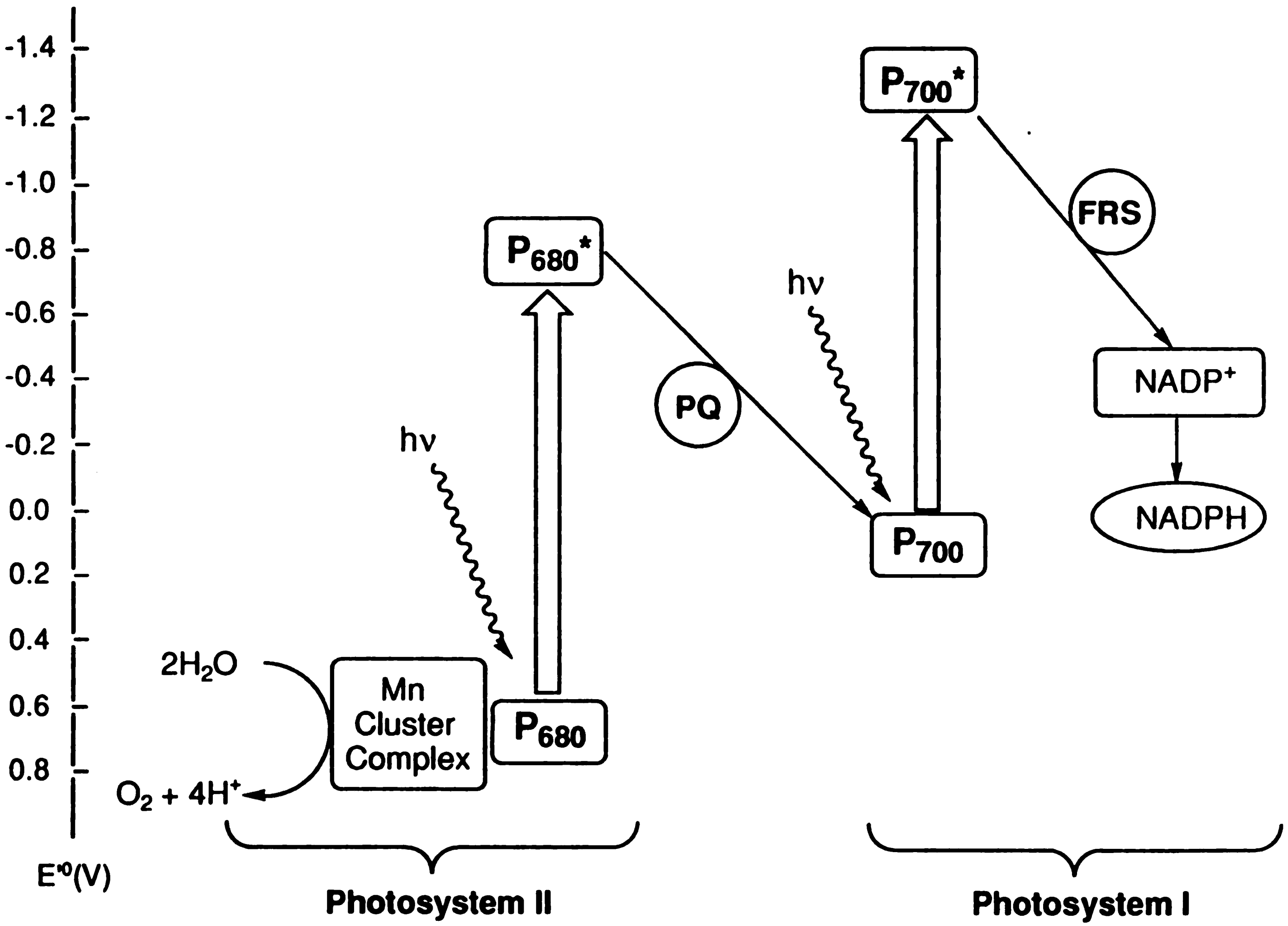

Figure 1.2 Schematic representation of photoinduced electron flow in Photosystems I and II.

Ph

ce

ni

Ph

ph

P6

cor

ove

fou

yiel

ther

NAI

CO_2

II. S

proce

separ

addit

found

NO_3^-

(cyto

(nitro

thoug

transi

funct

Photosystem I, electrons are passed from the excited state of the P700 reaction center through a series of carriers to ferredoxin (FRS), which in turn reduces nicotinamide adenine dinucleotide phosphate ($NADP^+$) to NADPH. In Photosystem II, excited P680 transfers an electron to a series of pheophytin/plastoquinone pigments (PQ) to create a charge-separated $P680^+/PQ^-$ pair. The $P680^+$ acquires an electron from a tetranuclear Mn cluster containing protein complex to return to its ground state. By turning this cycle over in successive one-electron steps, the tetranuclear Mn cluster is oxidized by four electrons whereupon it catalyzes the oxidation of two water molecules to yield four electrons, four protons and a molecule of oxygen.[8] The overall process therefore uses light energy to energetically run electrons uphill from H_2O to $NADP^+$, the biological electron acceptor, to yield NADPH, which in turn reduces CO_2 to give energy-rich carbohydrates.

II. Small Molecule Activation by Multielectron Transfer

Photosynthesis provides us with the two fundamental bioenergetic processes in nature: conversion of light into chemical energy by charge separation and multielectron transformations to activate small molecules. In addition to Photosystem II, many examples of multielectron redox reactions are found in enzymatic systems.[9-11] These include $SO_3^{2-} \rightarrow HS^-$ (sulfite reductase),[12] $NO_3^- \rightarrow NO_2^-$ (nitrate reductase),[13] $NO_2^- \rightarrow NH_3$ (nitrite reductase),[14] $O_2 \rightarrow H_2O$ (cytochrome *c* oxidase),[15] $O_2 \rightarrow H_2O$ (blue copper oxidases),[16] $N_2 \rightarrow NH_3$ (nitrogenase),[17,18] and $2H^+ \rightarrow H_2$ (hydrogenase).[19] In each case, the enzyme is thought to have one or more metals at the active site to promote the multielectron transformation. The mechanisms have been addressed by in vitro and in functional model studies for redox processes.[20,21] Bioinorganic and bioorganic

ch
bi
ele
po
mu
cor
acti
inv

III.

excit
excit
state
effec
the g
conv
molec
into a
quant
nonra
minim

photo
by pc
These

chemistry has sought to emulate the overall multielectron transformations of biology with a number of metal complexes,[22-24] such as the direct four-electron electrocatalytic reduction of O_2 to H_2O by ruthenated cyanophenyl cobalt porphyrins.[25] However, these studies have yet to successfully drive the multielectron transformations with light, a key step in designing energy conversion schemes. Accordingly, the development of new small molecule activation reactions by light-sensitive coordination compounds are important to investigate, especially those involving multielectron transfer reactivity.

III. Photochemical Conversion

The addition of a photon to a molecule in its ground state raises it to its excited state where the incident energy is stored. As a result, the electronically excited molecule is a stronger oxidant and a stronger reductant than its ground state parent. For this simple reason, a photon can be harvested by a molecule to effect the reactions that are kinetically or thermodynamically inaccessible from the ground state. Nevertheless, in order to mimic the high efficiency of sunlight conversion of the photosynthesis system, certain criteria of the excited state molecule are required.[26] The excited state energy must be effectively translated into a thermodynamically unfavorable chemical reaction at high photochemical quantum yield. Thus energy degrading processes such as intramolecular nonradiative decay and energy-wasting back electron-transfer reactions must be minimized.

In order to fulfill these criteria, many schemes rely on organizing the photosensitizer, donors, and acceptors within the organized assemblies provided by polymer-films,[27,28] membranes,[29,30] vesicles,[31,32] molecular systems.[3,5,33,34] These artificial photosynthetic systems have the advantage that specific

pr
sy
sp
st
di
m
Pa
ele
sto
enc
cha
stat
forv
long
phot

mana
with
water
surfa
electr
the c
band
H_2, ar
The s
oxidiz

properties of the photoinduced electron transfer reaction can be tuned by synthetically designing sensitizers, charge-relays, donors, bridges and acceptors spatially juxtaposed within the assembly.[35,36] Figure 1.3 shows the general strategy of the photochemical molecular device.[37] Light may be absorbed by a diverse array of photoactive redox metal systems ranging from metalloproteins to mononuclear metal complexes such as the ruthenium polypyridine complex.[38–40] Parallel to the function of chlorophyll in the reaction center of the green leaf, an electron is transferred from the photosensitizer one at a time to an electron storage center, where electrons are passed to reduce substrate. A frequently encountered problem in designing an artificial photosynthetic system is the fast charge recombination of the energy-releasing process in the charge separation state has to be prevented before the chemistry can be achieved. A highly efficient forward reaction when combined with a slow back electron transfer, results in a long-lived, charge separation state, which determines the overall efficiency of the photochemical process.

The time scales of the forward and back reactions can effectively be managed in the heterogeneous environment.[41–44] TiO_2 semiconductor particles with two metal/metal-oxide sites on a surface have been explored as promising water-splitting photocatalysts.[445–47] Figure 1.4a shows how water is split on the surface of TiO_2. Upon excitation across the band gap of the photocatalyst, electron-hole pairs are generated; negatively charged electrons get injected into the conduction band (CB) and positively charged holes remain in the valence band (VB). Electrons trapped in the metal site 1 (e.g. Pt cathode) reduce water to H_2, and holes trapped in the metal site 2 (e.g. RuO_2 anode) oxidize water to O_2. The system is driven by a sacrificial electron donor such as MeOH, which is oxidized to CO_2 (Figure 1.4b). In contrast, if the metal modified

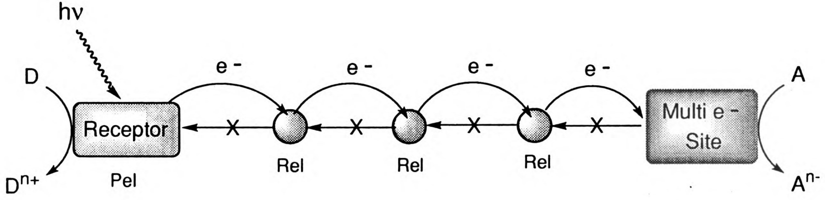

Figure 1.3 Molecular chemical device based on photoinduced electron transfer. Pel represents a photosensitizer whereas Rel represents an electron transfer relay.

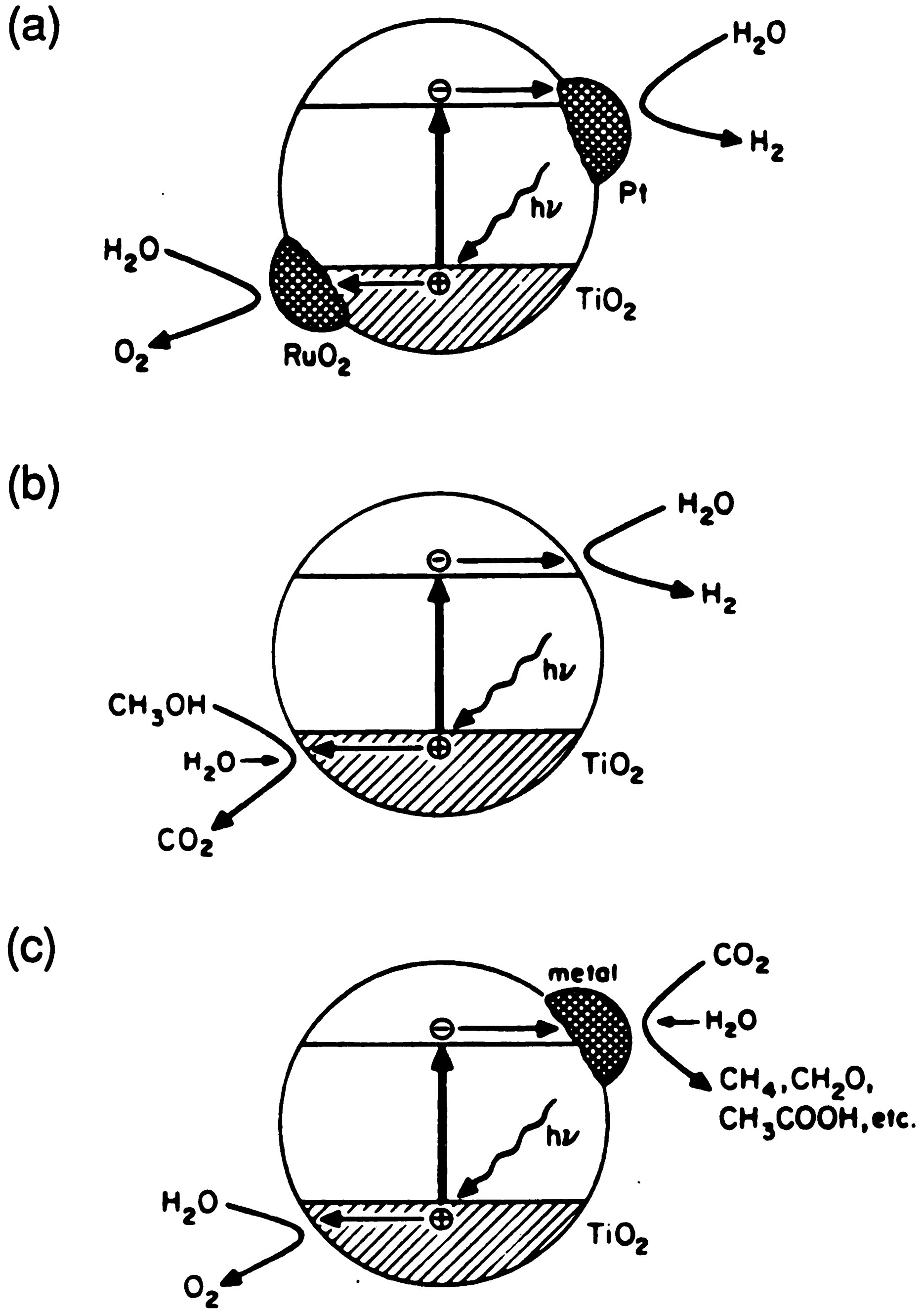

Figure 1.4 Photosplitting of water on (a) composite catalyst (b) catalyst with sacrifical donor (c) catalyst with sacrifical acceptor. (ref.46)

Ti(
CC
suc
(Fi
(E_g
lim
foci
sem
com
incre
form

abse
studi
four
Te. H
prima
via th
oxyg
oxom
result
organ
oxida
produ

extrao
elabora

TiO_2 catalysts (M_1 = Pd, Rh, Au, Cu, Ru, or Hg) are irradiated in the presence of CO_2 as a sacrificial electron acceptor, several reduced products can be observed such as methanol,[48] methane,[49,50] formic,[49] acetic acid,[50] and formaldehyde[51] (Figure 1.4c). TiO_2 is a quite stable photocatalyst, however, its large energy gap (E_g = 3.2 eV) in the ultraviolet region, which is 10% of the overall solar intensity, limits its application for solar energy conversion (Figure 1.1). Recent studies have focused on surface modification of the catalyst by deposition of composite semiconductors (e.g. CdS),[52] photosensitizers (e.g. organic dyes[53] or ruthenium complexes[54,55]), or transition metal dopants (e.g. Cr^{3+}, Fe^{3+}, Cu^{2+})[56] in order to increase the efficiency of charge-separation process, the selectivity of the product formation, and for tuning the photoresponse into the visible region.

Some photosensitizers are able to accomplish multielectron reactions in the absence of a solid-mediated redox reaction. Polyoxometalates are a widely studied example of a family of polynuclear complexes that can undergo up to four electron photoreduction.[57] Heteropoly oxometalates, $XM_{12}O_{40}^{n-}$ (X= P, Si, Te, H_2; M= Mo, W),[58,59] and isopoly tungstates, $[W_{12}O_{32}]^{4-}$,[60,61] photo-oxidize primary and secondary alcohols to their corresponding aldehydes and ketones via the multielectron-transfer steps shown in Figure 1.5. Upon excitation of the oxygen-to-metal charge-transfer transition, the photoexcited heteropoly-oxometalate reacts with the organic substrate by interelectron/hydrogen transfer resulting in the reduction of polyoxometalate, W_{12}^{4-} or W_{12}^{5-}, and oxidation of organic substrate. The reduced polyoxometalate can be re-oxidized to its original oxidation state by protons to produce hydrogen, or if oxygen is present, to produce water.[62]

As these heterogeneous and homogeneous systems show, an extraordinarily diverse array of photoactive redox metal systems have been elaborated. However, in each case, the basic redox chemistry of the excited state

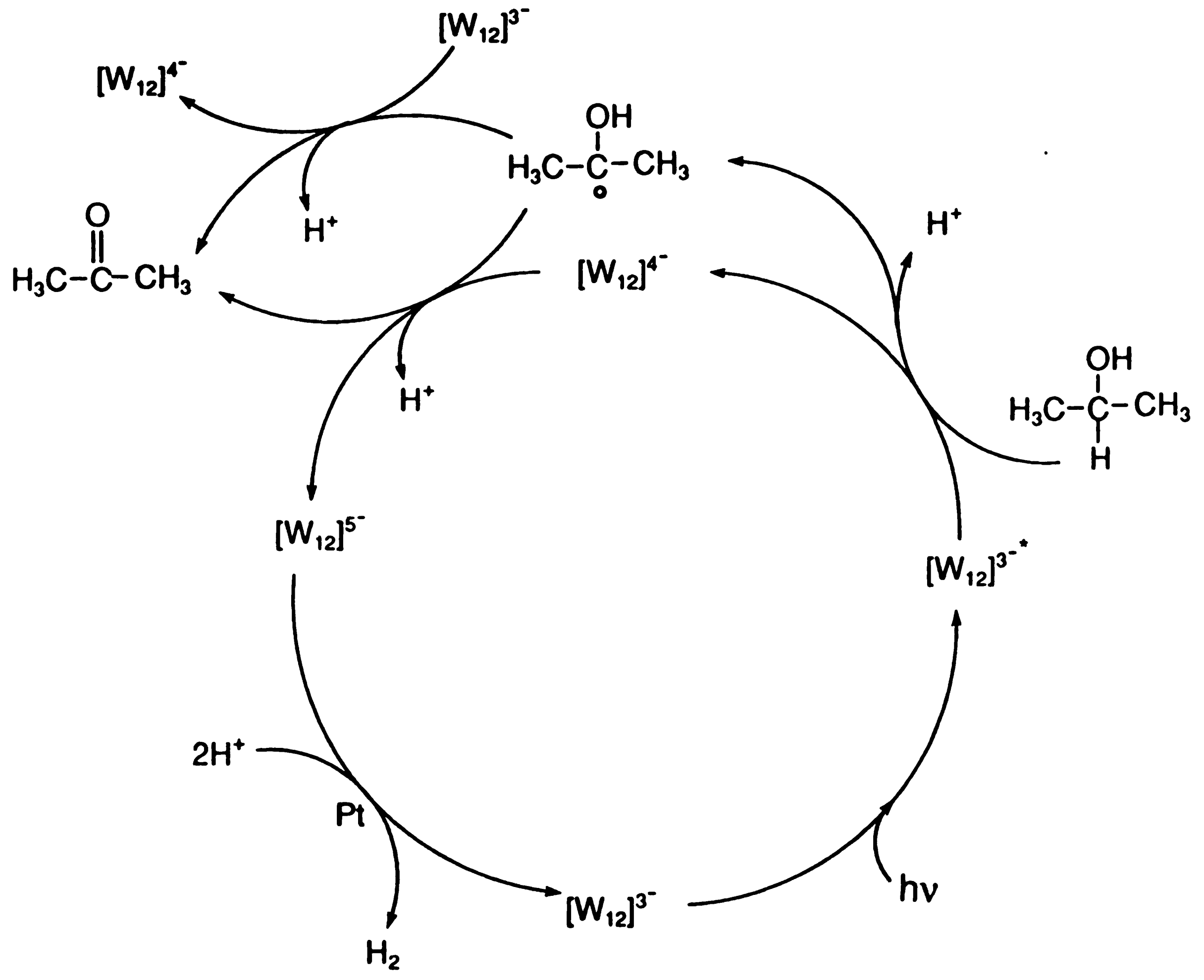

Figure 1.5 Schematic illustration of an alcohol-splitting cycle for conversion of isopropanol to acetone and hydrogen catalyzed by polyoxometalates.

is
ch
un
ele
sm
pre
mu

mul
func
new
obse
binu
be ex

IV.

d^7 ar
these
usual
$^1(\sigma^2$
M(CO
state
produ
gener
single

is the same, evolving little since the initial discovery of excited state redox chemistry over thirty years ago. Namely, the photoactive metal complexes undergo single electron transfer to or from their excited states. By itself, the single electron transfer step is limited inasmuch as most important reactions including small molecule activation processes involve two or more electrons. Thus, as is prevalent in the systems discussed heretofore, the single electron transfer step must be coupled to achieve the multielectron reactivity.

We wondered if an excited state could be designed to undergo a direct multilelectron reaction. The realization of this goal is important because it fundamentally represents a new reaction of excited states and therefore opens new avenues in the design of energy storage schemes. Because we wished to observe a multielectron reaction, we thought it would be logical to consider binuclear redox systems where the redox activity of the two metal subunits might be exploited for a rich redox chemistry.[63–65]

IV. Metal-Metal Binuclear Complexes

The photochemistry of binuclear complexes was popularized with the d^7—d^7 and d^9—d^9 metal-metal compounds.[66–70] The lowest energy transitions in these complexes are metal-localized $\sigma_b \rightarrow d\sigma^*$ and $d\pi^* \rightarrow d\sigma$ and their irradiation usually results in the cleavage of the metal-metal bond (Figure 1.6a). From the $^1(\sigma^2 \rightarrow \sigma\sigma^*)$ singlet excited state, metal-metal bond breaking correlates to $M(CO)_5^+$ and $M(CO)_5^-$ disproportionation products. Alternatively, if the singlet state nonradiatively decays to the lower lying $^3(\sigma\sigma^*)$ triplet state, dissociation produces $M(CO)_5$ radicals. More generally, homolysis of the metal-metal bond to generate reactive radical species is the general rule for binuclear metal-metal single bonded complexes. This process is also observed for d^5–d^5 ($Cp_2M_2(CO)_6$, M=

M′

(Cp

met

met

Hen

com

the

syst

com

(Fig

exen

two

face

orbit

pσ/p

state

show

energ

orbita

in the

the f

Chem

unsatu

(d^3

M= Mo, W), d^9—d^9 ($Co_2(CO)_6(PR_3)_2$), d^5—d^7 ($CpM(CO)_2M'(CO)_5$, M = Mo, W; M′ = Mn, Re), d^7—d^9 ($CpFe(CO)_2M'(CO)_3(PR_3)_3$, M = Mn, Re), and d^5—d^9 ($CpM(CO)_3Co(CO)_4$, M = Mo, W) complexes.[67] The disadvantage of these metal-metal single bonded systems is that the energy of the photon is diverted to metal-metal bond breaking. This results in the loss of polynuclearity in the excited state. Hence, the uncoupled, selective multielectron activation of substrates by these complexes is difficult to control.

Conversely, the structural integrity of metal-metal core can be preserved in the excited states of $d^8 \cdots d^8$,[71-74] $d^{10} \cdots d^{10}$ bimetallic,[75] or $d^{10} \cdots d^8$ heterobimetallic systems.[76] Excitation of the lowest energy $d\sigma^* \rightarrow p\sigma$ transition of these complexes yields an associative diradical species with a long-lived excited state (Figure 1.6b).[72] The excited state chemistry of this class of compounds is exemplified by the $d^8 \cdots d^8$ binuclear compound $Pt_2(P_2O_5H_2)_4^{4-}$, which consists of two square-planar tetracoordinated Pt(II) metal units held together in a face-to-face orientation by the four bridging $P_2O_5H_2^{2-}$ bidentate ligands. The d_{z^2} and p_z orbitals of the platinum centers overlap with each other to give $d\sigma/d\sigma^*$ and $p\sigma/p\sigma^*$ bonding/antibonding orbitals. Since $d\sigma$ and $d\sigma^*$ are filled, the ground state is expected to be nonbonding, although spectroscopically it has been shown there is a weak interaction between the two metal units. Upon the lowest energy $d\sigma^* \rightarrow p\sigma$ excitation, an electron is promoted from a localized antibonding orbital on the exterior of the M_2 unit ($d\sigma^*$ orbital) to a localized bonding orbital in the interior of the dinuclear cage ($p\sigma$ orbital). This electron promotion results in the formation of a net metal-metal bonding interaction in the excited state. Chemically, the excitation creates a hole on each of the coordinatively unsaturated metal centers thereby generating a very reactive associative diradical ($[d^8—d^8]^* = [\bullet M—M\bullet]^*$). The $^3A_{2u}$ excited state of

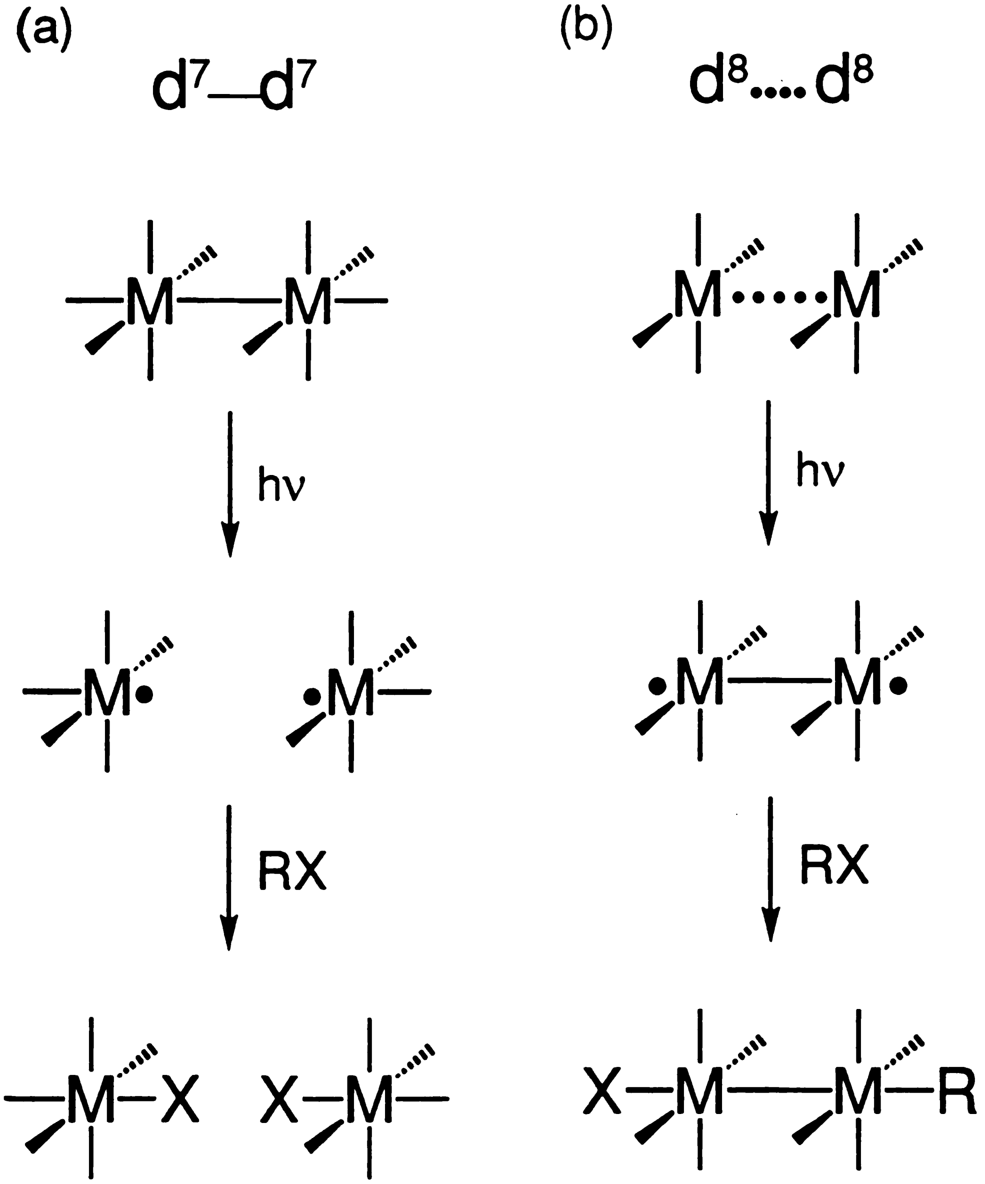

Figure 1.6 Photooxidation mechanisms for the reaction of an organic substrate (RX) with the photogenerated (a) "dissociative diradical" of d^7 and (b) "associative diradical" of d^8 dinuclear complexes.

Pt
0.:
tri
efl
su
del

pho
pho
mu
tran
that
sing
che
mul
met
the
binu
a zv
wea
prep
elec
the
exci
at th
the z
can r

$Pt_2(P_2O_5H_2)_4^{4-}$, which exhibits a long lifetime, 9 μs, and high quantum yield (ϕ_e = 0.5), enables $Pt_2(P_2O_5H_2)_4^{4-}$ to undergo excited state bimolecular reactions.[77] The triplet diradical activates organic substrate via single-electron or atom transfer to effect the overall two-electron photocatalytic reduction of the organic substrates such as the conversion of isopropyl alcohol to acetone[71] and the dehydrogenation of selected hydrocarbons to olefins.[73,78]

The above systems illustrate a general characteristic of classic photosystems: triplet excited states correlate to triplet-spin type primary photoproducts by means of electron transfer or atom abstraction.[79] Alternatively, multielectron processes such as oxidative-addition, reductive-elimination or atom-transfer, correlate to singlet products. Thus, spin conservation arguments suggest that successful multielectron photoreagents will acquire their reactivity from the singlet electronic excited states. The above analogy between one-electron chemistry and biradical excited states made us speculate as to whether multielectron transfer might be emphasized for excited states in which the two metal-localized electrons were not triplet coupled on individual metal atoms (as in the $d^8 \cdots d^8$ complexes) but rather singlet coupled on a single center of the binuclear core (i.e. $:M^-—M^+$). The preparation of this type of excited state, called a zwitterionic excited state, seems to suggest that the metal orbitals should be weakly coupled. In this case, the multielectron. zwitterionic excited state may be prepared by exciting a metal-to-metal charge transfer (MMCT) (Figure 1.7). Here electrons originally localized on the individual metal centers of a bimetallic core in the ground state, are paired upon the absorption of a photon to produce an excited state. The two-electron reduction of the substrate is anticipated to occur at the $:M^-$ site, and the two-electron oxidation occurs at the M^+ site. In this way, the zwitterionic excited state, possessing two-electron mixed-valence character, can realize direct multielectron reactivity from a discrete excited state.

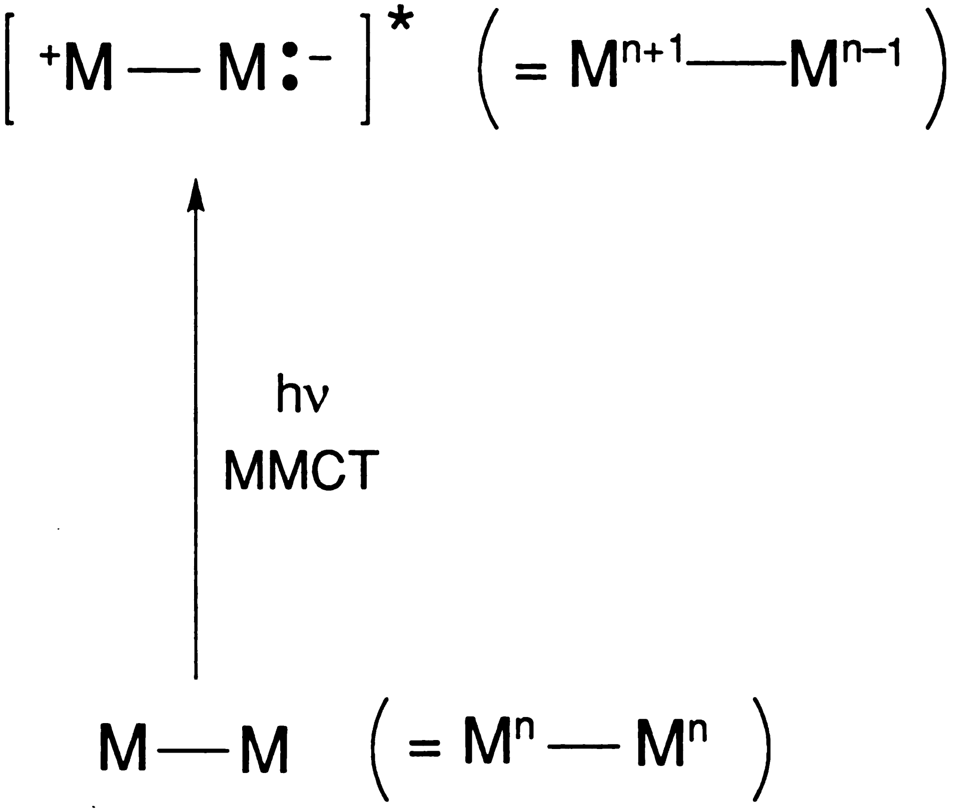

Figure 1.7 Localized two-electron mixed-valence excited state of binuclear metal complexes is produced upon metal-to-metal charge transfer (MMCT).

ma
sh
ex
be
me
(e.
ge
os
co
Th
[(N
ph
uns
[Co
pla
feat
M)

V.

opp
syst
phot
of th
meta

Can stable zwitterionic excited states be elaborated so that their chemistry may be explored? A cursory glance at the problem suggests that the metal centers should be widely separated to achieve zwitterionic character upon MMCT excitation. Precedent for this approach comes from Taube and coworkers' benchmark studies of mixed-valency in which electron localization between two metal centers may be observed[80] with the judicious choice of a bridging ligand (e.g. $[(NH_3)_5M^{III}–L–M^{II}(NH_3)_5]^{5+}$; M = Ru, Os; L = bipyrazine).[81] However, in general these complexes will not be practical excited state reagents because the oscillator strength for the MMCT transitions is too small and the metals are coordinatively saturated. Also the back electron transfer often occurs rapidly.[82] The oscillator strength can be increased with cyanide-bridged complexes, $[(NC)_5M^{II}(\mu\text{-NC})Co^{III}(CN)_5]^{6-}$ (M= Ru, Os, Fe). But the resulting redox isomeric photoproduct $[(NC)_5M^{III}(\mu\text{-NC})Co^{II}(CN)_5]^{6-}$ generated by IT excitation is unstable and often leads to the subsequent dissociation to $[M^{III}(CN)_6]^{3-}$ and $[Co^{II}(CN)_5]^{3-}$.[83] In perhaps one of the great ironies of inorganic chemistry, one place to find two electrons in weakly coupled metal orbitals is in complexes that feature the shortest distances between metals, quadruple bonded metal-metal ($M\overset{4}{-}M$) complexes.

V. Quadruply Bonded Metal-Metal Systems

Quadruply bonded metal-metal ($M\overset{4}{-}M$) complexes[84] offer an unique opportunity to explore excited state oxidation-reduction chemistry. These systems possess several other attractive features as polynuclear multielectron photoreagents. First, the presence of an open coordinate site in the axial position of the metal-metal bond provides a site for initial substrate activation. Second, the metal-metal multiple bond is an electron rich core that can provide many electrons in an oxidation-reduction transformation. Third, the lowest energy transitions are metal localized and lie in the visible spectral region. Fourth, the strong metal-metal bond makes photodissociative pathways less likely. Both theoretical calculations and experimental spectroscopic studies show that the bond strength of the metal-metal quadruple bond is in the range of 127-190 kcal/mol. Even under intense UV radiation, the metal-metal bond is usually retained.[85,86] Finally, and perhaps most important with regard to the theme of this thesis, the lowest energy transitions produce a long-lived zwitterionic excited state of $:\mathrm{M}^{-}\text{—}\mathrm{M}^{+}$ character. This excited state is of singlet character and unlike most singlet excited states, which typically exist for a few nanoseconds or even shorter,[87,88] this excited state can be quite long-lived to permit its bimolecular reaction.

A general molecular orbital diagram for $\mathrm{M}\overset{4}{-}\mathrm{M}$ complexes is shown in Figure 1.8. Quadruply bonded $\mathrm{M}\overset{4}{-}\mathrm{M}$ dimers are composed of two ML_4 fragments with four electrons delocalized in four degenerate d orbitals from each fragment to give a $\sigma^2\pi^4\delta^2$ ground state electronic configuration. The d_{z^2} orbitals overlap with each other to form a metal-metal σ bond, while d_{xz} and d_{yz} orbitals give two metal-metal π bonds. The d_{xy} orbitals on each metal are parallel to each other and consequently only weakly interact to give a δ bond. For two d^4 metals, as is the case with $\mathrm{Mo}^{\mathrm{II}}$ and W^{II}, the δ orbital is the highest occupied molecular orbital (HOMO), while the δ^* orbital is the lowest unoccupied molecular orbital (LUMO). Therefore the lowest energy, electronically allowed, transitions involve $\delta \rightarrow \delta^*$, $\pi \rightarrow \delta^*$, $\delta \rightarrow \pi^*$ promotions, and ligand-to-metal charge transfer (LMCT) or metal-to-ligand (MLCT) transitions lie to higher energy. Because the metal localized transitions are in the visible region, the photochemistry of these complexes may be studied by utilizing visible light.

While the molecular orbital model conceptually describes the qualitative bonding diagram for $\mathrm{M}\overset{4}{-}\mathrm{M}$ complexes, a valence bond model gives us a better

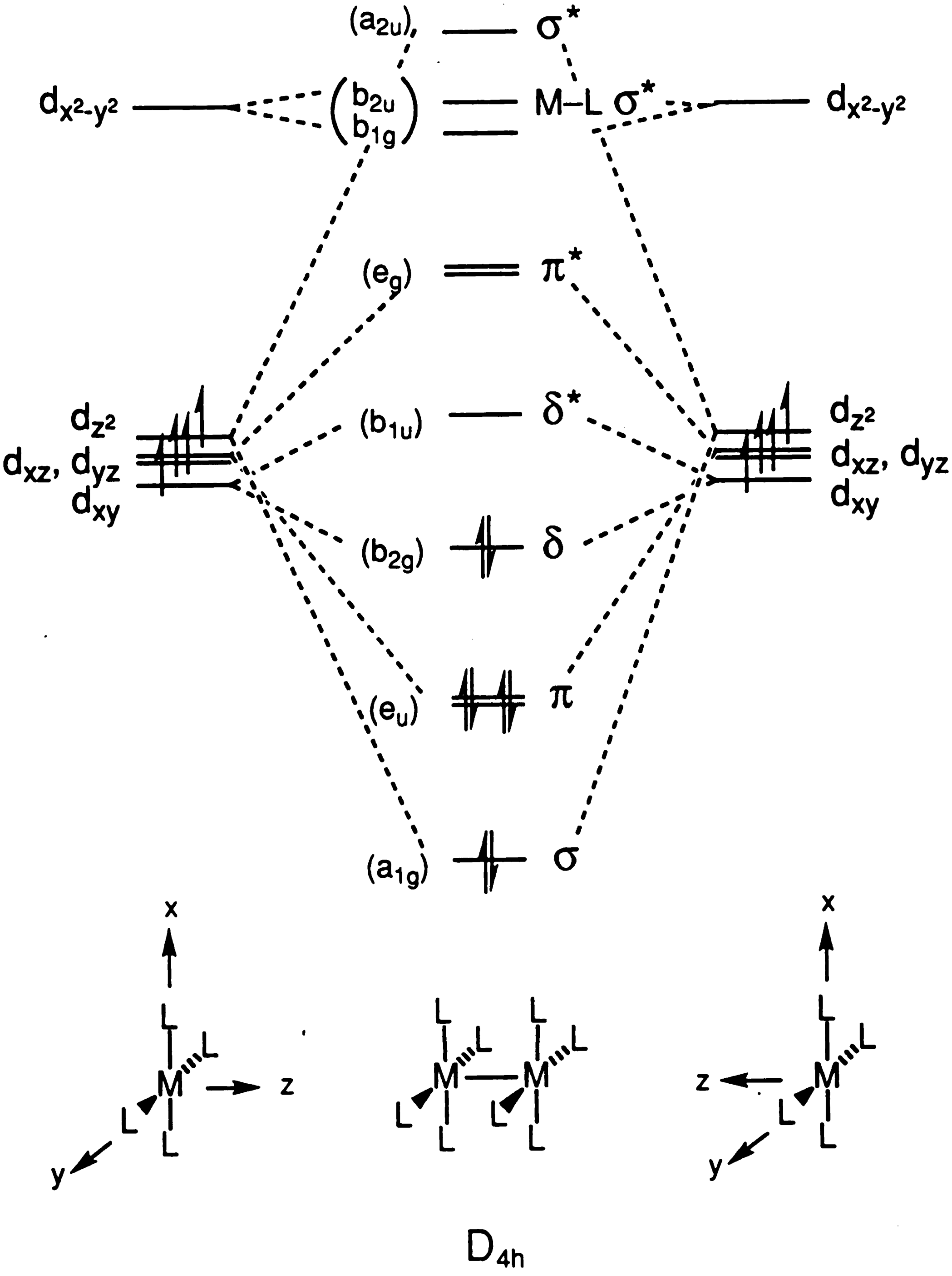

Figure 1.8 MO diagram of quadruply bonded M$\overset{4}{-}$M binuclear metal complexes.

an

for

we

tw

tw

lar

gi

zw

ele

gi

to y

aris

orb

pai

bon

stat

dira

the

whe

exci

MM

is ac

and more quantitative understanding of the states and their energies, especially for those associated with the δ orbitals. Because the overlap of the d_{xy} orbitals is weak, the δ bond of $M\overset{4}{-}M$ complexes is similar to the bonds formed from the two-electron, two-center weakly coupled orbitals of organic diradicals, such as twisted ethylene, and the stretched σ bond of a hydrogen molecule.[89–92] The large energies associated with pairing electrons in weakly coupled d_{xy} orbitals give rise to four states: two low-energy diradical states and two high-energy zwitterionic states as shown Figure 1.9. The two diradical states come from an electron in each singly occupied orbital of the metal site with spins opposed to give the singlet 1^1A_{1g} (in D_{4h} symmetry) $^1(\delta^2)$ ground state, and with spins parallel to yield the triplet $^3A_{2u}$ $^3(\delta\delta^*)$ excited state. The upper zwitterionic excited states arise from the symmetric 2^1A_{1g} and antisymmetric $^1A_{2u}$ linear combination of d_{xy} orbitals to form the corresponding $^1(\delta^*\delta^*)$ and $^1(\delta\delta^*)$ states with two electrons paired in either orbital of one metal site. As shown by Hay's general valence bond calculation of $Re_2Cl_8^{2-}$,[93] the energetic disposition of the diradical excited states is far below the ionic states, whereas the energy gaps between 1^1A_{1g}—$^3A_{2u}$ diradical states and $^1A_{2u}$—2^1A_{1g} ionic states are small and equal. Electronically, the singlet zwitterionic states correlate to a M^IM^{III} charge-separated center whereas the diradical states correlate to a symmetrical $M^{II}M^{II}$ configuration. Thus excitation of transitions associated with the δ manifold (eq. 1.3) amounts to MMCT in which an excited state of considerable $:M^-$—M^+ zwitterionic character is achieved.

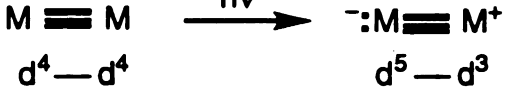

$$\underset{d^4-d^4}{M \equiv M} \xrightarrow{h\nu} \underset{d^5-d^3}{{}^-{:}M \equiv M^+} \qquad (1.3)$$

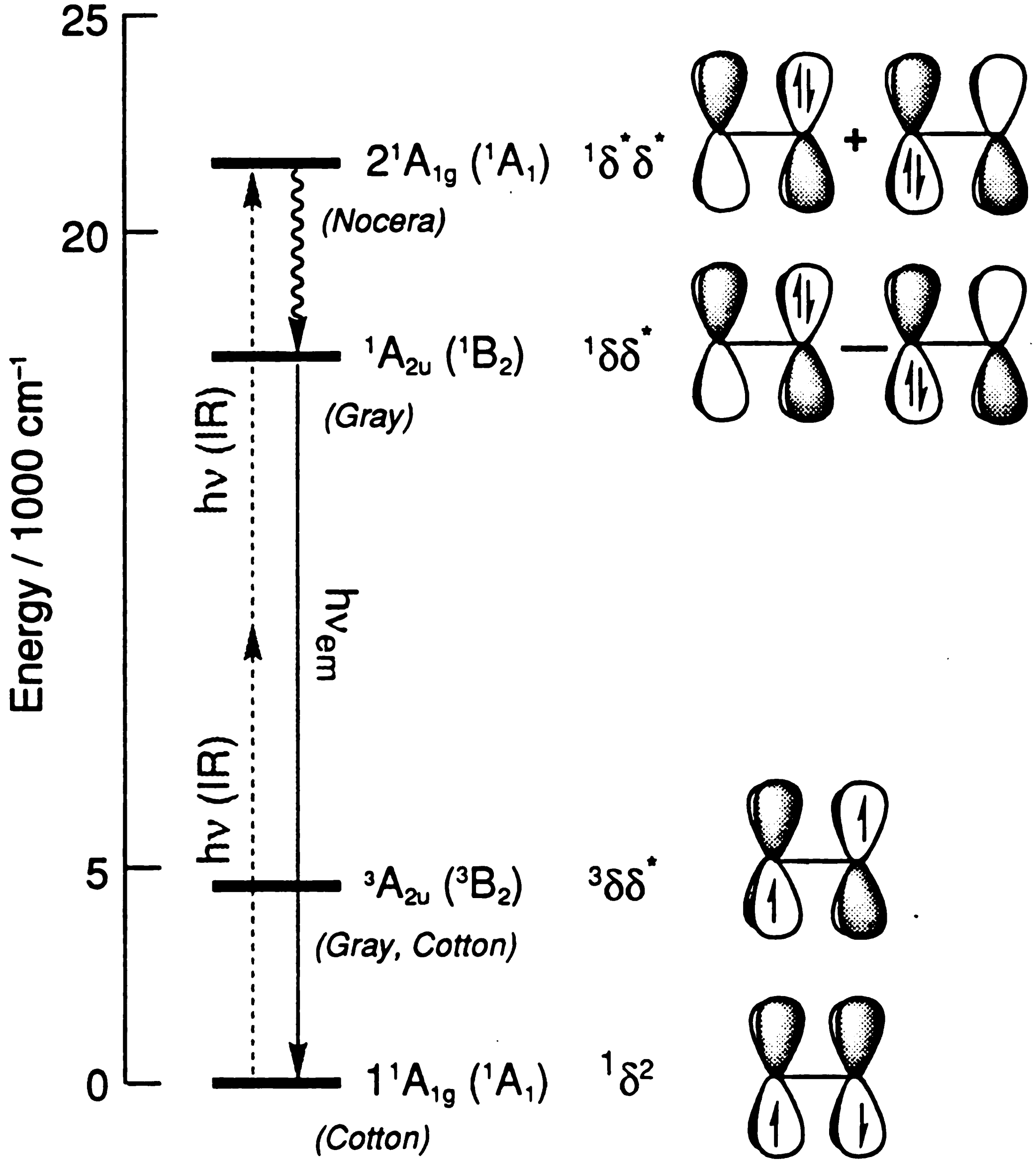

Figure 1.9 Energy level diagram for δ/δ* manifold of M$\stackrel{4}{-}$M complexes in valence bond description of the electronic states formed by the dxy orbitals with the corresponding MO formalism

The existence of zwitterionic character for $M\overset{4}{—}M$ complexes has been spectroscopically verified by recent two-photon spectroscopic experiments carried out in our laboratory.[94] By identifying the $^1(\delta^*\delta^*)$ excited state, a 4,890 cm^{-1} energy gap has been determined for the two zwitterionic excited states (i.e., $\Delta E(E\ ^1(\delta^*\delta^*) - E\ ^1(\delta^*\delta^*) = 4{,}890\ \mathrm{cm}^{-1})$. This gap is small, which should be the case for a zwitterionic state. Moreover, as mentioned above, the diradical energy gap, $^3A_{2u}$—$^1A_{1g}$, should be equivalent, to a first approximation, to that for the zwitterionic states, 2^1A_{1g}—1^1A_{1g}. This is observed experimentally. Cotton and coworkers have extrapolated their experimental measurements of the $^3A_{2u}$—$^1A_{1g}$ gap for twisted $M\overset{4}{—}M$ complexes to a torsional angle of $\chi = 0°$ and obtained an energy gap splitting of 4840 cm^{-1},[95] in excellent agreement with the 2^1A_{1g}—1^1A_{1g} gap measured by two-photon spectroscopy.

The spectroscopic results unequivocally establish that transitions associated with the δ-orbital manifold are MMCT in character, and yield an electron pair, singlet coupled, ($:M^-—M^+ = d^5—d^3$) within the binuclear core. More quantitatively, the spectroscopically ascertained values of ΔW and K (determined from the difference between the $^1(\delta^2 \rightarrow \delta\delta^*)$ and $^1(\delta^2 \rightarrow \delta^*\delta^*)$ energy gaps) in conjunction with the effective $d_{xy}(A)$—$d_{xy}(B)$ overlap (as evaluated from the oscillator strength of the $\delta \rightarrow \delta^*$ transition[96]) reveals that the δ^2 ground state possesses 34% ionic character, which increases significantly to 68% in the excited state. Nevertheless, the presence of a long-lived, ionic, excited state in $M\overset{4}{—}M$ complexes does not in itself ensure multielectron photochemistry. The $^1\delta\delta^*$ (Ψ_-) and $^1\delta^*\delta^*$ (Ψ_+) zwitterionic states are described by the following linear combinations,

$$\begin{aligned} \Psi_\pm \;=\; & :M^-—M^+ \pm M^+—M:^- \\ & [d^5—d^3] \pm [d^3—d^5] \end{aligned} \qquad (1.4)$$

A

M

is

or

di

po

VI

as

mo

su

rea

$^1(\delta$

di

di

tra

lig

inf

seq

to

ger

we

the

Although these states are ionic, they are nonpolar because $:\mathrm{M}^{-}\text{—}\mathrm{M}^{+}$ and $\mathrm{M}^{+}\text{—}\mathrm{M}:^{-}$ contribute equally to the linear combination as long as a center of inversion is maintained within the molecule and its environment. However, intermolecular or intramolecular perturbations that remove the center of inversion will lead to dissimilar contributions of the $:\mathrm{M}^{-}\text{—}\mathrm{M}^{+}/\mathrm{M}^{+}\text{—}\mathrm{M}:^{-}$ states in eq. (1.4), thereby polarizing the system.

VI. Thesis Outline

The zwitterionic nature of $\mathrm{M}\overset{4}{-}\mathrm{M}$ excited states presents these complexes as logical candidates for multielectron photochemistry. Unlike the singlet states of most transition metal complexes, the $^{1}(\delta\delta^{*})$ excited state of $\mathrm{M}\overset{4}{-}\mathrm{M}$ dimers are sufficiently long-lived ($\tau \sim 100$ ns)[97] in some cases to permit bimolecular reactivity. The longevity of the MMCT state most probably arises from the large $^{1}(\delta\delta^{*})\text{—}^{3}(\delta\delta^{*})$ energy gap which inhibits intersystem crossing.

Chapter III outlines mechanistic studies of the photoreactions of a dimolybdenum tetraphosphate, $\mathrm{Mo_2[O_2P(OC_6H_5)_2]_4}$, in the presence of dihalocarbons. In these complexes, the zwitterionic excited state can not be trapped by intramolecular ligand rearrangement because the diaryl phosphate ligands are too bulky and in their bidentate coordination geometry, structurally inflexible. Mechanistic studies reveal that the reaction proceeds by two sequential one-electron steps at the axial coordination site of the bimetallic core to yield the overall two-electron transformation. This chemistry has been generalized by reacting the $\mathrm{M}\overset{4}{-}\mathrm{M}$ complex with unsaturated dihalocarbons as well as saturated halocarbons as substrates.

In Chapters IV and V complexes are chosen with ligands that can stabilize the mixed-valence $\mathrm{M^{I}\text{—}M^{III}}$ intermediate coordination by rearranging to edge

br
D
or
pr
ca
dia
M
ph
im
tra
tra
diff

mix
the
with
Mo
stat
low
pho
ana
of th

pho
appr
chen

bridging positions. The terminal halide monodentate ligands of $M_2Cl_4(PR_3)_4$ (with D_{2d} geometry) and $M_2Cl_4(PP)_2$ (with D_{2h} geometry) complexes (where M = Mo or W) give the structural flexibility to form edge-bridging intermediates. We proposed that discrete multielectron transformations might be achieved in these cases. Chapter IV details the photochemistry of the $M_2Cl_4(PP)_2$ complexes with diaryl/dialkyl disulfides and Chapter V presents the photochemistry of the $M_2Cl_4(PR_3)_4$ complexes with dihalocarbons. For $M_2Cl_4(PP)_2$ compounds, the photochemistry proceeds with visible excitation of MMCT states that are immediately adjacent in energy to the $\delta\delta^*$ excited state. In contrast, these transitions are obscured in the $M_2Cl_4(PR_3)_4$ (M = Mo, W) complexes by LMCT transitions. Consequently, the photochemistry for these two family of compounds differs.

Whereas the approach taken in Chapters IV and V is to trap the critical mixed-valence $M^{I}—M^{III}$ intermediate by an internal ligand arrangement to break the symmetry of the bimetallic core, Chapter VI attempts to trap the intermediate with the asymmetry induced by a heterobimetallic core. Our hypothesis is that $Mo\overset{4}{-}W$ bimetallics may exhibit better energy-storage behavior in the excited state because the mixed-valence character of a $Mo^{I}—W^{III}$ excited state will be lower than the $Mo^{III}—W^{I}$ counterpart. Chapter VI will compare the photophysical properties of $Mo\overset{4}{-}W$ species with their $Mo\overset{4}{-}Mo$ and $W\overset{4}{-}W$ analogs, and examine the influence of the asymmetric core on the photoreactivity of this class of photoreagents.

In summary, we have systematically explored the multielectron photochemistry of a unique class of photoreagents, provided by a systematic approach to the realization of the first excited state multielectron pathways in chemistry. The nature of the substrates and the $M\overset{4}{-}M$ electronically excited complexes, and the affect of environment in contributing to the novel photochemical observations will be rationally developed in this dissertation.

I

V

se

va

co

(N

pr

pr

su

pe

bi

N

pu

Ch

wa

di

a

CHAPTER II

EXPERIMENTAL

I. General Procedures

All manipulations were performed under the argon atmosphere of a Vacuum Atmospheres drybox or the manifold of a Schlenk line. For the most air-sensitive compounds, syntheses were performed on the manifold of a high vacuum line (10^{-6} to 10^{-7} torr). Syntheses of quadruply bonded metal-metal complexes were accomplished with standard Schlenk techniques. $K_4Mo_2Cl_8$,[98] $(NH_4)_5Mo_2Cl_9$,[99] $Mo_2(O_2CCH_3)_4$,[100] and iodobenzene dichloride ($PhICl_2$)[101] were prepared by published procedures. Tungsten(IV) tetrachloride (WCl_4) was also prepared according to a literature method[102] but was further purified by sublimating the product from tungsten oxide impurities. Molybdenum(V) pentachloride (Mo_2Cl_{10}), tungsten(VI) hexachloride (WCl_6), diphenylphosphate, bidentate phosphines, chlorotrimethylsilane (Me_3SiCl), dialkyl disulfides and $NOBF_4$ were purchased from Aldrich Chemicals and used without further purification as were trialkylphosphines, which were purchased from Strem Chemicals. Diphenyl disulfide was recrystallized and dried under vacuum.

Solvents used for synthesis were dried by general procedures.[103] Toluene was freshly distilled from sodium/potassium benzophenone ketyl, and dichloromethane was distilled from P_2O_5, then stored over 4-Å molecular sieves in a 1-liter flask equipped with a Kontes high-vacuum valve. The methanol used for th

N

a

c

us

p

P

ec

d

pu

dy

fl

a

fr

sc

fo

II

A.

lig

(C

M

ab

the syntheses of dimolybdenum tetrakis(diphenylphosphates) was refluxed over NaOMe for no less than 6 h and freshly distilled prior to use; the amount of Na added to MeOH was 20% more than the amount required to react with the water contained in a freshly opened bottle. All other chemicals were reagent grade and used as received unless otherwise noted.

All solvents used for spectroscopic and photochemical experiments were purchased from Burdick and Jackson Laboratories (Spectroscopic grade). Purified solvents were stored in glass containers that consisted of a 1-liter flask equipped with a Kontes high-vacuum valve. 1,2-Dichloroethane, 1,2-dichloroethylene, and 1,2-dichlorocyclohexane were degassed by seven freeze-pump-thaw cycles and stored over activated (heated to 250 °C under 10^{-6} torr dynamic vacuum for 12 h) Linde 4 Å molecular sieves contained in a storage flask; ortho-dichlorobenzene was refluxed over P_2O_5 under a nitrogen atmosphere. Tetrahydrofuran, toluene and benzene were subjected to seven freeze-pump-thaw cycles and subsequently distilled into flasks containing sodium-potassium alloy with a small amount of benzophenone; the purple ketyl form of benzophenone formed over a two-day period.

II. Synthesis

A. Tetrakis(diphenylphosphate) Dimolybdenum Complexes

The Mo_2(II,II) tetrakis(diphenylphosphate) was prepared by a simple ligand substitution reaction. The anion $(C_6H_5O)_2PO_2^-$ was generated by stirring $(C_6H_5O)_2P(O)OH$ (3.25 g, 13 mmol) with NaOMe (0.702 g, 13 mmol) in 60 mL of MeOH. After 10 min, $(NH_4)_5Mo_2Cl_9 \cdot H_2O$ (0.5 g, 0.8 mmol) was added to the above solution, which was then heated to reflux for 3 h. The pink precipitate, formed during refluxing, was collected by suction filtration and washed with three 15 mL portions of MeOH. Aliquots for all washings were delivered by cannula. The solid was dried in vacuo (yield: 0.67 g, 70%). The $Mo_2^{II,II}$ tetrakis(diphenylphosphate) complex is extremely air-sensitive, decomposing within seconds upon exposure to air. The compound, though not soluble in most organic solvents, exhibits fairly good solubilities in halocarbons and THF. UV-vis, λ_{max} (ε) in CH_2Cl_2: 515 nm (156 $M^{-1}cm^{-1}$) and 404 nm (38 $M^{-1}cm^{-1}$).

B. Homonuclear Dimolybdenum and Ditungsten Complexes.

B.1. Syntheses of $Mo_2Cl_4(PR_3)_4$ (PR_3 = PMe_3, PMe_2Ph, $PMePh_2$)[104]

Complexes of $Mo_2Cl_4(PR_3)_4$ were prepared typically by the following procedure. The $K_4Mo_2Cl_8$ or $(NH_4)_5Mo_2Cl_9$ (0.5g, 0.8 mmol) salt was dissolved in dry methanol (25 mL), followed by adding four equivalents of trialkylphosphines. The reaction solution was refluxed for 4 h to form a green precipitate, which was then filtered off, washed with water and methanol, and dried in vacuo. The blue solid, $Mo_2Cl_4(PR_3)_4$, can be purified by filtering a CH_2Cl_2 solution of $Mo_2Cl_4(PR_3)_4$ through a Florisil column under nitrogen; the solvent was removed under reduced pressure. Compounds were identified by UV-vis, ^1H and ^{31}P NMR.

B.2 Syntheses of $Mo_2Cl_4(dppm)_2$[105]

$Mo_2Cl_4(dppm)_2$ was prepared by the same method described for the $Mo_2Cl_4(PR_3)_4$ complexes but the bidentate phosphine ligand, dppm, was used in place of PR_3. UV-vis, λ_{max} (ε) in CH_2Cl_2: 634 nm (2490 $M^{-1}cm^{-1}$), 462 nm (900 $M^{-1}cm^{-1}$) and 325 nm (5600 M^{-1} cm^{-1}).

B.3. Syntheses of $W_2Cl_4(PR_3)_4$ (PR_3 = PMe_3, PMe_2Ph, $PMePh_2$, PBu_3)[106]

Sodium amalgam (0.41%, 90 g, 16.04 mmol of Na) was freshly prepared in a three-neck round bottom flask under argon. To this liquid, 135 mL of dry THF was introduced into the flask, which was cooled to –78 °C with a dry-ice/acetone, and tungsten(IV) tetrachloride (2.6 g, 8.0 mmol) was added followed by the addition of two equivalents of phosphine, PR_3. The reaction solution was stirred at –30 °C (chloroform/liq. N_2 bath) for half an hour, then slowly warmed to 0 °C with an ice bath and, finally warmed to room temperature over an hour upon the removal of the ice bath. The deep brown-green solution was filtered through Celite and the solvent was removed from the filtrate in vacuo. The residue was extracted with hexane (or CH_2Cl_2 when PR_3 = $PMePh_2$ owing to the poor sloubility of $W_2Cl_4(PMePh_2)_4$). The extract was filtered and concentrated to 3 mL. The dark green $W_2Cl_4(PR_3)_4$ complex was precipitated out by adding MeOH to the concentrated filtrate. (Note: different $W_2Cl_4(PR_3)_4$ complexes have different solubilities in THF and CH_2Cl_2. The longer the alkyl chain, the better the solubility in these solvents.) Compounds were identified by UV-vis, ^1H and ^{31}P NMR.

C. Heteronuclear Molybdenum-Tungsten Complexes

C.1. Synthesis of $Mo(\eta^6\text{-}PhPMePh)(PMePh_2)_3$[107]

Molybdenum(V) pentachloride (0.65 g, 2.38 mmol) was dissolved in a 135 mL of dry THF solution containing methyl(diphenyl)phosphine (2.4 g, 11.9 mmol) at 0 °C under argon atmosphere. (Note: Argon is necessary in this case since nitrogen is found to act as a ligand and coordinates to the metal site.) Excess Grignard magnesium (1.26 g of Mg turnings) was slowly added to the ice-cold c

v

t

t

f

n

w

p

M

re

M

m

un

40

4.

m-

N

C.

th

w

9.

be

ph

fla

orange THF solution over one-hour with vigorous stirring. The reaction solution was kept stirring at 0 °C for an additional hour and warmed up to room temperature over half an hour. The reaction solution changed from rusty orange to olive green after ca. 30 min and then turned orange. This orange solution was filtered through Celite by cannula techniques. The filtrate was concentrated to 30 mL under vacuum but not too concentrated to induce the formation of oligomers, which is indicated by the solution turning black-green. An orange powder was precipitated by the dropwise addition of MeOH and filtered, followed by three MeOH washings to remove excess phosphine from the solid. The product was recrystallized from benzene/MeOH in order to remove oligomer impurities. $Mo(\eta^6\text{-PhPMePh})(PMePh_2)_3$ is extremely air-sensitive especially when the mother liquid is around. It is better to dry the product by evaporating MeOH under an argon stream overnight before drying under high vacuum (yield: 0.84 g, 40%). ^1H NMR(C_6D_6) δ 7.55 (m, 6 H, o-PhP–Mo), 7.3–7.2(m, 9 H, m,p-PhP–Mo), 4.42 (m, 2 H, o-η^6-Ph), 4.16 (m, 1 H, p-η^6-Ph), 3.72 (m, 2H, m-η^6-Ph), 3.60 (m, 2H, m-η^6-Ph), 1.77 (br, 9H, Me_2P–Mo), 1.20 (d, 6H, $^2J_{HP}$= 4 Hz, Me_2P–η^6-Ph). ^{31}P NMR(C_6D_6): δ 15.8 (s, 3P, P–Mo), -46.7 (s, 1 P, η^6-Ph–P).

C.2. Synthesis of $Mo(\eta^6\text{–PhPMe}_2)(PMe_2Ph)_3$[108]

The experimental set-up is similar to $Mo(\eta^6\text{-PhPMePh})(PMePh_2)_3$ except that the reaction requires heat. Molybdenum pentachloride (0.50 g, 1.83 mmol) was dissolved in 45 mL of dry THF containing dimethyl(phenyl)phosphine (1.3 g, 9.4 mmol) at room temperature under an argon atmosphere. (Caution: water must be rigorously excluded from the reaction set-up because free dimethyl(phenyl)-phosphine reacts with water vigorously and will ignite in the presence of flammable material). Excess Grignard magnesium (2 g of Mg turnings) was slowly

(
r
l
v
F
c
n
N

C

zi
pi
co
so
dr
m
m
th
s
ar
he
fi
ar

added to the THF solution with vigorous stirring. The reaction solution was then heated to 70 °C for 2h. The solution was filtered through Celite and concentrated. Precipitation was induced by the dropwise addition of MeOH. The resulting filtrate was kept at –20 °C overnight to induce more precipitate. The bright-orange solid, which formed on the sides of the reaction flask, was washed with MeOH. $Mo(\eta^6\text{-}PhPMe_2)(PMe_2Ph)_3$ is even more air-sensitive than the its $PMePh_2$ analog, both in solid state and in solution. ^1H NMR(C_6D_6) δ 7.5 (m, 6 H, o-PhP–Mo), 7.3–7.2 (m, 9 H, m,p-PhP–Mo), 4.0 (m, 2 H, o-η^6-Ph), 3.4 (m, 1 H, p-η^6-Ph), 3.2 (m, 2H, m-η^6-Ph), 1.5 (br, 1.8H, Me_2P–Mo), 1.0 (d, 6H, $^2J_{HP}$= 4 Hz, Me_2P–η^6-Ph). ^{31}P NMR(C_6D_6): δ 15.8 (s, 3P, P–Mo), –46.7 (s, 1 P, η^6-Ph–P).

C.3. Synthesis of $WCl_4(PPh_3)_2$[109]

Tungsten(VI) hexachloride (5.6 g, 14.1 mmol) and dry granulated mossy zinc (7.5g) were placed in round bottom flask. The mossy Zn amalgam was prepared prior to its use by the dropwise addition of 2 mL of 12 M HCl (aq) containing HgO (0.2 g, Matheson, Coleman and Bell) to mossy Zn in 80 mL H_2O solution. The amalgamated Zn was filtered, washed with H_2O and acetone and dried in the oven. Dichloromethane (90 mL) was added to flask containing the mossy zinc and tungsten complex under argon via a side-arm. The solution was mixed well by shaking the sealed flask for 1 min and the pressure was released through the side-arm stopcock. Triphenylphosphine (11.25g, 42.9 mmol) was slowly (~3 min) added to the saturated solution of WCl_6. The flask was shaken and the build-up in pressure was relieved periodically until the tungsten hexacholride had totally reacted. The resulting yellowish-orange solid was filtered and the co-deposited zinc was removed by picking out the pieces under an argon flow. The solid was washed with CH_2Cl_2 and MeOH to remove the tungsten oxide impurities. The product was dried in vacuo (yield: 5.4g, 45%). UV-vis (CH_2Cl_2): 420 nm. IR(Nujol mull, CsI) ν(M–Cl): 317 cm^{-1} (strong) and 325 cm^{-1} (shoulder). ^1H NMR($CDCl_3$) δ 11.2 (d, 2 H, o-PhP), 8.2 (d, 2 H, m-PhP), 7.88 (t, 1 H, p-PhP).

C.4. Synthesis of $MoWCl_4(PMePh_2)_4$[110]

In a glove bag inside the dry box, a 40 mL benzene solution of Mo(η^6-PhPMePh)($PMePh_2)_3$ (0.9 g, 1.0 mmol) in a dropping funnel was added over 30 min to a 100 mL suspension of benzene solution containing yellow $WCl_4(PPh_3)_2$ (2.25 g, 2.7 mmol). This part of the reaction is very moisture-sensitive and all the glassware must be flamed dried under 10^{-3} torr vacuum; otherwise the product yield will drop to near zero and impurities, such as $WOCl_2(PMePh_2)_3$, will be produced in significant yields. The entire reaction set-up was removed from the dry box and subsequent manipulations were carried out with Schlenk techniques. After an additional half hour of stirring, the resulting blue-green solution was filtered through Celite by the cannula technique and the solvent was removed from the filtrate. The residue was redissolved in toluene and filtered to remove excess $WCl_4(PPh_3)_2$. The toluene filtrate was then concentrated to 5 mL and MeOH was added to induce precipitation. The blue-green precipitate was filtered, washed with MeOH three times, and dried in vacuo (Yield: 0.6 g, 49%). UV-vis, λ_{max} (ε) in C_6H_6: 650 nm (2609 $M^{-1}cm^{-1}$), 460 nm (394 $M^{-1}cm^{-1}$) and 320 nm (7133 $M^{-1}cm^{-1}$). ^1H NMR(C_6D_6): δ 8.0–7.5 (m, 16 H, ortho-PhP–M, M= Mo, W), 7.0–6.8 (m, 24 H, m,p-PhP–M, M = Mo, W), 2.1 (t, virtual coupling, 6 H, MeP–W, J = 4 Hz), 1.9 (t, virtual coupling, 6 H, MeP–Mo, J = 3 Hz). ^{31}P NMR(C_6D_6): δ −12.05 (t, 2 x 0.86 P, P–Mo–W (I = 0), $^3J_{pp}$ = 23.5 Hz), −12.05 (dt, 2 × 0.14 P, P–

Mo–^{183}W, $^2J_{pw}$ = 47 Hz, $^3J_{pp}$ = 23.5 Hz), 23.03 (t, 2 × 0.86 P, P–W (I = 0), $^3J_{pp}$ = 23.5 Hz), 23.03 (dt, 2 × 0.14 P, P–Mo–^{183}W, $^1J_{pw}$ = 266 Hz, $^3J_{pp}$ = 23.5 Hz).

C.5. Synthesis of $MoWCl_4(PMe_2Ph)_4$[110,111]

Mo(η^6-PhPMe$_2$)(PMe$_2$Ph)$_3$ (60 mg, 0.093 mmol) was added dropwise into a benzene solution of $WCl_4(PPh_3)_2$ (80 mg, 0.094 mmol) and dark green $MoWCl_4(PMe_2Ph)_4$ was produced (yield: 48 mg, 53%). The solid was isolated as described in Section 3.4. UV-Vis (C_6H_6): 630 nm. ^{1}H NMR(C_6D_6): δ 7.7, 7.23 (d,m, 8 H, ortho-PhP–M, M = Mo, W), 7.0, 6.9 (d,m, 12 H, m,p-PhP–M, M = Mo, W), 1.9, 1.8 (d,t, virtual coupling, 12 H, MeP–Mo, J = 3.6 Hz). ^{31}P NMR(C_6D_6): δ –19.62 (t, 2P, P–Mo, $^3J_{pp}$ = 24.0 Hz), 17.84 (t, 2 × 0.86 P, P–W (I = 0), $^3J_{pp}$ = 24.0 Hz), 17.84 (dt, 2 × 0.14 P, P–^{183}W, $^1J_{pw}$ = 280 Hz, $^3J_{pp}$ = 24.0 Hz).

C.6. Synthesis of $MoWCl_4(PMe_3)_4$[110]

Trimethylphosphine (40 mg, 0.53 mmol) was added to a benzene solution of $MoWCl_4(PMePh_2)_4$ (130 mg, 0.106 mmol). The reaction solution was sealed under vacuum and heated to 60 °C for 3 h thereby ensuring complete ligand exchange. The ligand PMePh$_2$, excess PMe$_3$, and the solvent were removed under vacuum. The resulting blue residue was washed with MeOH to yield the dark blue-green product, $MoWCl_4(PMe_3)_4$ (yield: 20 mg, 26%). UV-Vis (C_6H_6): 630 nm. ^{1}H NMR(C_6D_6): δ 1.5 (m, 36 H, MeP–M, M= Mo, W). ^{31}P NMR(C_6D_6): δ -27.4 (t, 2P, P–Mo, $^3J_{pp}$ = 24.4 Hz), 10.9 (t, 2 × 0.86 P, P–W (I= 0), $^3J_{pp}$ = 24.4 Hz), 10.9 (dt, 2 × 0.14 P, P–^{183}W, $^1J_{pw}$ = 269 Hz, $^3J_{pp}$ = 24.4 Hz).

C.7. Synthesis of $MoWCl_4(dppm)_2$[112]

$MoWCl_4(PMePh_2)_4$ (70 mg, 0.057 mmol) and bis(diphenylphosphino)-methane (90 mg, 0.234 mmol) were suspended in dry 1-propanol (20 mL). The blue-green suspension solution was refluxed overnight to form a green precipitate, which was collected by filtration, washed with hexanes, and dried in vacuo (Yield: 44 mg, 63%). UV-Vis (THF): 675, 317 nm. ^1H NMR(CD_2Cl_2, –40 °C): δ 7.5–7.0 (m, 40 H, PhP–M, M = Mo, W), 4.7 (m, 4 H, CH_2P–M, M = Mo, W). ^{31}P NMR(CD_2Cl_2, –40 °C) exhibits a AA´BB´X pattern: δ –2.5 (m, 2P, P–Mo), 35.4 (m, 2 P, P–W).

III. Reactions

A. Photochemistry of $Mo_2[O_2P(OC_6H_5)_2]_4$ with Dihalocarbons

Dichlorocarbon solutions containing 2-4 mgs of $Mo_2[O_2P(OC_6H_5)_2]_4$ were irradiated at $\lambda > 495$ nm and the photolysis was monitored by UV-vis spectra. Photolysis was terminated when the near-IR absorption reached a maximum, indicating the formation of the mixed-valence $Mo_2^{II,III}$ complex. UV-vis, λ_{max} in CH_2Cl_2: 1492, 542 and 420 nm.

B. Photochemistry of $Mo_2Cl_4(dppm)_2$ with PhSSPh

$Mo_2Cl_4(dppm)_2$ (0.05 g, 0.045 mmol) was dissolved in CH_2Cl_2 containing a twenty-fold molar excess of diphenyl disulfide and irradiated at $\lambda > 435$ nm (16 ± 0.5 °C). The solution was concentrated to 5 mL and the photoproduct was precipitated by adding hexane to the reaction solution. The compound was further purified by chromatography on a Florisil packed column with CH_2Cl_2/CH_3CN as an eluent. FAB/MS displayed a mass ion cluster with a peak at 1246 amu, corresponding to the molecular weight of $Mo_2Cl_5(dppm)_2(SPh)$.

Suitable single crystals of $Mo_2Cl_5(dppm)_2(SPh){\cdot}2C_7H_8$ for X-ray structural determination were obtained by layering a toluene solution of the photoproduct with cyclohexane in a Schlenk tube. The same photoproduct was obtained for an excitation wavelength range of 305 - 435 nm either in CH_2Cl_2 or toluene; only the yield was perturbed by the nature of the solvent (33% for $\lambda > 435$ nm in CH_2Cl_2 and 52% for $\lambda > 335$ nm in toluene). FAB/MS of $Mo_2Cl_5(dppm)_2(SPh)$: 1246 ($[M]^+$); 1211 ($[M-Cl]^+$) and 1137 ($[M-SC_6H_5]^+$) amu. UV-vis for $Mo_2Cl_5(dppm)_2(SPh)$ in CH_2Cl_2: 527 (752), 457 (1120), and 407 nm (898 $M^{-1}cm^{-1}$).

C. Thermal Reactions of $Mo_2Cl_4(dppm)_2$ with PhSSPh[113]

$Mo_2Cl_4(dppm)_2$ (0.06 g, 0.054 mmol) and PhSSPh (0.06 g, 0.28 mmol) were mixed in toluene and rigorously shielded from light. No reaction was observed at room temperature. Under reflux conditions for 12 h, an unidentified orange-brown solid precipitated out of the solution and the product was isolated by washing with hexane to remove excess disulfide. Parent ion clusters at 1263 and 1279 amu in the FAB/MS are consistent with a trinuclear cluster product. UV-vis (CH_2Cl_2): 460 (m) and 375 nm (sh).

D. Photochemistry of $W_2Cl_4(PR_3)_4$ with CH_2Cl_2

Dichloromethane solutions containing 2-4 mgs of $W_2Cl_4(PR_3)_4$ were irradiated at wavelength $\lambda > 375$ nm and the photolysis was monitored by UV-vis spectra. Photolysis was terminated when the near-IR absorption reached a maximum, indicating the formation of the mixed-valence $W_2^{II,III}$ complex (UV-vis(CH_2Cl_2): $\lambda_{abs,max}$ = 1336, 419, 383 and 315 nm for $PR_3 = PMe_3$; $\lambda_{abs,max}$ =

1360, 427, and 344 nm for $PR_3 = PMe_2Ph$; and $\lambda_{abs,max}$ = 1410, 400, and 334 nm for $PR_3 = PBu_3$). The photolyzed solution (1 mL) was transferred to an EPR tube, followed by adding 2-methyl tetrahydrofuran (2-MeTHF) to form a glass at –170 °C and was characterized by EPR ($g_{\parallel}$ = 1.950, 1.950, and 1.941 and $g_{\perp}$ = 1.855, 1.847, and 1.856 for $PR_3 = PMe_3$, PMe_2Ph, PBu_3, respectively). Continued irradiation of the remaining solution led to the disappearance of the near-infrared absorption with the concomitant appearance of an absorption at ~480 nm.

E. Thermal oxidations of $W_2Cl_4(PR_3)_4$ with $PhICl_2$

Thermal oxidations of $W_2Cl_4(PR_3)_4$ were accomplished with $PhICl_2$ or $NOBF_4$. For the former, 0.01 mmol of $PhICl_2$ was added dropwise to an equivalent amount of $W_2Cl_4(PR_3)_4$ in 5 mL of CH_2Cl_2. The color of the solution changed from green to red-brown instantly (UV-vis(CH_2Cl_2): $\lambda_{abs,max}$ = 1340, 469, 428, 376, and 315 nm for $PR_3 = PMe_3$; $\lambda_{abs,max}$ = 1366, and 421 nm for $PR_3 = PMe_2Ph$; and $\lambda_{abs,max}$ = 1415, 507, 439, 403 and 331 nm for $PR_3 = PBu_3$. EPR (CH_2Cl_2/2-MeTHF, –170 °C): $g_{\parallel}$ = 1.952, 1.952 and 1.940 and $g_{\perp}$ = 1.857, 1.854 and 1.852 for $PR_3 = PMe_3$, PMe_2Ph, PBu_3, respectively).

F. Thermal oxidations of $W_2Cl_4(PR_3)_4$ with $NOBF_4$

The oxidation of $W_2Cl_4(PMe_3)_4$ (4 mg) in CH_2Cl_2 was also carried out by dropwise addition of $NOBF_4$ in MeOH. The solution promptly turned from green to yellow-orange, and NO was removed by several freeze-pump-thaw cycles. The compound is extremely air-sensitive, but microcrystalline solid can be obtained by slowly removing solvent (UV-vis(CH_2Cl_2): $\lambda_{abs,max}$ = 1468, 474, and 375; $\lambda_{abs,max}$ = 1505, 497, and 398 nm; and $\lambda_{abs,max}$ = 1514, 483, and 388 nm for $PR_3 = PMe_3$,

I
a
r
t

I

A

s
c
c
s
w
h
v
s
s
c

B

a
p
p
v

PMe_2Ph, PBu_3, respectively. EPR (CH_2Cl_2/2-MeTHF, –170 °C): $g_{\parallel} = 1.980, 1.985$ and 1.980 and $g_{\perp} = 1.840, 1.836$ and 1.834 for $PR_3 = PMe_3$, PMe_2Ph, PBu_3, respectively). When solvent is completely removed, the compound is susceptible to rapid oxidation, and blue tungsten oxo compounds are obtained.

IV. Instrumentation and Methods

A. Absorption Spectroscopy

Absorption spectra were recorded on Cary 17D or Cary 2300 spectrometers. Extinction coefficients were determined by using high-vacuum cells consisting of a 1-cm quartz cuvette and a 10-mL side arm. These two chambers were separated with two Kontes high-vacuum quick-release teflon stopcocks. For measurements of molar absorptivity coefficients, weighed samples were placed in the cuvette and isolated by the Kontes valve. The appropriate high purity solvent was transferred to the 10-mL side arm by bulb-to-bulb vacuum distillation or by syringe from a calibrated volumetric vessel, and three subsequent freeze-pump-thaw cycles were performed before mixing with the sample. Extinction coefficients were calculated from Beer-Lambert plots composed of at least seven points.

B. Photolysis[114]

Sample irradiations for photochemical experiments were executed by using a Hanovia 1000-W Hg/Xe high-pressure lamp. The beam was collimated and passed through a 10-cm circulating water filter. Photolysis experiments were performed in two-arm evacuable cells equipped with Kontes quick-release teflon valves. Solutions were prepared by bulb-to-bulb distillation of solvent on a high-vacuum manifold. Sample temperatures were thermostatted at constant temperature (15.0 ± 0.5 °C) in all photoreactions. Excitation wavelengths in the ultraviolet and visible spectral regions were selected by using colored glass high-energy cutoff filters from Schott. For quantum yield measurements, the excitation wavelength was isolated by using an interference filter purchased from Oriel Corporation with a half-width of less than 10 nm at the given mercury line. Absorption spectra for photolysis and quantum yield experiments were recorded on a Cary 2300 or Cary 17D spectrometer. Quantum yields for dimolybdenum diphenylphosphate photochemistry were determined on 7 M solutions of the dichlorocarbon in benzene by monitoring the disappearance of $Mo_2[O_2P(OC_6H_5)_2]_4$ at 515 nm and appearance of $Mo_2[O_2P(OC_6H_5)_2]_4^+$ at 1494 nm ($\varepsilon = 362\ M^{-1}cm^{-1}$). The absolute quantum yield for photoreduction of 1,2-dichloroethane was measured by using a ferrioxalate actinometer;[115] the quantum yields for reaction of all other halocarbon solutions were measured relative to 1,2-dichloroethane. Quantum yields for the photochemistry of $M_2Cl_4(dppm)_2$ with disulfides were determined on CH_2Cl_2 solutions containing 1.4×10^{-3} M $M_2Cl_4(dppm)_2$ and a twenty-fold excess of diphenyl disulfide. The quantum yield, determined by monitoring the disappearance of the $\delta^2 \rightarrow {}^1\delta\delta^*$ transition of $M_2Cl_4(dppm)_2$, was standardized by using a ferrioxalate actinometer.

C. Mass Spectrometry

C.1 GC/MS

Volatile organic photoproducts were identified by GC/MS on a JEOL JMS-AX505H double focusing MS coupled to a Hewlett-Packard 5890J GC. Separations were achieved on a Poraplot U fused silica capillary column from

Chromp
organic
photoch
temperat
product
ranged f
40 to 1
headspa
O
photorea
GC/TRI
54 supp
(0.32 m
maintain
to 200 °
LMCT
5MS J&
0.25-μm
for 2 mi
spectrom
to 400 m
mL/min.

C.2. FA

Fa
performe

Chrompack (25 m length, 0.32 mm i.d., 10-µm film thickness). For gas phase organic photoproducts obtained from dimolybdenum diphenylphosphate photochemistry, the m/z scans ranged from 15 to 400 and the GC column temperature was programmed from 30 to 200 °C at 10 °C/min. For gas phase products isolated from ditungsten LMCT photoreacted solutions, the scans ranged from 0 to 200 m/z and the GC column temperature was programmed from 40 to 180 °C at 10 °C/min. The volatile sample was introduced from a 2 mL headspace by splitless injection.

Organic liquid products isolated from dimolybdenum diphenylphosphate photoreacted solutions by vacuum distillation were analyzed on a HP 5890 GC/TRIO-1 MS instrument up to masses of one thousand. The column is an SE-54 support-coated open tubular capillary column from Alltech with 30 m length (0.32 mm i.d., 0.25-µm film thickness). The mass spectrometer ion source was maintained at 200 °C, and the GC column temperature was programmed from 35 to 200 °C at 5 °C/min. Organic liquid photoproducts separated from ditungsten LMCT photoreacted solutions by vacuum distillation were analyzed on a DB-5MS J&W fused silica capillary column from Alltech (30 m length, 0.32 mm i.d., 0.25-µm film thickness). The GC column temperature was programmed at 40 °C for 2 min, and then it was ramped from 40 to 200 °C at 10 °C/min. The mass spectrometer ion source was maintained at 280 °C and the scans ranged from 20 to 400 m/z. For both instruments, the helium carrier gas was set at a flow rate of 1 mL/min. 1 µL of liquid sample was employed by splitless injection.

C.2. FAB/MS

Fast atom bombardment mass spectrometric analyses (FAB/MS) were performed on a JEOL HX-110 double focusing mass spectrometer housed in

Nationa

Facility.

instrume

C.3 ES/

E

Finnegar

mobile

vaporiza

Nitrogen

D. Nuc

^{1}H

spectrom

externall

deuterate

under hig

E. Elec

EP

using a X

amplitud

from dir

frequenc

12 GHz c

National Institutes of Health/Michigan State University Mass Spectrometry Facility. Samples were dissolved in 2-(octyloxy)nitrobenzene matrices and the instrument was operated in the positive ion detection mode.

C.3 ES/MS

Electrospray mass spectrometric (ES/MS) analyses were obtained with a Finnegan mat (San Jose, CA) quadrupole mass spectrometer using a CH_3CN mobile phase. A CH_3CN solution of the sample was infused directly into the vaporization nozzle of the electrospray ion source at a flow rate of 3 μL min^{-1}. Nitrogen was used as the nebulizing gas at a pressure of 35 PSI.

D. Nuclear Magnetic Spectroscopy (NMR)

^1H and $^{31}P\{^1H\}$ NMR spectra were obtained on a Varian VXR-300 spectrometer, with the latter experiment recorded at 121.4 MHz and referenced externally to 85% H_3PO_4. Deuterated methylene chloride (Aldrich, 99.6+%) and deuterated chloroform (99.8%, Cambridge Isotope Laboratories) were dried under high vacuum conditions as described in Section A of Chapter II.

E. Electron Paramagnetic Spectroscopy (EPR)

EPR spectra were recorded at –170 °C on a Varian E-4 spectrometer by using a X-band TE 102 cavity with 100 kHz field modulation, a 1.0 G modulation amplitude, and a microwave power of 19.8 mW. The g values were determined from direct measurement of the magnetic field strength and the microwave frequency, which was measured with a Hewlett-Packard 5245 counter/5255 3-12 GHz converter.

F. Ste

E
Michiga
of the di
the ditur
samples
standard
quantum

where x
the avera
corrected
the soluti

G. Tim

Li
instrume
were mad
LASER (
Michigan
and 650
Quanta-R
Quanta-R

F. Steady-State Luminescence Spectroscopy

Emission spectra were recorded on a spectrometer constructed at Michigan State University.[116] The R1104 Hamamatsu PMT was used in the case of the dimolybdenum complexes and the R316 Hamamatsu PMT in the case of the ditungsten complexes. Absolute emission quantum yields of optically dilute samples ($A<0.2$) were measured using $Mo_2Cl_4(PMe_3)_4$ as a quantum yield standard ($\phi_{em} = 0.013$ at $\lambda_{exc} = 585$ nm in 2-methylpentane at 300 K).[117] The quantum yield was calculated from the following equation:[118]

$$\Phi_x = \Phi_r \times \left[\frac{A_r(\lambda_r)}{A_x(\lambda_x)}\right] \times \left[\frac{\eta_x^{\,2}}{\eta_r^{\,2}}\right] \times \left[\frac{D_x}{D_r}\right] \tag{2.1}$$

where x and r designate the unknown and standard solutions, respectively, η is the average refractive index of the solution, D is the integrated area under the corrected emission spectrum, and $A(\lambda)$ is the absorbance per unit length (cm) of the solution at the exciting wavelength λ.

G. Time-Resolved Laser Spectroscopy

Lifetimes were measured on a time-resolved picosecond lifetime instrument.[119] Picosecond and nanosecond transient absorption measurements were made with the pulse-probe technique with instrumentation[120] housed in the LASER (Laser Applications in Science and Engineering Research) Laboratory at Michigan State University. Transient absorption spectra were collected at 355 and 650 nm. The latter excitation wavelength was achieved by pumping a Quanta-Ray PDL-2 dye laser (DCM, Exciton) with the second harmonic of a Quanta-Ray DCR-2A Nd:YAG laser. The transient spectra were collected using a

SPEX 16
elsewher
the Nd:Y
sample c
circumve
Instrume
intensifie
Princeton
allowed
range app

H. Cry

A. Data

X-
$Mo_2Cl_4($
structure
Michigan
performed
The inten
scans at a
counting t
beam coll
crystal pa
Table 4.1
angles, an

SPEX 1680A monochromator and Hamamatsu R928 photomultiplier as described elsewhere.[120] Excitation at 355 nm was provided by third harmonic generation of the Nd:YAG laser. UV excitation led to high background fluorescence of the sample cells, thus precluding the use of the photomultiplier for detection. To circumvent these difficulties, the monochromator and PMT were replaced by an Instruments SA HR-320 spectrograph and Princeton Instruments IRY-1024 intensified photodiode array detector. The intensifier was driven by an EG&G Princeton Applied Research model 1302 fast pulser for 20 ns. This combination allowed the transient absorption measurements to be acquired over a 150 nm range approximately 50 ns after laser excitation.

H. Crystallography

A. Data collection of $Mo_2Cl_4(dppm)_2(\mu\text{-}Cl)(\mu\text{-}SPh)$

X-ray quality crystals were obtained by layering a toluene solution of $Mo_2Cl_4(dppm)_2(\mu\text{-}Cl)(\mu\text{-}SPh)$ with cyclohexane in a Schlenk tube. Crystal structure determinations were performed in the X-ray Crystal Structure Facility at Michigan State University. Preliminary examination and data collection were performed with Mo Kα radiation ($\lambda = 0.71073$ Å) on a Nicolet P3F diffractometer. The intensity data were collected at 202(3)K by using Wyckoff omega(ω) scans at a rate of 4°/min (in ω) to a maximum 2θ of 40°. The ratio of peak counting time to background counting time was 1:1. The diameter of the incident beam collimator was 1.5 mm and the crystal to detector distance was 19 cm. The crystal parameters and details of intensity collection and refinement are listed in Table 4.1, and complete tables of positional parameters, bond distances, bond angles, anisotropic thermal parameters, and structure factors are given in Table 4.2

to Tab

station

penta

dimen

orient

matrix

the se

param

23.88

calcu

sever

with

absen

refine

B. I

not

on t

rang

pola

coef

Inte

ave

inte

to Table 4.4 discussed in Chapter IV. All calculations were performed on a VAX station 3100 computer by using SDP/VAX.[121]

A deep maroon rod-shaped crystal of bis(diphenylphosphinomethane) pentacholro(μ-phenylsulfido) dimolybdenum(III,III) having approximate dimensions of 0.20 × 0.20 × 0.45 mm, was mounted on a glass fiber in a random orientation using Exxon "Paratone-N" oil. Cell constants and an orientation matrix for data collection were obtained from least-squares refinement, by using the setting angles of 25 reflections in the range $15° < 2\theta < 20°$. The monoclinic cell parameters and calculated volume are: a = 15.270(14), b = 17.926(15), c = 23.881(11) Å; β = 92.33(5); V = 6531.5(6)$Å^3$. For Z = 4 and F.W. = 1431.40 the calculated density is 1.46 g/cm^3. As a check on crystal quality, omega scans of several intense reflections were measured; the width at half-height was 0.26° with a take-off angle of 6.0°, indicating good crystal quality. From the systematic absences of h0l (l = 2n) and 0k0 (k = 2n), and from subsequent least-squares refinement, the space group was determined to be P21/C (No. 14).

B. Data Reduction

A total of 6670 reflections were collected, of which 6092 were unique and not systematically absent (R_{MERGE}(I)= 0.007). A linear decay correction, based on three representative reflections, was applied; the correction factors on F ranged from 0.997 to 1.000 with an average value of 0.998. Lorentz and polarization corrections were applied to the data. The linear absorption coefficient is 7.5 cm^{-1} for Mo Kα radiation. No absorption correction was made. Intensities of equivalent reflections were averaged. The agreement factors for the averaging of the 294 observed and accepted reflections was 4.3% based on intensity and 3.0% based on F_o.[122]

C. Structure Solution and Refinement of $Mo_2Cl_4(dppm)_2(\mu$-$Cl)(\mu$-$SPh)$

The structure was solved by using the direct methods program SHELXS86.[123] A total of 22 atoms were located from an E-map; the remaining atoms were located in succeeding difference Fourier syntheses. Hydrogen atoms were refined isotropically and included in the refinement but restrained to ride on the atom to which they are bonded. The structure was refined by full-matrix least-squares where the function minimized was $\Sigma w(|F_o|-|F_c|)^2$ and the weight w is defined as $4F_o^2/\sigma(F_o^2)^2$.

Scattering factors were taken from Cromer and Waber.[124] Anomalous dispersion effects were included in F_c;[125] the values for $\Delta f'$ and $\Delta f''$ were those of Cromer.[126] Only the 3160 reflections having intensities greater than 2.0 times their standard deviation were used in the refinements. The final cycle of refinement, which included 389 variable parameters, converged (largest parameter shift was 0.03 times is esd) with $R = 0.082$ and $R_w = 0.071$. The standard deviation of an observation of unit weight was 1.79. The highest peak in the final difference Fourier had a height of 0.90 e/Å^3 with an estimated error based on σF[127] of 0.19; the minimum negative peak had a height of -0.94 e/Å^3 with an estimated error based on σF of 0.19. Plots of $\Sigma w(|F_o|-|F_c|)^2$ vs. $|Fo|$, reflection order in data collection, $\sin\theta/\lambda$, and various classes of indices showed the 16 "worst" reflections with $|F_o|<<|F_c|$.

1,

T

I. Bac

T

dimers

perform

of the

substrat

aqueous

photopr

oxidized

CHAPTER III

PHOTOREDUCTION OF 1,2-DICHLOROALKANES AND 1,2-DICHLOROALKENES BY TETRAKIS(DIPHENYLPHOSPHATO)DIMOLYBDENUM(II,II)

I. Background

The general class of Mo_2O_8 ($O_8 = (SO_4^{2-})_4$,[128] $(HPO_4^{2-})_4$,[129] $(OH_2)_x$[130] dimers exhibits a rich ultraviolet photochemistry. Most studies have been performed in the presence of reducible substrates and, therefore, photo-oxidation of the metal core typically occurs cleanly with the concomitant reduction of substrate. Ultraviolet irradiation of $Mo_2(SO_4)_4^{4-}$ and $Mo_2(aq)_x^{4+}$ in acidic aqueous solutions photoreduces protons to hydrogen and the corresponding photoproducts of one-electron oxidized species $Mo_2(SO_4)_4^{3-}$, and two-electron oxidized species $Mo_2(\mu\text{-}OH)_2(aq)_x^{4+}$, as described by eqs. 3.1 and 3.2,

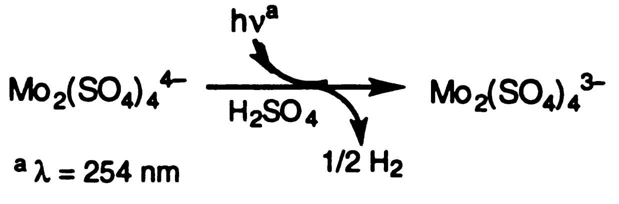

$$\mathrm{Mo_2(SO_4)_4^{4-}} \xrightarrow[\mathrm{H_2SO_4}\ \searrow\ 1/2\,\mathrm{H_2}]{h\nu^{a}} \mathrm{Mo_2(SO_4)_4^{3-}} \qquad (3.1)$$

$^{a}\lambda = 254$ nm

For eq

of acid

irradia

similar

a prim

interm

substa

investi

phosph

tripled

oxidize

a seco

Mo$_2$(H

Mo$_2$

^{a} 40

Carefu

Mo$_2$(H

from th

^{1}($\pi\pi$*

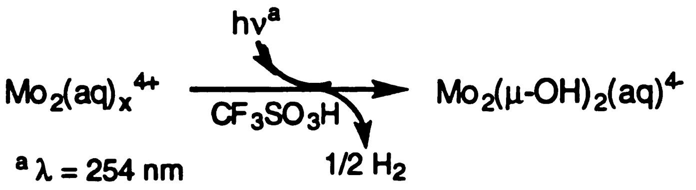

(3.2)

For eq. (3.1), the photoreaction quantum yield of 0.17 at 254 nm is independent of acid concentration from 0.001 to 5.0 M H_2SO_4, but becomes negligible as the irradiation wavelength is extended into the visible. The reaction in eq. (3.2) is similarly efficient ($\phi_p = 0.035$), but it is not known whether the ultimate product is a primary photoproduct or a thermal product of a photochemically generated intermediate.

Insight into the mechanism of Mo_2O_8 photochemistry is provided substantially by the $Mo_2(HPO_4)_4^{n-}$ (n = 2,3,4) system, which has been investigated in detail in our group. Ultraviolet irradiation ($\lambda > 335$ nm) of phosphoric acid solutions of $Mo_2(HPO_4)_4^{4-}$ leads to the production of H_2 and the tripled bond dimer, $Mo_2(HPO_4)_4^{2-}$. Further studies shows the one-electron oxidized complex, $Mo_2(HPO_4)_4^{3-}$, as the primary photoproduct, which undergoes a secondary photolysis to give the two-electron fully oxidized complex $Mo_2(HPO_4)_4^{2-}$,

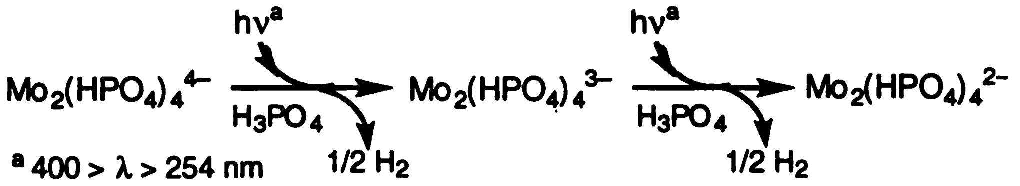

(3.3)

Careful examination of the electronic absorption and action spectra of the $Mo_2(HPO_4)_4^{n-}$ series of complexes reveals that the photochemistry is derived from the $\pi \rightarrow \pi^*$ metal-localized transition. Photoreduction from a high energy $^1(\pi\pi^*)$ excited state conforms well with $Mo_2(SO_4)_4^{4-}$ and $Mo_2(aq)_x^{4+}$

ph
en
an

M
rec
pro
hy
hy

bo
Co
occ
lyi
ina
pro
the
pho
que
pre
proc

stru
Mo
spec
Mo
little

photochemistry described by eqs. (3.1) and (3.2), which also is derived when the energy of irradiation is coincident with the $^1(\pi\pi^*)$ excited state of $Mo_2(SO_4)_4^{4-}$ and $Mo_2(aq)_x^{4+}$ complexes.

Figure 3.1 summarizes the proposed mechanism for the photoprocess of Mo_2O_8 complexes in acidic aqueous solution. Excitation produces the powerfully reducing $^1(\pi\pi^*)$ excited state of Mo_2O_8, which is capable of directly reducing protons to H atoms. Hydrogen production comes from either annihilation of two hydrogen atoms, or sequential oxidation of the Mo_2O_8 starting reactant by a hydrogen atom to yield H^- followed by protonation.

A general to emerge from these photochemical studies is that quadruply bonded Mo_2O_8 systems do not exhibit appreciable lifetimes in acidic solution. Consequently, photoactivation of substrates by $M\overset{4}{-}M$ complexes typically occurs from metal-localized states that are high in energy and not from the low-lying δ^* metal localized excited states.[128,129] One reason for $^1(\delta\delta^*)$ photoinactivity is the propensity of this excited state to be efficiently quenched by protons in acidic aqueous solutions.[131] This suggested to us that the chemistry of the $^1(\delta\delta^*)$ excited state could be exploited by undertaking studies of $Mo_2^{II,II}$ phosphates in aprotic environments, where the energy-wasting, proton-quenching reactions of the $^1(\delta\delta^*)$ excited state would be circumvented thus preserving it for reaction with substrate. In this manner, substrate activation processes of $M\overset{4}{-}M$ species might be achieved with visible light.

On this premise, Dr. I-Jy Chang in our research group synthesized and structurally characterized the dimolybdenum diphenylphosphate, $Mo_2[O_2P(OC_6H_5)_2]_4$. As shown in Figure 3.2, comparison of the absorption spectra of $Mo_2[O_2P(OC_6H_5)_2]_4$ in CH_2Cl_2 and aqueous solutions of $Mo_2(HPO_4)_4^{4-}$ reveals that substitution of HPO_4^{2-} by diphenyl phosphate does little to perturb the electronic structure of the quadruple bonded metal-metal

$Mo_2(HPO_4)_4^{4-}$
H^+
6.0

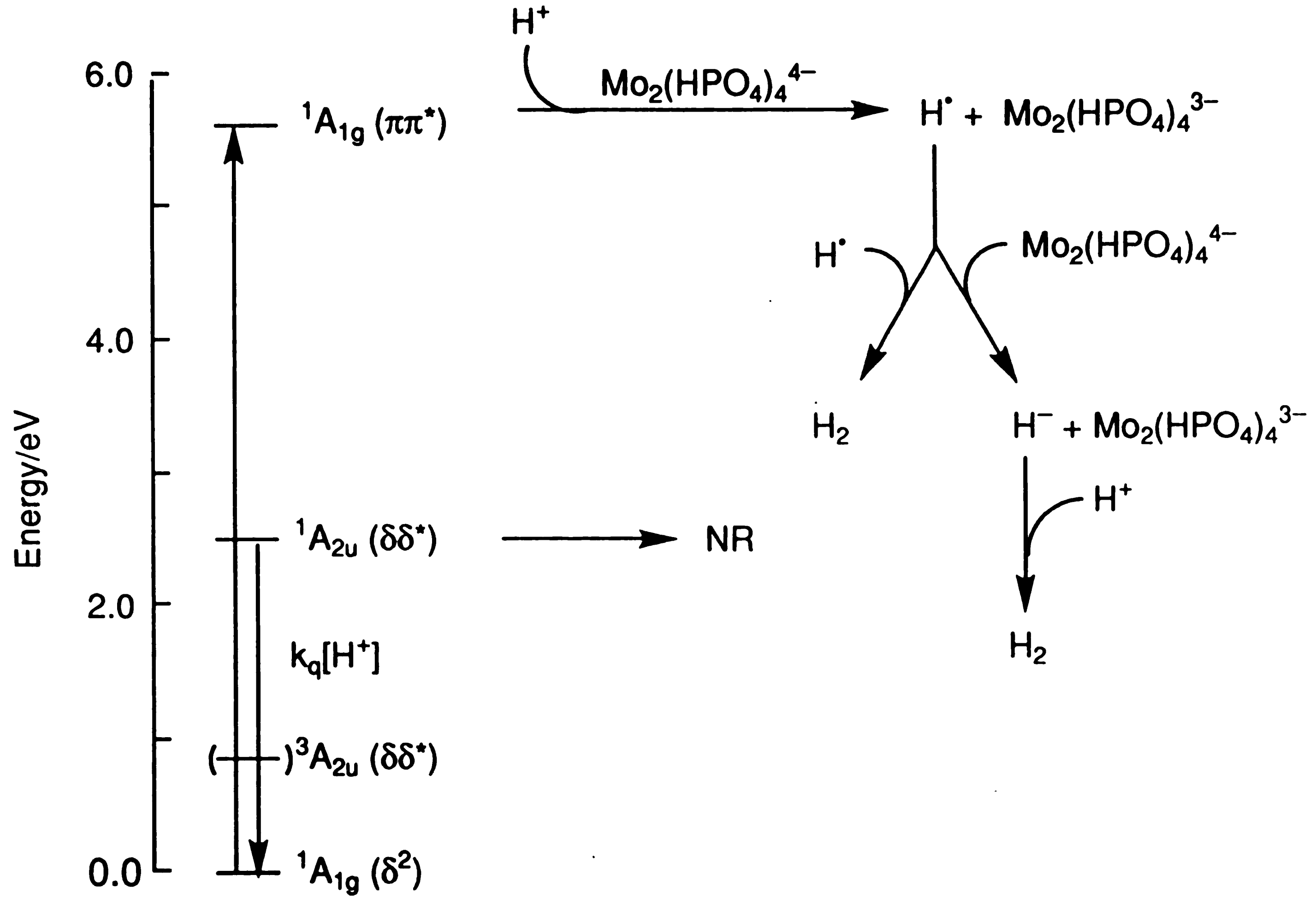

Figure 3.1 Energy level diagram summarizing the mechanism for the photochemistry of the quadruply bonded $Mo_2[HPO_4]_4^{4-}$ in acidic solution.

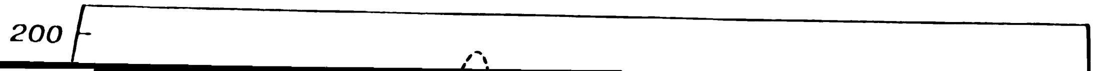
200

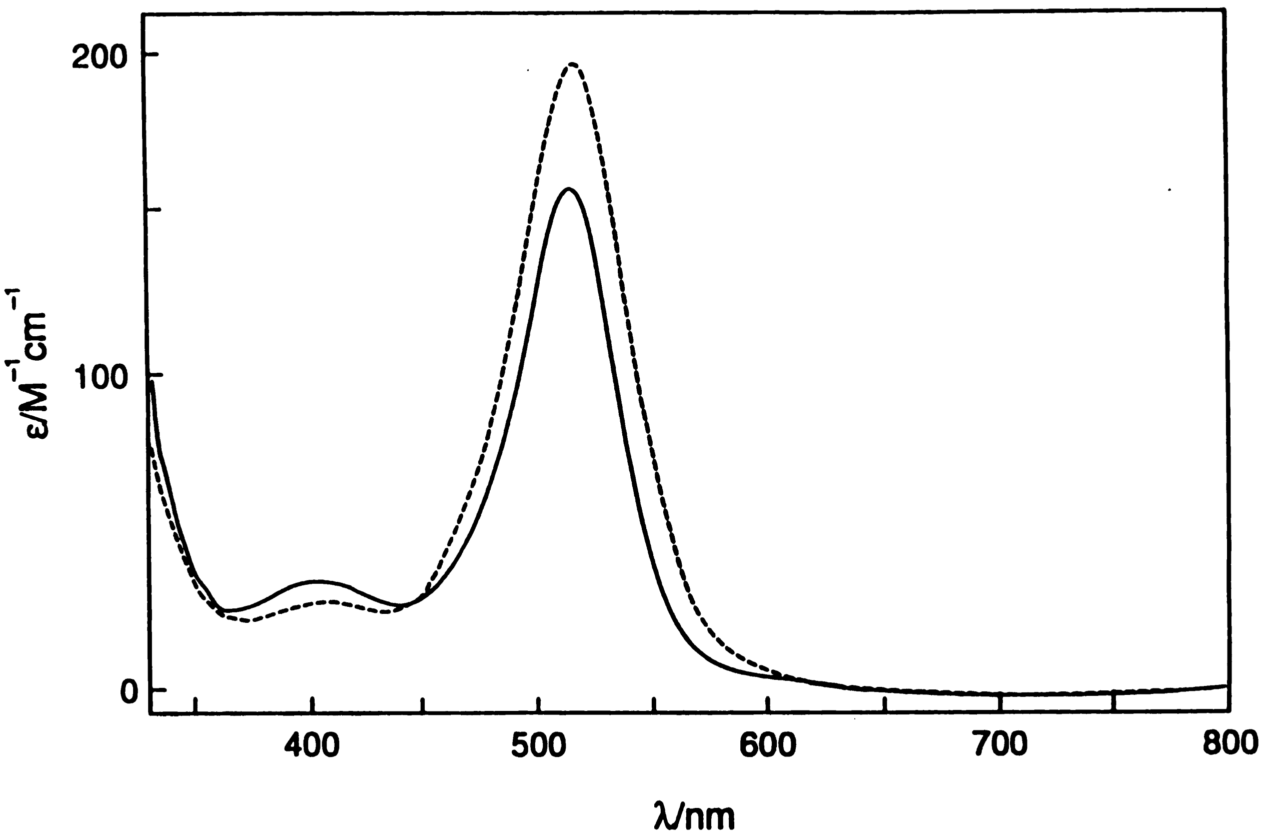

Figure 3.2 Electronic absorption spectra of (a) $Mo_2[O_2P(O_6CH_5)_2]_4$ (—) in CH_2Cl_2 solution and (b) $Mo_2(HPO_4)_4^{4-}$ (– – –) in 2 M H_3PO_4 at 25 °C.

system

compa

, and i

which

spectro

former

solutio

conju

($E_{1/2}$(M

activat

comple

dihaloc

II. Re

A. Pl

indefin

dihalo

wavele

electro

reactio

$2Mo_2$[

system. The lowest energy absorption band (λ_{max} = 515 nm, ε = 156 $M^{-1}cm^{-1}$) is comparable in energy and intensity to the $^1(\delta^2 \rightarrow \delta\delta^*)$ transition of $Mo_2(HPO_4)_4^{4-}$, and is similarly flanked to higher energy by a band at 404 nm (ε = 38 $M^{-1}cm^{-1}$), which has tentatively been assigned to the $\pi \rightarrow \delta^*$ transition. In spite of these spectroscopic similarities between $Mo_2[O_2P(OC_6H_5)_2]_4$ and $Mo_2(HPO_4)_4^{4-}$, the former is distinguished by a weak luminescence ($\phi_{em} \sim 5 \times 10^{-4}$) in nonaqueous solution and a $^1(\delta\delta^*)$ excited state lifetime of 68 ns. This appreciable lifetime, in conjunction with the energy of the $^1(\delta\delta^*)$ excited state ($E_{1/2}(Mo_2[O_2P(OC_6H_5)_2]_4^{+/*})$ = 2.24 eV),[132] engenders the photochemical activation of dichloroethane upon low-energy excitation of the quadruple bond complex. We set out to generalize the chemistry of this system with dihalocarbons, and to provide mechanistic insight into the photoredox process.

II. Results and Discussion

A. Photochemistry

Whereas 1,2-dichloroethane solutions of $Mo_2[O_2P(OC_6H_5)_2]_4$ are indefinitely stable in the absence of light, we have observed prompt reaction of dihalocarbon solutions of $Mo_2[O_2P(OC_6H_5)_2]_4$ upon visible irradiation with wavelengths of light energetically coincident with the $\delta\delta^*$ transition. The two-electron conversion of 1,2-dichloroethane to ethylene occurs by the following reaction,[133]

$$2Mo_2[O_2P(OC_6H_5)_2]_4 + ClCH_2CH_2Cl \xrightarrow{h\nu} 2Mo_2[O_2P(OC_6H_5)_2]_4Cl + CH_2CH_2 \qquad (3.4)$$

The $Mo_2[O_2P(OC_6H_5)_2]_4$ dimer also reacts with other 1,2-dihalocarbons including 1,2-dichlorocyclohexane (DCC), cis-1,2-dichloroethylene (DCEE), and o-dichlorobenzene (DCB). Figure 3.3 shows an example of the spectral change of the $Mo_2[O_2P(OC_6H_5)_2]_4$ photochemistry in DCEE. Irradiation at $\lambda > 495$ nm causes the disappearance of the $^1(\delta\delta^*)$ absorption band at 515 nm and an increase of absorption in the near-infrared spectral region. Isosbestic points are observed in the visible region during the initial stages of photolysis. The appearance of a vibrationally structured absorption in the near-IR region (λ_{max} = 1494 nm, $\varepsilon = 362\ M^{-1}cm^{-1}$) is consistent with the production of a mixed-valence $Mo_2^{II,III}$ complex, $Mo_2[O_2P(OC_6H_5)_2]_4Cl$, which has been identified by FAB/MS.[133] The absorption bands of the $Mo_2^{II,III}$ photoproduct at 600 nm and 1494 nm are comparable in energy and intensity to the corresponding $^2(\pi \rightarrow \delta)$ and $^2(\delta \rightarrow \delta^*)$ transitions of $Mo_2[O_2P(OC_6H_5)_2]_4BF_4$,[128,134] which has been structurally and spectroscopically characterized.[135] A red shift in the $^2(\delta \rightarrow \delta^*)$ absorption band with respect to the BF_4^- salt is attributed to the presence of chloride ion in photolyzed solutions.[135] The 308 cm^{-1} progression on the the near-IR $^2(\delta \rightarrow \delta^*)$ transition of the $Mo_2^{II,III}$ complex conforms well with the symmetric metal-metal stretching vibration. As with dimolybdenum phosphate and sulfate,[136] the large red-shift of the $^2(\delta \rightarrow \delta^*)$ transition is not due to a lengthening of the Mo—Mo bond length, which increases by only 0.05 Å upon one-electron oxidation of the metal-metal core (2.141 Å and 2.191 Å for quadruple bond and mixed-valence complexes, respectively).[137] Rather, the shift is explained by the absence of two electron spin pairing terms for a $\sigma^2\pi^4\delta^1$ ground state configuration shown in Figure 3.4.[96] This spectral shift is also observed in the mixed-valence dimolybdenum sulfate system.

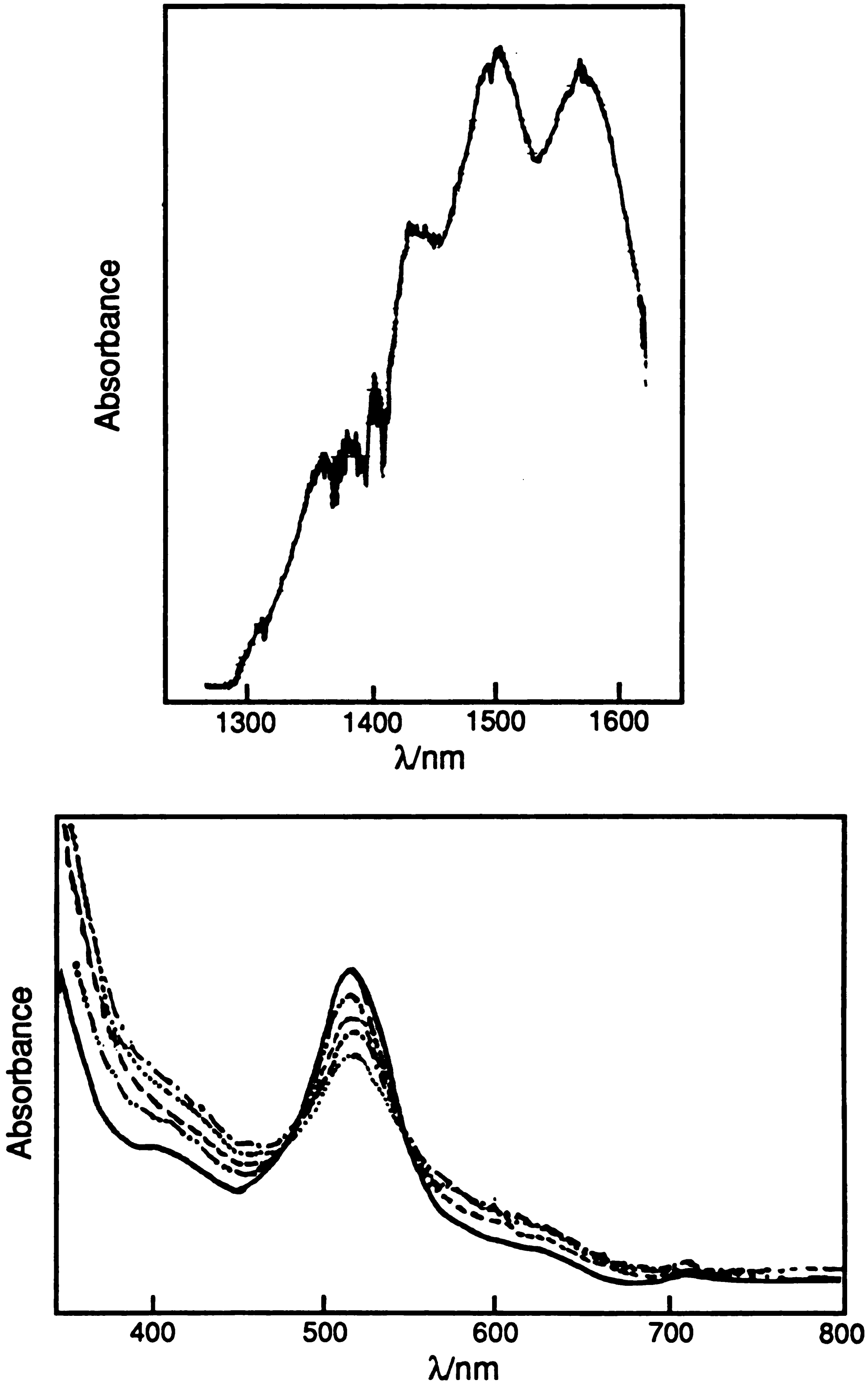

Figure 3.3 Spectral changes resulting from the photolysis ($\lambda > 495$ nm) of $C_2H_2Cl_2$ solution of $Mo_2[O_2P(O_6CH_5)_2]_4$.

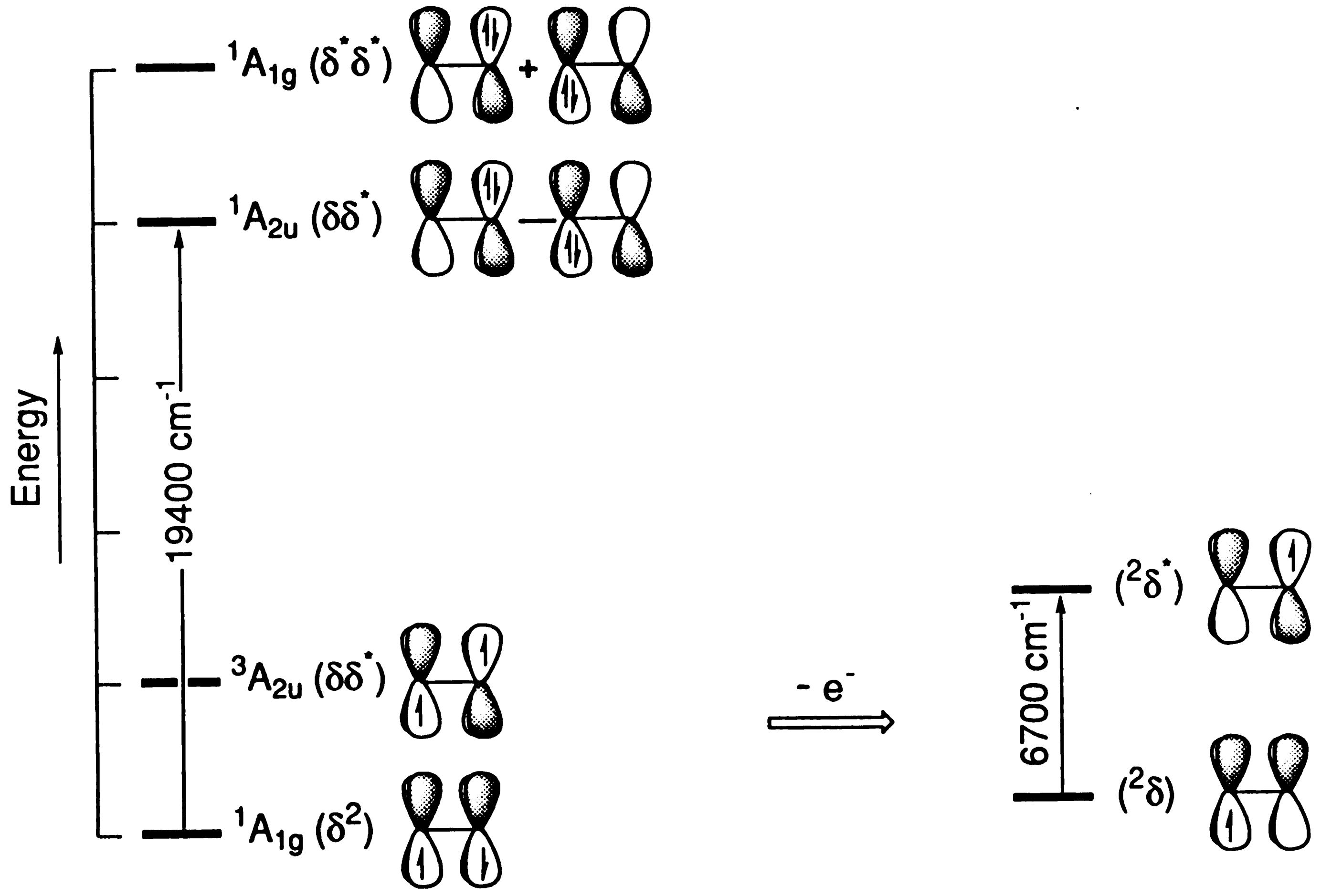

Figure 3.4 Valence bond description of the electronic states formed by the d_{xy} orbitals with the corresponding MO formalism (left). With the removal of one electron, a transition of doublet states is observed (right).

With respect to the organic photoproducts, the DCC and DCE photochemistry is analogous inasmuch as GC/MS shows the exclusive production of the unsaturated olefin (Figure 3.5: cyclohexene, $[M]^+ = 82$ m/z, $([M] - CH_3)^+ = 67$ m/z, $([M] - C_2H_4)^+ = 54$ m/z, $([M] - C_3H_3)^+ = 41$ m/z and $([M] - C_3H_5)^+ = 39$ m/z).[138] However, when the substrate is an unsaturated dichlorocarbon the organic photoproduct is not the olefinic hydrocarbon. Consider the photochemistry of DCB. Elimination of chlorine from DCB would result in benzyne, which is efficiently trapped by furan to yield α-naphthol. Yet when $Mo_2[O_2P(OC_6H_5)_2]_4$ is irradiated in the presence of DCB and furan, α-naphthol is not detected; GC/MS reveals chlorobenzene as the principal photoproduct (Figure 3.6a). In addition to chlorobenzene, a high boiling fraction is also isolated from the photoreaction mixture; its GC/MS (Figure 3.6b) shows it to be primarily tri-chlorobiphenyl. The photoproduction of mono-chlorinated product is consistent with chlorine abstraction by the photoexcited quadruply bonded species, but subsequent elimination of chlorine from the incipient chlorobenzyl radical does not occur. The appearance of polychlorinated biphenyls is consistent with initial chlorine atom abstraction owing to the known reaction of the chlorobenzyl radical with DCB,[139]

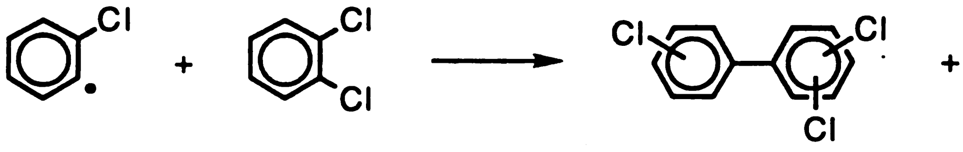

(3.5)

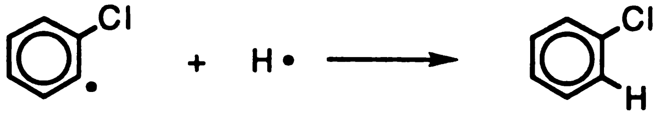

(3.6)

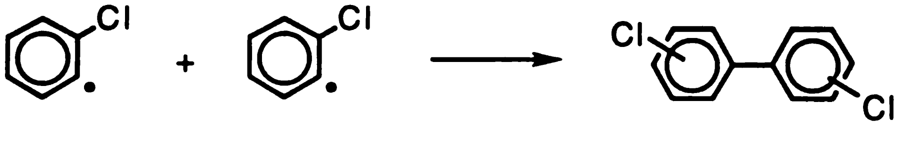

(3.7)

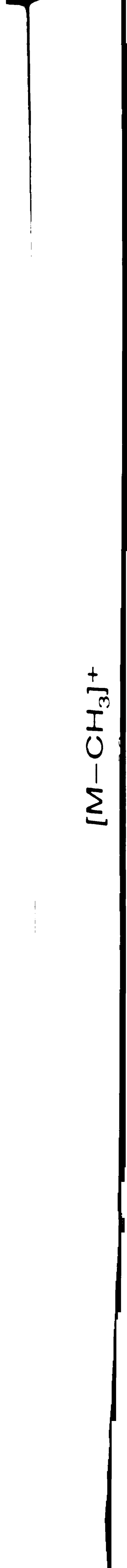
[M−CH3]+

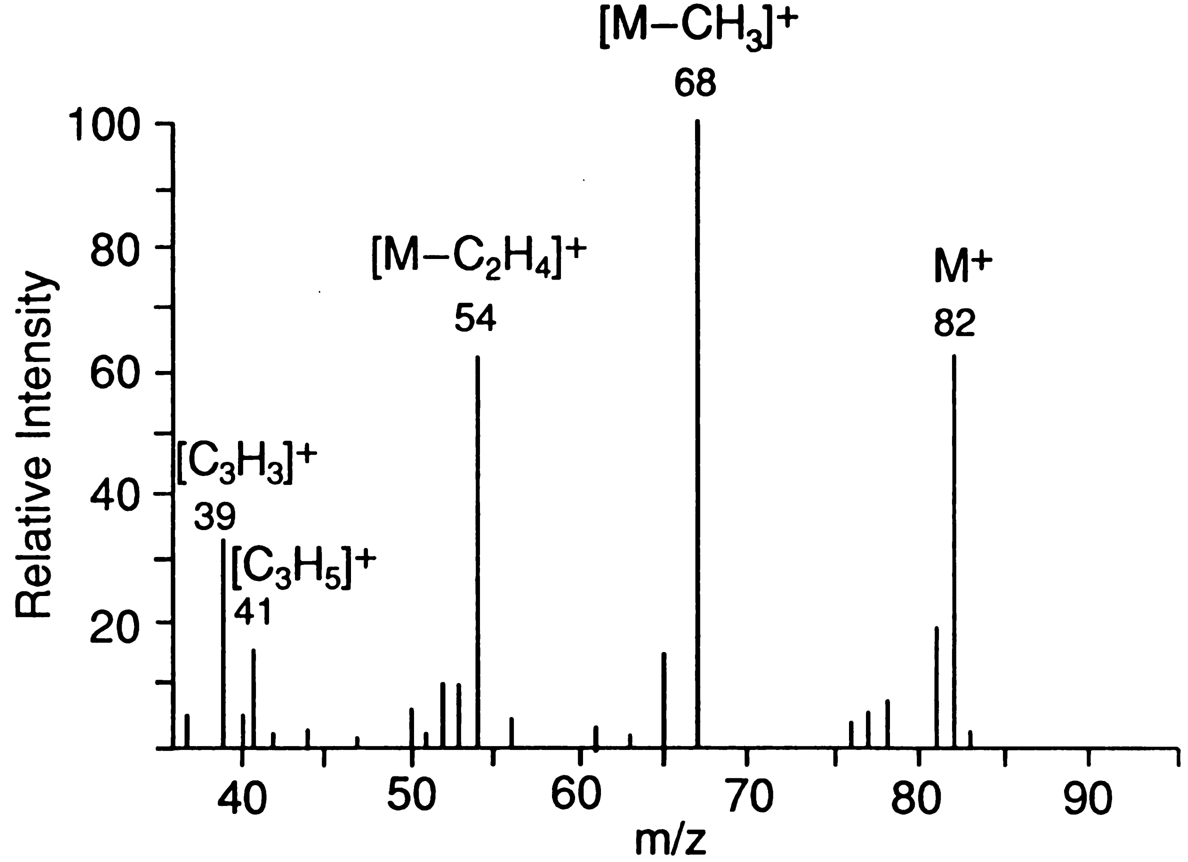

Figure 3.5 Mass spectra of the organic products resulting from the photoreaction of trans-dichlorocyclohexane and $Mo_2[O_2P(OC_6H_5)_2]_4$ with cyclohexene obtained as the photoproduct. [M]+ denotes parent ion peak mass fragment.

Fi
ph
(a
(b

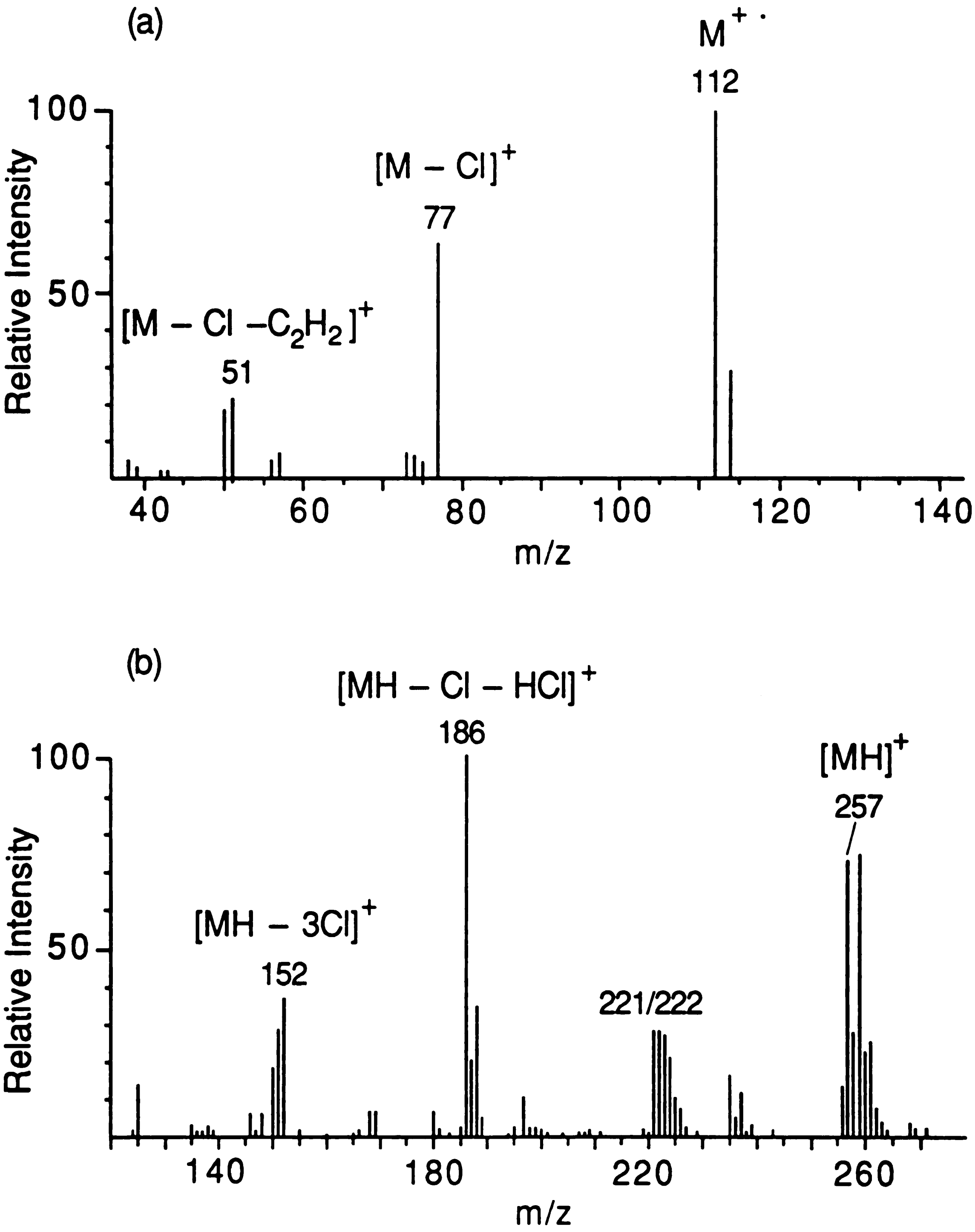

Figure 3.6 Mass spectra of the organic products resulting from the photoreaction of o-dichlorobenzene and $Mo_2[O_2P(OC_6H_5)_2]_4$ with (a) chlorobenzene obtained as the primary product and (b) tri-chlorobiphenyl obtained as a secondary product in ~3% yield.

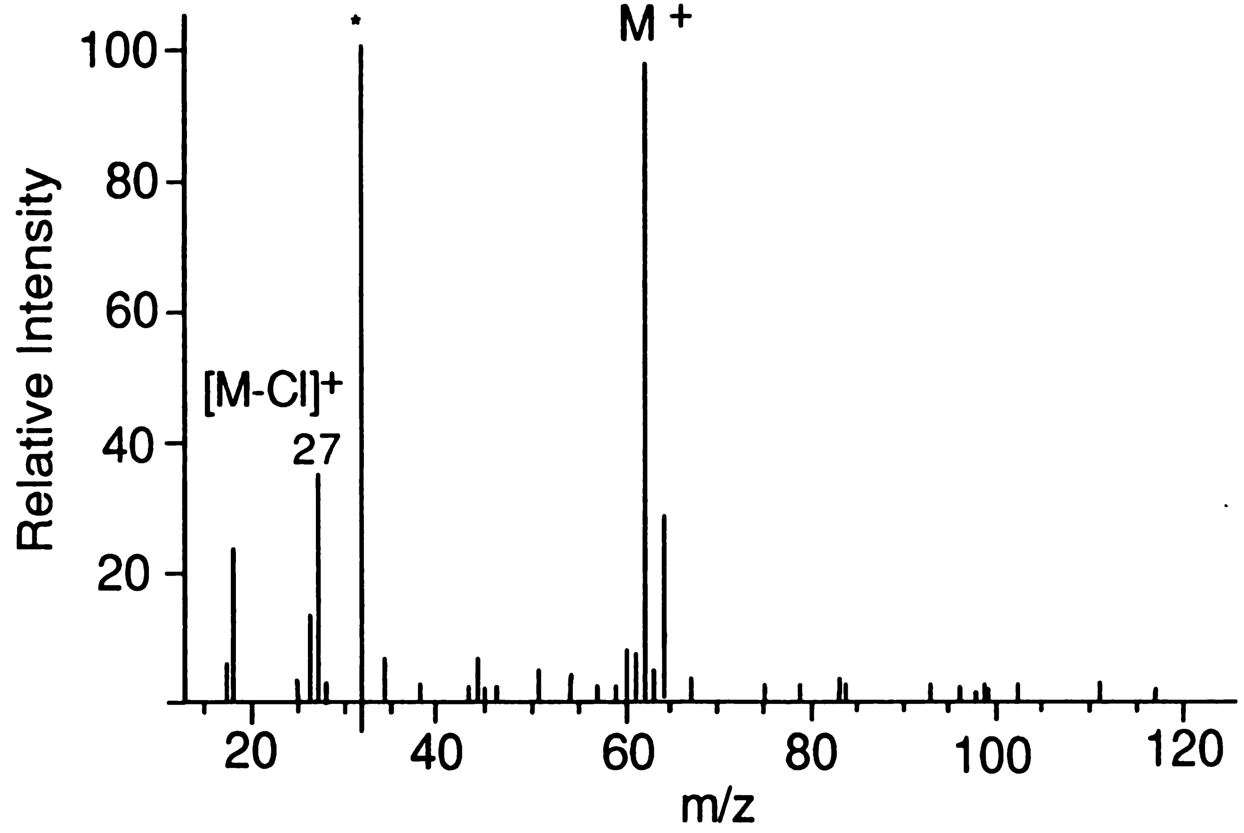

Figure 3.7 Mass spectra of the organic products resulting from the photoreaction of cis-dichloroethylene and $Mo_2[O_2P(OC_6H_5)_2]_4$ with chloroethylene obtained a the photoproduct. The star mark * indicates the presence of O_2 as a background from the air.

The pl

with t

chloroc

summa

Mo$_2$[C

saturat

monoh

species

comple

the tri

rationa

the r

Mo$_2$[C

reduc

Mo$_2^{II,I}$

much

~1.0 V

The photoreactivity $Mo_2[O_2P(OC_6H_5)_2]_4$ with DCEE is similar to that of DCB with the monohalohgenated olefin observed as the photoproduct (Figure 3.7: chloroethylene, $[M]^+ = 62$ m/z; $([M] - Cl)^+ = 27$ m/z).

The general result to emerge from our product distribution studies is summarized by eqs. 3.8 and 3.9. Initial chlorine abstraction by photoexcited $Mo_2[O_2P(OC_6H_5)_2]_4$ leads to the olefinic hydrocarbon when the substrate is a saturated dichlorocarbon whereas unsaturated dihalocarbons react to produce monohalogenated olefin.

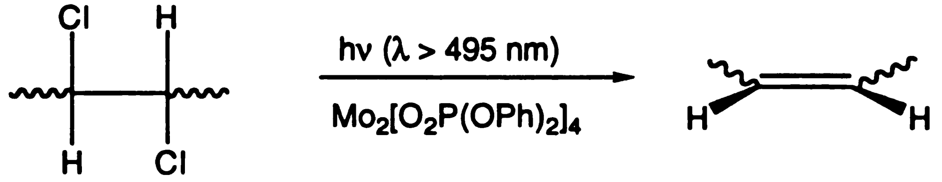

(3.8)

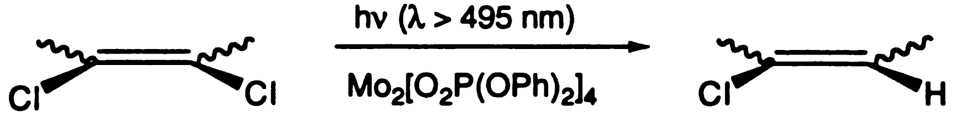

(3.9)

In both cases, the inorganic photoproduct is the mixed-valence $Mo_2^{II,III}$ species; the photoreaction terminates at the one-electron oxidized $Mo_2^{II,III}$ metal complex rather than fully oxidized $Mo_2^{III,III}$ species. The difficulty in obtaining the triply bonded dimolybdenyum sulfate and diphenylphosphate systems can be rationalized on the basis of the oxidation-reduction chemistry. Table 3.1 collects the reduction potentials for $Mo_2(SO_4)_4^{4-}$, $Mo_2(HPO_4)_4^{4-}$, and $Mo_2[O_2P(OC_6H_5)_2]_4$.[129,136] As compared with previously reported oxidation-reduction properties of multiply bonded "Mo_2O_8" complexes, the $Mo_2^{II,III}/Mo_2^{II,II}$ reduction potentials of the sulfate and diphenylphosphate are much the same, and significantly positive to that for the phosphate compound by ~1.0 V shift, in spite of the structural and electronic similarities among HPO_4^{2-},

SO_4^{2-} and $O_2P(OR)_2^-$ ligands. The HPO_4^{2-} is distinguished from $O_2P(OR)_2^-$ and SO_4^{2-} by its chemical properties. An equilibrium with protons of the phosphate ligand can be established in aqueous solution,[129] whereas the SO_4^{2-} and $O_2P(OR)_2^-$ ligands are not affected by proton association. Consequently, the inability to generate the triply bonded sulfate complex is not due to the intrinsic instability of this species, but rather because the reduction potential for the generation of the triply bonded complex lies positive of the potential for water oxidation. Similarly, attempts to prepare the triply bonded dimolybdenum diphenylphosphate are also frustrated by the very positive $Mo_2^{III,III}/Mo_2^{II,III}$ couple. Although oxidation of the quadruple bond complex by $NOBF_4$ proceeds smoothly to the $Mo_2[O_2P(OC_6H_5)_2]_4^+$, subsequent oxidation to $Mo_2[O_2P(OC_6H_5)_2]_4^{2+}$ can not be achieved by $NOBF_4$ (the NO^+/NO couple is estimated to be ~0.85 to 1.0 V vs. SCE in nonaqueous solution[135]), not even by stronger one-electron oxidants, such as tris(4-bromophenyl)aminium hexachloroantimonate ($E_{1/2}$ = 1.04 V vs. SCE) or dichloroiodobenzene (estimated 0.9 to 1.2 V vs. SCE). This may be a result from kinetic barriers for generating the dication that cannot be overcome by carrying out the reaction at elevated temperatures owing to decomposition of the mixed-valence dimer upon heating. Alternatively, electrochemical methods may offer the triply bonded dication species. Bulk electrolysis of solution by holding the potential of platinum electrodes at potentials as high as 1.7 V vs. SCE led to the disappearance of the near-infrared absorption of the mixed-valence dimer and the appearance of weak absorptions in the visible.[135] Although the species in solution failed to crystallize, the spectral changes accompanying bulk electrolysis are consistent with the formation of the triply bonded dimer, and we suspect that the electrochemical preparation of this triply bonded species is plausible.

Tabl

Mo_2(

Phosp

D

[a] refere

Table 3.1 Formal Reduction Potentials of the Mo_2(II,III)/(II,II) and Mo_2(III,III)/(II,III) Couples of Dimolybdenum *Tetrakis* Sulfate, Phosphate, and Diphenylphosphate Complexes

Complex	$E_{1/2}$/V vs SCE Mo_2(II,III)/(II,II)	$E_{1/2}$/V vs SCE Mo_2(III,III)/(II,III)
Sulfate	+0.25[a]	~1.20[d]
Phosphate	−0.67[b]	−0.24[b]
Diphenylphosphate	+0.06[c]	+1.00[c]

[a] reference 136. [b] reference 129. [c] ref 135 [d] Estimated see c for reference

B. Q

organi
selecte
consis
dihalo
dihalo
less th
barrie
unsatu

Mo_2[
quantu
ability
transit
transfe
metal
coordi
likely
electro
the cr
Figure
Mo_2[C
Inspec
insula

B. Quantum Yields

Table 3.2 summarizes the organic reactants, the corresponding principle organic photoproducts and the quantum yields of the photoreaction for the selected substrates with $Mo_2[O_2P(OC_6H_5)_2]_4$. The quantum yield studies are consistent with the nature of the organic photoproducts. For saturated dihalocarbons, the quantum yield falls in the range of 0.04. For unsaturated dihalocarbons, the quantum yields drops off dramatically to 10^{-2} to 10^{-4} times less than that of saturated dihalocarbons. This may be due to the greater kinetic barrier for breaking the more thermodynamically stable C—Cl bond of the unsaturated halocarbon.

The quantum yields for photoreduction of dihalocarbons by $Mo_2[O_2P(OC_6H_5)_2]_4$ is also solvent dependent. As shown in Table 3.2, the quantum yields for photoreaction decrease dramatically with the increasing ability of solvent to ligate the metal core. The reduction of alkyl halides by transition metal donors can occur by outer-sphere[140] or inner-sphere electron transfer pathways,[140d,e,141] with the latter being especially important for transition metal reductants featuring open coordination sites. In view of the vacant axial coordination sites of the metal-metal core, an inner-sphere reaction pathway is likely to play a significant role in the photoreduction of alkyl halides by the electronically excited $Mo_2^{II,II}$ diphenylphosphate complex. In the case of THF, the crystal structure of $Mo_2[O_2P(OC_6H_5)_2]_4 \cdot 2THF$[142] supports this contention. Figure 3.8a shows the space filling computer generated model of $Mo_2[O_2P(OC_6H_5)_2]_4 \cdot 2THF$, situated just off-axis of its metal-metal bond.[131] Inspection of the model reveals that the ligating solvent molecules completely insulate the metal-metal core from substrate. Alternatively, with the solvent

Tab

Mo

Solv

[a]Qua

with

Conce

Table 3.2 Quantum Yield Data for the Photoreaction between $Mo_2[O_2P(OC_6H_5)_2]_4$ and 1,2-Dichlorocarbon in Various Nonaqueous Solvents.

1,2-Dichlorocarbon	Solvent	ϕ_p[a]
1,2-dichloroethane	C_6H_6	0.029
1,2-dichloroethane	THF	0.014
1,2-dichloroethane	CH_3CN	0.0012
1,2-dichlorocyclohexane	C_6H_6	0.040
1,2-dichloroethylene	C_6H_6	5.5×10^{-6}
o-dichlorobenzene	C_6H_6	1.4×10^{-4}

[a] Quantum yield for the photoreaction (λ_{exc} = 546 nm) of $Mo_2[O_2P(OC_6H_5)_2]_4$ with dichlorocarbon as determined by using a ferrioxalate actinometer. Concentration of chlorocarbon is 7 M.

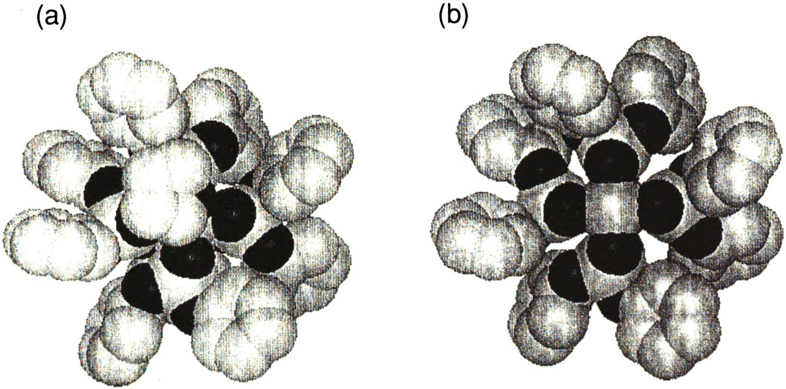

Figure 3.8 Computer generated space-filling models of (a) $Mo_2[O_2P(OC_6H_5)_2]_4$ •2THF and (b) $Mo_2[O_2P(OC_6H_5)_2]_4$.

remo

show

Mo_2[

phot

THF.

attac

show

C.

with

phot

exci

Chlo

prod

Mo_2

equi

phot

spec

removed, the metal-metal core is clearly visible to axially approaching substrates shown in Figure 3.8b. Consequently, the photoreduction of DCE by $Mo_2[O_2P(OC_6H_5)_2]_4$ is severely impeded. Therefore, the quantum yield for the photoreduction of DCE by $Mo_2[O_2P(OC_6H_5)_2]_4$ is significantly diminished in THF. These data suggest that the photoreaction is confined predominantly to attack by substrate at the axial coordination site of the metal-metal core as shown in eq. (3.10),

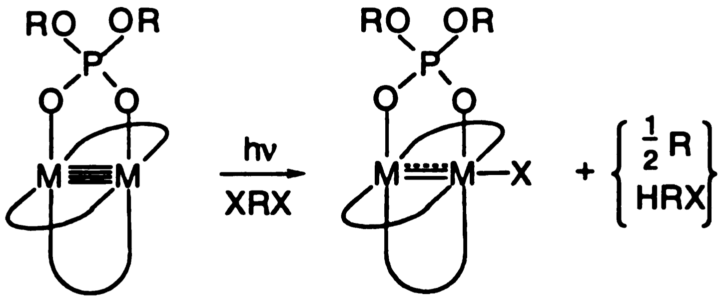

(3.10)

C. Mechanism

The mechanism for the reduction of saturated dihalocarbons is consistent with the reaction pathways shown in Figure 3.9. In contrast to the $Mo_2(HPO_4)_4{}^{4-}$ photochemical scheme of Figure 3.1, the visible photoreaction from the $\delta\delta^*$ excited state of $Mo_2[O_2P(OC_6H_5)_2]_4$ is observed in nonaqueous solutions. Chlorine abstraction by the electronically excited $Mo_2[O_2P(OC_6H_5)_2]_4$ complex produces ~•CHCHCl~ and the mixed-valence $Mo_2{}^{II,III}$ complex, $Mo_2[O_2P(OC_6H_5)_2]_4Cl$. Subsequent reaction of the radical with another equivalent of the $Mo_2{}^{II,II}$ reactant, which is in excess, directly yields the observed photoproducts. The photogenerated chloroalkane radical is a very reactive species. It can either react within or external to the solvent cage of the primary


6.0
¹A₁g (ππ*)

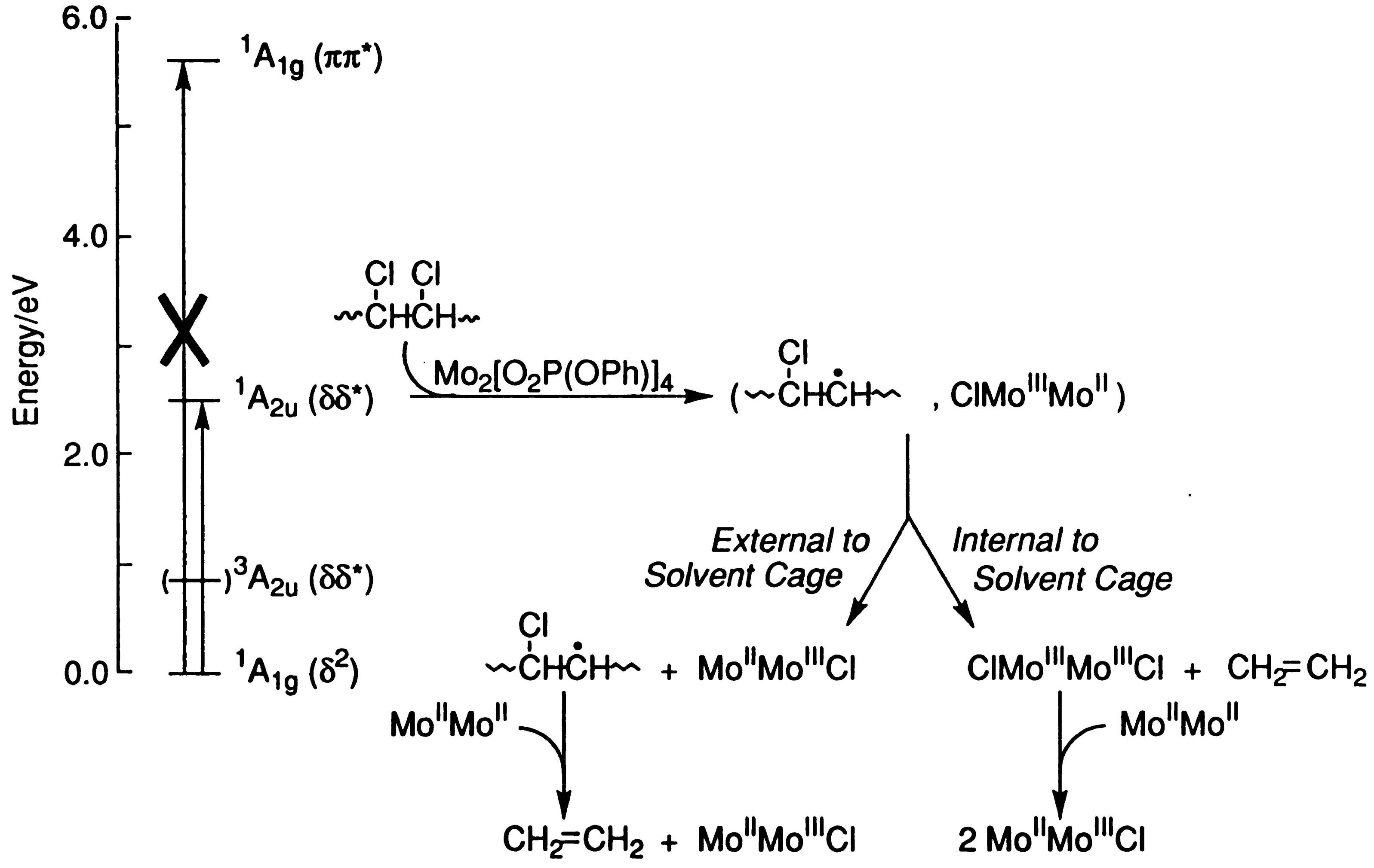

Figure 3.9 Energy level diagram summarizing the mechanism for the photochemical reduction of saturated 1,2-dichlorocarbons by $Mo_2[O_2P(OC_6H_5)_2]_4$.

pho
prin
bon
that
the
also
mix
Mo
Mo
Mo
then
stoic

diha
phot
quac
elim
appa
to re
solv
chlo
star
ator
the
pol
and
abs

photoproducts. When the photogenerated radical escapes the solvent cage of the primary photoproducts, its thermodynamically favorable reaction with quadruply bonded $Mo_2^{II,II}$ species yields ethylene or cyclohexene.[133] It should be noted that the dissociation of chloroalkane radicals to give $^\bullet Cl$ and olefins has a rate in the range of 10^7 sec^{-1};[143] thus, this pathway resulting in the olefin formation is also possible. Alternatively, if the organic radical intermediate is scavenged by the mixed-valence complex inside the solvent cage, then the fully oxidized $Mo_2^{III,III}Cl_2$ complex is produced. Based on the energetics of the $Mo_2^{II,II}/Mo_2^{II,III}$ and $Mo_2^{II,III}/Mo_2^{III,III}$ couples, $Mo_2^{III,III}Cl_2$ and unreacted $Mo_2^{II,II}$ diphenylphosphate can undergo comproportionation to give the thermodynamically favored $Mo_2^{II,III}Cl$ mixed-valence species. Thus, the overall stoichiometry of the photoreaction is independent of these two pathways.

A mechanism that accounts for the photochemistry of unsaturated dihalocarbons is illustrated in Figure 3.10. The presence of the monochlorinated photoproduct indicates that the chlorine atom abstraction by the photoexcited quadruply bonded species is also a primary photoprocess, but subsequent elimination of chlorine from the unsaturated chlorocarbon radicals does not apparently happen. The photogenerated vinylic and benzylic radicals are stable to reduction. They can abstract a hydrogen atom from either another substrate or solvent molecule to produce the monohalogenated olefin. Alternatively, a chloroalkene radical $\sim {}^\bullet C{=}CCl$ may undergo electron transfer with the $Mo_2^{II,II}$ starting reagent to produce a carbanion followed by protonation. If the hydrogen atom abstraction to produce the monohalogenated olefin dominates the reaction, the radical can go on to react with olefin starting material to produce polyaromatic halocarbons. However, this reaction occurs in small yields (<3%) and appears to be an insignificant side reaction. Therefore, hydrogen atom abstraction may not be indicative of the primary reaction pathway.


6.0
$^1A_{1g}$ ($\pi\pi^*$)

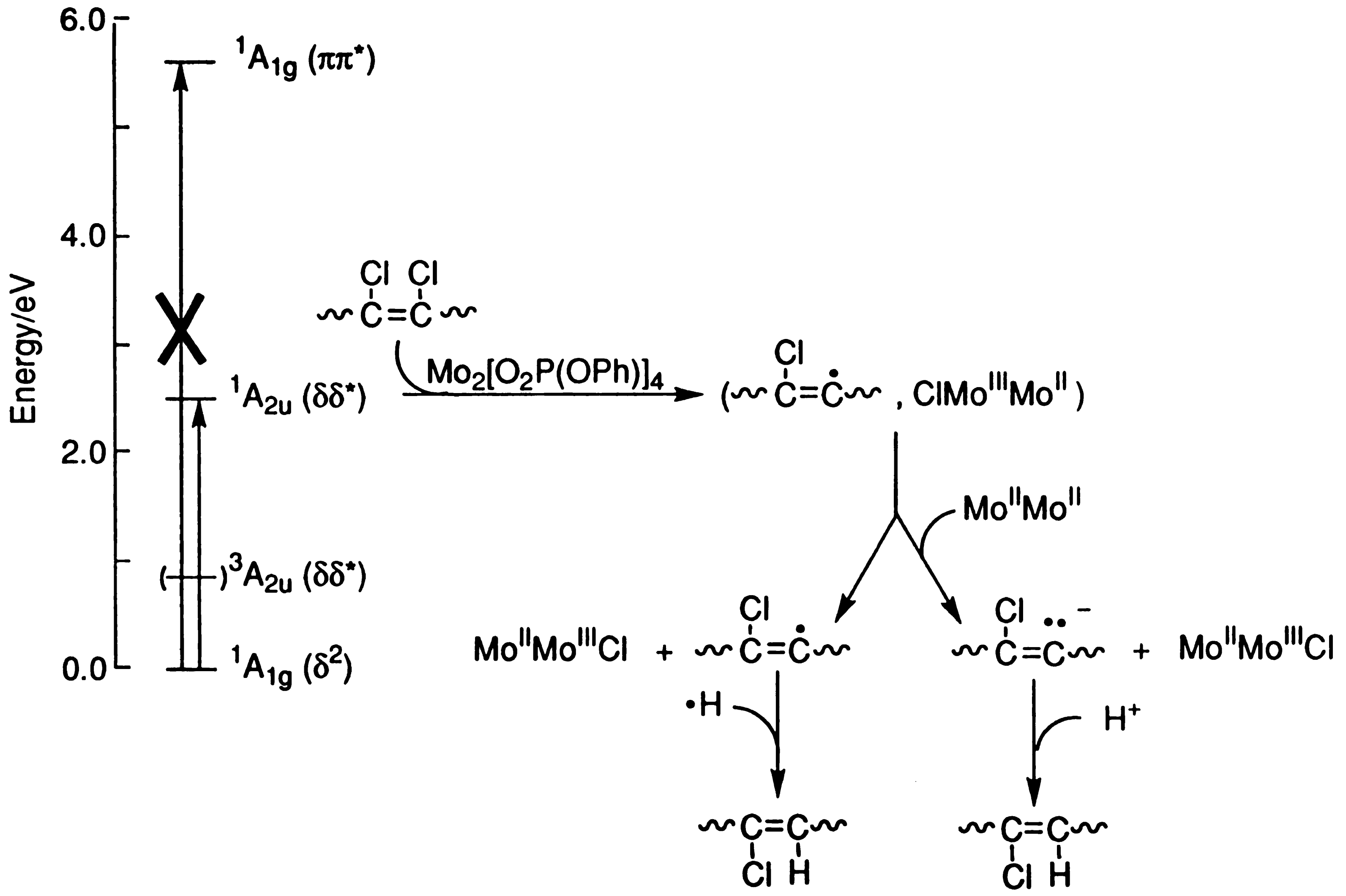

Figure 3.10 Energy level diagram summarizing the mechanism for the photochemical reduction of unsaturated 1,2-dichlorocarbons by $Mo_2[O_2P(OC_6H_5)_2]_4$.

On the other hand, if the carbanion is the important intermediate, then it is conceivable that the production of the radical is circumvented and the carbanion is produced directly. It should be noted that the photoreduction of dichlorocarbons by $Mo_2[O_2P(OC_6H_5)_2]_4$ can be correlated with the general reaction chemistry observed in the electroreduction of 1,2-dihaloalkanes and 1,2-dihaloalkenes.[144] For instance, the early studies of von Stackelburg and Stracke established that the electroreduction of 1,2-dihalides afforded olefinic hydrocarbons.[145] Reductions of 1,2-dihalobenzenes may take place via a carbanion, which is then trapped by a proton to produce the monosubstituted halo-benzenes.[146] Also, the two-electron electrochemical reduction of cis-2,3-dichloroacrylonitrile to 2-chloroacyrlonitrile is believed to occur via the carbanion.[147] Recently, aromatic and vinylic dibromides have been shown to react with low valent metallo-porphyrins by X^+ atom departure to produce a carbanion.[140c] This E2 mechanism presumably is preferred owing to the presence of the π^* orbital. This observation implies that the first halogen is eliminated as a cation and the carbanion is produced directly. However, in this case, the direct production of the carbanion may be precluded by the high potential for production of $Mo_2^{III,III}$, which is necessary for direct X^+ transfer. Alternatively, a carbanion may be produced by electron transfer of the chloroalkene radical $\sim\!{}^{\bullet}C{=}CCl\!\sim$ with the $Mo_2^{II,II}$ starting reagent. In either case, the monohalogenated product is obtained by protonation of the carbanion.

While the above studies paint a general picture as to the mechanism of dihalocarbon reductions by $Mo_2[O_2P(OC_6H_5)_2]_4$, a more precise mechanism for the photoreduction of aromatic and vinylic dihalides should be garnered when quantum yields are measured (if the reaction of the primary photoproduct is rate determining) and H/D isotope studies are performed for photoreactions carried out in the presence of proton donors and radical scavengers.

I

I. B

photo

the p

surro

bider

photo

from

react

pathv

coord

Mo$_2$

Mo$_2$

oxid

redu

of th

obtai

CHAPTER IV

PHOTOREDUCTION OF DIARYL DISULFIDES BY QUADRUPLY BONDED DIMOLYBDENUM AND DITUNGSTEN COMPLEXES

I. Background

The M_2O_8 studies of Chapter III indicate that two-electron photoprocesses to be exceptional reaction pathways and the precise nature of the photooxidation product depends intimately on the coordination environment surrounding the bimetallic core.[148] When the metal core is strapped by four bidentate ligands (D_{4h}), d^3—d^4 mixed-valence species are the common photoproduct. Although the photoactivation range of $M\overset{4}{-}M$ dimers has moved from UV to visible in the Mo_2 diphenylphosphate system, the excited-state reaction chemistry is still limited primarily to sequential single electron transfer pathway. The structural inflexibility of the four bidentate ligands renders the coordination sphere incapable of accommodating the increased charge of a $Mo_2^{III,III}$ core and hence the reaction terminates at the one-electron oxidized $Mo_2^{II,III}$ metal complex. As we have discussed in Chapter III, a two-electron oxidized photoproduct may be accessed if the bimetallic core is made more reducing. Substitution of $O_2P(OR)_2^-$ by HPO_4^{2-} increases the reduction potential of the dimolybdenum core by 1.0 V and, accordingly, a $Mo_2^{III,III}$ tetraphosphate is obtained on the photochemical reduction of protons to hydrogen.[129] However,

d^4—c

core i

biden

halide

bridg

plane

oxida

additi

reduc

photo

and (

subst

chlori

the te

Here,

facilit

metal

ESBC

specie

d^4—d^4→d^3—d^3 photoconversions of this type are unusual when the bimetallic core is spanned by four bidentate ligands.

Two-electron chemistry is typically observed when two of the four bidentate ligands of a M$\underline{4}$M core are replaced by monodentate ligands, usually halides. Quadruply bonded binuclear systems $M_2X_4(PP)_2$ (M_2 = Mo_2, W_2; PP = bridging phosphine; X = halide)[84] feature sterically uncongested equatorial planes and the terminal halides can easily move to edge-bridging positions upon oxidation of the metal core to form edge-sharing bioctahedral (ESBO) species. In addition, the bidentate or chelating function of PP ligands in these complexes reduces the possibility of circumventing photoredox chemistry by photosubstitution of the phosphine ligands. It is well established that $M_2X_4(P\ P)_2$ and (P P = bidentate phosphine) complexes thermally reduce a variety of substrates (YZ), such as diselenides,[113149,150] halogens,[151] and hydrogen chloride.[152,153] These two-electron thermal reactions involve the rearrangement of the terminal halide ligands to yield $M_2X_4YZ(P\ P)_2$ ESBO products,[152154,155]

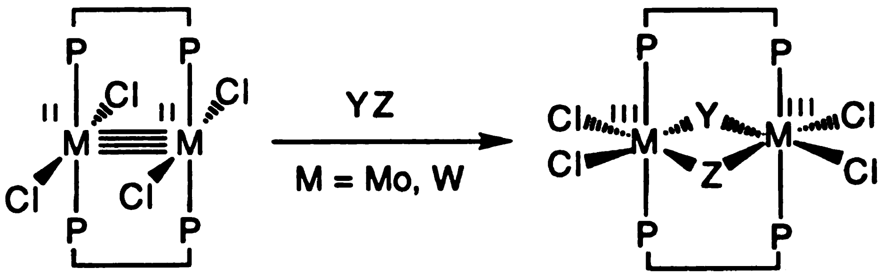

(4.1)

Here, the ability of the ligand coordination sphere to stabilize an ESBO structure facilitates the reaction by enforcing an octahedral geometry about the individual metal centers of the oxidized bimetallic core.

For the same reason, our group has previously shown that formation of ESBO species is also prominent in the two-electron photochemistry of these species.[156] Early work in our group established the two-electron photochemical oxid

the e

W_2C

analy

The

direc

edge

of M

phot

phot

the f

com

studi

the p

the

bioc

term

path

repre

II.

A.

CH_2

oxidative-addition of CH_3I to $W_2Cl_4(dppm)_2$.[157] This reaction is also attributed to the excitation of the metal-localized $\delta\pi^*$ and $\pi\delta^*$ transitions. The photoproduct, $W_2Cl_4(dppm)_2(CH_3)(I)$, was characterized by chemical and spectroscopic analyses, and ^{13}C-NMR shows the methyl group to be in the terminal position. The cis-addition to one end of the tungsten bimetallic core is consistent with the direct addition of the substrate to the open coordination site of a photogenerated edge-sharing bioctahedral intermediate. The observation of simple photoaddition of MeI to a terminal coordination site of the ditungsten core suggests a photoreaction pathway in which substrate is activated at the $:M^-$ site of the photoactivated $:M^-—M^+$ core. This reaction is important as it represents one of the first examples of a discrete multielectron photoreaction of a transition metal complex. We wished to generalize this type of photoreactivity with further studies of $M_2X_4(dppm)_2$ (M = Mo or W, dppm = diphenyl(phosphino)methane) in the presence of other substrates such as RSSR (R = Et, Ph).

Terminal coordination of the methyl group is consistent with addition of the substrate to an open coordination site of a photogenerated edge-sharing bioctahedral intermediate. The observation of simple photoaddition of MeI to a terminal coordination site of the ditungsten core suggests a photoreaction pathway in which substrate is activated at a distinct tungsten atom, and represents one of the first examples of a discrete multielectron photoreaction.

II. Results and Discussion

A. Photochemistry

Figure 4.1 shows the spectral changes associated with the irradiation of CH_2Cl_2 solutions ($\lambda > 435$ nm) of $Mo_2Cl_4(dppm)_2$ and PhSSPh. While isosbestic

poi
abs
isos
pho
Mo
and
Mo
(λ>
isol

brid
X-ra
Mo
repo
with
4.3.
penta
mono
cryst
angle
distar
quadr

points are maintained during the course of the photoreaction in the low energy absorption range for the disappearance of the $^1(\delta^2 \rightarrow \delta\delta^*)$ absorption band, isosbestic behavior in the ultraviolet spectral region is not observed. The photoproduct is isolated with a yield of 33%. The absorption spectrum of $Mo_2Cl_5(dppm)_2(SPh)$ compares well to that of the final photoreaction ($\lambda_{max} = 527$ and 457 nm) as shown in Figure 4.2. When the solvent is toluene, irradiation of $Mo_2Cl_4(dppm)_2$ with excess PhSSPh from low (λ>435 nm) to high energy (λ>335 nm) under the same conditions produces the same final product in 52% isolated yields.

The identification of the $Mo_2Cl_5(dppm)_2(SPh)$ ESBO, with SPh^- in the bridging position of the $Mo_2^{III,III}$ core, as the final photoproduct is confirmed by X-ray crystallography. Specifically, the toluene co-solavte was obtained, $Mo_2Cl_5(dppm)_2(SPh){\bullet}C_7H_8$. The molecular structure is similar to that previously reported by Cotton and coworkers,[113] and differs only in the solvent packing within the lattice. The structure of $Mo_2Cl_5(dppm)_2(SPh) \bullet C_7H_8$ is shown in Figure 4.3. Deep maroon rod-shaped crystals of the bis(diphenylphosphinomethane)-pentachloro(μ-phenylsulfido) dimolybdenum(III,III) of the oxidized complex are monoclinic with a P21/C space group. Tables 4.1 and 4.2 gives a summary of crystal data and the selected positional parameters, respectively; selected bond angles and bond distances are listed in Tables 4.3 and 4.4. The Mo—Mo bond distance of 2.787(3) Å for the oxidized dimer is 0.649 Å greater than its quadruple bond parent complex, $Mo_2Cl_4(dppm)_2$ (2.138 Å). Because of the

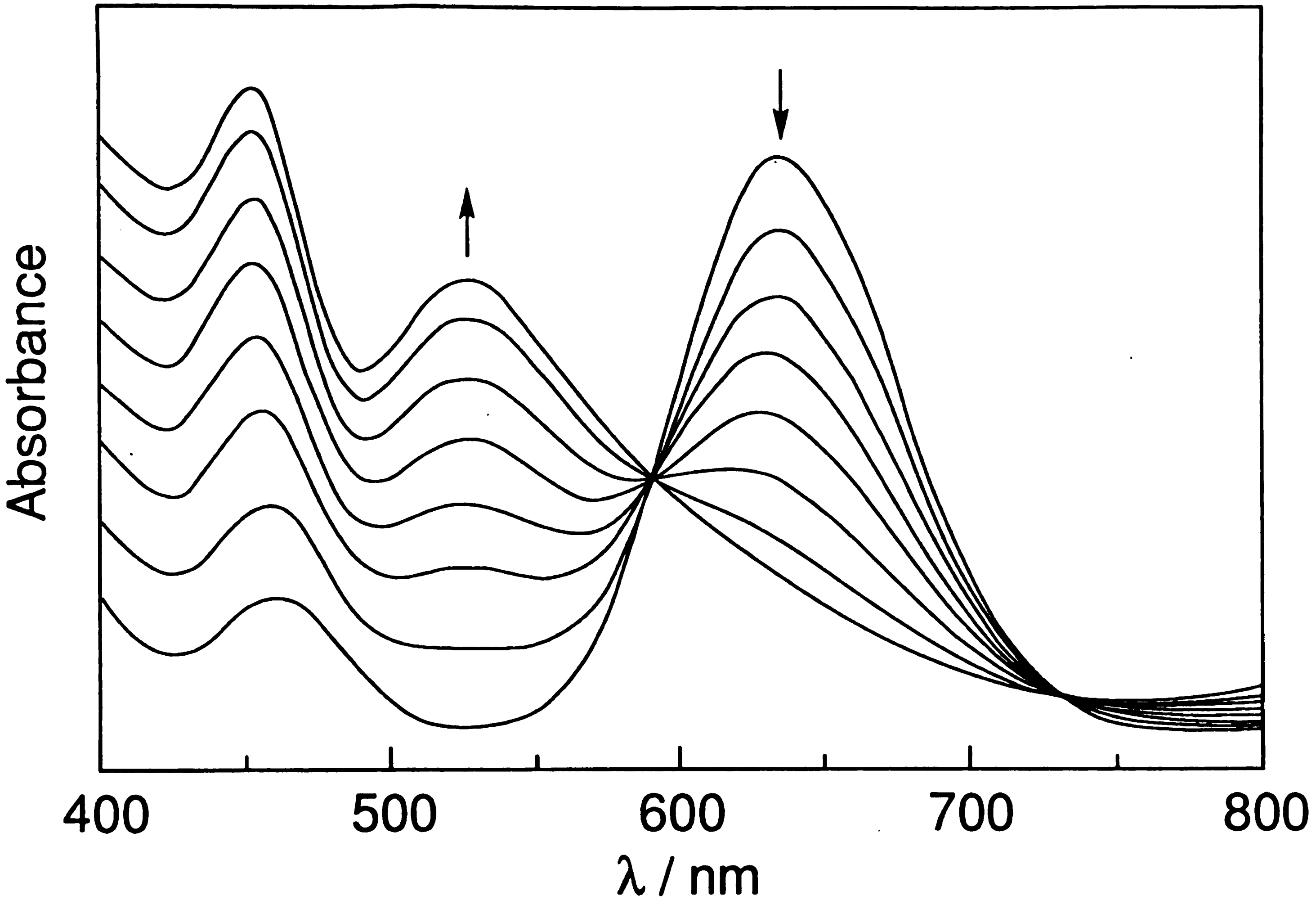

Figure 4.1 Electronic absorption spectral changes during the photolysis ($\lambda_{exc} > 435$ nm) of $Mo_2Cl_4(dppm)_2$ with a twenty-fold excess PhSSPh in deoxygenated dichloromethane at 16°C. Spectra were recorded at 0 to 240 mins in 30 min intervals.

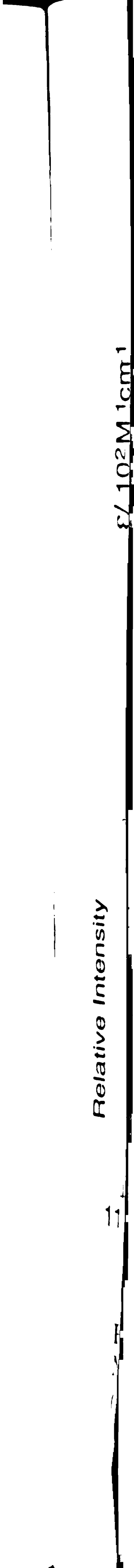
ε/ 10²M⁻¹cm⁻¹
Relative Intensity

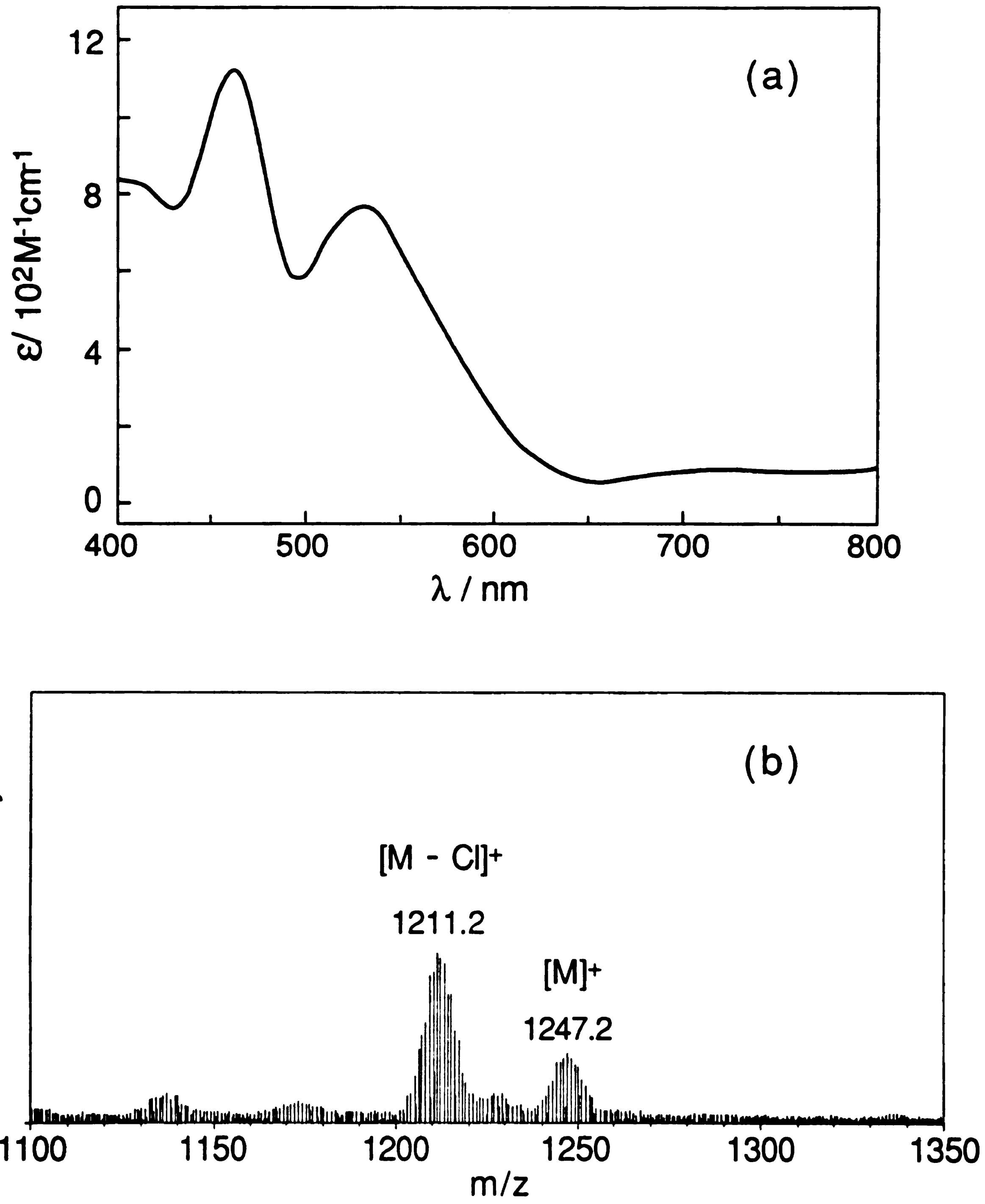

Figure 4.2 (a) Electronic absorption spectrum of $Mo_2Cl_4(dppm)_2(\mu\text{-}Cl)(\mu\text{-}SPh)$ in CH_2Cl_2 solution at room temperature. (b) FAB-MS spectrum of $Mo_2Cl_4(dppm)_2(\mu\text{-}Cl)(\mu\text{-}SPh)$.

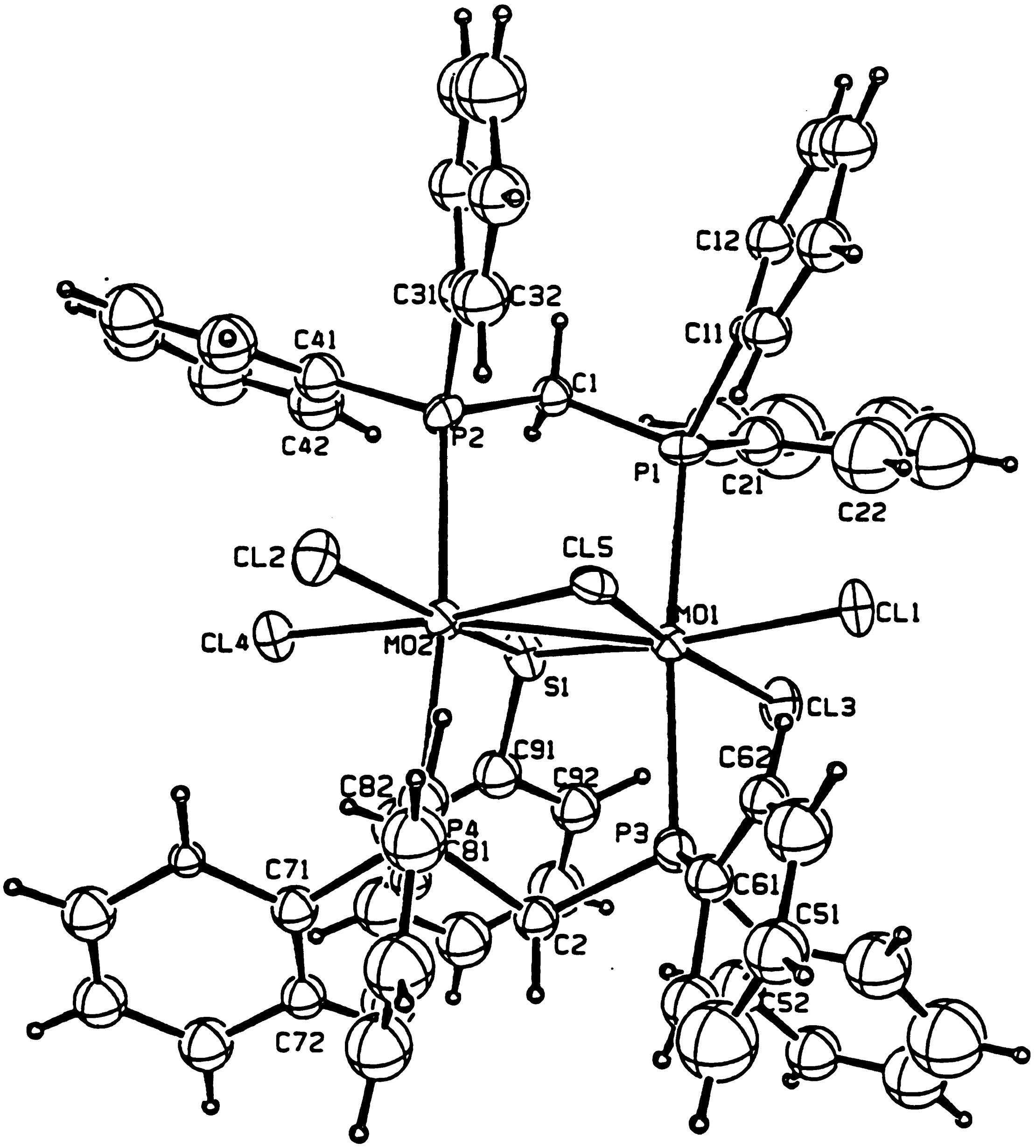

Figure 4.3 ORTEP view of molecular structure of photoproduct $Mo_2Cl_4(dppm)_2(\mu\text{-}Cl)(\mu\text{-}SPh)\cdot 2C_7H_8$. Thermal ellipsoids are drawn at 50% probability.

Tab

---

[a] R =

[b] R_w =

Table 4.1. Crystallographic Data for $Mo_2Cl_4(dppm)_2(\mu\text{-}Cl)(\mu\text{-}SPh){\bullet}2C_7H_8$

chem formula	$C_{56}H_{49}Cl_5Mo_2P_4S$: $2C_7H_8$
fw	1431.40
space group	*P*2₁/c (No. 14)
a	15.270(14) Å
b	17.926(15) Å
c	23.881(11) Å
α	90°
β	92.33(5)°
γ	90°
V	6531.5(6) $Å^3$
Z	4
T	202(3) K
λ (Mo Kα)	0.71073 Å
ρ_{calc}	1.46 g cm^{-3}
μ	7.5 cm^{-1}
$R(F_0)$	0.082[a]
$R_w(F_0)$	0.071[b]

[a] $R = \sum ||F_0| - |F_c|| / \sum |F_0|$.

[b] $R_w = [\sum w(|F_0| - |F_c|)^2 / \sum w |F_0|^2]^{1/2}$; $w = 1/(\sigma^2 |F_0|)$.

Table 4.2 Positional Parameters and Equivalent Isotropic Displacement Parameters (Å^2) for $Mo_2Cl_4(dppm)_2(\mu\text{-}Cl)(\mu\text{-}SPh)\cdot 2C_7H_8$

atom	x	y	z	B_{eq}, Å^2
Mo(1)	0.2552(1)	0.4268(1)	0.14521(8)	1.67(4)
Mo(2)	0.3166(1)	0.3275(1)	0.22759(8)	1.75(4)
Cl(1)	0.2899(4)	0.4639(3)	0.0499(2)	2.5(1)
Cl(2)	0.4289(4)	0.2293(3)	0.2371(2)	2.9(1)
Cl(3)	0.1425(4)	0.5196(3)	0.1317(2)	2.9(2)
Cl(4)	0.2936(4)	0.2991(3)	0.3239(2)	2.4(1)
Cl(5)	0.3665(3)	0.3360(3)	0.1343(2)	2.1(1)
S(1)	0.2166(4)	0.4282(3)	0.2417(2)	2.2(1)
P(1)	0.3636(4)	0.5299(4)	0.1784(3)	2.1(1)
P(2)	0.4383(4)	0.4187(4)	0.2640(2)	2.1(1)
P(3)	0.1440(4)	0.3302(4)	0.1036(2)	2.2(1)
P(4)	0.1994(4)	0.2255(3)	0.1991(2)	1.9(1)
C(1)	0.403(1)	0.516(1)	0.2511(8)	1.9(5)*
C(2)	0.105(1)	0.269(1)	0.1602(8)	2.2(5)*
C(11)	0.465(1)	0.548(1)	0.1416(7)	1.0(4)*
C(12)	0.509(1)	0.611(1)	0.1529(9)	2.7(5)*
C(13)	0.588(1)	0.627(1)	0.1236(8)	3.0(6)*
C(14)	0.617(1)	0.579(1)	0.0850(9)	3.3(6)*
C(15)	0.567(1)	0.514(1)	0.0722(9)	3.0(5)*
C(16)	0.497(1)	0.499(1)	0.1028(8)	2.5(5)*
C(21)	0.318(1)	0.621(1)	0.1804(9)	3.0(6)*

Table 4.2 Positional Parameters and Equivalent Isotropic Displacement Parameters (Å^2) for $Mo_2Cl_4(dppm)_2(\mu\text{-}Cl)(\mu\text{-}SPh)\cdot 2C_7H_8$ (cont'd)

atom	x	y	z	B_{eq}, Å^2
C(22)	0.296(2)	0.656(2)	0.129(1)	7.2(9)*
C(23)	0.260(2)	0.727(2)	0.123(1)	7.5(9)*
C(24)	0.246(2)	0.764(2)	0.171(1)	7.3(9)*
C(25)	0.251(2)	0.731(2)	0.222(1)	10(1)*
C(26)	0.296(2)	0.659(2)	0.226(1)	6.0(7)*
C(31)	0.549(1)	0.417(1)	0.2392(8)	2.3(5)*
C(32)	0.576(1)	0.369(1)	0.1979(9)	3.5(6)*
C(33)	0.662(1)	0.371(1)	0.1790(9)	3.7(6)*
C(34)	0.721(2)	0.420(2)	0.204(1)	5.2(7)*
C(35)	0.695(2)	0.466(1)	0.2456(9)	4.2(6)*
C(36)	0.611(1)	0.467(1)	0.2634(9)	3.2(6)*
C(41)	0.459(1)	0.413(1)	0.3401(9)	2.8(5)*
C(42)	0.405(2)	0.456(1)	0.3752(9)	3.9(6)*
C(43)	0.423(2)	0.450(1)	0.435(1)	5.0(7)*
C(44)	0.487(2)	0.400(1)	0.454(1)	4.7(7)*
C(45)	0.531(2)	0.353(1)	0.419(1)	4.6(7)*
C(46)	0.513(1)	0.359(1)	0.3609(9)	4.0(6)*
C(51)	0.040(1)	0.368(1)	0.0728(8)	2.1(5)*
C(52)	-0.026(1)	0.385(1)	0.107(1)	3.6(6)*
C(53)	-0.104(1)	0.416(1)	0.0813(9)	3.5(6)*
C(54)	-0.112(2)	0.426(1)	0.025(1)	4.9(7)*

Table 4.2 Positional Parameters and Equivalent Isotropic Displacement Parameters (Å^2) for $Mo_2Cl_4(dppm)_2(\mu\text{-}Cl)(\mu\text{-}SPh)\bullet 2C_7H_8$ (cont'd)

atom	x	y	z	B_{eq}, Å^2
C(55)	-0.046(2)	0.405(2)	-0.007(1)	7.0(9)*
C(56)	0.035(2)	0.378(1)	0.016(1)	4.9(7)*
C(61)	0.182(1)	0.266(1)	0.0482(8)	2.3(5)*
C(62)	0.251(1)	0.280(1)	0.0185(8)	2.3(5)*
C(63)	0.271(2)	0.231(1)	-0.0248(9)	4.1(6)*
C(64)	0.219(1)	0.171(1)	-0.0378(9)	3.7(6)*
C(65)	0.142(2)	0.156(2)	-0.008(1)	6.2(8)*
C(66)	0.120(1)	0.206(1)	0.0344(9)	3.3(6)*
C(71)	0.145(1)	0.178(1)	0.2573(8)	2.4(5)*
C(72)	0.057(1)	0.183(1)	0.2658(8)	2.2(5)*
C(73)	0.023(1)	0.143(1)	0.3105(8)	3.3(6)*
C(74)	0.080(1)	0.105(1)	0.3477(9)	3.2(6)*
C(75)	0.167(1)	0.101(1)	0.3394(9)	3.2(6)*
C(76)	0.206(1)	0.138(1)	0.2934(7)	1.4(4)*
C(81)	0.229(1)	0.147(1)	0.1557(8)	1.7(5)*
C(82)	0.309(1)	0.139(1)	0.1339(8)	2.3(5)*
C(83)	0.331(2)	0.076(1)	0.1015(9)	3.8(6)*
C(84)	0.266(2)	0.024(1)	0.088(1)	4.5(7)*
C(85)	0.187(2)	0.029(1)	0.1120(9)	4.2(6)*
C(86)	0.166(1)	0.091(1)	0.1441(9)	3.1(6)*
C(91)	0.106(1)	0.414(1)	0.2633(9)	2.9(5)*

Table 4.2 Positional Parameters and Equivalent Isotropic Displacement Parameters (Å^2) for $Mo_2Cl_4(dppm)_2(\mu\text{-}Cl)(\mu\text{-}SPh)\cdot 2C_7H_8$ (cont'd)

atom	x	y	z	B_{eq}, Å^2
C(92)	0.045(1)	0.464(1)	0.2444(9)	3.1(6)*
C(93)	-0.041(2)	0.461(1)	0.2642(9)	4.3(6)*
C(94)	-0.063(2)	0.403(1)	0.2988(9)	4.1(6)*
C(95)	-0.001(2)	0.353(1)	0.319(1)	4.6(7)*
C(96)	0.084(2)	0.356(1)	0.2983(9)	4.4(6)*
C(101)	0.404(2)	0.777(1)	-0.075(1)	4.1(6)*
C(102)	0.487(2)	0.754(1)	-0.0559(9)	3.7(6)*
C(103)	0.490(2)	0.693(1)	-0.0184(9)	3.9(6)*
C(104)	0.419(2)	0.663(2)	0.002(1)	5.4(7)*
C(105)	0.340(2)	0.689(2)	-0.015(1)	5.5(7)*
C(106)	0.332(2)	0.747(2)	-0.052(1)	6.4(8)*
C(107)	0.403(2)	0.840(2)	-0.116(1)	8.1(9)*
C(111)	0.115(2)	0.634(2)	0.461(1)	10(1)*
C(112)	0.111(2)	0.689(2)	0.421(1)	7.1(8)*
C(113)	0.118(2)	0.672(2)	0.365(1)	10(1)*
C(114)	0.130(3)	0.600(2)	0.348(2)	14(2)*
C(115)	0.130(3)	0.548(3)	0.386(2)	15(2)*
C(116)	0.115(3)	0.559(2)	0.444(2)	15(2)*
C(117)	0.107(2)	0.655(2)	0.522(1)	12(1)*

Starred atoms were refined isotropically. Anisotropically refined atoms are given in the form of the isotropic equivalent thermal parameter defined as:
$(4/3)\ [a^2B_{11} + b^2B_{22} + c^2B_{33} + ab(\cos\gamma)B_{12} + ac(\cos\beta)B_{13} + bc(\cos\alpha)B_{23}]$

Table 4.3 Selected Bond Lengths (Å) and The Standard Deviations for for $Mo_2Cl_4(dppm)_2(\mu\text{-}Cl)(\mu\text{-}SPh)\bullet 2C_7H_8$

Bond Lengths		Bond Lengths	
Mo(1)—Mo(2)	2.787(3)	S(1)—C(91)	1.80(2)
Mo(1)—Cl(1)	2.450(6)	P(1)—C(1)	1.83(2)
Mo(1)—Cl(3)	2.407(6)	P(1)—C(11)	1.84(2)
Mo(1)—Cl(5)	2.376(6)	P(1)—C(21)	1.79(2)
Mo(1)—S(1)	2.401(6)	P(2)—C(1)	1.85(2)
Mo(1)—P(1)	2.584(6)	P(2)—C(31)	1.82(2)
Mo(1)—P(3)	2.595(6)	P(2)—C(41)	1.83(2)
Mo(2)—Cl(2)	2.462(6)	P(3)—C(2)	1.86(2)
Mo(2)—Cl(4)	2.395(6)	P(3)—C(51)	1.85(2)
Mo(2)—Cl(5)	2.389(5)	P(3)—C(61)	1.86(2)
Mo(2)—S(1)	2.397(6)	P(4)—C(2)	1.86(2)
Mo(2)—P(2)	2.599(6)	P(4)—C(71)	1.85(2)
Mo(2)—P(4)	2.628(6)	P(4)—C(81)	1.81(2)

Table 4.4 Selected Bond Angles (deg) and The Standard Deviations for $Mo_2Cl_4(dppm)_2(\mu\text{-}Cl)(\mu\text{-}SPh)\cdot 2C_7H_8$

Bond Angles		Bond Angles	
Mo(2)—Mo(1)—Cl(1)	138.6(2)	Mo(1)—Mo(2)—Cl(2)	137.3(2)
Mo(2)—Mo(1)—Cl(3)	139.0(2)	Mo(1)—Mo(2)—Cl(4)	139.0(2)
Mo(2)—Mo(1)—Cl(5)	54.4(1)	Mo(1)—Mo(2)—Cl(5)	54.0(1)
Mo(2)—Mo(1)—S(1)	54.4(2)	Mo(1)—Mo(2)—S(1)	54.6(1)
Mo(2)—Mo(1)—P(1)	92.7(2)	Mo(1)—Mo(2)—P(2)	92.9(2)
Mo(2)—Mo(1)—P(3)	92.3(2)	Mo(1)—Mo(2)—P(4)	93.2(2)
Cl(1)—Mo(1)—Cl(3)	82.4(2)	Cl(2)—Mo(2)—Cl(4)	83.6(2)
Cl(1)—Mo(1)—Cl(5)	84.4(2)	Cl(2)—Mo(2)—Cl(5)	83.3(2)
Cl(1)—Mo(1)—S(1)	163.6(2)	Cl(2)—Mo(2)—S(1)	166.2(2)
Cl(1)—Mo(1)—P(1)	86.0(2)	Cl(2)—Mo(2)—P(2)	86.1(2)
Cl(1)—Mo(1)—P(3)	89.3(2)	Cl(2)—Mo(2)—P(4)	89.5(2)
Cl(3)—Mo(1)—Cl(5)	166.0(2)	Cl(4)—Mo(2)—Cl(5)	166.9(2)
Cl(3)—Mo(1)—S(1)	85.4(2)	Cl(4)—Mo(2)—S(1)	84.6(2)
Cl(3)—Mo(1)—P(1)	89.6(2)	Cl(4)—Mo(2)—P(2)	86.7(2)
Cl(3)—Mo(1)—P(3)	87.5(2)	Cl(4)—Mo(2)—P(4)	88.6(2)
Cl(5)—Mo(1)—S(1)	108.5(2)	Cl(5)—Mo(2)—S(1)	108.2(2)
Cl(5)—Mo(1)—P(1)	94.1(2)	Cl(5)—Mo(2)—P(2)	91.2(2)
Cl(5)—Mo(1)—P(3)	87.7(2)	Cl(5)—Mo(2)—P(4)	92.5(2)
S(1)—Mo(1)—P(1)	83.0(2)	S(1)—Mo(2)—P(2)	86.0(2)
S(1)—Mo(1)—P(3)	101.1(2)	S(1)—Mo(2)—P(4)	97.4(2)
P(1)—Mo(1)—P(3)	174.8(2)	P(2)—Mo(2)—P(4)	173.9(2)

Table 4.4 Selected Bond Angles (deg) and The Standard Deviations for $Mo_2Cl_4(dppm)_2(\mu\text{-}Cl)(\mu\text{-}SPh)\bullet 2C_7H_8$ (cont'd)

Bond Angles		Bond Angles	
Mo(1)—Cl(5)—Mo(2)	71.6(2)	Mo(1)—P(3)—C(61)	117.6(7)
Mo(1)—S(1)—Mo(2)	71.0(2)	Mo(2)—P(2)—C(1)	109.8(7)
Mo(1)—S(1)—C(91)	122.9(7)	Mo(2)—P(2)—C(31)	122.9(7)
Mo(2)—S(1)—C(91)	122.8(8)	Mo(2)—P(2)—C(41)	112.7(8)
Mo(1)—P(1)—C(1)	112.1(7)	Mo(2)—P(4)—C(2)	110.2(7)
Mo(1)—P(1)—C(11)	121.2(6)	Mo(2)—P(4)—C(71)	116.5(7)
Mo(1)—P(1)—C(21)	114.7(7)	Mo(2)—P(4)—C(81)	120.3(7)
Mo(1)—P(3)—C(2)	109.9(9)	P(1)—C(1)—P(2)	112.(1)
Mo(1)—P(3)—C(51)	116.5(7)	P(3)—C(2)—P(4)	110.(1)

longer metal-metal bond distance in the triply bonded species, there is less steric strain associated with the bridging bidentate phosphine ligands. The Mo_2P_2 segments of the five-membered $Mo_2(P_2C)$ rings are planar and orthogonal to each other (dihedral angle of 93° average), compared to 96° and 100° of the parent complex. In the equatorial plane, terminal chlorine atoms trans to the bridging sulfur atom have longer $Mo–Cl_t$ bond lengths ($(Mo—Cl_t)_{avg}$ 2.456 Å) than those cis to the bridging sulfur atom (ave. 2.401 Å), while the bridging chlorine atoms have even shorter $Mo—Cl_{br}$ bond distances ($d(Mo—Cl_{br})_{avg}$ = 2.383 Å). This Mo—Cl bond length difference within the binuclear core can be attributed to the trans effect of SR^- group, which is a stronger π donor as compared to Cl^-. Support for this intrepretation comes from the crystal structure of $Mo_2Cl_6(dppm)_2$, which shows similar Mo—Cl bond distances for the bridging and terminal chlorines. There are no significant differences between the Mo—P bond distances in the crystal structures of $Mo_2Cl_5(dppm)_2(SPh)$ and $Mo_2Cl_6(dppm)_2$.

Whereas $Mo_2Cl_4(dppm)_2$ converts to $Mo_2Cl_5(dppm)_2(SPh)$ in CH_2Cl_2, evidence for reactive intermediates is provided when the photolysis is halted prior to its completion in toluene. In contrast to the isoenergetic disappearance of the $^1(\delta^2 \rightarrow \delta\delta^*)$ absorption band in Figure 4.1, toluene solutions display a 600-nm absorption in the low energy spectral region (Figure 4.4). The compound responsible for this absorption has not been successfully crystallized, even at low temperature. However, FAB/MS and ES/MS analysis of solids isolated during intermediate stages of the photolysis showed the presence of $Mo_2Cl_4(dppm)_2(SPh)_2$ as the major product, with $Mo_2Cl_5(dppm)_2(SPh)$ present as well (Figure 4.5). Partially photolyzed solutions containing $Mo_2Cl_4(dppm)_2(SPh)_2$, left standing in the dark, converted completely to $Mo_2Cl_5(dppm)_2(SPh)$ as monitored by UV-vis spectroscopy and FAB/MS. We believe that $Mo_2Cl_4(dppm)_2(SPh)_2$ may be present in both the CH_2Cl_2 and

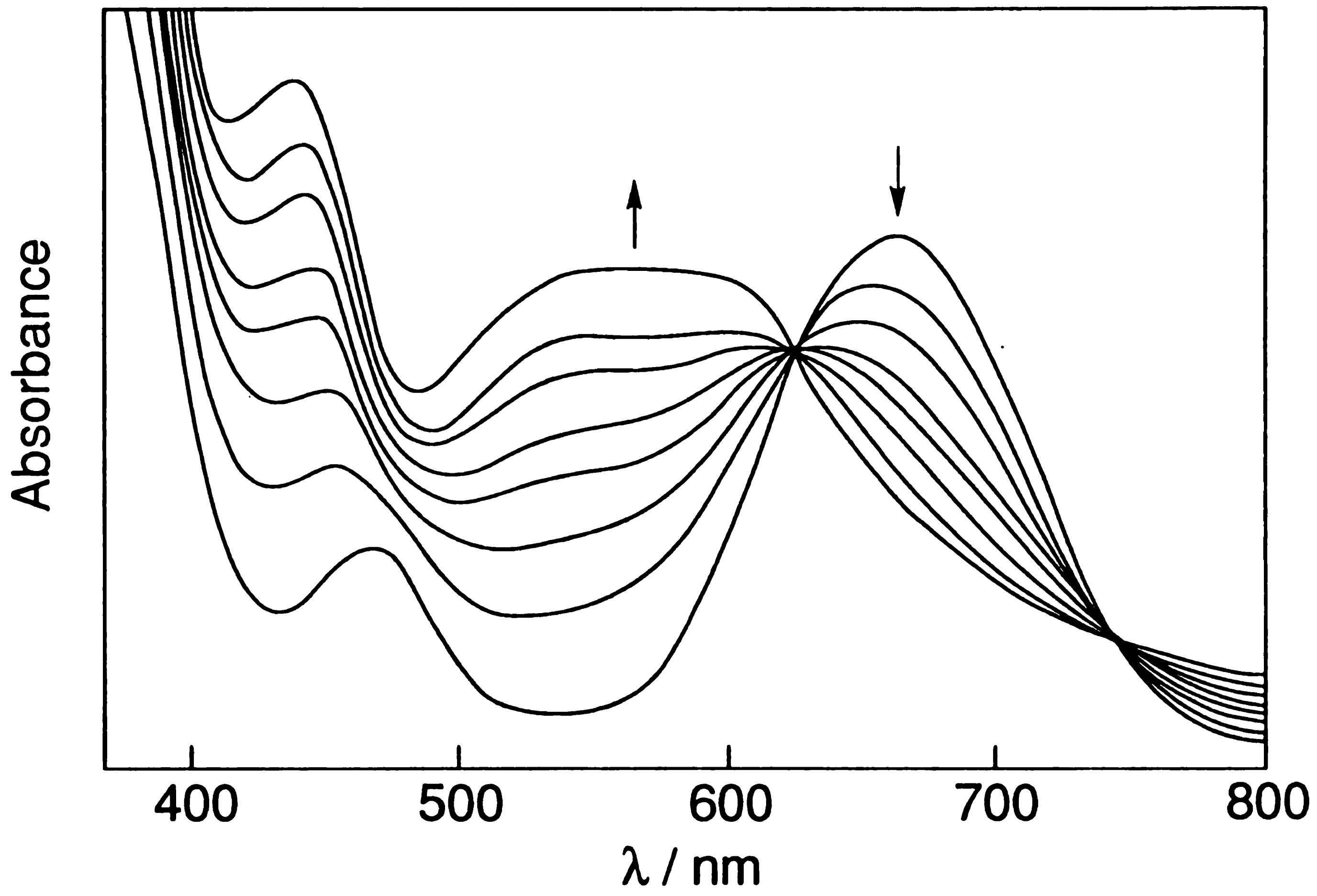

Figure 4.4 Electronic absorption spectral changes during the photolysis ($\lambda_{exc} > 365$ nm) of toluene solution of $Mo_2Cl_4(dppm)_2$ with excess PhSSPh at 8 °C; spectra were recorded at 0, 36, 70, 105, 140, 185, 235 and 300 mins. The irradiation was interrupted when the 600-nm band had attained a maximum absorption value.

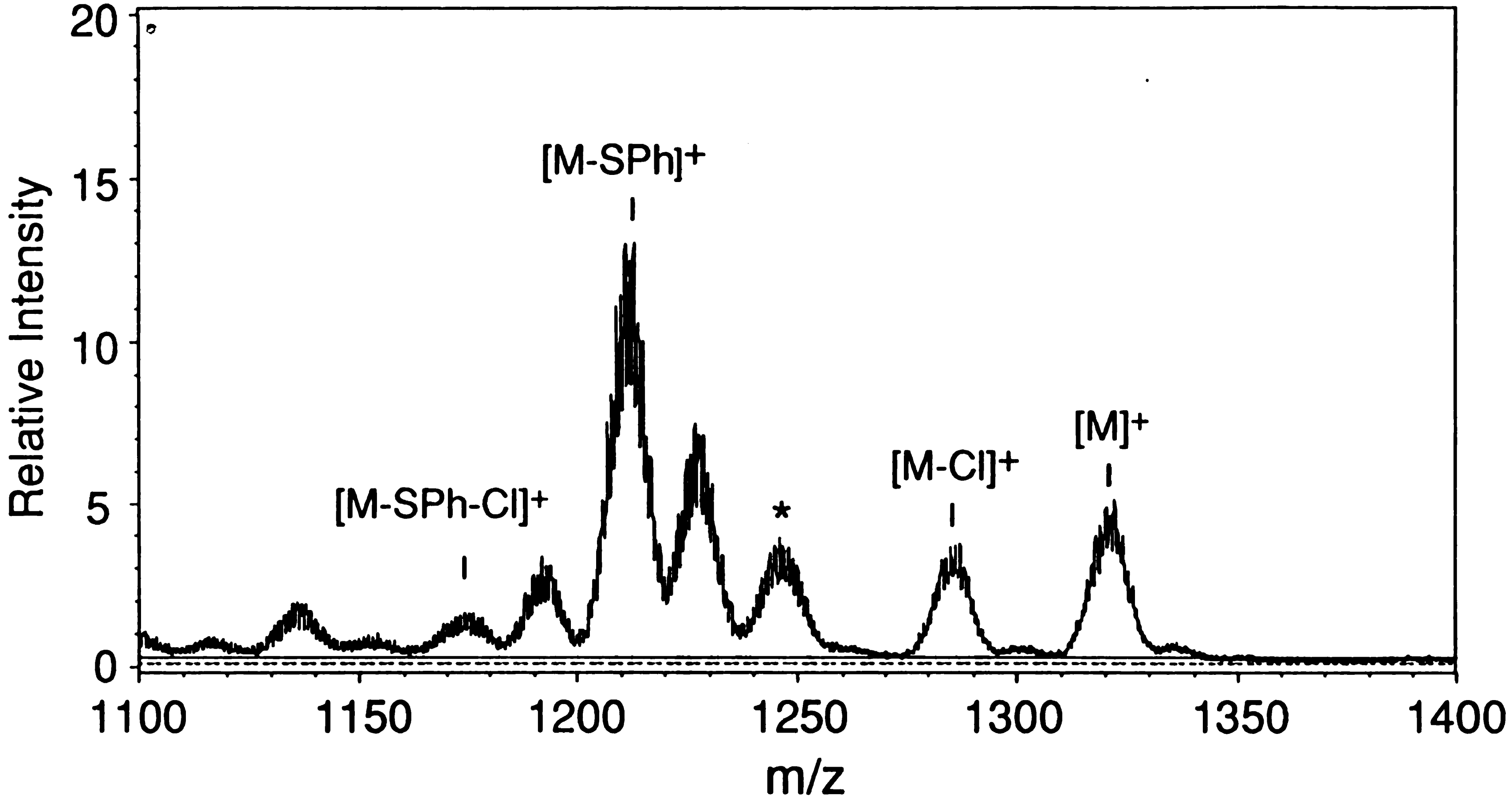

Figure 4.5 FAB-MS spectrum of the product isolated from the photolyzed ($\lambda_{exc} > 365$ nm) toluene solutions of $Mo_2Cl_4(dppm)_2$ showing the presence of $Mo_2Cl_4(dppm)_2(SPh)_2$. The asterisk is $Mo_2Cl_5(dppm)_2(SPh)$.

toluene photolyses, but its stability appears to be solvent dependent, reacting with facility in CH_2Cl_2 but stable enough in toluene solutions to be observed. It should be noted that no photoreaction of $Mo_2Cl_4(dppm)_2$ occurred in neat CH_2Cl_2, even when irradiated in the ultraviolet region, indicating that no charge transfer to solvent (CTTS) chemistry is involved. Thus, the possibility of the formation of $\cdot CH_2Cl + \cdot Cl$ in the photochemical reaction may be ruled out.[158]

Similar photochemistry for $Mo_2Cl_4(dppm)_2$ is observed in the presence of EtSSEt. The intensities of the 630-nm and higher energy 470-nm absorption bands decrease upon irradiation at $\lambda > 260$ nm, and two additional bands at 510 nm and 420 nm appear (Figure 4.6a). The photoproduct is confirmed to be $Mo_2Cl_5(dppm)_2(SEt)$ by FAB/MS; spectra display a parent ion mass cluster at 1200 amu. (Figure 4.6b). During the early course of the reaction, an isosbestic point is observed at 595 nm, but it is not maintained with continued photolysis, therefore suggesting that the mechanism proceeds by more than one step. Toluene solutions produce the same result at a solvent cutoff wavelength $\lambda > 285$ nm with the exception that small amounts of a brown precipitate form.

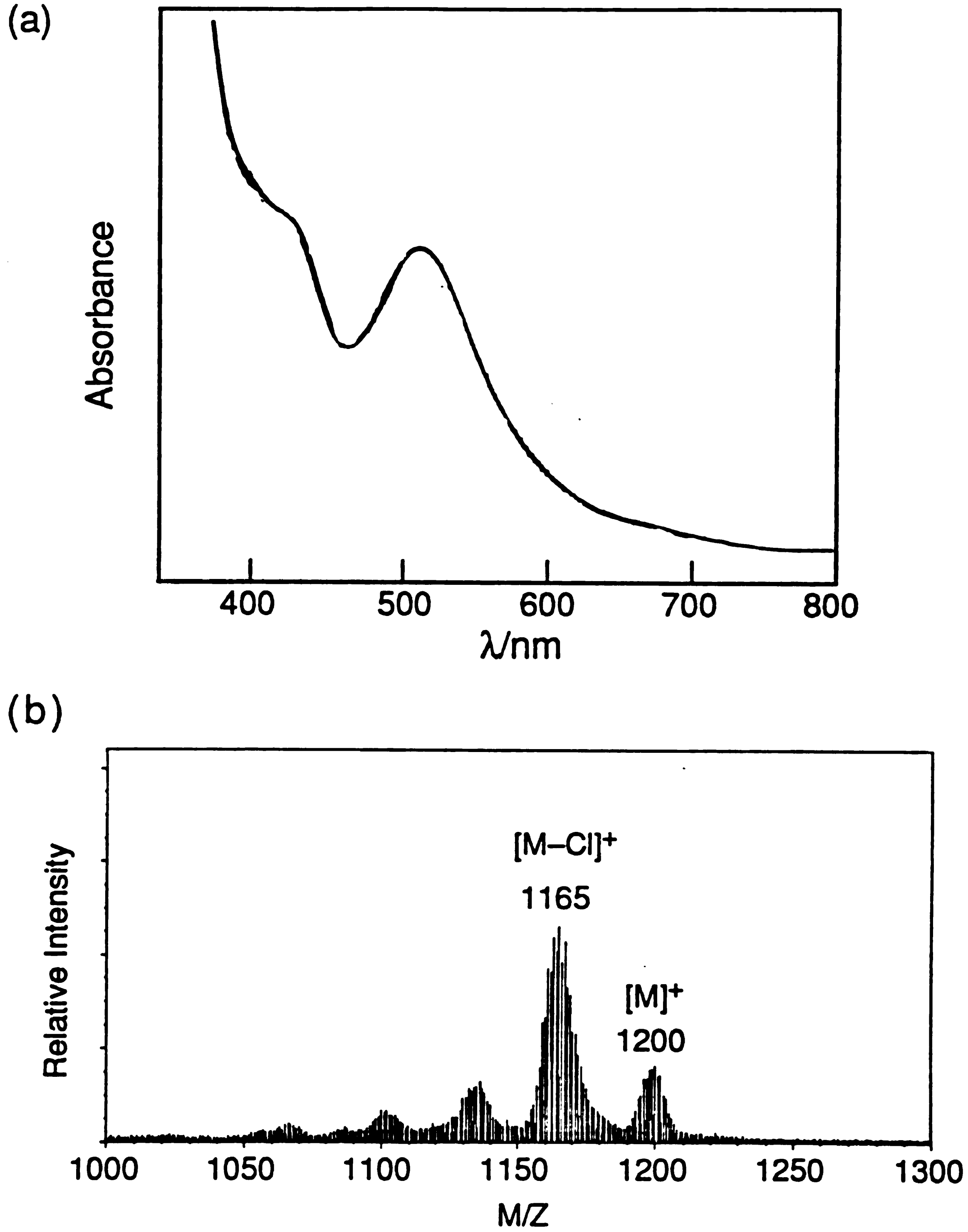

Figure 4.6 (a) Electronic absorption spectrum of $Mo_2Cl_4(dppm)_2(\mu\text{-}Cl)(\mu\text{-}SEt)$ in CH_2Cl_2 solution at room temperature. (b) FAB-MS spectrum of the product isolated from the photolyzed ($\lambda_{exc} > 235$ nm) CH_2Cl_2 solutions of $Mo_2Cl_4(dppm)_2$ with 40-fold excess of EtSSEt, consistent with $Mo_2Cl_4(dppm)_2(\mu\text{-}Cl)(\mu\text{-}SEt)$.

B. Thermal Chemistry

The formation of the $Mo_2^{III,III}$ ESBO from $Mo_2Cl_4(dppm)_2$ is unique to the photochemical reaction pathway. Solutions of $Mo_2Cl_4(dppm)_2$ and PhSSPh are indefinitely stable at room temperature. Upon refluxing for 12 h, toluene solutions of $Mo_2Cl_4(dppm)_2$ with excess PhSSPh or PhSH produce an as of yet unidentified orange-brown solid. The thermal product gives an absorption at 460 nm (m), 375 nm (sh) (Figure 4.7a) and the FAB/MS is consistent with a higher nuclearity cluster species. Similarly, the reaction of $Mo_2Cl_4(dppm)_2$ with EtSSEt in refluxing toluene for 36 h produces a purple-brown product. The electronic absorption spectrum displays one transition in the visible region at 450 nm (Figure 4.7b), and FAB/MS of the thermoproduct also shows a trinuclear type of clusters with mass ion peaks at 1263 and 1279 amu. Red crystals of thin platelets were obtained by slow diffusion of cyclohexane in a CH_2Cl_2 solution, but failed to get X-ray quality crystals. Presumably the difficulty in oxidizing the $Mo_2^{II,II}$ core hinders the formation of the $Mo_2^{III,III}$ ESBO along a thermal reaction pathway.

This is not the case, however, when tungsten is substituted for molybdenum. Electronic absorption, FAB/MS, and ES/MS spectra of thermally and photochemically ($\lambda > 495$ nm) reacted toluene solutions of $W_2Cl_4(dppm)_2$ and PhSSPh are identical to samples of the ESBO, $W_2Cl_4(dppm)_2(SPh)_2$, which have been previously synthesized and characterized.[113] Although the same product is obtained in both cases, the thermal reaction occurs over days as opposed to only hours for the photolysis.

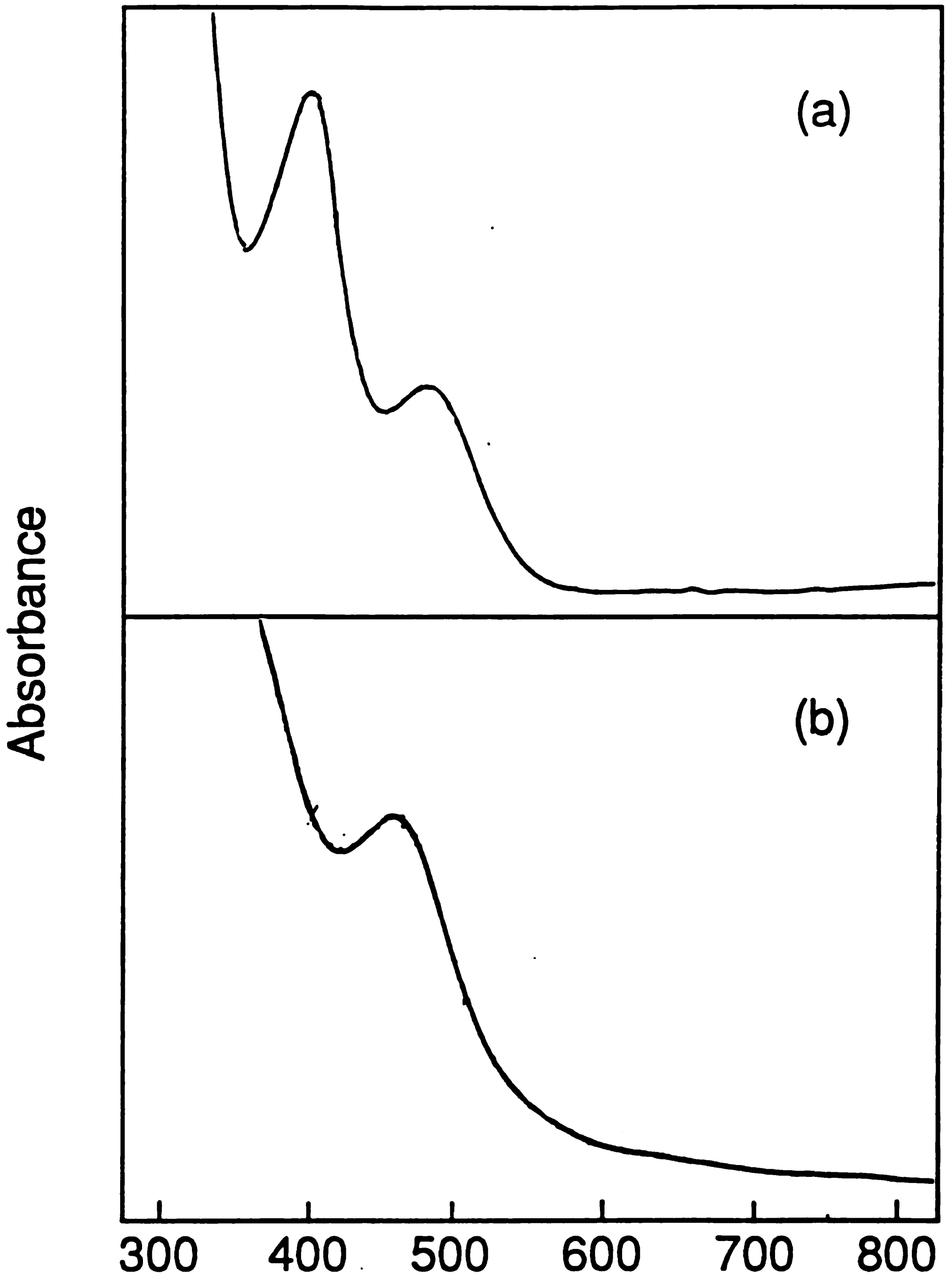

Figure 4.7 Electronic absorption spectrum of the isolated brown product from reactions of $Mo_2Cl_4(dppm)_2$ with (a) excess PhSSPh refluxing in toluene solutions for 12 hours (b) excess EtSSEt refluxing in toluene solutions for 36 hours.

C. Quantum Yields

Table 4.5 summarizes the wavelength dependence of the photoreaction quantum yield, ϕ_p. The action spectrum of $M_2Cl_4(dppm)_2$/PhSSPh photochemistry parallels its absorption spectrum, shown in Figure 4.8 and is consistent with reactivity originating from the metal complex. The onset of $Mo_2Cl_4(dppm)_2$ photoreactivity occurs at λ = ~436 nm (ϕ_p = 0.01), and ϕ_p increases monotonically between 320-380 nm, asymptotically approaching a limiting quantum yield of 0.27 at $\lambda<313$ nm. The band centered at 330 nm appears to be responsible for the photoreactions. The action spectrum tracks the rising absorption edge of transitions immediately to higher energy of the $^1(\delta^2 \rightarrow \delta\delta^*)$ transition (λ_{max} = 635 nm). This coincidence between the wavelengths of absorptions immediately to higher energy of $^1(\delta^2 \rightarrow \delta\delta^*)$ and the action spectrum of $Mo_2Cl_4(dppm)_2$ is preserved in $W_2Cl_4(dppm)_2$ photochemistry. The ~50 nm red-shift of the $W_2Cl_4(dppm)_2$ action spectrum as compared to its $Mo_2Cl_4(dppm)_2$ homolog is consistent with a respective 50 nm red-shift of the absorption spectrum of the ditungsten complex (see Figure 4.8).

When the substrate is diethyl disulfide, the quantum yields decreases dramatically to 0.0014 and 0.061 for the corresponding wavelength 365 and 313 nm. The result can be rationalized by the increased bond strength of AlkS—SAlk (Alk = alkyl group) substrates as compared to PhS—SPh (bond dissociation energies are ~55 and 74 kcal, respectively).[159] The increased activation barrier to sulfur-sulfur bond claevage in AlkS—SAlk substrates is sufficient to significantly perturb the efficiency of the photoreaction.

The wavelength dependence of $M_2Cl_4(dppm)_2$/PhSSPh photochemistry excludes the possibility of a reaction derived from direct homolysis of the disulfide bond to produce RS• radicals. Organic disulfides add to acetylenes to

Table 4.5 Wavelength Dependence of Quantum Yields for Photoreaction of $Mo_2Cl_4(dppm)_2$ and $W_2Cl_4(dppm)_2$ with PhSSPh.

λ_{exc}/nm	ϕ_p [$Mo_2Cl_4(dppm)_2$] [a]	ϕ_p [$W_2Cl_4(dppm)_2$] [b]
546	$<10^{-5}$	0.025
436	0.010	0.048
405	0.11	0.075
365	0.23	0.15
313	0.27	0.39

[a] T = 16 °C in CH_2Cl_2; [b] T = 0 °C in toluene.

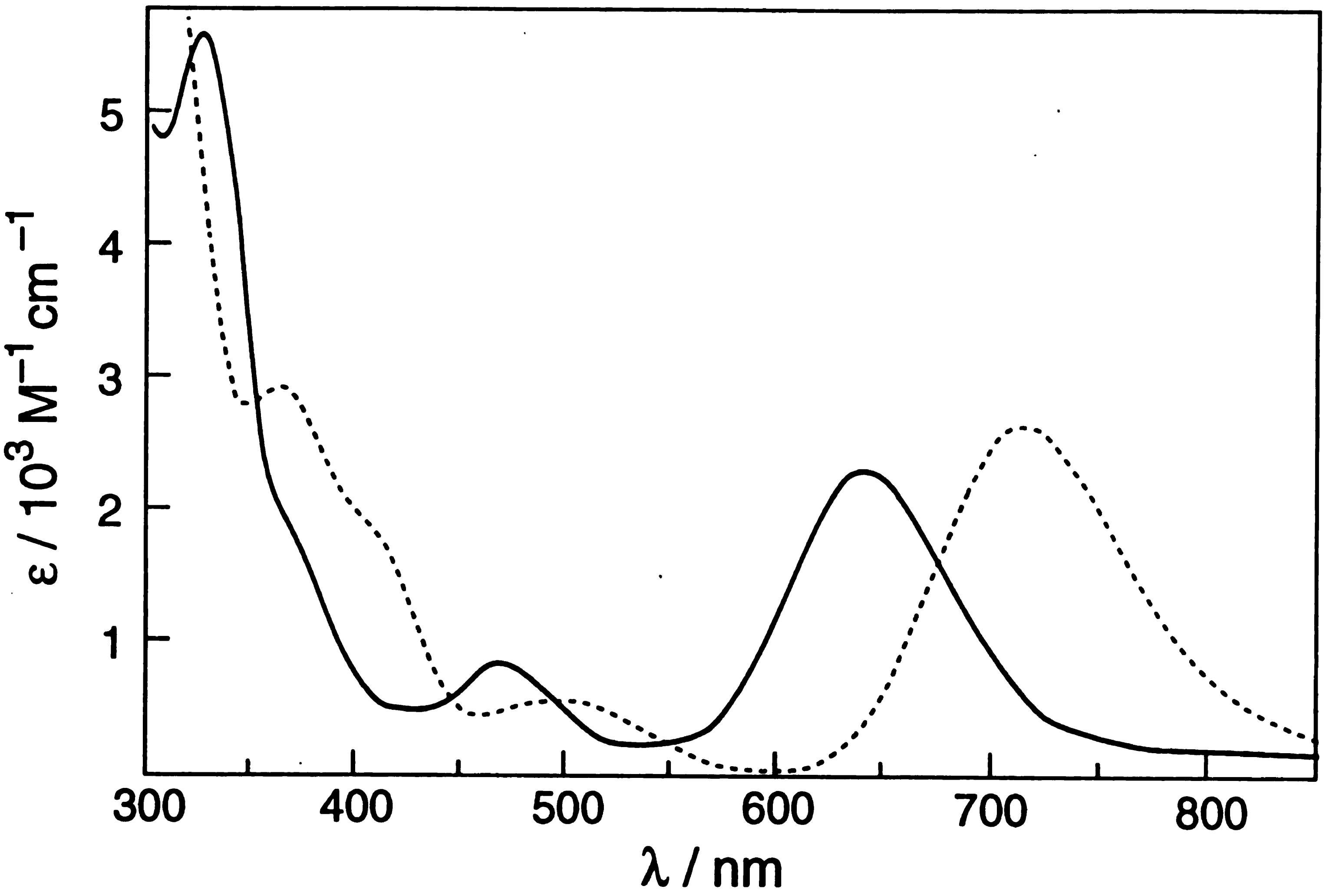

Figure 4.8 Electronic absorption spectra of $Mo_2Cl_4(dppm)_2$ (—) and $W_2Cl_4(dppm)_2$ (——) complexes in toluene.

afford 1,2-diarylmercaptoethenes in high yields via a free radical pathway, resulting from the photochemically induced cleavage of the disulfide bond, but the reaction occurs at higher wavelengths than reported here.[160] Benzene solutions of PhSSPh in either the presence of methylacetylene or 1-heptyne are irradiated with wavelengths coincident with $M_2Cl_4(dppm)_2$ photochemistry. No reaction is observed for $\lambda > 380$ nm and only trace amount of reaction is observed at lower excitation wavelengths. With decreasing wavelength, the 1:1 adduct is observed with the highest yields occurring for irradiation wavelengths coincident with the absorption maximum of PhSSPh at $\lambda = 240$ nm, a result that is consistent with Heiba and Dessau's original observations of free radical addition of PhSSPh to these alkynes.[161] The parallels between the quantum yields listed in Table 4.5 and the absorption profiles of the quadruply bonded metal-metal complexes, and their disparity with the action spectrum of RSSR photochemistry, establish that $M_2Cl_4(dppm)_2$/RSSR photochemistry is derived from the quadruple bond complex.

A comparison of the action spectra of dimolybdenum and ditungsten complexes provides additional insight into the excited state responsible for the observed photochemistry. Substitution of Mo by W in quadruply bonded metal-metal halophosphine complexes is known to lead to a blue shift in ligand-to-metal transitions owing to the greater difficulty associated with reducing W^{II}.[162] Conversely, metal-localized transitions exhibit a red shift owing to decreased two-electron contributions to the overall transition energy of the tungsten complex.[163] Figure 4.8 shows the absorption spectra of $Mo_2Cl_4(dppm)_2$ and $W_2Cl_4(dppm)_2$. As expected on the basis of these arguments, the metal-localized $^1(\delta^2 \rightarrow \delta\delta^*)$ transition shifts from 635 nm for $Mo_2Cl_4(dppm)_2$ to 710 nm for $W_2Cl_4(dppm)_2$. More pertinent to the photochemistry described here, a red shift is clearly observed in the excitation window of the photochemistry. That this Mo → W red shift is accomapnied by a similar red shift in the action spectra implies that the parentage of $M_2Cl_4(dppm)_2$ (D_{2h}) photochemistry is from a metal-localized excited state.

D. Transient Absorption Studies

Photochemical studies were complemented by the investigations of the transient absorption spectroscopy of $M_2X_4(PP)_2$ complexes upon visible and near-ultraviolet excitation.[164] In the case of M = Mo, a complete wavelength study could not be achieved owing to stimulated emission of dppm (λ_{max} = 460 nm, $\tau \sim 1$ ns)[165] when samples were excited with high energy light (λ_{exc} = 355 nm). Specifically, simulated emission in the 450-520 nm spectral range, although weak, was problematic because the ΔODs for the transient absorption bands of $Mo_2Cl_4(dppm)_2$ in this range were small. The stimulated emission was eliminated upon replacement of the dppm by dmpm (bis(dimethylphosphino)methane) thereby allowing us to obtain sufficiently high signal-to-noise to detect absorptions with ΔODs<0.05. Because $Mo_2Cl_4(dmpm)_2$ is structurally and electronically analogous to $Mo_2Cl_4(dppm)_2$, we believe the transient spectroscopy of the dmpm system to be representative of $Mo_2Cl_4(dppm)_2$. Evidence for the electronic similarity of the two complexes comes from the absorption profile of $Mo_2Cl_4(dmpm)_2$ and $Mo_2Cl_4(dppm)_2$, which are nearly identical but blue-shifted by ~40 nm for the former complex.[166] Moreover, $Mo_2Cl_4(dmpm)_2$ photochemistry is parallel to that of $Mo_2Cl_4(dppm)_2$ with the production of $Mo_2Cl_5(dmpm)_2(SPh)$ as the photoproduct. For the case of $W_2Cl_4(dppm)_2$, these complicating problems do not arise. A red-shift in the electronic absorption spectrum of the complexes transitions with regard to the intraligand transitions of the dppm permitted us to obtain transient spectra at high and low energy excitation without interference from stimulated emission from the sample.

Figure 4.9 shows transient absorption profiles for $Mo_2Cl_4(dmpm)_2$ following a 3 ps excitation pulse at 600 nm. A prominent feature at 460 nm decays monoexponentially to ground state with a lifetime of 40(8) ps. Concurrent with this absorption decay is the recovery of the $^1(\delta\delta^*)$ bleach at 630 nm on the same time scale thereby establishing the assignment of the transient absorption in Figure 4.9 to the $^1(\delta\delta^*)$ excited state. The excitation of the $^1(\delta\delta^*)$ state of $W_2Cl_4(dppm)_2$ also affords a short-lived intermediate (< 1 ns), which is generally true of all $M_2X_4(PP)_2$ complexes that we have surveyed to date. The short lifetimes of the $^1(\delta\delta^*)$ transient accounts for the absence of $M_2Cl_4(dppm)_2$/RSSR photochemistry upon $^1(\delta^2 \rightarrow \delta\delta^*)$ excitation.

A long-lived intermediate is observed, however, when the absorption profile immediately to higher energy of the $^1(\delta^2 \rightarrow \delta\delta^*)$ transition is excited. High energy excitation of $Mo_2Cl_4(dmpm)_2$ in dichloromethane at λ_{exc} = 355 nm displays a transient absorption profile at λ_{max} = 520 nm with a lifetime of 5 μs,[164] which is spectrally similar to the absorption spectrum of the edge-sharing bioctahedron, $Mo_2Cl_6(dmpm)_2$, as shown in Figure 4.10a[167,168] A similar result is obtained for $W_2Cl_4(dppm)_2$ in benzene at room temperature. Figure 4.10b shows that the transient absorption, which decays even more slowly (τ = 46 μs) than that observed for its molybdenum congener, is also similar to $W_2Cl_6(dppm)_2$.[150,167]

Figure 4.9 Time evolution of the disappearance of the picosecond transient absorption of $Mo_2Cl_4(dmpm)_2$ in dichloromethane. The spectra were obtained 2, 20 and 50 ps after a 600 nm, 3 ps excitation pulse. The inset shows a plot of the ln(ΔOD) for the transient absorption at 630 nm vs time. (ref. 164)

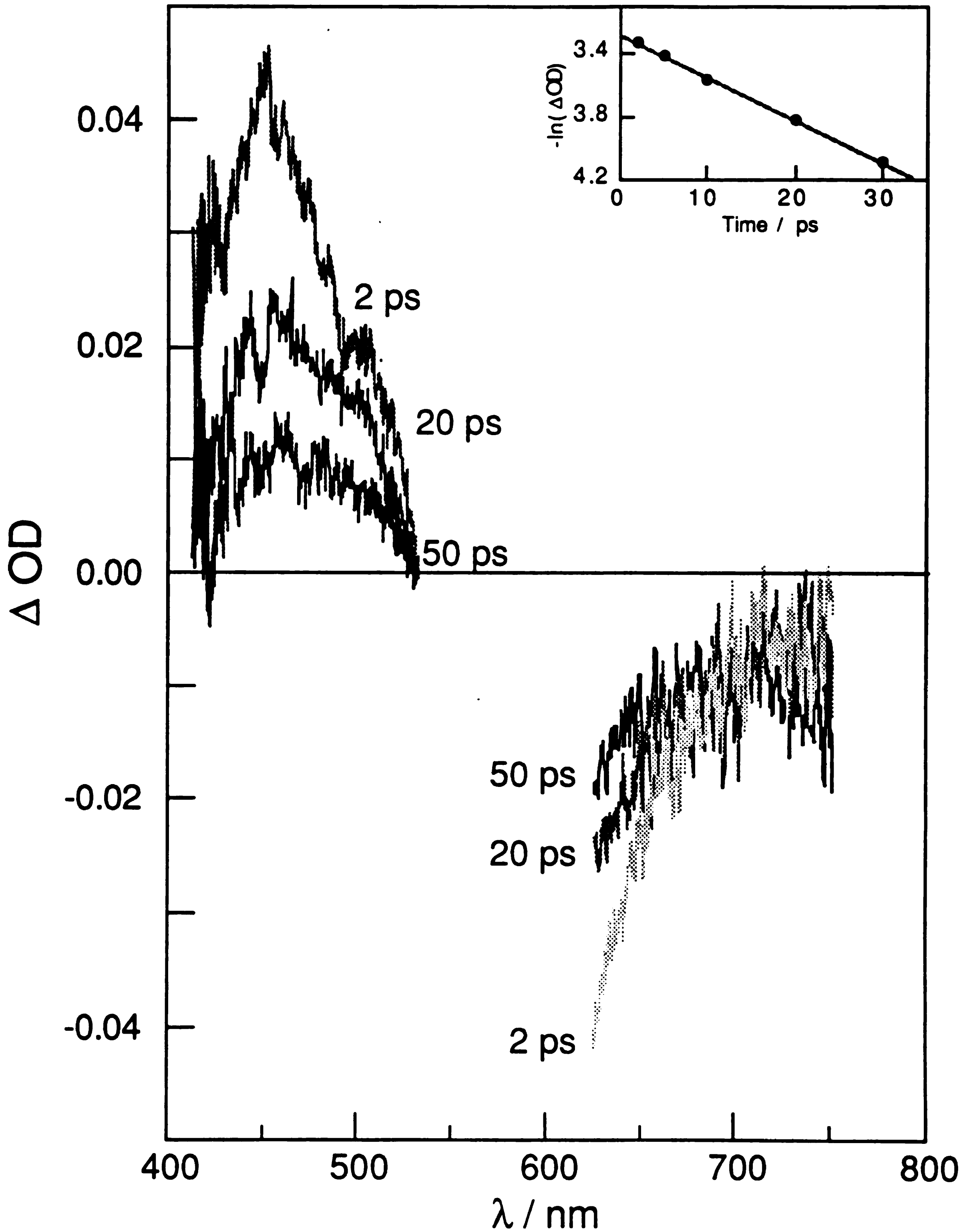
0.04
0.02
0.00
-0.02
-0.04
Δ OD
400
500
600
700
800
λ / nm
2 ps
20 ps
50 ps
50 ps
20 ps
2 ps
3.4
3.8
4.2
-ln(ΔOD)
0
10
20
30
Time / ps

Figure 4.9

Figure 4.10 Transient difference spectra (O) of a deoxygenated (a) dichloromethane solution of $Mo_2Cl_4(dmpm)_2$ recorded 1 μs after 355 nm, 10 ns excitation, and electronic absorption spectrum of $Mo_2Cl_6(dmpm)_2$ (—) in dichloromethane, (b) benzene solution of $W_2Cl_4(dppm)_2$ collected 100 ns after 532 nm, 10 ns excitation, and electronic absorption spectrum of $W_2Cl_6(dppm)_2$ (—) in dichloromethane. (ref. 164)

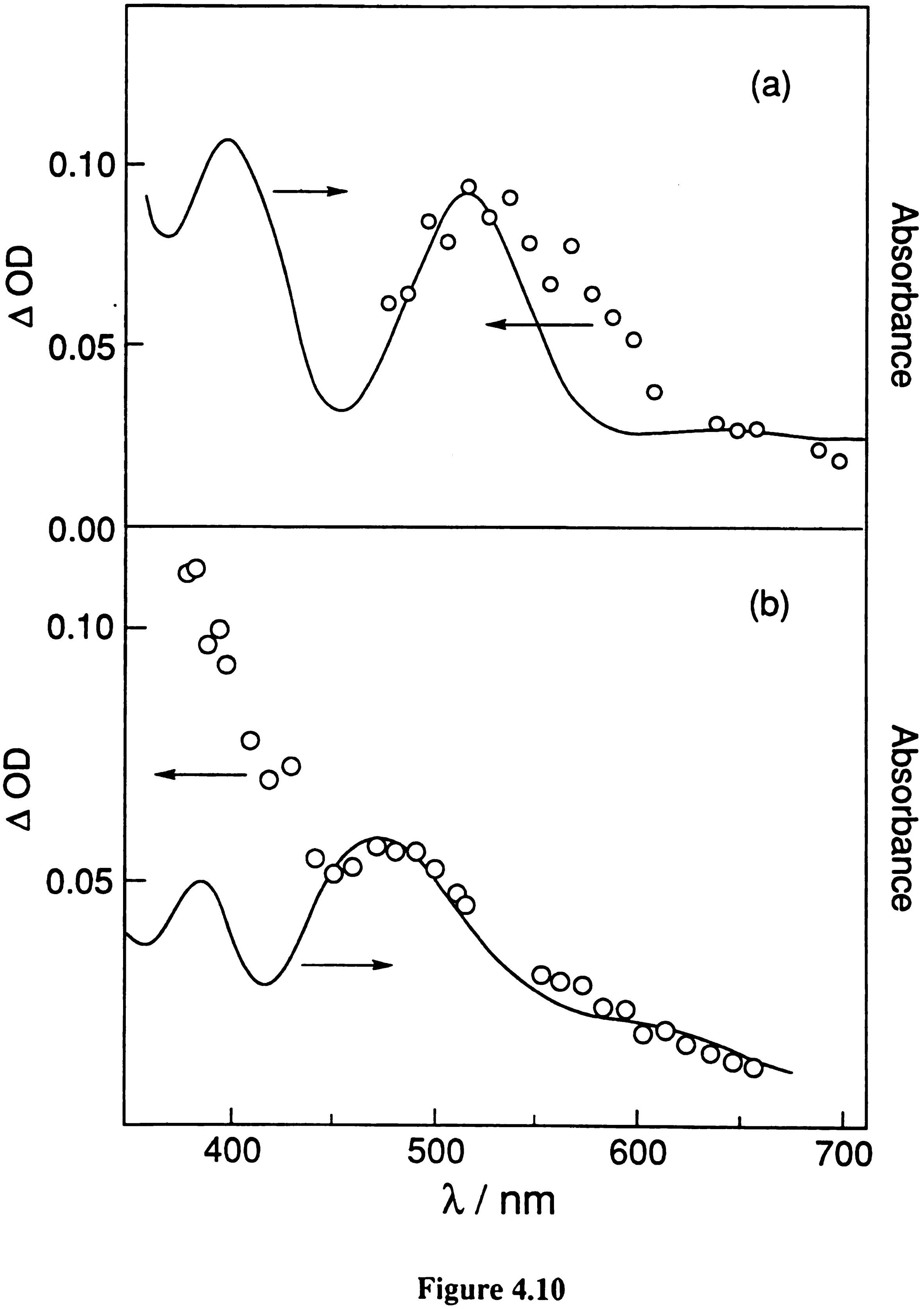
(a)
(b)
0.10
0.05
0.00
0.10
0.05
Δ OD
Δ OD
Absorbance
Absorbance
400
500
600
700
λ / nm

Figure 4.10

The correlation between the spectra of the long-lived non-luminescent transients and the edge-sharing bioctahedra suggests that the transient may be derived from a chemically distorted ESBO-intermediate shown in eq. (4.2),

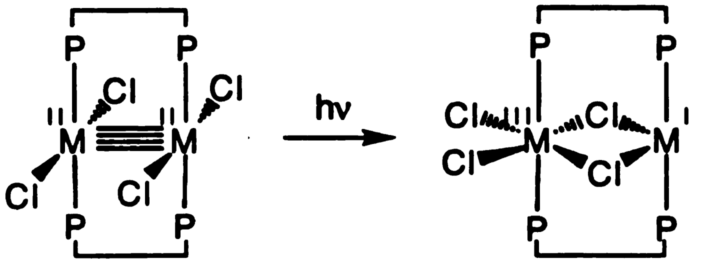

(4.2)

Although the electron counts of the chemically distorted ESBO transient ($M_2^{I,III} = d^5—d^3$) and $M_2X_6(PP)_2$ complexes ($M_2^{III,III} = d^3—d^3$) are different, the spectra of the two species may be similar for several reasons. The energy ordering of the molecular orbitals of an ESBO are $\sigma << \pi < \delta^*{\sim}\delta < \pi^* << \sigma^*$ with a very small δ^*/δ splitting.[149, 168, 169] Consequently, transitions such as $\pi \rightarrow \delta^*$, $\pi \rightarrow \delta$ and $\delta^* \rightarrow \pi^*$ in $d^3—d^3$ are predicted to be energetically similar to $\delta \rightarrow \pi^*$ and $\delta^* \rightarrow \pi^*$ in a chemically distorted $d^5—d^3$ ESBO. Even greater similarities between the spectra of the two intermediates will result if the two additional electrons of the chemically distorted intermediate occupied the in-plane π orbital of the ESBO as a lone pair. In this case, the electron count of a chemically distorted ESBO would be $d^3—d^3$ $(\pi_{\text{in-plane}})^2$ and metal-based transitions within the metal-based d-orbitals would be similar to the native $d^3—d^3$ ESBO.

The formation of such an intermediate is consistent with the electronic structure of quadruply bonded metal-metal complexes. Metal-localized excited states associated with promotion of electrons to and from the δ and δ* orbitals exhibit charge transfer character (i.e. $M_2^{II,II*} \equiv M_2^{I,III}$).[94,96] Intramolecular chemical distortion to an ESBO can stabilize this charge transfer within the bimetallic core by providing cooperative stabilization with an octahedral geometry about a partially oxidized metal center and diminished donation of electron density from the halides about the partially reduced metal center. Whereas the activation barrier associated with the intramolecular ligand rearrangement may prevent access to an ESBO-type intermediate from the $^1(\delta\delta^*)$ excited state, population of the higher energy metal-localized transitions can lead to diminished metal-metal π bonding relative to that in the ground state molecule (Figure 4.11). This feature is expected to enhance the formation of a bioctahedral intermediate because interactions of the metal d_{yz} (or d_{xz}) orbitals with those of ligands in the equatorial plane of an edge-sharing bioctahedron occur at the expense of M—M π interactions. Notwithstanding, the generation of long-lived intermediates upon excitation of the absorption profile to higher energy of the $^1(\delta^2 \rightarrow \delta\delta^*)$ transition is consistent with our observations of $M_2Cl_4(dppm)_2$ photochemistry over this same excitation range.

The photochemistry of $M_2Cl_4(dppm)_2$ is analogous in many ways to the thermal oxidative-addition chemistry of mononuclear d^8 square planar metal complexes. In the d^8 archetype, Vaska's complex, trans-$IrCl(CO)(PR_3)_2$, a reduced, coordinatively unsaturated ML_4 center adds substrate to yield an octahedral, two-electron oxidized metal center.[170] The same is true of $M_2Cl_4(dppm)_2$ inasmuch as the ML_4 fragments composing the quadruply bonded metal-metal core are oxidized to yield a two-electron oxidized ESBO. The analogy is even more striking when a chemically-distorted ESBO is considered. A ML_4 fragment provides the reducing equivalent to and accepts two terminal ligands from its ML_4 neighbor thereby creating a single active site susceptible to substrate addition. More practically, the presence of a chemically distorted intermediate is necessary for $M_2Cl_4(dppm)_2$ photochemistry. As transient spectroscopy shows, the $^1(\delta\delta^*)$ excited state is too short for its reaction with

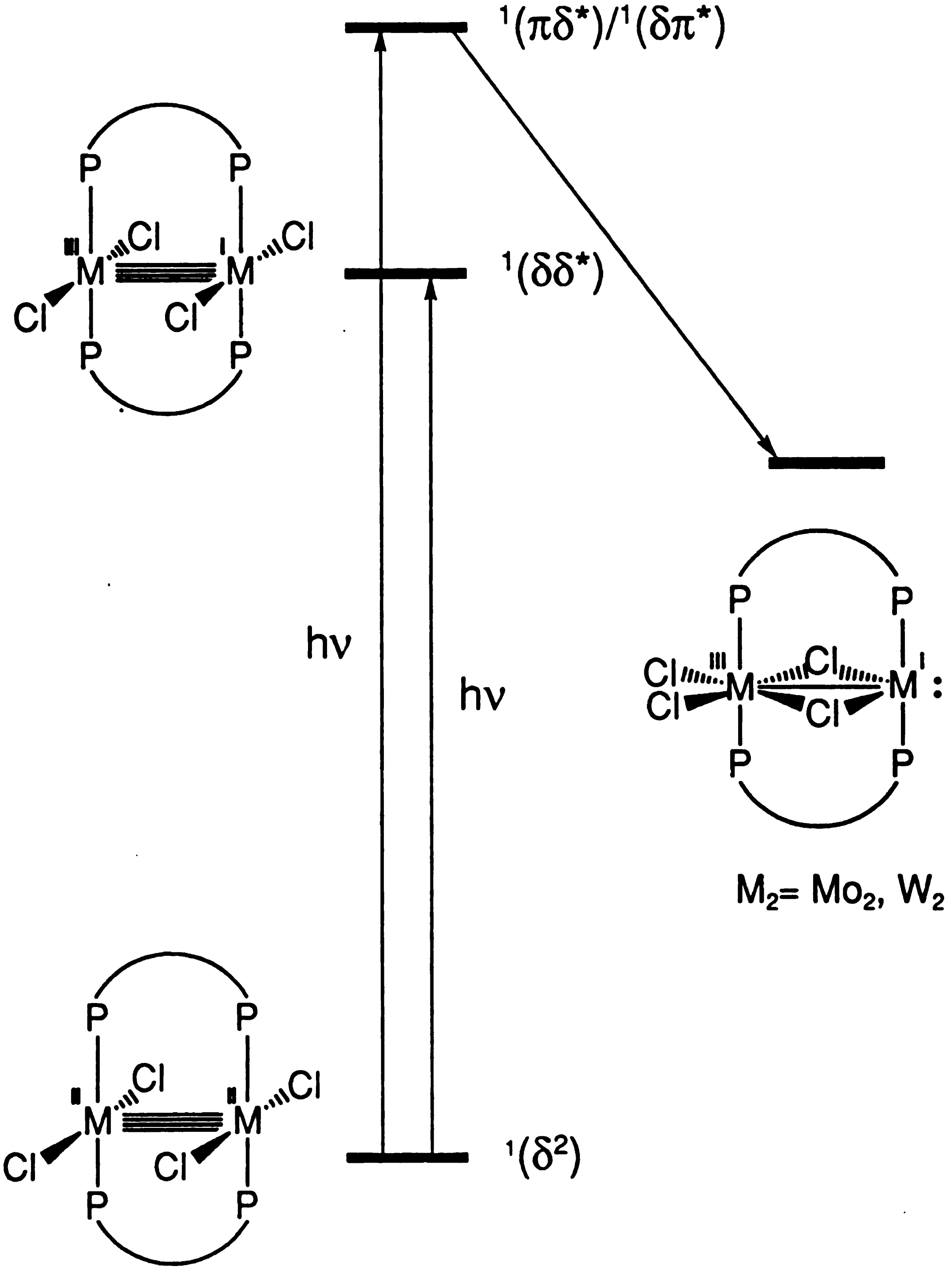

Figure 4.11 Energy level diagram summarizing the formation of the edge-sharing bioctahedral distortion of the $^1(\pi\delta^*)$ (or $^1(\delta\pi^*)$) excited state of the $M_2Cl_4(PP)_2$ complexes to stabilize the charge transfer mixed-valence state.

substrate. However a chemically distorted intermediate provides a means of trapping the charge separated character of the metal-localized excited states of quadruply bonded metal-metal complexes at sufficiently long lifetime to permit their reaction with substrate.

E. Proposed Mechanism

Although the characteristic $^2(\delta \rightarrow \delta^*)$ absorption of the mixed-valence $M^{II}M^{III}$ species in the near-infrared region is not observed during the course of the photoreaction of $Mo_2Cl_4(dppm)_2$ with PhSSPh, this does not necessarily exclude the possibility of a one-electron reaction sequence. It has been shown that the photoreaction of $Mo_2Cl_4(dppm)_2$ in the presence of PhSSPh and TolSSTol (Tol = $CH_3C_6H_5$) yields a cross-over product, $Mo_2Cl_4(dppm)_2(STol)(SPh)$, in addition to the formation of $Mo_2Cl_4(dppm)_2(SPh)_2$ and $Mo_2Cl_4(dppm)_2(STol)_2$.[131] The presence of the mixed crossover product $Mo_2Cl_4(dppm)_2(SPh)(STol)$ appears to support a radical pathway as follows,

$$M_2^{II,II}Cl_4(dppm)_2 \xrightarrow{h\nu} M_2^{II,II}Cl_4(dppm)_2^* \qquad (4.3)$$

$$M_2^{II,II}Cl_4(dppm)_2^* + RSSR \longrightarrow M_2^{II,III}Cl_4(dppm)_2(SR) + \bullet SR \qquad (4.4)$$

$$\begin{tikzcd}
2M_2^{II,III}Cl_4(dppm)_2(SR) \arrow[r, "\bullet SR"] \arrow[dr, "\bullet Cl"'] & M_2^{III,III}Cl_4(dppm)_2(SR)_2 + M_2^{II,II}Cl_4(dppm)_2 \quad (4.5) \\
 & M_2^{III,III}Cl_5(dppm)_2(SR) + M_2^{II,II}Cl_3(dppm)_2(SR) \quad (4.6)
\end{tikzcd}$$

The primary step involves one-electron oxidation of electronically excited $M_2^{II,II}Cl_4(dppm)_2$ by the substrate RSSR to yield the mixed valence $M_2^{II,III}Cl_4(dppm)_2(SR)$ intermediate. Disproportionation upon Cl atom abstraction yields $M_2^{II,III}Cl_5(dppm)_2(SR)$ and $M_2^{II,II}Cl_3(dppm)_2$. Alternatively, disproportionation by •SR atom transfer generates $M_2^{III,III}Cl_4(dppm)_2(SR)_2$ and $M_2^{II,II}Cl_4(dppm)_2$. The formation of the $Mo_2Cl_5(dppm)_2(SR)$ is consistent with what we have previously observed for the formation of $W_2Cl_5(dppm)_2Y$ and $W_2Cl_4(dppm)_2Y_2$ photoproducts upon the photolysis of the parent quadruple bond complex in the presence of substrate Y—Y (e.g. alkyl iodides).[157,171] The $W_2Cl_4(dppm)_2$ complex photoreacts with substrate to produce a mixed-valence primary photoproduct that disproportionates by either chlorine or Y atom transfer. A similar disproportionation mechanism involving halogen atom transfer between mixed-valence intermediates for the photochemical reaction of diplatinum pyrophosphite with aryl halides has been proposed.[172] For the case here, only $Mo_2Cl_5(dppm)_2(SR)$ is observed in the disproportionation due to the limited stability of $Mo_2Cl_4(dppm)_2(SR)_2$, which further converts to $Mo_2Cl_5(dppm)_2(SR)$.

Nevertheless, the possibility for direct addition to the bimetallic core in a two electron step. While the crossover experiments with TolS—STol and PhS—SPh appear to exclude this possibility, this experiment should be carried out again under more careful conditions. The crossover photoproducts were isolated only by FAB/MS. Moreover, TolS—STol and PhS—SPh will form STol—SPh standing in room light. Until these experiments are carefully performed, the precise mechanism remains undefined.

III. Conclusion

From the observations above, we conclude that the photochemical pathways differ from the thermal reaction routes. $Mo_2Cl_5(dppm)_2(SR)$ compounds can be prepared cleanly by photolysis of $Mo_2Cl_4(dppm)_2$ in the presence of RSSR. The photoreaction to produce these compounds in high yields is completely general. We believe that the previous preparation[113] of $Mo_2Cl_5(dppm)_2(SPh)$ was actually obtained photochemically and not thermally since no product formation is observed when the reaction is carried out in complete absence of light, even when solutions are heated to the boiling point of toluene. The production of $Mo_2^{III,III}Cl_5(dppm)_2(SR)$ and $Mo_2^{III,III}Cl_4(dppm)_2(SR)_2$ may occur by the free radical chemistry of eqs. 4.3-4.6. Alternatively these two products could form from the direct addition of persulfide to the bimetallic core. Notwithstanding these intimate mechanistic details, the wavelength dependence of quantum yields coupled with transient studies clearly indicates that the photochemistry is derived from metal-localized MMCT excited state of the bimetallic complex.

CHAPTER V

CHARGE TRANSFER PHOTOCHEMISTRY OF QUADRUPLY BONDED DITUNGSTEN HALOPHOSPHINE COMPLEXES

I. Background

A comaprison of the photochemistry of the Mo_2O_8 and $M_2X_4(P\,P)_2$ compounds shows that the ligands about the bimetallic core play an important role in determining the oxidation-reduction photochemistry of $M\overset{4}{-}M$ complexes. The photochemistry of these classes of $M\overset{4}{-}M$ complexes is the scheme below,

$M\overset{4}{-}M$ (D_{4h}) Complexes

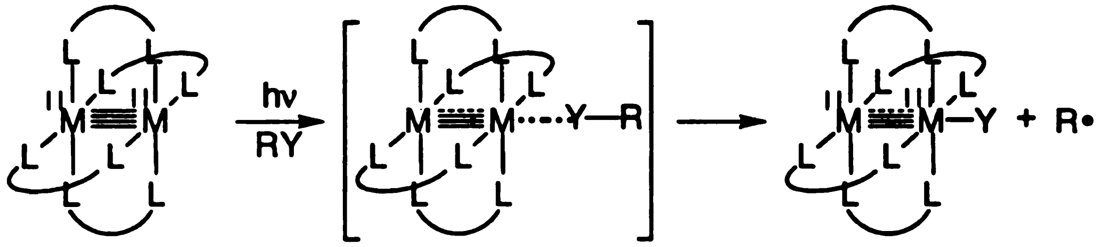

$M\overset{4}{-}M$ (D_{2h}) Complexes

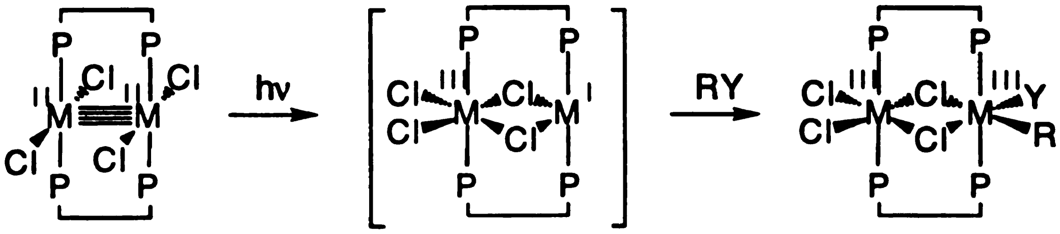

The bimetallic core is oxidized by either one or two electrons, depending on the coordination environment of the $\mathrm{M}\overset{4}{-}\mathrm{M}$ center. A $M_2^{III,III}$ core necessarily demands that the coordination number of the bimetallic core increase. This can not be accommodated by the 'lantern' geometry of the Mo_2O_8 compounds and the $\mathrm{M}\overset{4}{-}\mathrm{M}$ photoproduct is oxidzed by a single electron. However, when two of the bidentate ligands are replaced by terminal ligands of the D_{2h} complexes, complementary redox reactivity of both metal centers is achieved. As described in Chapter IV, two-electron photoreduction of substrate (RY) is accomplished by the D_{2h} class of $\mathrm{M}\overset{4}{-}\mathrm{M}$ complexes, $M_2X_4(P\ P)_2$, to yield a d^3—d^3 edge-sharing bioctahedron species (ESBO).[171] Here, the photochemistry is facilitated by the ability of the ligand coordination sphere to stabilize the d^3—d^3 core by providing an octahedral geometry about each of the oxidized metal centers.

Can the multielectron photochemistry of $\mathrm{M}\overset{4}{-}\mathrm{M}$ compounds be generalized toclasses of compounds other than the D_{2h} systems? We decided to investigate the $M_2Cl_4(PR_3)_4$ complexes, which are structurally congruent to $M_2X_4(P\ P)_2$,

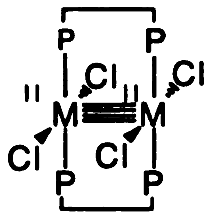

D_{2h}

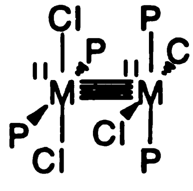

D_{2d}

As with their D_{2h} $M_2X_4(P\ P)_2$ homologs, the $M_2X_4(PR_3)_4$ complexes may also undergo two-electron redox chemistry. These complexes are capable of sustaining bioctahedral geometries in either edge-sharing (ESBO) or face-sharing (FSBO) conformations,[173]

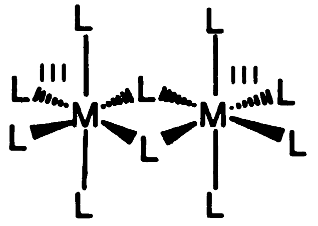

ESBO

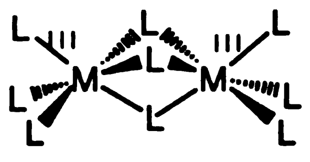

FSBO

These structural types are prevalent in the thermal oxidative-addition chemistry of $M_2X_4(PR_3)_4$ species. For instance, oxidiation of $Mo_2X_4(PMe_3)_4$ by I_2 (X = I),[173b] or $PhICl_2$ (X= Cl)[137f] results in formation of the FSBO complex, $Mo_2X_7(PMe_3)_2^-$ with the loss of two phosphines. In the case of labile phosphines such as PEt_3, $P(n\text{-}Pr)_3$, $Mo_2Cl_4(PR_3)_4$ thermal reacts with CCl_4 and to yield $Mo_2Cl_9^{3-}$.[174] Reaction of dimolybdenum complexes to ESBOs by simple oxidative-addition is more unusual. Attempts to generate these species by oxidation of $Mo_2Cl_4(PR_3)_4$ by $NOPF_6$[175] or electrolysis often leads to decomposition of the oxidized product.[176] In contrast, ditungsten ESBO complexes do exist, but they are obtained from reduction of WCl_4 with one equivalent of sodium amalgam.[177] Attempts to convert $WCl_3(PR_3)_3$ to either the known $W_2Cl_6(PR_3)_4$ ESBO complex or the known $W_2Cl_6(PR_3)_3$ FSBO complex have also failed.[173c]

The parallels in the reaction chemistry of $M_2X_4(PR_3)_4$ (D_{2d}) and $M_2X_4(PP)_2$ (D_{2h}) complexes to produce bioctahedral, two-electron products might suggest that these complexes will exhibit similar photochemistry. However such a correlation is based on ground state reactivity alone and it does not consider the nature of the excited state. Although the D_{2d} and D_{2h} $M\overset{4}{-}M$ halophosphine complexes possess $^1(\delta\delta^*)$ as their lowest energy excited state, the excited states to higher energy are of different parentages for the two classes of complexes. The absorption spectra for $M_2X_4(PR_3)_4$ complexes are dominated by ligand-to-metal charge transfer (LMCT) transitions in the near-ultraviolet spectral region[162] whereas $M_2X_4(P\ P)_2$ complexes display metal localized, near-ultraviolet absorptions.[163] Accordingly replacement of these metal-localized states by the LMCT states of the D_{2d} complexes may be manifested by significantly divergent photochemistry.

Accordingly, studies were undertaken to compare the photochemistry of $M\overset{4}{-}M$ D_{2d} complexes to their D_{2h} counterparts. Specifically, we have investigated the visible and near-ultraviolet photochemistry of $W_2Cl_4(PR_3)_4$ (PR_3 = PMe_3, PMe_2Ph, PBu_3) in CH_2Cl_2 and benzene. The photochemistry of $Mo_2Cl_4(PR_3)_4$ (PR_3 = PEt_3, $PEtPh_2$, PBu_3) complexes has previously been investigated,[85] but the excitation wavelengths were in the hard ultraviolet (λ_{exc} = 254 nm). Under these high energy conditions, photodegradation of the complex was observed to yield $Mo_2Cl_9^{3-}$. Rupture of the metal-metal bond is not found in the case of $Mo_2Cl_4(PR_3)_4$ in halocarbon solvents, either, despite the existence of the stable $MoCl_{4-x}(PR_3)_{2+x}$ ($x = 2, 3, 4$) monomers.[178] In our studies, by moving to lower energy excitation wavelengths, $W_2Cl_4(PR_3)_4$ smoothly converts to photooxidized bimetallic products. The observed photochemistry is correlated with photophysic studies of time-resolved absorption and emission spectroscopies. These results are compared to those obtained from our photochemical studies of the $W_2Cl_4(P\ P)_2$ homologs described in Chapter IV.

II. Results

A. Photochemistry of $W_2Cl_4(PR_3)_4$

Dichlorocarbon solutions of $W_2Cl_4(PR_3)_4$ are indefinitely stable in the absence of light. However, irradiation in the near ultraviolet ($300 < \lambda_{exc} < 400$ nm) engenders prompt reaction at room temperature. The photochemistry is similar for the three phosphine complexes, and it is exemplified by the absorption spectral changes for $W_2Cl_4(PMe_3)_4$, shown in Figure 5.1. The disappearance of the $^1(\delta^2 \rightarrow \delta\delta^*)$ band at 655 nm is accompanied by the appearance of an intense near infrared absorption at 1340 nm and weaker absorption bands at 419 and 383 nm. Isosbestic points are maintained at 584 and 313 nm during the early stages of the photolysis. The near-infrared absorption is a signature of the $^2(\delta \rightarrow \delta^*)$ transition for a $W_2^{II,III}$ mixed-valence compound, as described in Chapter III. With continued photolysis, the near-infrared and visible absorptions completely disappear with the concomitant growth of an absorption at 483 nm. The isolated product exhibits a parent ion peak of 808 amu in the FAB/MS and ^{31}P NMR spectra of the final photoproduct show two singlets with a 2:1 intensity, consistent with the production of the previously characterized $W_2Cl_6(PMe_3)_3$ face-sharing bioctahedron.[177,179] Photochemistry of $W_2Cl_4(PBu_3)_4$ shows the same results. The final product is also characterized by FAB/MS and ^{31}P NMR spectra shown in Figures 5.2 and 5.3. When the dihalocarbon is dichloroethane, similar $W_2Cl_4(PMe_2Ph)_4$ photochemistry is observed with the photoreduction of dichloroethane signified by the disappearance of the $^1(\delta^2 \rightarrow \delta\delta^*)$ transition at 667 nm and the concomitant growth of the mixed-valence $W_2^{II,III}$ absorption at 1360, 427 and 343 nm as shown in Figure 5.4.

As inferred from electronic absorption spectra, solutions displaying the near-infrared absorption band are paramagnetic. The X-band EPR spectrum of a frozen CH_2Cl_2/2-MeTHF solution (T = −170 °C) collected at an intermediate stage of the photolysis (Figure 5.5) displays an axial doublet, $g_{\parallel} = 1.950$ and $g_{\perp} = 1.855$. Similar signals have been observed from many mixed-valence $M\overset{3.5}{—}M$ species such as $Mo_2[O_2P(OC_6H_5)_2]_4^+$, $Mo_2(HPO_4)_4^{3-}$ and $Mo_2(SO_4)_4^{3-}$ and they indicate a species in which the unpaired electron is coupled between two equivalent tungsten nuclei.[180] The disappearance of the near-infrared band is accompanied by a similar disappearance of the EPR signal.

Figure 5.1 Electronic absorption spectral changes during the photolysis (λ_{exc} > 375 nm) of $W_2Cl_4(PMe_3)_4$ in deoxygenated dichloromethane at 15.0 °C at ~5 h intervals. Panel (a) shows the photolysis reaction proceeding to a maximum absorption in the near-IR region. Panel (b) shows the spectral changes occurring with continued photolysis of the solution. The absorbance scale of the near-infrared relative to the visible spectral region in both panels is expanded by a factor of 6.

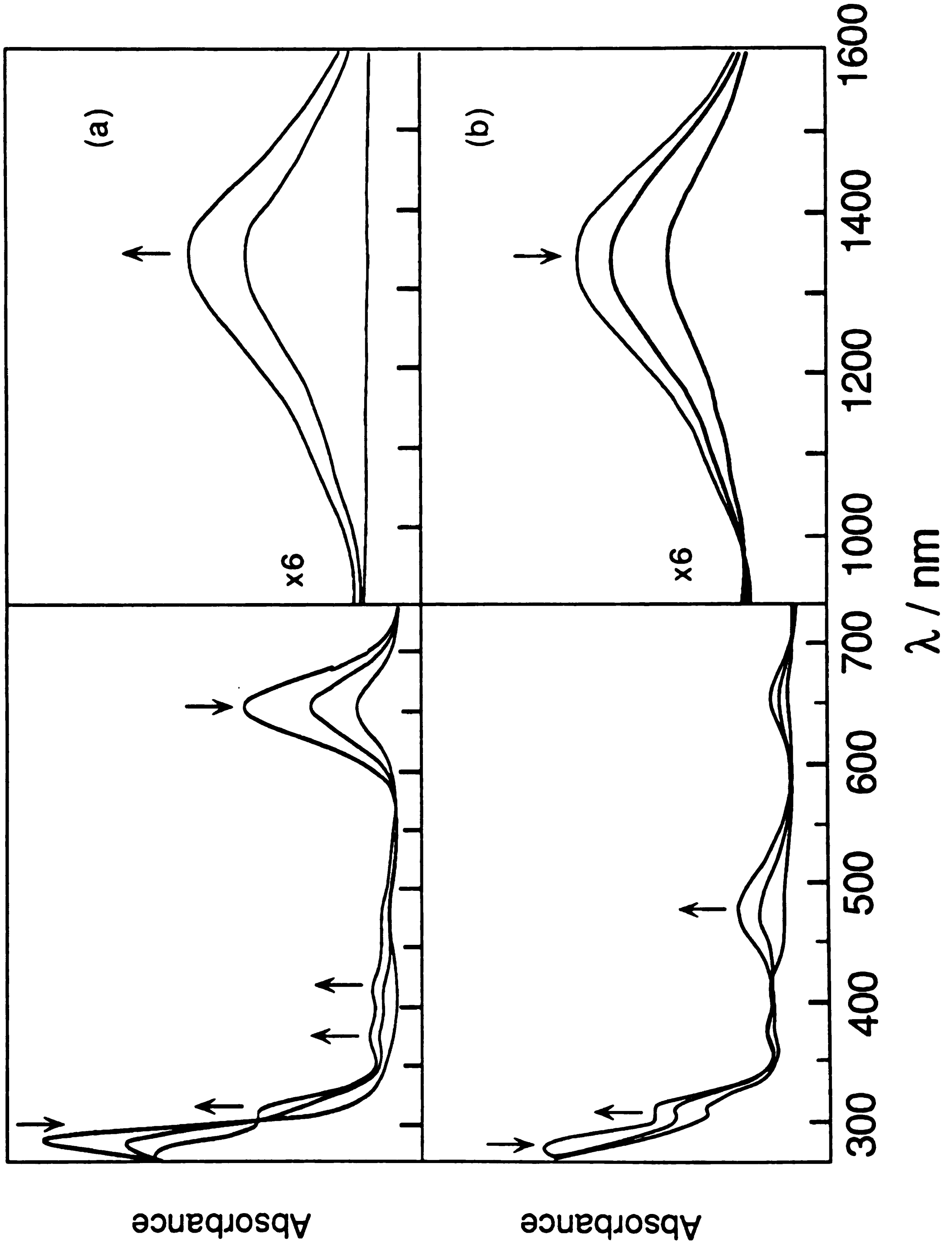
Absorbance
Absorbance
(a)
(b)
x6
x6
300
400
500
600
700
1000
1200
1400
1600
λ / nm

Figure 5.1

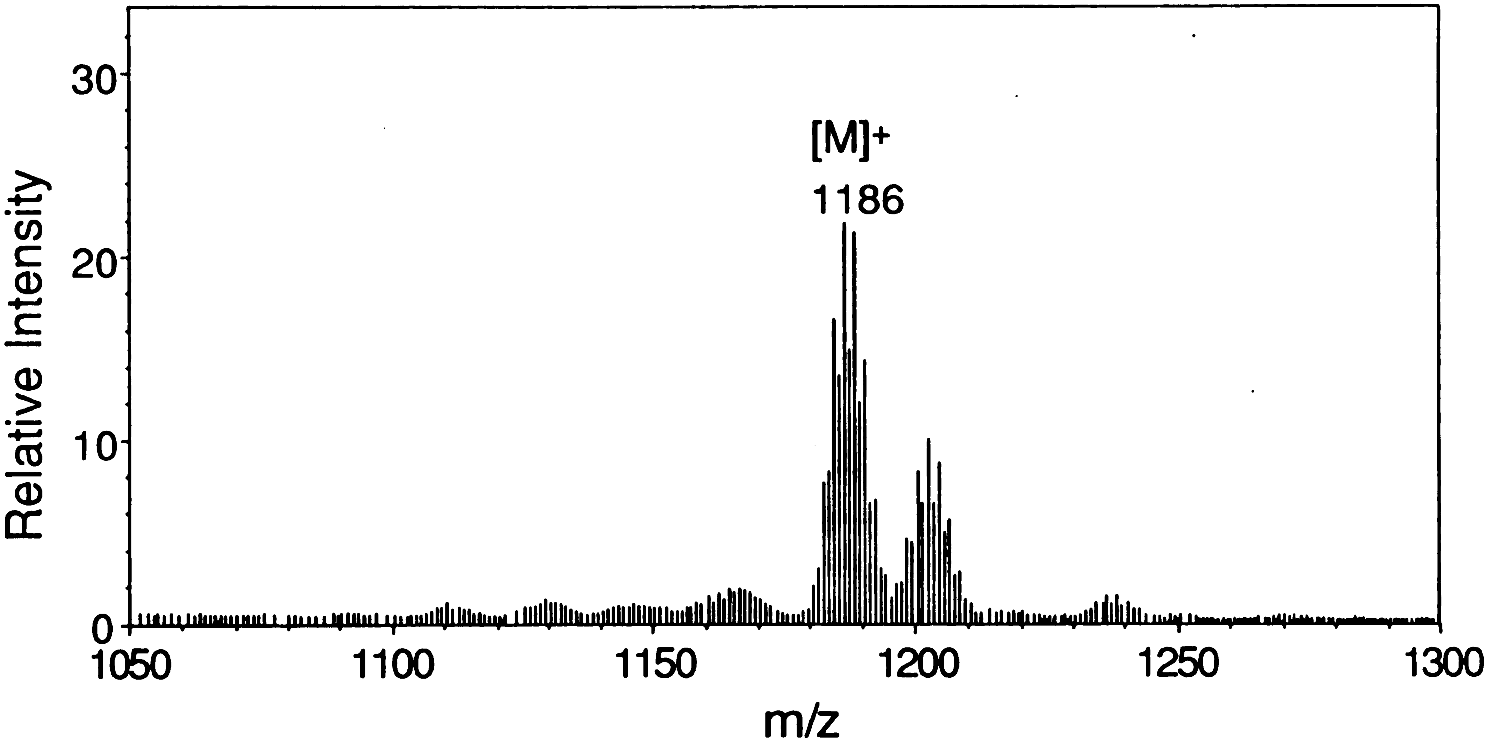

Figure 5.2 FAB-MS spectrum of the final products resulting from the photoreaction of $W_2Cl_4(PBu_3)_4$ with dichloromethane.

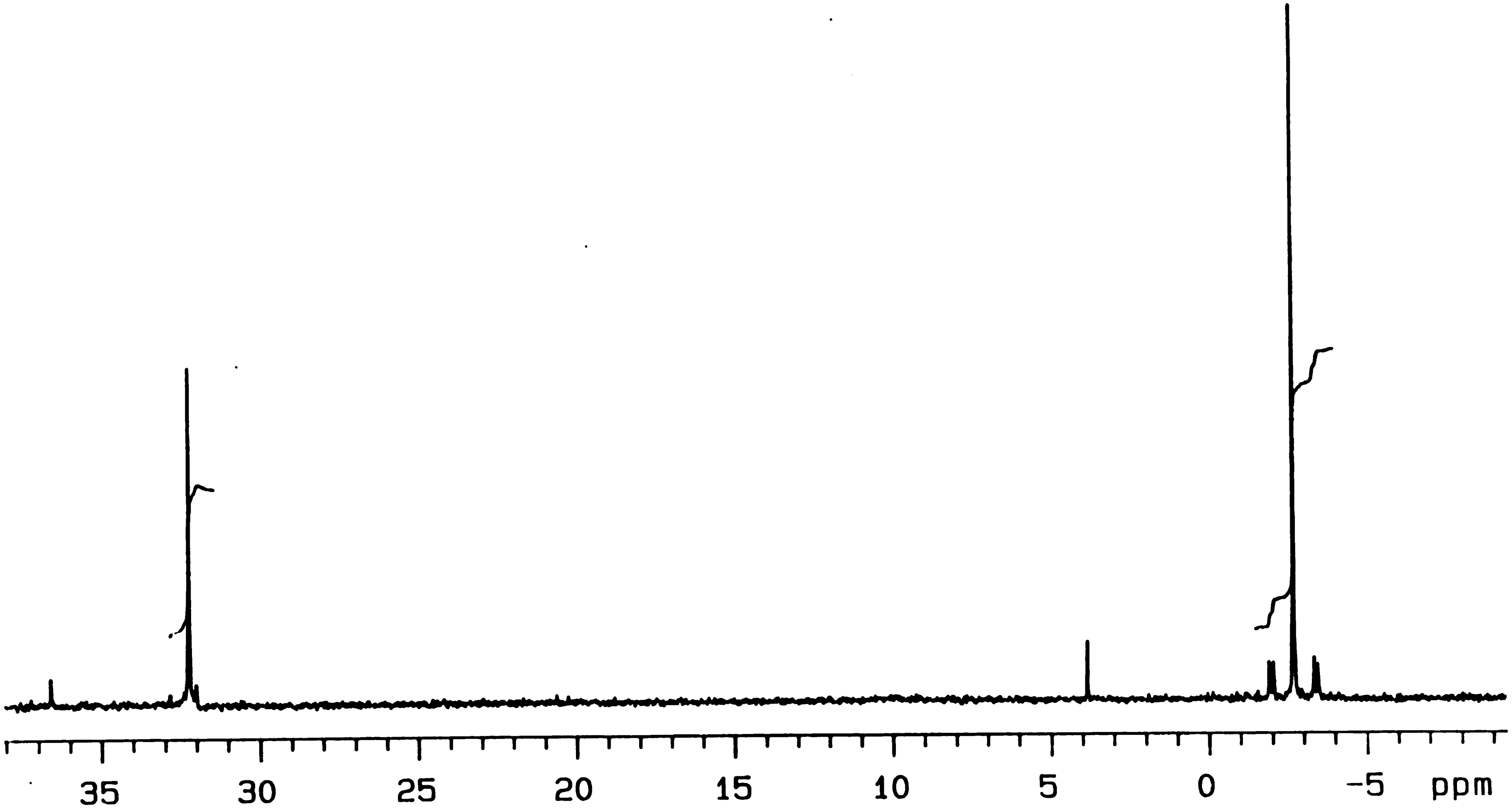

Figure 5.3 ^{31}P NMR spectrum of the final products resulting from the photoreaction of $W_2Cl_4(PBu_3)_4$ with dichloromethane-d_2.

Figure 5.4 Electronic absorption spectral changes during the photolysis (λ_{exc} > 375 nm) of $W_2Cl_4(PMe_2Ph)_4$ in deoxygenated dichloroethane at 15.0 °C at ~6 h intervals. Panel (a) shows the photolysis reaction proceeding to a maximum absorption in the near-IR region. Panel (b) shows the spectral changes occurring with continued photolysis of the solution.

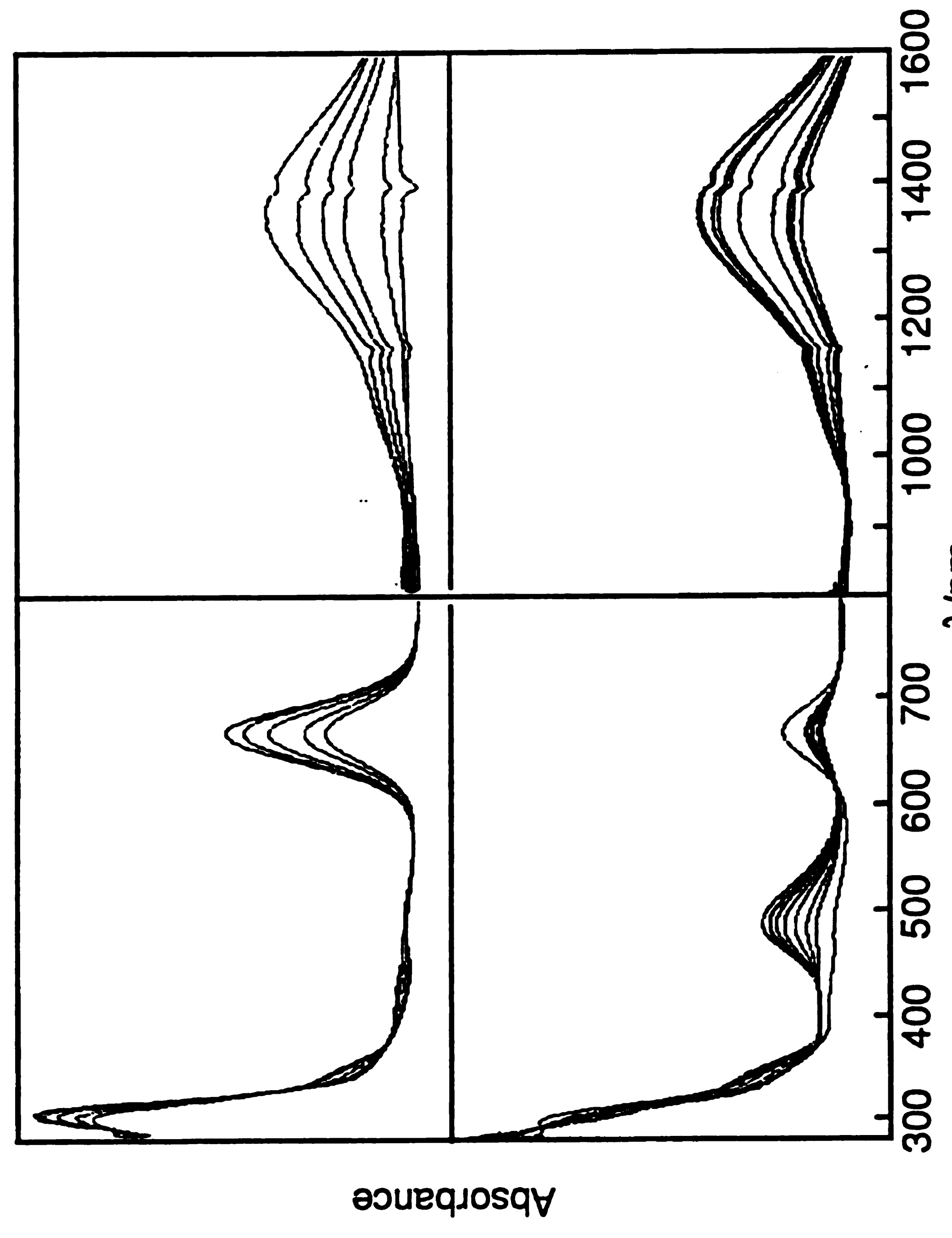

Figure 5.4

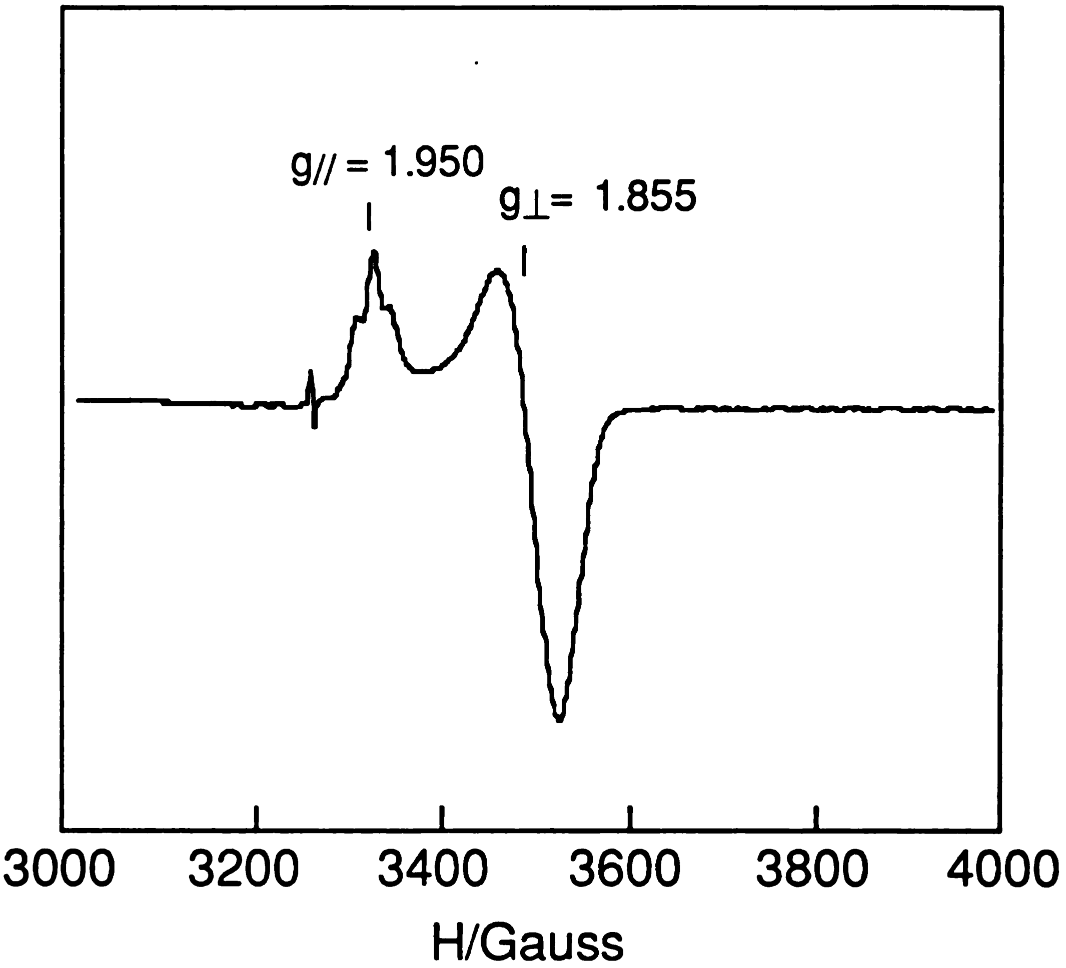

Figure 5.5 The X-band EPR spectrum of $W_2Cl_4(PMe_3)_4$ in frozen CH_2Cl_2/2-MeTHF solutions (T = –170 °C) exhibiting the maximum near-infrared absorption in panel (a) of Figure 5.1.

B. Comparison to Thermal Oxidation Chemistry

The spectroscopic results suggesting the presence of a $W_2^{II,III}$ species during the initial stages of photolysis are substantiated by the thermal oxidation chemistry of $W_2Cl_4(PR_3)_4$ complexes. Dichloromethane solutions of $W_2Cl_4(PMe_3)_4$ are efficiently oxidized by one equivalent of $PhICl_2$ or $NOBF_4$. The absorption spectrum and EPR spectrum of the product obtained by $PhICl_2$ oxidation ($\lambda_{abs,max}$ = 1340, 428, 376, and 315 nm; $g_{||} = 1.952$ and $g_{\perp} = 1.857$) were identical to the spectra obtained by $W_2Cl_4(PMe_3)_4$ photolysis shown in Figures 5.6a and 5.7a. Recently, Cotton and coworkers have characterized the reaction chemistry of $W_2Cl_4(PMe_3)_4$ with $PhICl_2$ by isolating and structurally characterizing the mixed-valence complex, 1,3,6-$W_2Cl_5(PMe_3)_3$.[181] Here, oxidation of the $W_2^{II,II}$ core is accompanied by chloride substitution of phosphine to maintain the overall neutral charge of the complex. An axial doublet EPR signal and near-infrared absorption profile are also observed for the $NOBF_4$ oxidation product of $W_2Cl_4(PMe_3)_4$. However, the spectra of this oxidation reaction, shown in Figures 5.6b and 5.7b, are not the same ($\lambda_{abs,max}$ = 1468, 474, and 375; $g_{||} = 1.980$ and $g_{\perp} = 1.840$) as those obtained from photolysis and $PhICl_2$ thermal oxidation. EPR spectra of one-electron oxidized mixed-valence $W_2^{II,III}$ species for other phosphines, PMe_2Ph and PBu_3, are also shown for comparison in Figures 5.8 and 5.9. As Shrock has shown,[106] NO^+ oxidation of $W_2Cl_4(PR_3)_4$ affords the unsubstituted one-electron oxidized $W_2Cl_4(PR_3)_4^+$ complex in the absence of anionic, coordinating ligands.

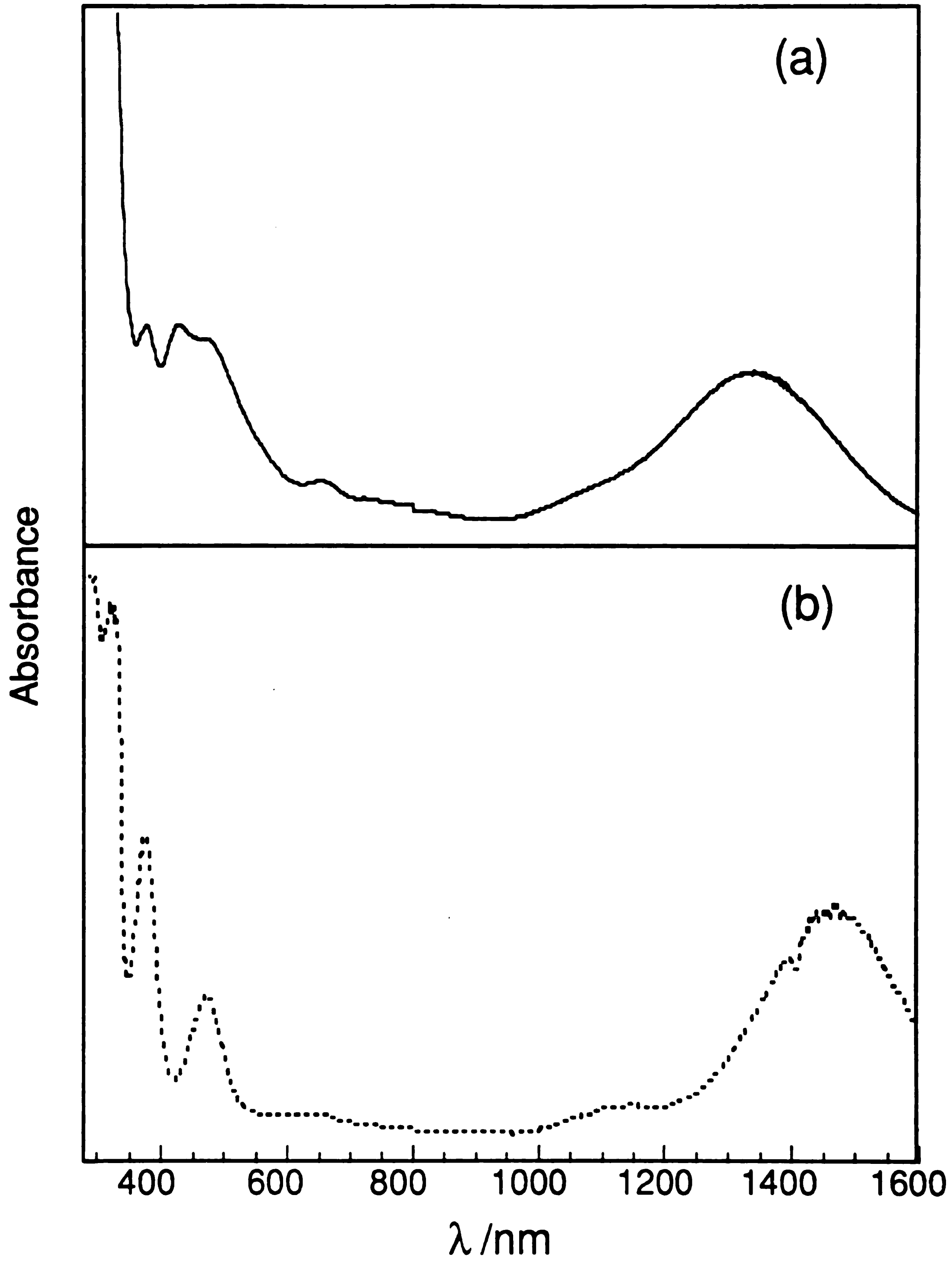

Figure 5.6 Electronic absorption spectra of the product resulting from the thermal oxidation of $W_2Cl_4(PMe_3)_4$ by one equivalent of (a) $PhICl_2$ in dichloromethane (——) (b) $NOBF_4$ in CH_2Cl_2/MeOH solutions(- - - -).

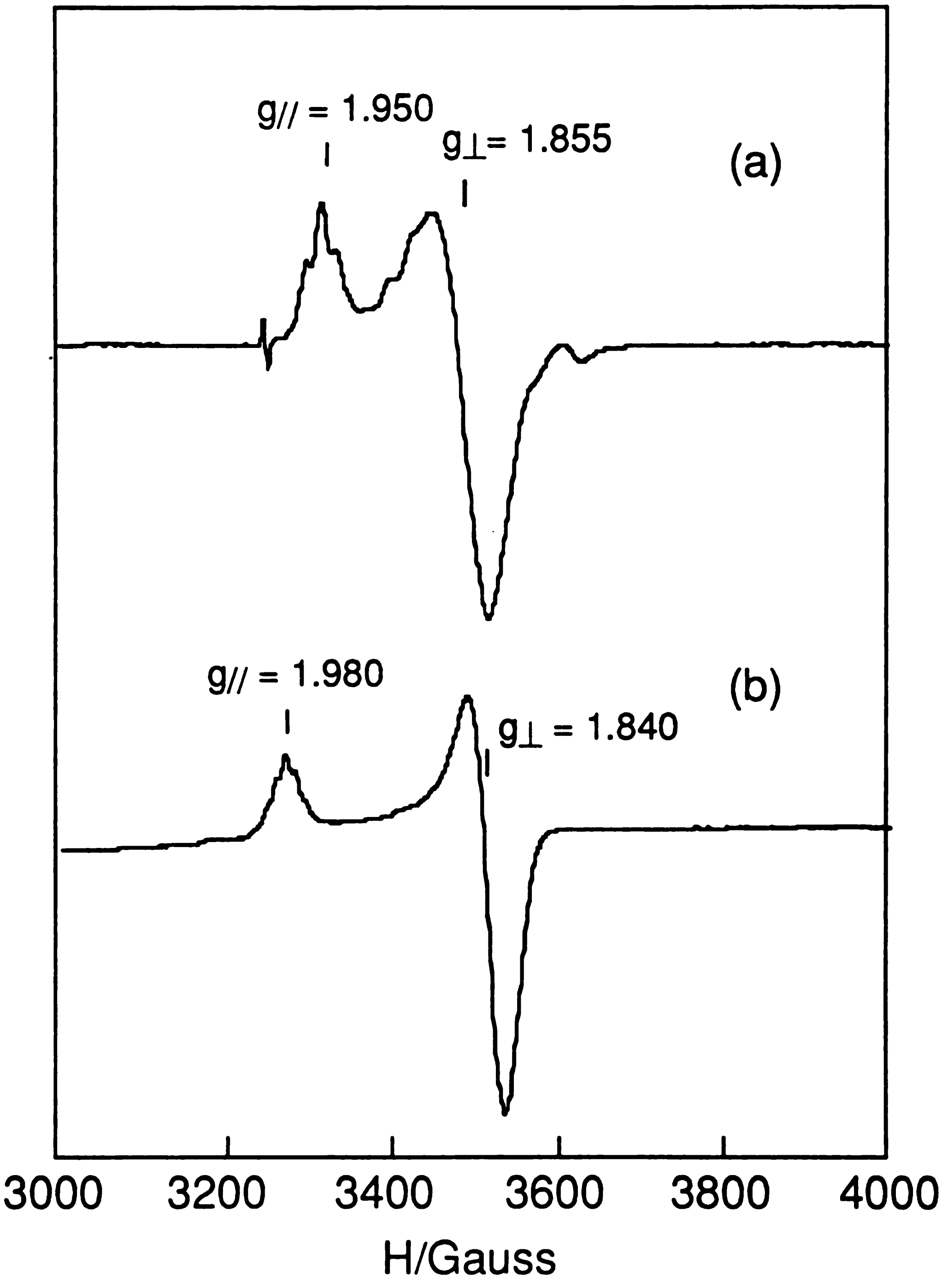

Figure 5.7 The X-band EPR spectrum of the product resulting from the thermal oxidation of $W_2Cl_4(PMe_3)_4$ by one equivalent of (a) $PhICl_2$ in frozen CH_2Cl_2/2-MeTHF solutions (b) $NOBF_4$ in frozen CH_2Cl_2/MeOH solutions. Both spectra are obtained at T = –170 °C.

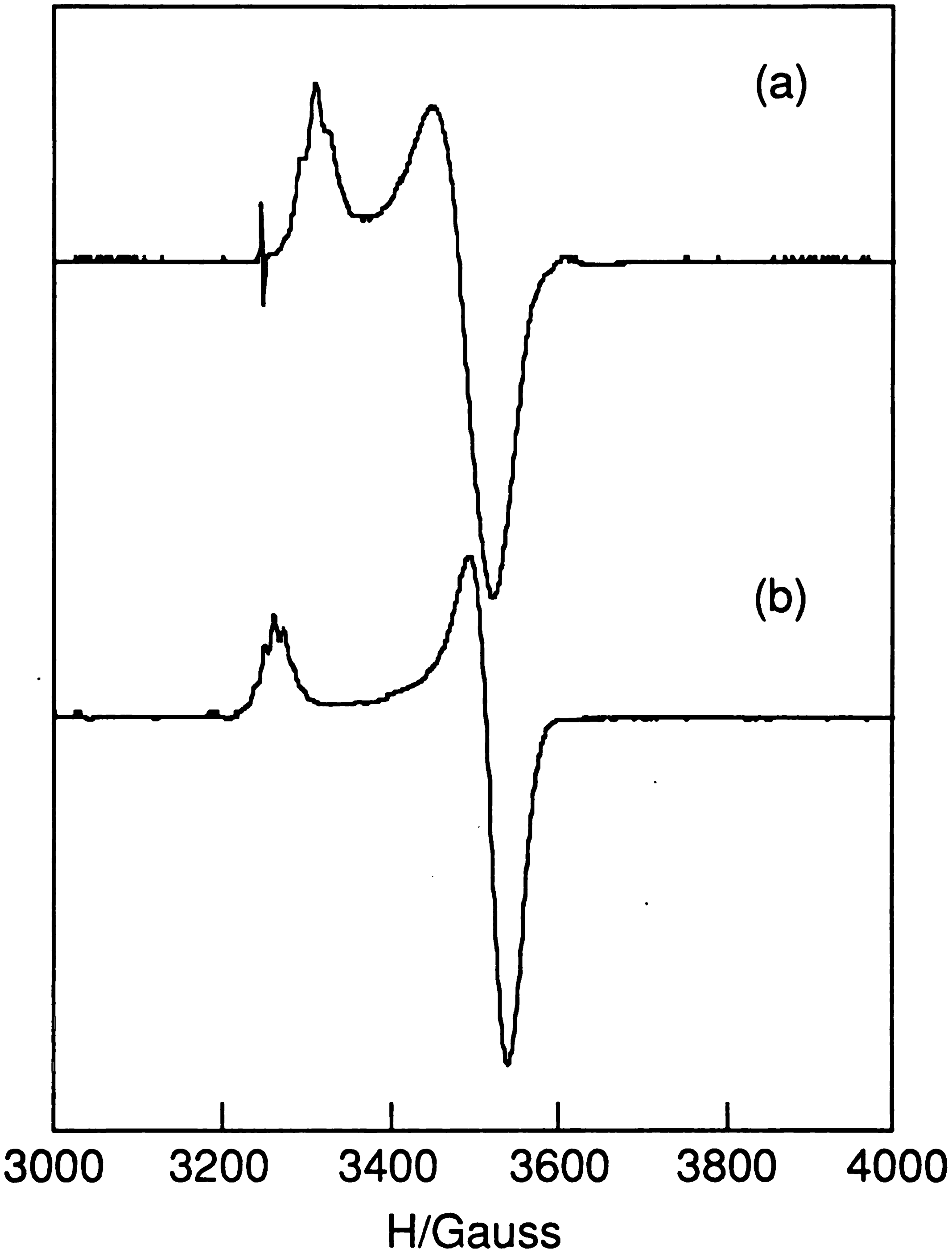

Figure 5.8 The X-band EPR spectrum of the product resulting from the thermal oxidation of $W_2Cl_4(PMe_2Ph)_4$ by one equivalent of (a) $PhICl_2$ in frozen CH_2Cl_2/2-MeTHF solutions (b) $NOBF_4$ in frozen CH_2Cl_2/MeOH solutions. Both spectra are obtained at T = −170 °C.

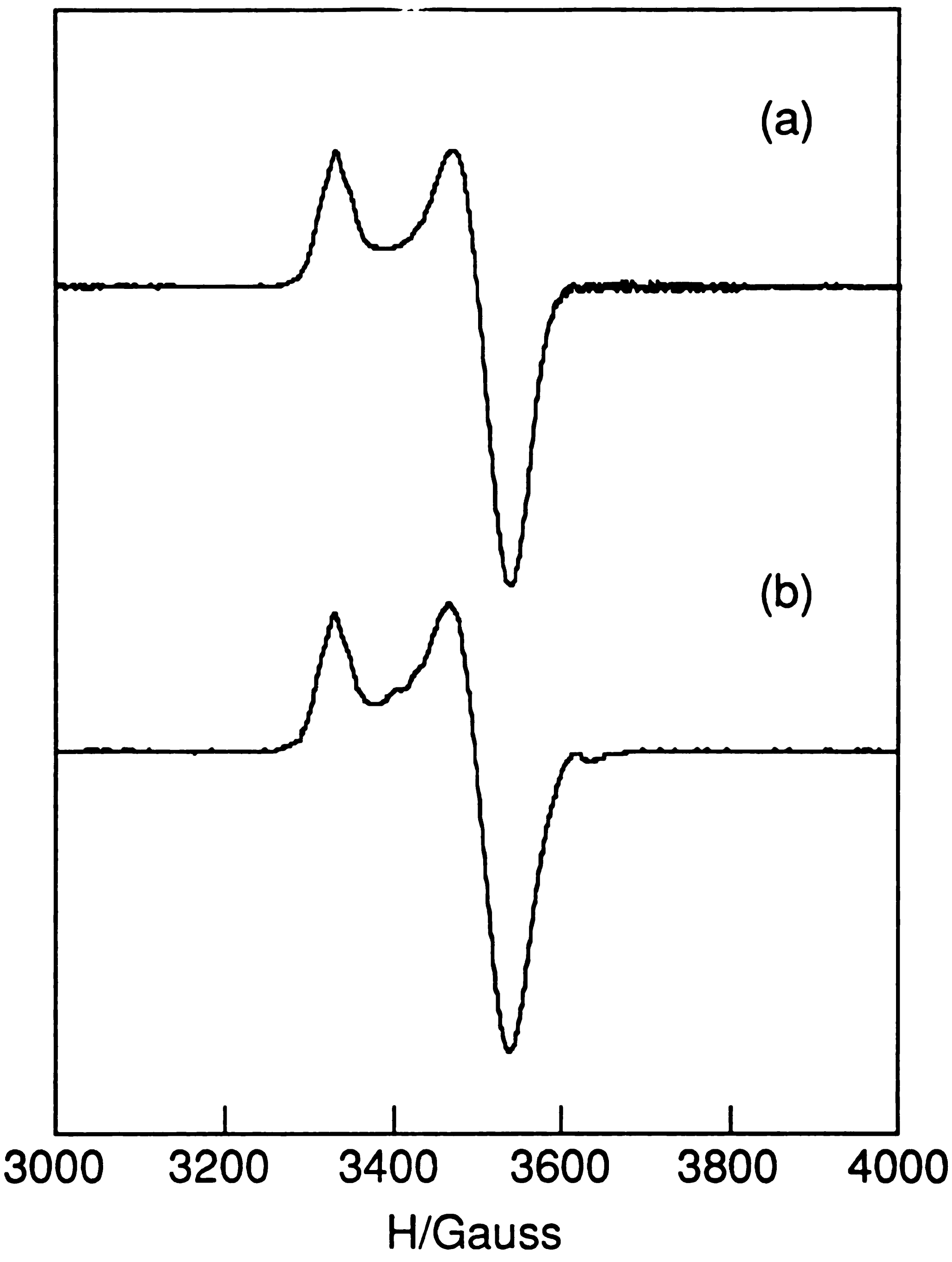

Figure 5.9 The X-band EPR spectrum of frozen CH_2Cl_2/2-MeTHF solutions (T = –170 °C) of (a) the photoproduct exhibiting the maximum near-infrared absorption, and of (b) the product resulting from the thermal oxidation of $W_2Cl_4(PBu_3)_4$ by one equivalent of $PhICl_2$.

C. Organic Photoproduct Analysis

Organic photoproducts of the photoreaction were analyzed by gas chromatography/mass spectrometry (GC/MS). The inset of Figure 5.10a shows a typical GC of the gas collected above photolyzed solutions. Besides a solvent peak (not shown), a single product is observed to elute from the GC column whose mass spectrum is identical to chloromethane (CH_3Cl: $[M]^+ = 50$ m/z, $[M-Cl]^+ = 15$ m/z).[182] An additional product is observed for sufficiently concentrated solutions of the $W_2Cl_4(PR_3)_4$ photoreactant (> 8 mM). Photolyzed solutions exhibit a peak in the gas chromatogram whose intensity increases as the concentration of the photoreactant is increased; GC/MS (Figure 5.10b) shows the exclusive production of dichloroethane ($ClCH_2CH_2Cl$: $[M]^+ = 98$ m/z, $[M - HCl]^+ = 62$ m/z, $[M - HCl - Cl]^+ = 27$ m/z). No photochemical reaction was observed upon irradiation of $W_2Cl_4(PR_3)_4$ complexes in neat CH_3CN or benzene.

D. Photophysics and Transient Absorption Studies

The $W_2Cl_4(PR_3)_4$ complexes all exhibit a red luminescence, which decays monoexponentially, upon excitation of the $^1(\delta^2 \rightarrow \delta\delta^*)$ transition. Table 5.1 lists the luminescence maxima and the lifetime decay constants in benzene and CH_2Cl_2.[183] The excited state lifetimes are typical of $^1(\delta\delta^*)$ excited states, as is the slight shift of the emission band to lower energies and increased bandwidth with increasing solvent polarity. Solvent dependent photophysical properties of the $^1(\delta\delta^*)$ excited state have been observed previously[184] and they are consistent with solvent stabilizing the zwitterionic character of excited states associated with the population and depopulation of the δ/δ^* levels.[94] The correlation of the shorter lifetimes with decreasing emission energy in Table 5.1 follows expected

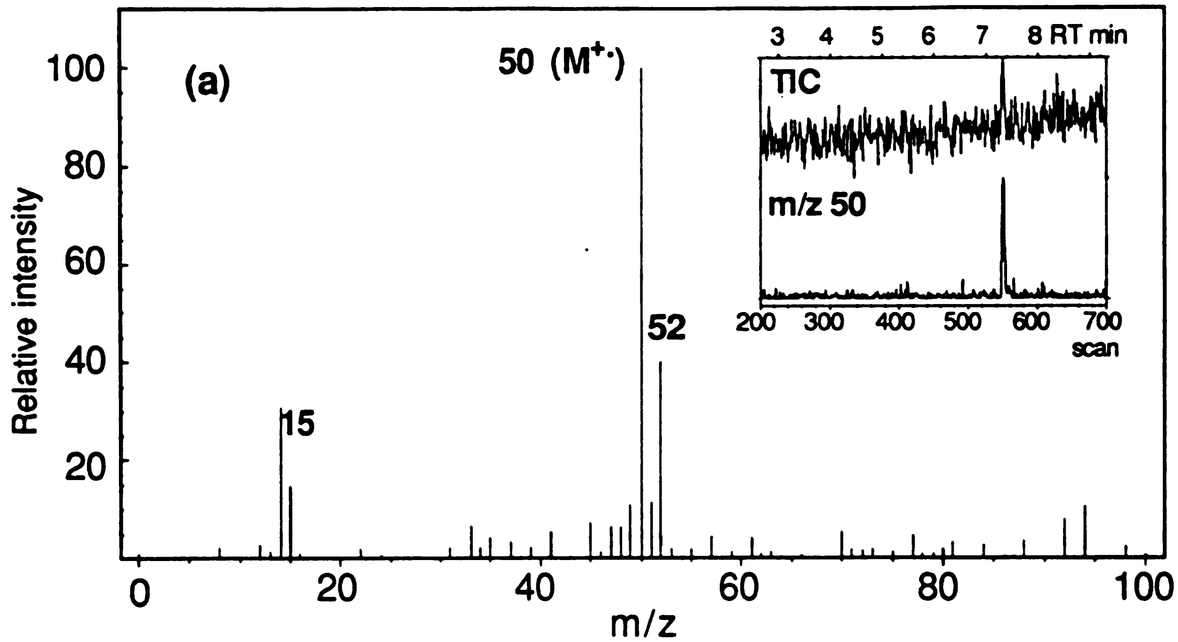

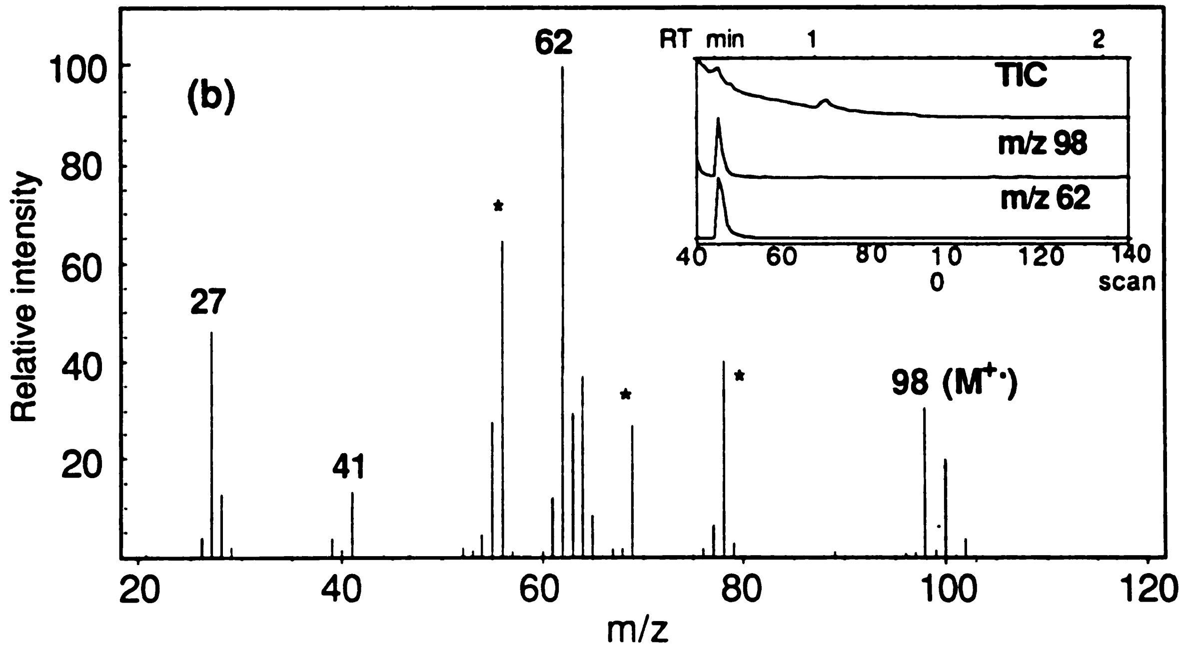

Figure 5.10 Gas chromatogram (inset) of (a) the volatile organic products resulting from the photolysis reaction of $W_2Cl_4(PMe_3)_4$ (1.5 mM) in CH_2Cl_2. (b) the coupling product resulting from dimeration of chloromethyl radicals at higher concentrations. The retention times during which the CH_2Cl_2 solvent peak elutes from the GC column is shown on the side.

Table 5.1 Photophysical properties of $W_2Cl_4(PR_3)_4$ complexes in benzene and dichloromethane at room temperature.

$W_2Cl_4(PR_3)_4$	in benzen		in CH_2Cl_2	
	$\lambda_{em,max}$ / nm[a]	τ/ns	$\lambda_{em,max}$ / nm[a]	τ/ns
PMe_3	717 (850)	50	719 (961)	41
PMe_2Ph	728 (676)	43	731 (749)	43
PBu_3	723 (784)	54	723 (859)	44

[a] The values in parantheses indicate the emission band's full-width at half-maximum in cm^{-1}.

energy gap considerations,[185] which predict an increase in the nonradiative decay rate constant with decreasing energy gap.

The transient absorption spectra of $W_2Cl_4(PR_3)_4$ complexes have been measured in dihalocarbon (e.g. CH_2Cl_2) and hydrocarbon (e.g. benzene) solvents for excitation of the $^1(\delta^2 \rightarrow \delta\delta^*)$ transition and excitation of states lying in the near-ultraviolet spectral region. Figure 5.11 shows the transient absorption profiles for $W_2Cl_4(PMe_3)_4$ following a 8 ns excitation pulse at 650 nm. The same transient absorption profile is obtained for either solvent. A prominent feature at 350 nm decays monoexponentially to ground state with a lifetime similar to that measured for the luminescence decay of the $^1(\delta\delta^*)$ excited state (see Table 5.1). Concurrent with this absorption decay is the recovery of the $^1(\delta^2 \rightarrow \delta\delta^*)$ bleach at 700 nm over the same time scale thereby establishing the assignment of the transient absorption in Figure 5.11 to the $^1(\delta\delta^*)$ excited state.

Solvent dependent behavior of $W_2Cl_4(PR_3)_4$ transient spectra is observed for solutions excited at higher energy wavelength 355 nm. When the solvent is CH_2Cl_2, $W_2Cl_4(PR_3)_4$ exhibits a transient absorption spectrum after the $^1\delta\delta^*$ excited state has decayed to ground state. As discussed below, the 'transient' appears to result from laser photolysis, which occurs readily for $W_2Cl_4(PMe_3)_4$, thereby complicating the collection of transient absorption data. Because laser photolysis of the sample was diminished for $W_2Cl_4(PBu_3)_4$, we were able to signal average transient data reliably at 355 nm excitation of this complex. As shown in Figure 5.12, a transient absorption maximizing at 370 nm and a transient bleaching at $\lambda > 500$ nm are observed 50 ns after the excitation pulse. The transient spectrum at the longer wavelengths is consistent with the bleach of the $^1(\delta^2 \rightarrow \pi\delta^*)$ ($\lambda = 540$ nm) absorption of the ground state molecule. Addition of the $W_2Cl_4(PBu_3)_4$ ground state absorption spectrum to the difference spectrum

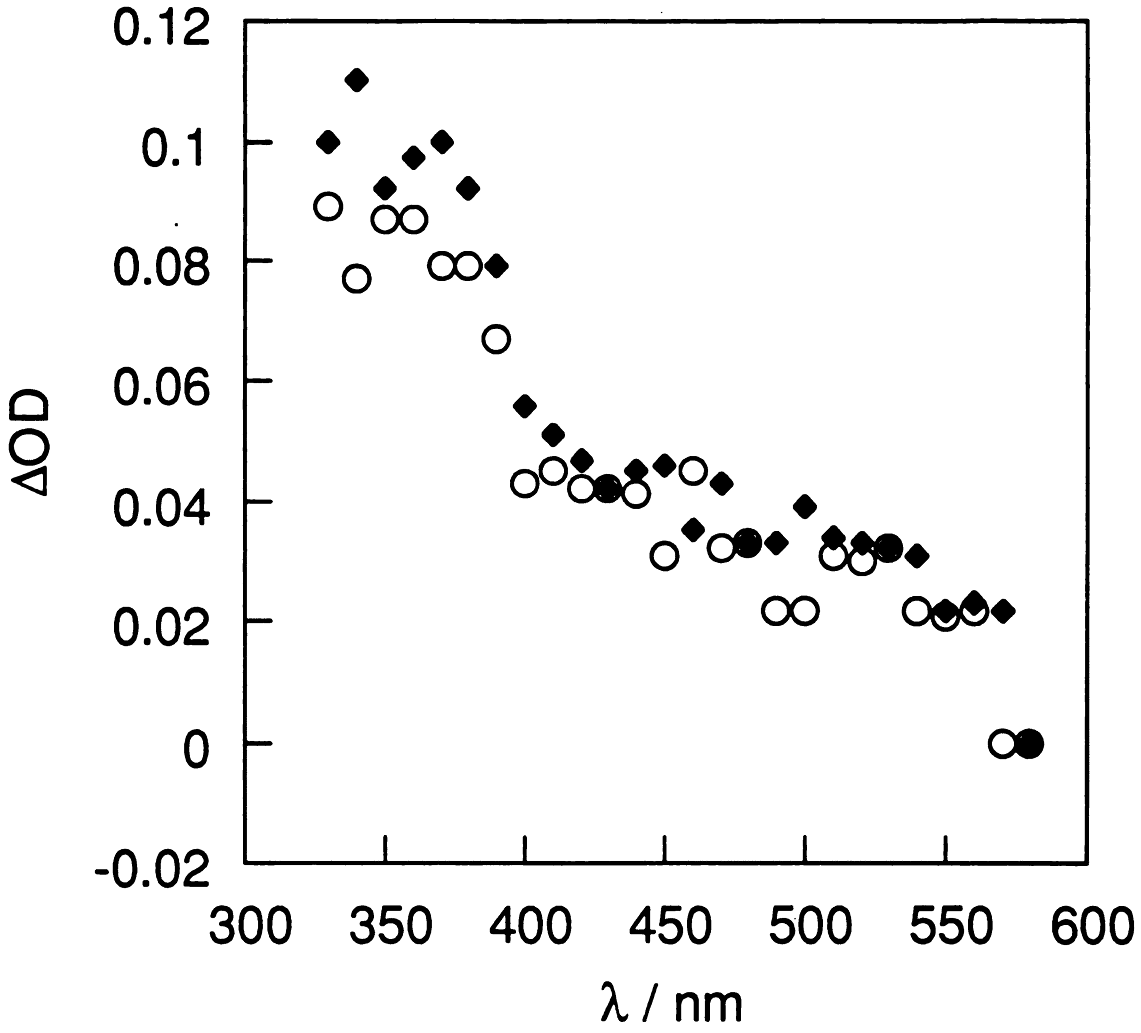

Figure 5.11 Transient difference spectra of $W_2Cl_4(PMe_3)_4$ in deoxygenated dichloromethane (◆) and benzene (O) recorded immediately after a 650 nm, 8 ns laser excitation pulse.

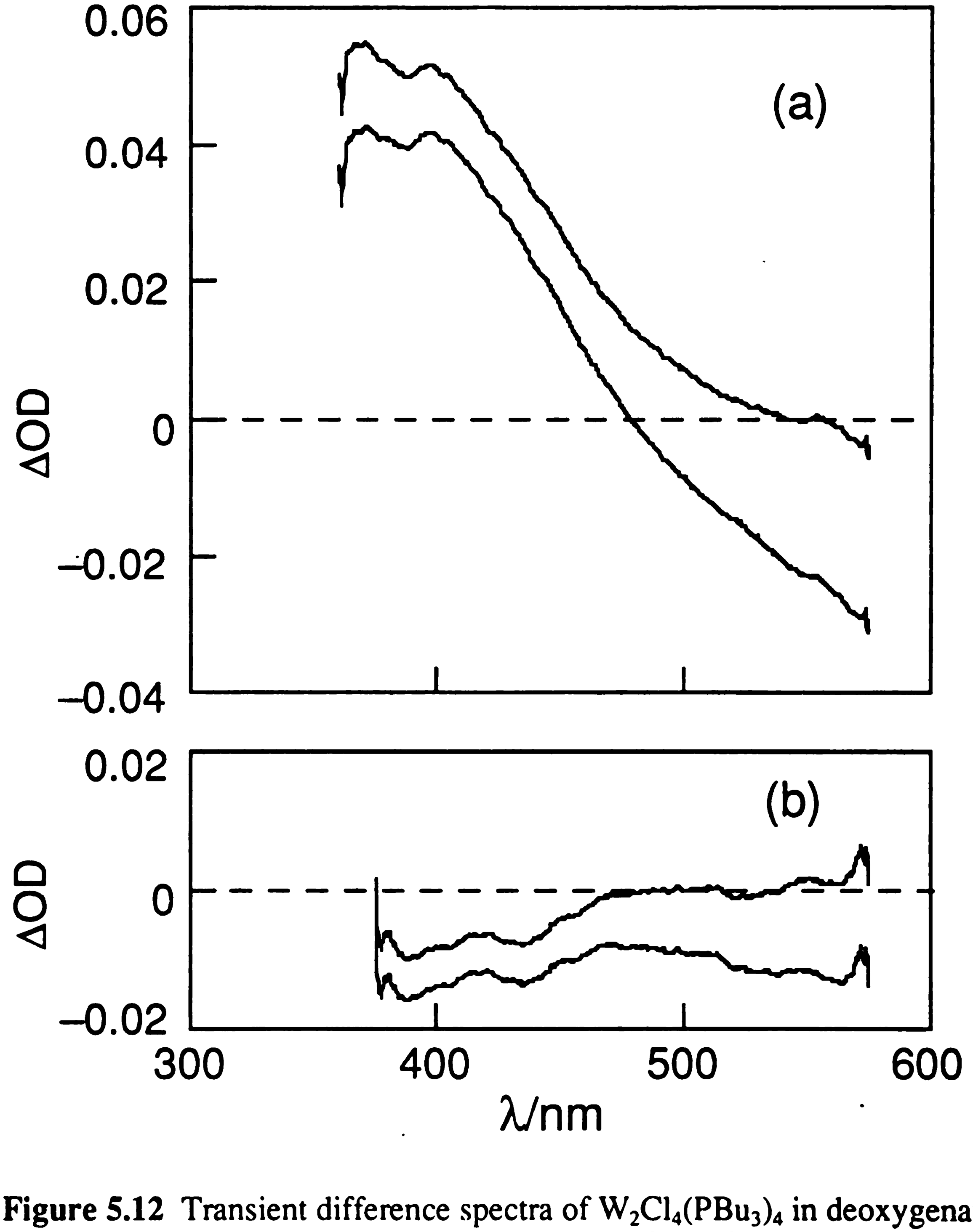

Figure 5.12 Transient difference spectra of $W_2Cl_4(PBu_3)_4$ in deoxygenated (a) dichloromethane and (b) benzene recorded 50 ns after a 355 nm, 10 ns laser excitation pulse. The bottom trace in panels (a) and (b) is the difference spectrum and the top trace is the transient's absorption spectrum generated by the addition of the ground state absorption spectrum of $W_2Cl_4(PBu_3)_4$ to the difference spectrum.

shows the transient to possess two absorption bands between 370 and 420 nm followed by a monotonic decrease to an absorbance = 0 at $\lambda > 500$ nm. An overlay of the absorption spectrum of photolyzed solutions of $W_2Cl_4(PBu_3)_4$ in CH_2Cl_2 (same spectrum as in Figure 5.1) reveals that the transient absorption is in fact the primary photoproduct. Conversely, benzene solutions of $W_2Cl_4(PBu_3)_4$ excited at 355 nm exhibit no transient absorption at times longer than the $^1\delta\delta^*$ excited state lifetime. Figure 5.12b shows only a slight bleach at $\lambda > 500$ nm, and addition of the $W_2Cl_4(PBu_3)_4$ ground state absorption profile to the transient difference spectrum yields a baseline trace.

III. Discussion

Photolysis of $W_2Cl_4(PMe_3)_4$ in CH_2Cl_2 gives a one-electron oxidized $W_2^{II,III}$ core, and subsequent reaction yields a fully oxidized $W_2^{III,III}$ product. Comparison of the absorption and EPR spectra of photolyzed solutions to those obtained from independently oxidized solutions of $W_2Cl_4(PMe_3)_4$ reveal the primary photoproduct to be $W_2Cl_5(PMe_3)_3$, which reacts over time to produce the face-sharing bioctahedron, $W_2Cl_6(PMe_3)_3$. These results, in conjunction with analysis of the organic products, give rise to the following photoreaction scheme,

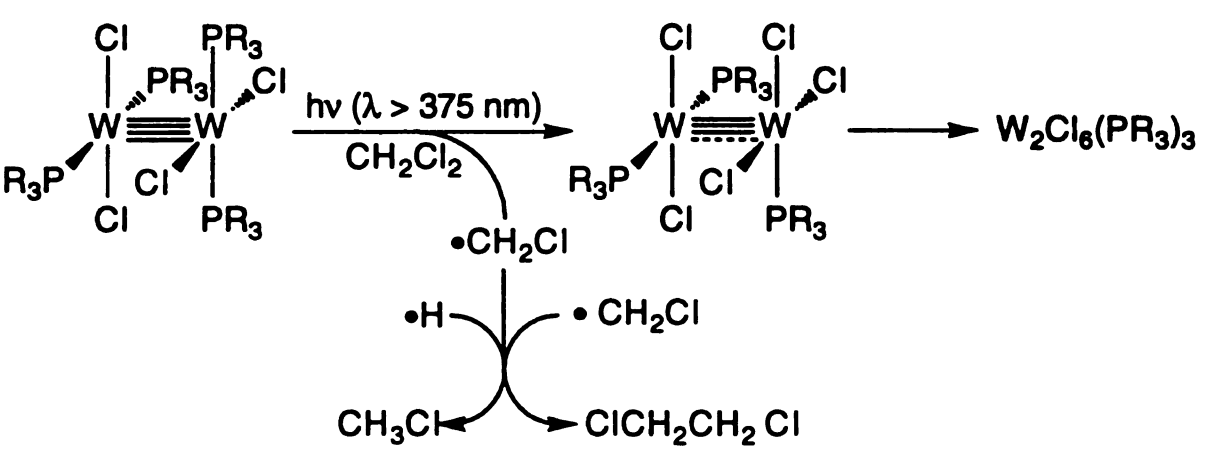

The chlorohydrocarbon photoproducts are consistent with initial chlorine atom abstraction by the photoexcited quadruple bond species to produce the chloromethyl radical. At low concentrations of the primary photoproduct, hydrogen abstraction from solvent appears to be sufficiently efficient to compete with dimerization and chloromethane is the only product observed by GC/MS. As the concentration of the primary photoproduct is increased (with increasing concentration of the $M\overset{4}{-}M$ photoreagent), the chloromethyl radicals couple to produce dichloroethane.

The above reaction scheme is consistent with LMCT photochemistry for the $W_2Cl_4(PR_3)_4$ complexes. The strong near ultraviolet absorption of $W_2Cl_4(PMe_3)_4$ (λ_{max} = 293 nm) has been previously assigned to the $e(\sigma(MP) \rightarrow \delta^*)$ LMCT transition based on the absorption band's strong $\perp$ z-polarization, a vibronic progression in $a_1\nu(MP)$, and the relative insensitivity of the transition with respect to halide.[162] Excitation into this LMCT manifold will generate a highly reducing bimetallic $W_2^{I,II}$ core, which is capable of reducing the C—X bond in chlorohydrocarbon solvents thereby leading to the photoinitiated radical chemistry of the above scheme. The LMCT excited state appears to be short-lived, and hence it is able to react only with substrates in high concentration, as is the case here where the substrate is solvent. Consequently, the observed 'transient' spectrum in Figure 5.12 is not that of the native LMCT excited state but rather correlates directly with the primary product of the photolysis reaction. In the absence of the C—X bond, reduction of substrate is circumvented and the excited state converts smoothly and rapidly back to ground state. Hence absorptions attributable to a photo-oxidized species are not observed in the laser flash photolysis spectrum of $W_2Cl_4(PBu_3)_4$ in benzene, and correspondingly no photoreaction is observed. Moreover, the $^1(\delta\delta^*)$ excited state does not appear to be reducing enough to activate the C—X or C—H bonds of solvent. Therefore excitation of the $^1(\delta\delta^*)$ excited state $W_2Cl_4(PR_3)_4$ in CH_2Cl_2 or benzene yields the same transient species, which is unreactive and decays to ground state at the $^1(\delta\delta^*)$ luminescence decay rate.

The transient spectroscopy and LMCT photochemistry of $W_2Cl_4(PR_3)_4$ is in direct contrast to that observed for $W_2Cl_4(PP)_2$, which derives its photoreactivity from MMCT excited states. These differences can be explained by the different electronic structures of the two classes of compounds. Figure 5.13 shows the qualitative correlation MO diagram[163] of D_{2h} and D_{2d} geometries based on the theoretical calculation of the model compound $Mo_2Cl_4(PH_3)_4$.[186,187] The relative energetics of the metal-metal based orbitals are displayed as a function of a C_4 rotation of one MCl_2P_2 unit about the metal-metal bonded axis where a P–M–M–P torsion angle of 0° defines the D_{2h} structure. At 90° rotation, the D_{2d} conformation is obtained. The cylindrically symmetric M–M σ bond is not affected by internal rotation about the M—M axis and hence the energy of these orbitals remain relatively constant in the correlation diagram. But π components are affected considerably. In the D_{2d} limiting structure, the π orbitals are degenerate by symmetry considerations. However these orbitals lose their degeneracy upon rotation with a maximum splitting obtained for the D_{2h} structure. The spiltting is due to the difference in π bonding ability of the halide and phosphine ligands. The δ/δ^* energy gap is also affected by rotation. As a trans-MX_2P_2 unit rotates away from either of the eclipsed conformations, the d_{xy} orbital overlap decreases until it reaches zero at the staggered conformations (45° rotation angle). However, when the MCl_2P_2 units are eclipsed, the d_{xy} overlap is maximized and to a first approximation the δ orbitals are energetically similar in the D_{2h} and D_{2d} structures.

Representative ground state absorption spectra of Mo and W homologs for the D_{2d} system, shown in Figure 5.14, conform to the predictions of the

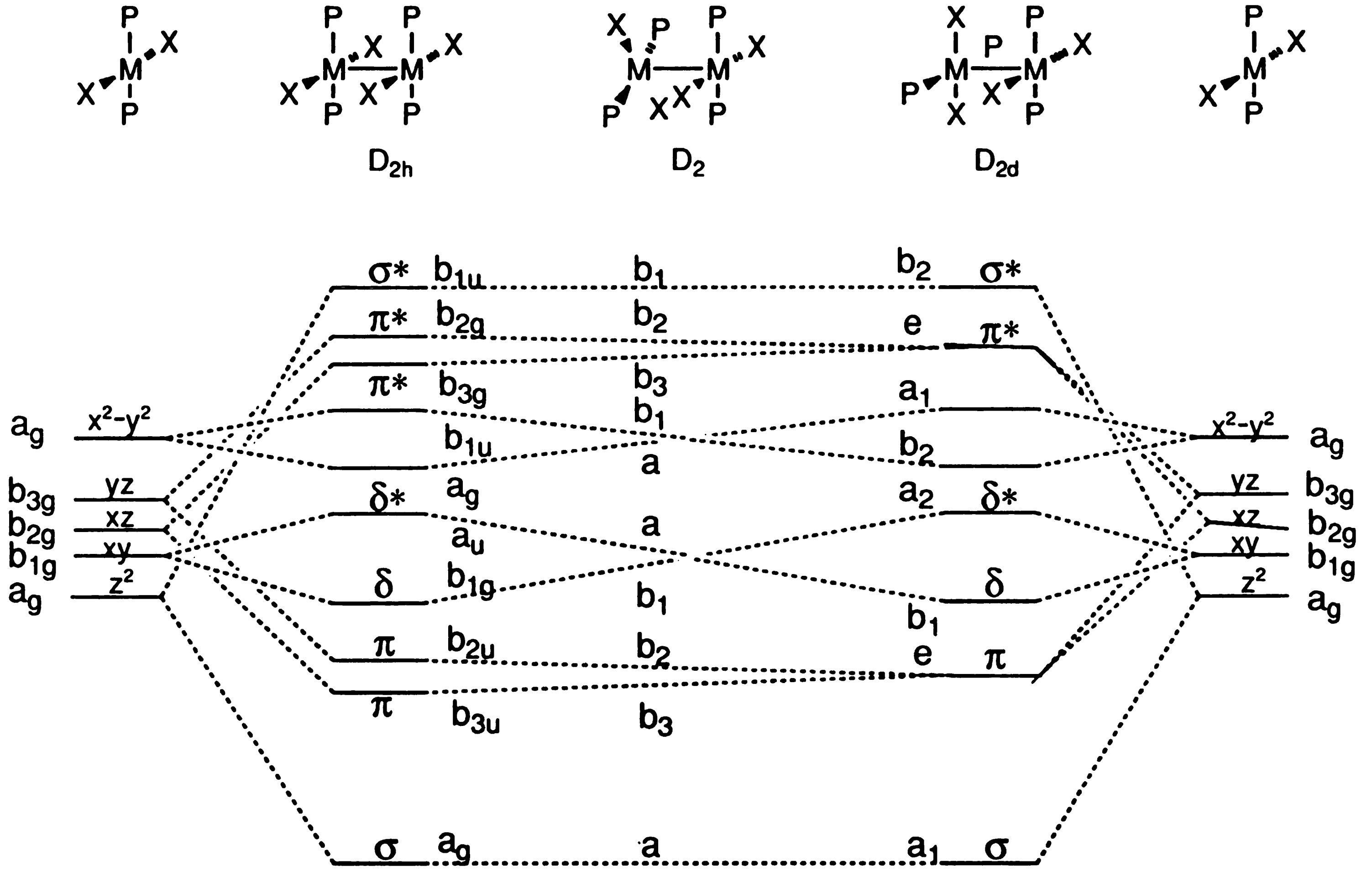

Figure 5.13 Qualitative correlation MO diagram of D_{2h} and D_{2d} geometries based on the theoretical calculation of the model compound $Mo_2Cl_4(PH_3)_4$. (ref. 163)

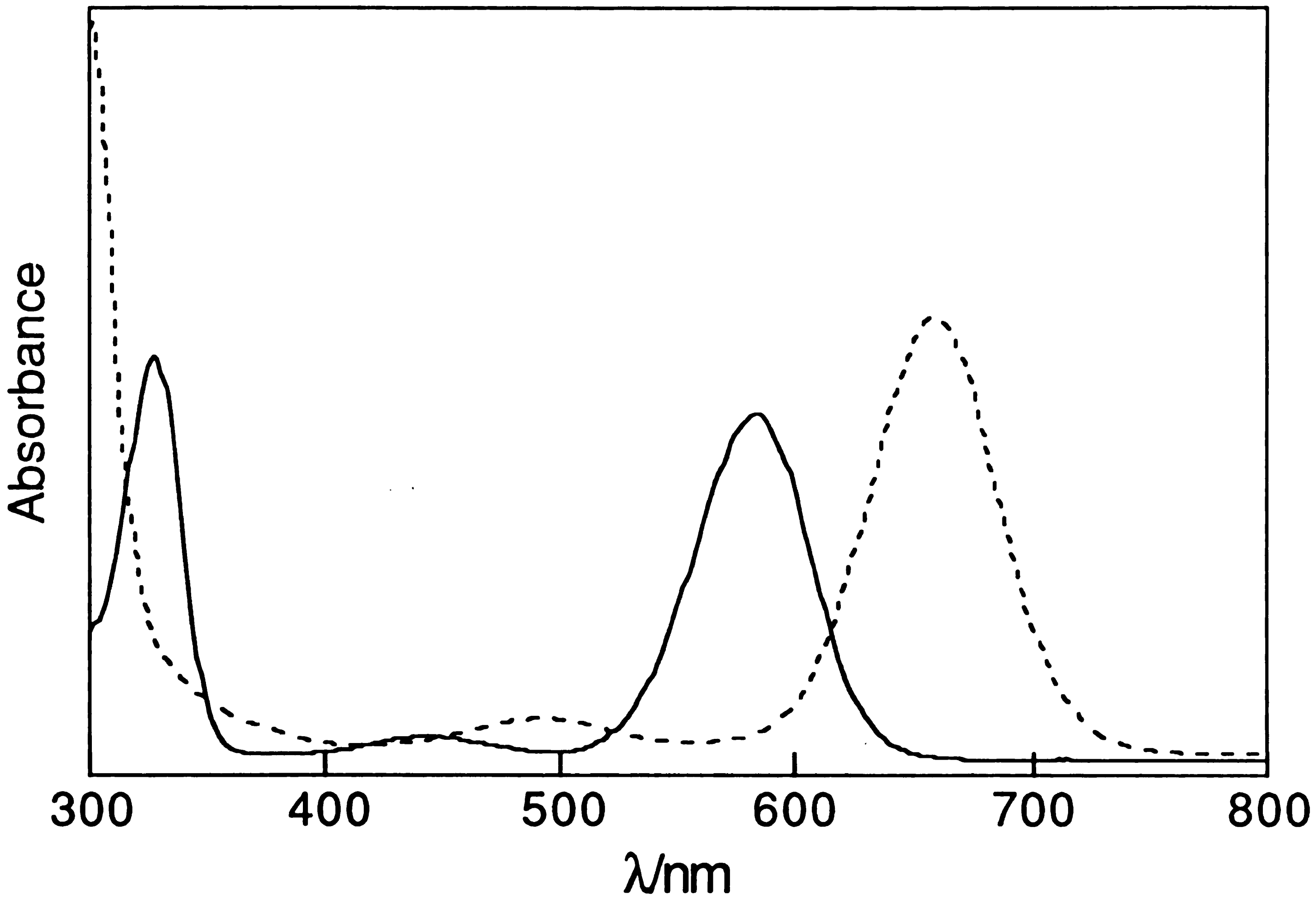

Figure 5.14 Electronic absorption spectra of (a) $Mo_2Cl_4(PMe_3)_4$ (—) and $W_2Cl_4(PMe_3)_4$ (- - -) in benzene.

correlation diagram. The spectroscopic assignment of the D_{2d} complexes has been intensively studied for the series of $M_2X_4(PMe_3)_4$ (M = Mo, W; X = Cl, Br, I).[162,188] The first absorption band in the 550 – 650 nm region and the second small band in the 400 – 500 nm region have been assigned to be the $\delta \rightarrow \delta^*$and $\pi \rightarrow \delta^*$ transitions, respectively, and the strong absorption at around 300 nm has been correlated with a $\sigma(MP) \rightarrow \delta^*$ transition. A comparsion of the absorption spectra for the $M_2Cl_4(PR_3)_4$ in Figure 5.2 and $M_2Cl_4(P\ P)_2$ (M = Mo, W) in Figure 4.9 reveals that both the D_{2d} and D_{2h} complexes display a red-shift in the $^1(\delta^2 \rightarrow \delta\delta^*)$ and $^1(\delta^2 \rightarrow \pi\delta^*)$ transitions. The red shift upon substitution of W for Mo is an indication of metal-localized transitions as discussed in Chapter IV. However the near-ultraviolet profiles exhibit disparate behavior. For $M_2Cl_4(PR_3)_4$ complexes, a distinct blue shift specific to LMCT transitions is observed in the near-ultraviolet spectral region with replacement of a metal-localized Mo by W.[162] This blue-shift is due to the destabilization of the metal-metal levels relative to the ligand levels. This is in contrast to the red-shift in the spectra of $M_2Cl_4(P\ P)_2$ in the same region resulting from metal localized absorptions. Accordingly replacement of these metal-localized states of the D_{2h} complexes by the LMCT states of the D_{2d} complexes is manifested in the significantly divergent photochemistry between these two families of $M \overset{4}{-} M$ compounds.

IV. Conclusion

The formation of a mixed valence photoproduct, $W_2Cl_5(PR_3)_3$ and the organic photoproduct analysis reveal that $W_2Cl_4(PR_3)_4$ photochemistry with dihalocarbons occurs via single electron pathways originating from the excitation of a LMCT absorption manifold. Because near-ultraviolet excitation of $M_2Cl_4(P\ P)_2$ produces a long-lived ESBO transient derived from a discrete excited state of the $M\overset{4}{-}M$ complex, the photochemistry is not confined to solvent and the $M\overset{4}{-}M$ (D_{2h}) halophosphine systems exhibit multielectron activation of a wide variety of substrates. However, this is not the case for $M\overset{4}{-}M$ (D_{2d}) complexes. The metal localized excited states that lead to discrete multielectron photoreactivity of $W_2Cl_4(P\,P)_2$ are obscured by the LMCT transitions in the absorption spectra of $W_2Cl_4(PR_3)_4$ complexes. The consequences of this state inversion in the D_{2d} complexes is that excitation in the near-ultraviolet produces a short-lived, highly reduced metal core that is only able to react with solvent via a free radical pathway. Hence, substrate activation occurs in one electron steps that are difficult to control with $M_2X_4(PR_3)_4$ as the photoreagent. Accordingly, these studies suggest that the multielectron activation of substrates by $M\overset{4}{-}M$ halophosphine excited states is best accomplished with $M_2Cl_4(P\,P)_2$ binuclear complexes or with $M_2X_4L_4$ complexes in which the $L \rightarrow M$ charge transfer states are removed to high energies.

CHAPTER VI

SPECTROSCOPIC STUDIES OF QUADRUPLY BONDED HETEROBIMETALLIC MOLYBDENUM-TUNGSTEN COMPLEXES

I. Background

The zwitterionic character of $M\overset{4}{-}M$ complexes can be accessed chemically only upon low symmetry distortion within the molecule or its environment. As described in Chapters IV and V, this low symmetry distortion is intramolecular in nature. In the zwitterionic excited state of the $M\overset{4}{-}M$ complexes, one center of the binuclear core is oxidized thereby driving distortion to a coordinatively unsaturated ESBO intermediate as described by eq. (4.2). Such a ligand rearrangement provides cooperative stabilization of a charge-separated core by achieving an octahedral geometry about the oxidized M^{III} center and by diminishing the donation of electron density from the halides about the reduced M^{I} center. While this intramolecular ligand distortion traps the zwitterionic character of $M\overset{4}{-}M$ excited states, it also stabilizes the excited state thereby lowering the energy and hence reactivity of the photogenerated intermediate. This may explain why our studies of $M\overset{4}{-}M$ complexes to date show us that these complexers can photoactivate only weak substrate bonds such as C—I of alkyl iodides or S—S of persulfides.

The heterobimetallic cores of $MoWCl_4(PR_3)_4$ and $MoWCl_4(PP)_2$ complexes present a alternative and straightforward means to trap the charge transfer excited character of $M\overset{4}{-}M$ metal-localized excited states without relying on an energy dissipating intramolecular rearrangement of the ligating coordination sphere. Because tungsten is easier to oxidize than molybdenum, the energy wells of $Mo^{I}W^{III}$ and $Mo^{III}W^{I}$ are asymmetric, and therefore the energy of $Mo^{I}W^{III}$ charge separated state should be stabilized with respect to $Mo^{III}W^{I}$; this is schematically represented in Figure 6.1. With the low symmetry distortion intrinsic to the nature of the heterobimetallic core, the zwitterionic state may be stabilized without the need for a ligand distortion. As diagrammed on the state diagram of Figure 6.2, the $Mo\overset{4}{-}W$ bimetallic compounds may exhibit better energy-storage behavior in the excited state and therefore may provide us with a more activated photogenerated intermediate than can be obtained from the homobinuclear Mo_2, and W_2 analogs.

Thus we plan to undertake the systematic exploration of the two-electron photooxidation chemistry of $Mo\overset{4}{-}W$ heterobimetallics and compare the results of these photosensitizers to the phototransformations of the analogous $Mo\overset{4}{-}Mo$ and $W\overset{4}{-}W$ complexes. The nature of the addition product is especially intriguing because the formation of a $Mo^{I}W^{III}$ edge-sharing intermediate should be reflected in a product displaying substrate addition at the Mo center. Thus a simple photoproduct characterization will in itself be enlightening. However before a systematic photochemical study can be meaningfully undertaken, the excited state dynamics of $Mo\overset{4}{-}W$ heterobimetallics need to be defined. This is the focus of the work in this Chpater. The spectroscopic properties of heteronuclear quadruply bonded $Mo^{II}W^{II}$ complexes in D_{2d} and D_{2h} symmetries are presented and compared with the homonuclear $Mo_2^{II,II}$ and $W_2^{II,II}$ congeners.

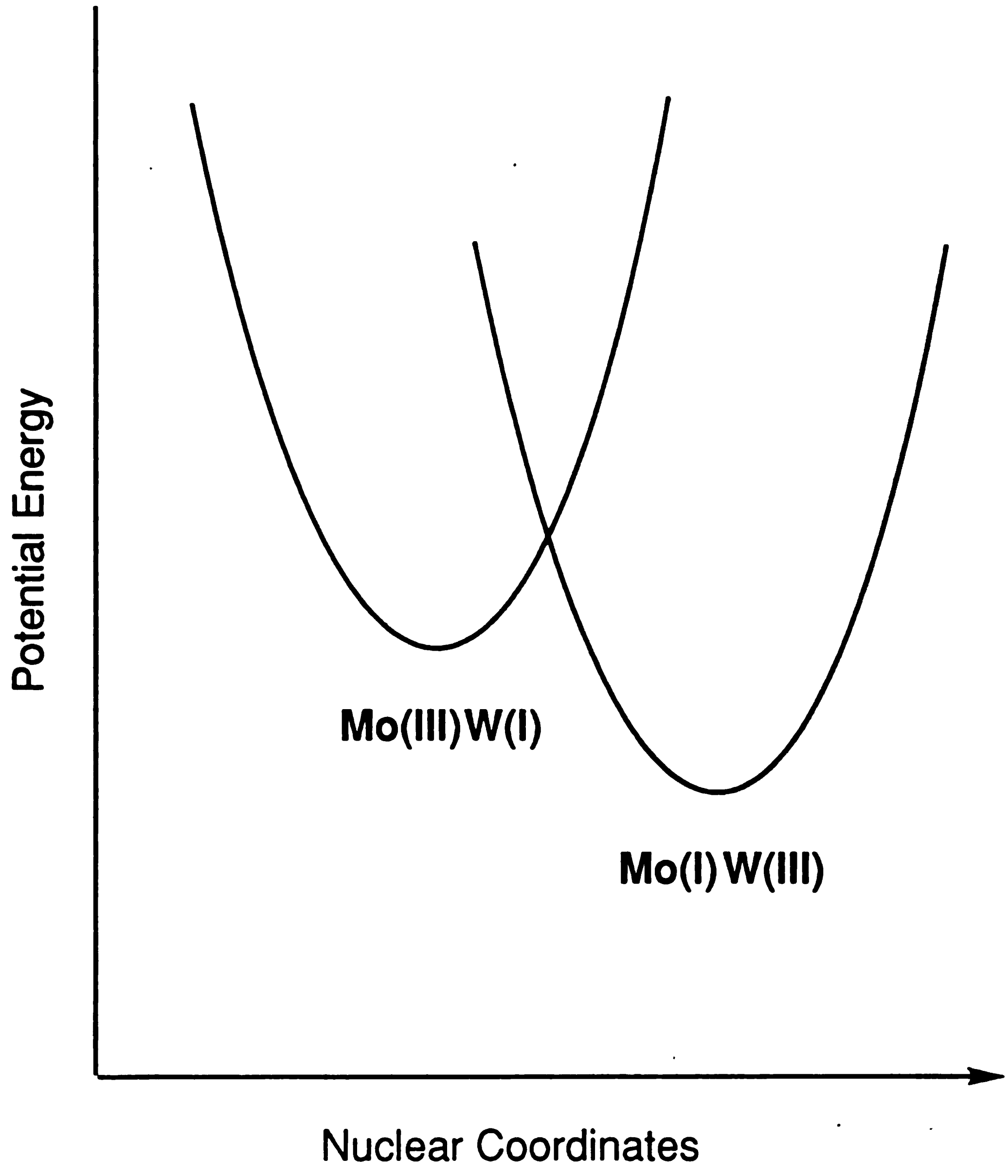

Figure 6.1 Schematic potential energy curves of the mixed-valence states of Mo(I)–W(III) vs. Mo(III)–W(I) in heterobimetallic systems.

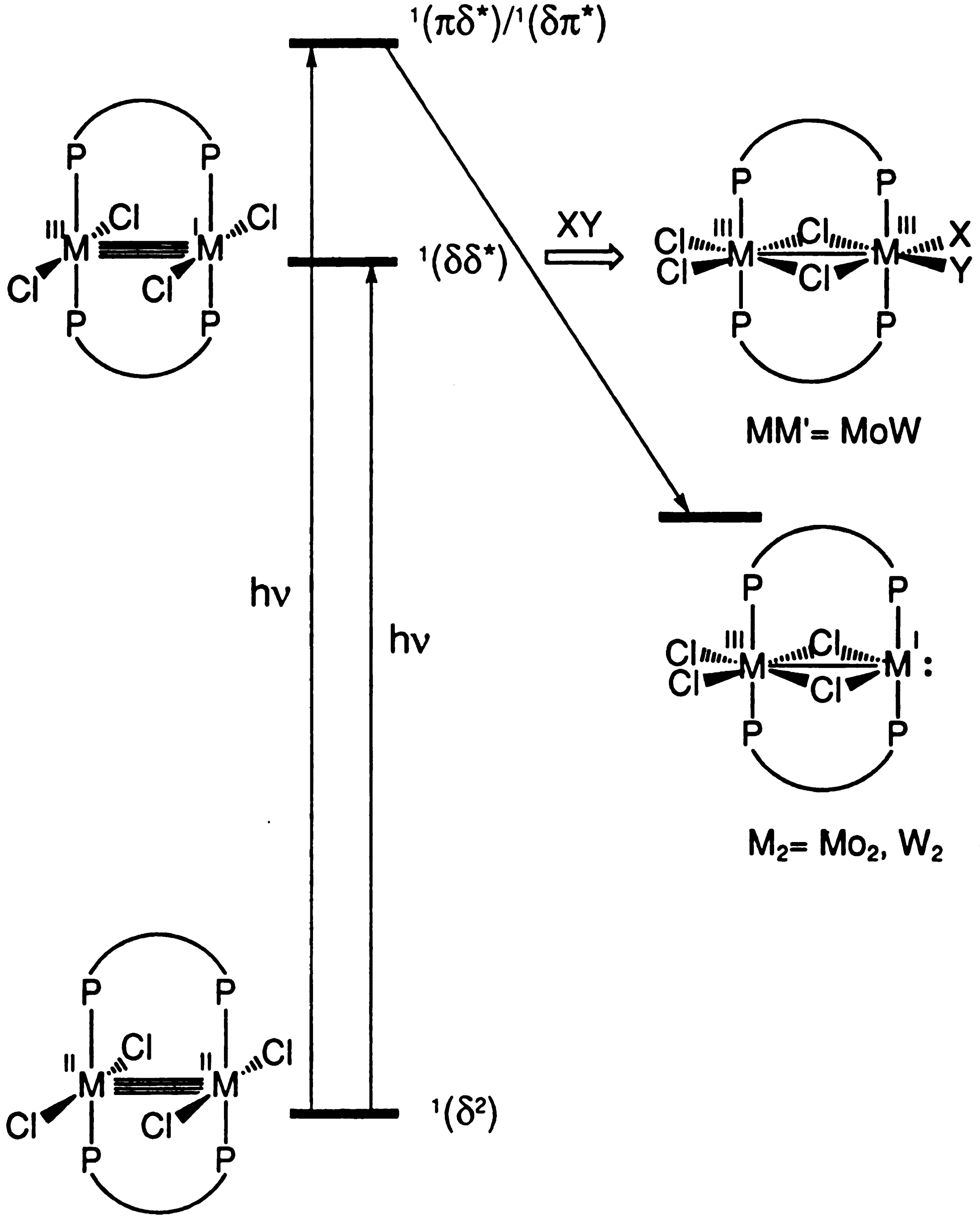

Figure 6.2 Proposed scheme for the formation of the Mo(I)-W(III) excited state. Upon δδ* excitation, the charge transfer mixed-valence state can be stabilized without utilizing the edge-sharing bioctahedral distorted intermediate.

II. Results and Discussion

A. NMR Studies of $MoWCl_4(PR_3)_4$ and $MoWCl_4(dppm)_2$

The ^{31}P NMR spectra of shows characteristic signatures of $Mo^{II}W^{II}$ cores, and therefore ^{31}P NMR is an important tool in the chemistry of these species. Figures 6.3, 6.4, and 6.5 show the ^{31}P NMR spectra of $MoWCl_4(PR_3)_4$ (D_{2d}) complexes (PR_3 = $PMePh_2$, PMe_2Ph, PMe_3) in C_6D_6 at room temperature. Two intense triplets are observed for molybdenum and tungsten isotopes with $I = 0$ due to equivalent ^{31}P nuclei coupling across the quadruple bond ($J_{PP} \sim 24$ Hz). The downfield resonance is assigned to the tungsten site based on $^{183}W{-}^{31}P$ coupling, which gives rise to a doublet of triplets with coupling $^{1}J_{PW} = 280$ Hz for the ^{31}P nuclei on W and a doublet of triplets (only the outer satellite peaks are observed) with coupling $^{2}J(^{183}W{-}^{31}P) \sim 47$ Hz for those on Mo. The results clearly show that the phosphines on the tungsten atoms are less shielded with respect to those on molybdenum atoms in the heteronuclear species.

Due to the sample solubility, ^{31}P NMR spectrum of $MoWCl_4(dppm)_2$ (D_{2h}) complex was taken in CD_2Cl_2 but recorded at –40 °C to prevent the oxidation of the sample in the halogenated solvent.[112] As was the case for the D_{2d} complexes, two resonancesassociated with the Mo and W centers are observed in the ^{31}P NMR spectrum of $MoWCl_4(dppm)_2$ (Figure 6.6). However, the spectrum is more complicated than its D_{2d} counterpart, exhibiting an $AA'BB'X$ spin pattern.

These ^{31}P NMR spectra of the heterobimetallics are clrearly distinguished from the singlet observed in the spectra of the Mo_2 and W_2 congeners. A comparison of the chemical shifts and coupling constants (J) for these heterobimetallics vs. the homobimetallics is listed in Table 6.1. These results indicate that the electron density on the molybdenum is higher than that on the

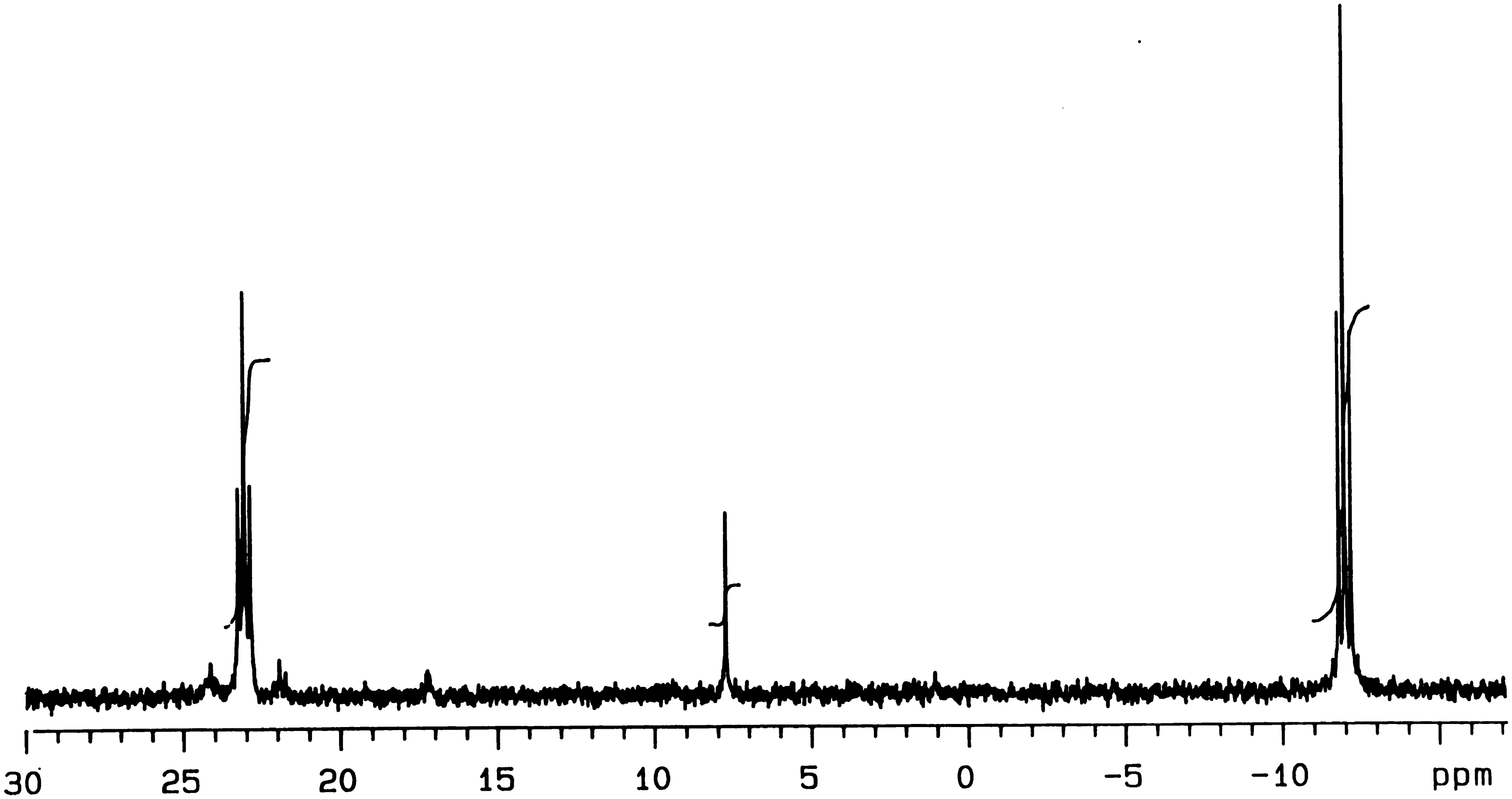

Figure 6.3 $^{31}P\{^1H\}$ NMR spectrum of $MoWCl_4(PMePh_2)_4$ at 202.4 MHz in benzene-d_6 at room temperature. The asterisk indicates the presence of its Mo_2 congener with approximately 6.8%.

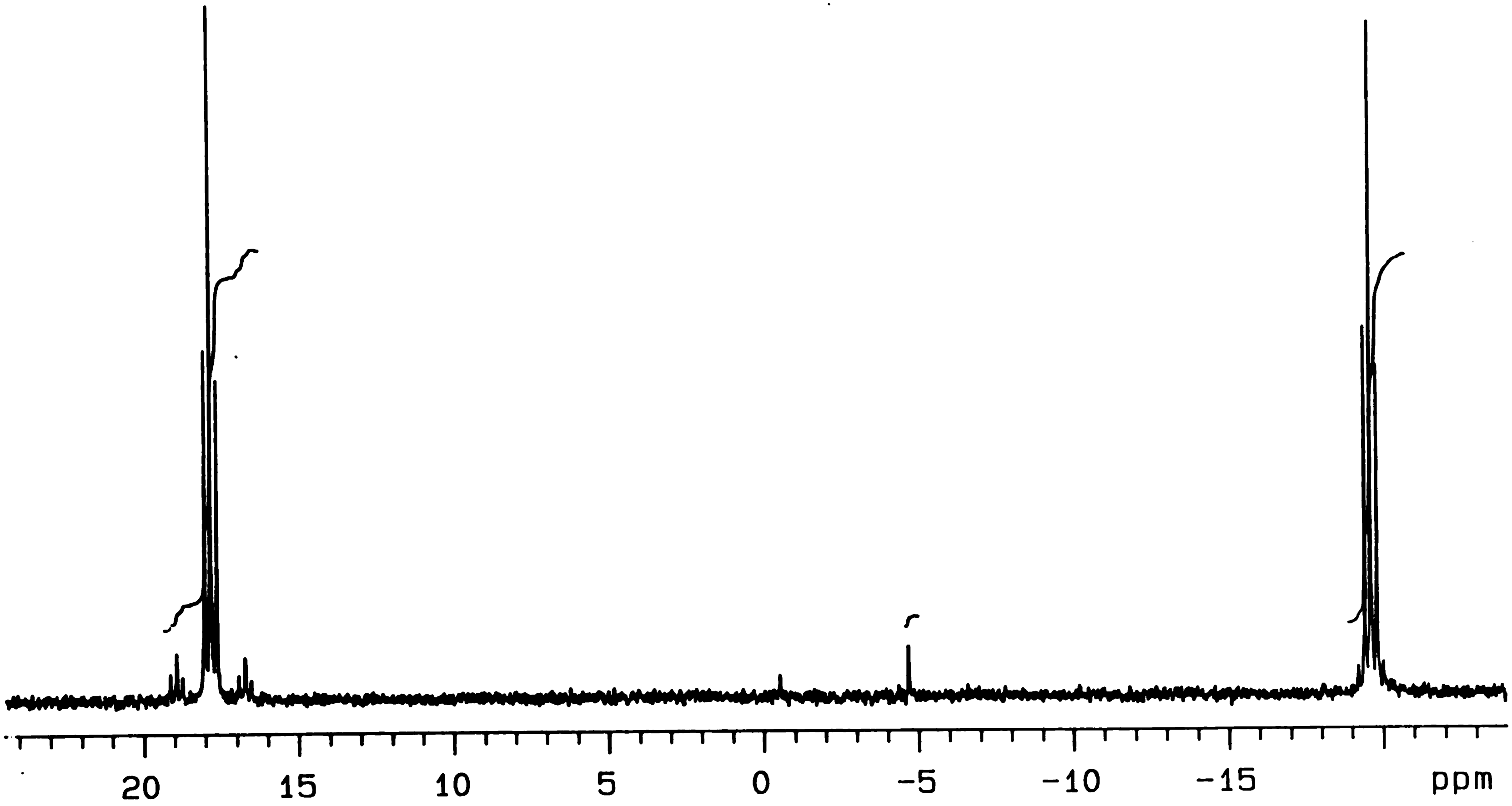

Figure 6.4 $^{31}P\{^1H\}$ NMR spectrum of $MoWCl_4(PMe_2Ph)_4$ at 202.4 MHz in benzene-d_6 at room temperature. The asterisk indicates the presence of its Mo_2 congener with approximately 1.2%.

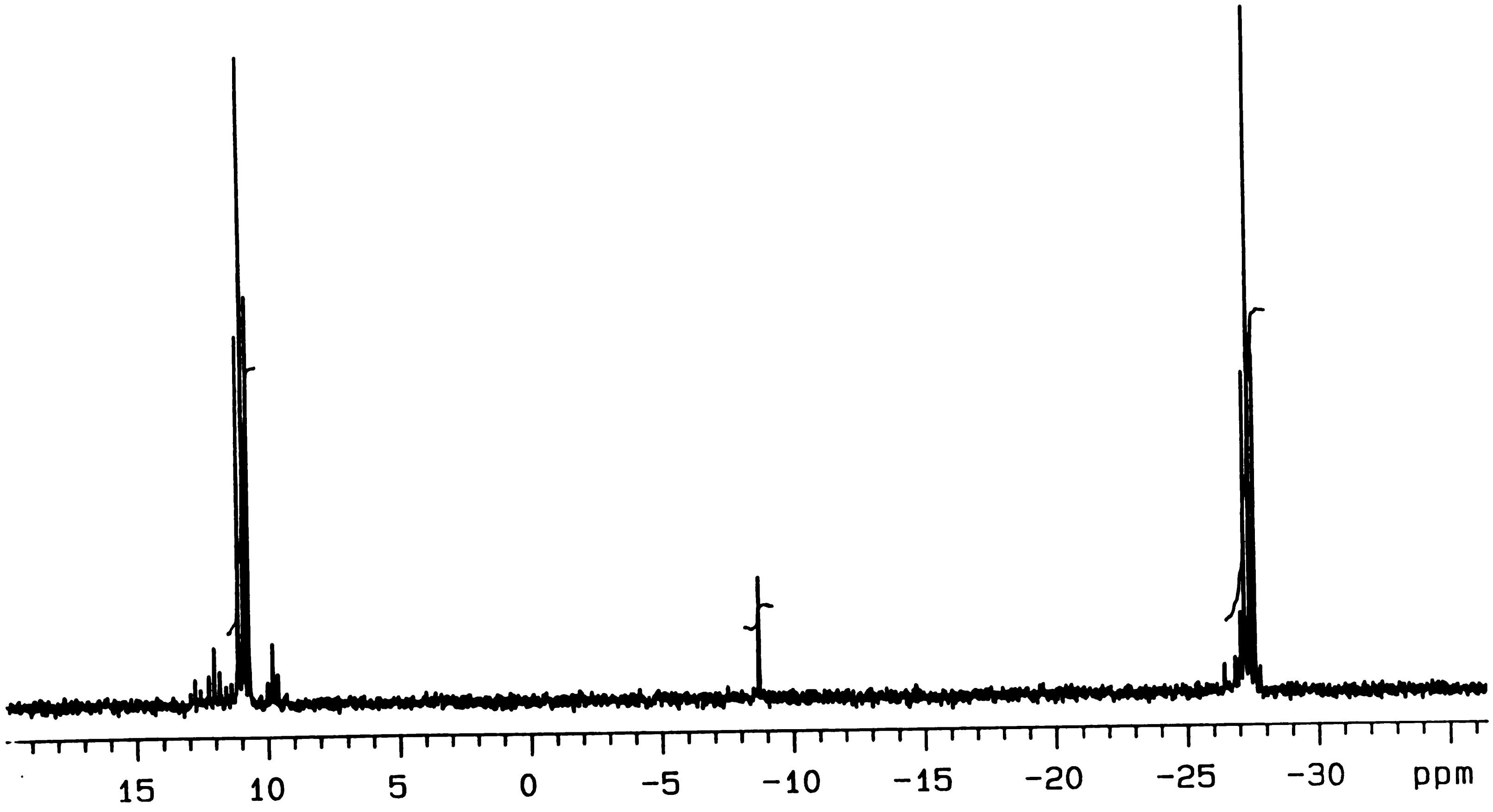

Figure 6.5 $^{31}P\{^{1}H\}$ NMR spectrum of $MoWCl_4(PMe_3)_4$ at 202.4 MHz in benzene-d_6 at room temperature. The asterisk indicates the presence of its Mo_2 congener with approximately 4.4%.

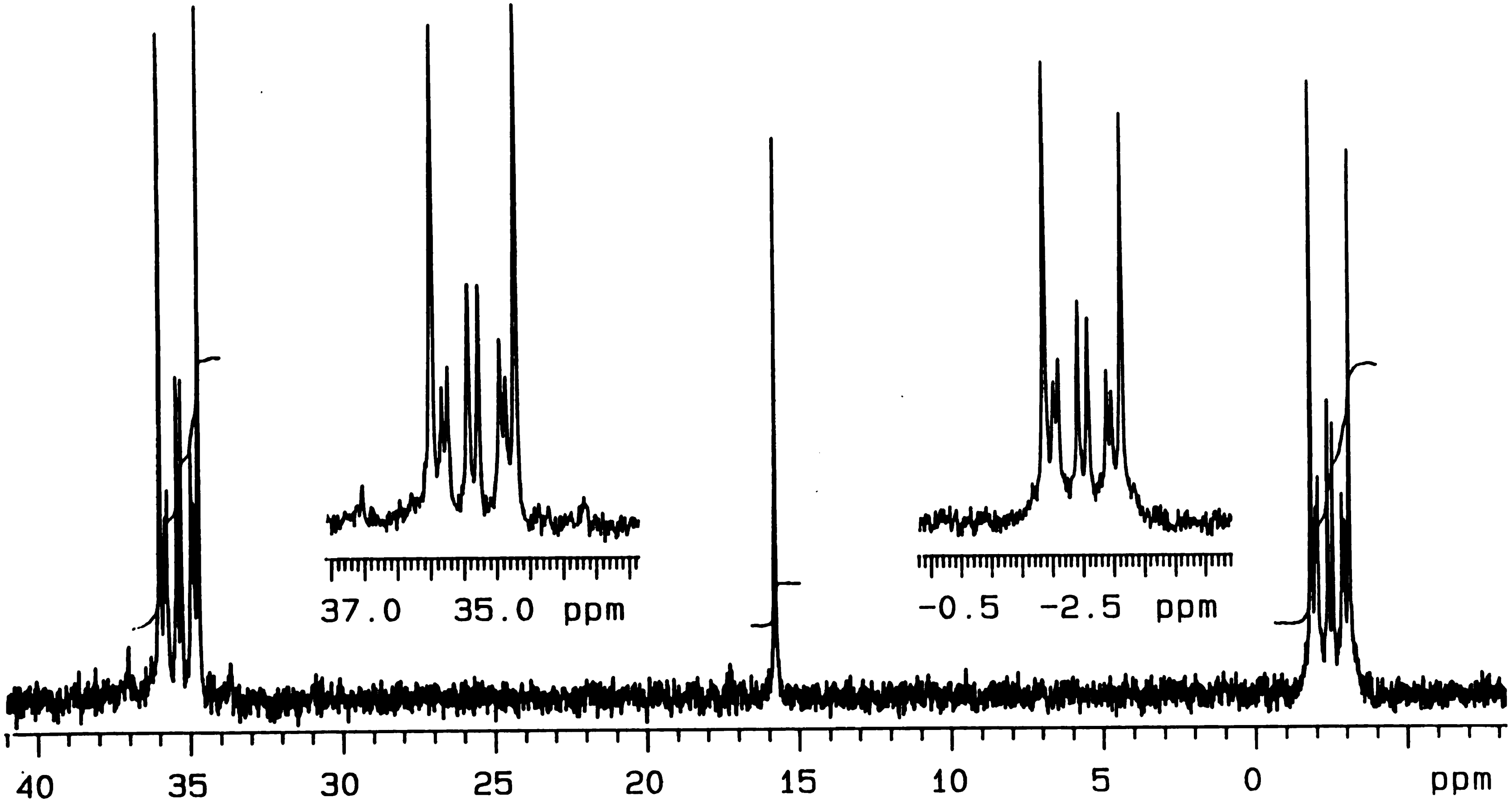

Figure 6.6 $^{31}P\{^1H\}$ NMR spectrum of $MoWCl_4(dppm)_2$ at 202.4 MHz in CD_2Cl_2 at –40 °C. The asterisk indicates the presence of its Mo_2 congener with approximately 8%.

Table 6.1 ^{31}P NMR Chemical Shift[a,b] and coupling constants (J)[b] of $M_2Cl_4(PR_3)_4$ (M_2 = Mo_2, MoW, W_2)[e]

$M_2Cl_4(PR_3)_4$	Mo_2[c]	MoW[c]					W_2[d]			
	$\delta_{(P-Mo)}$	$\delta_{(P-Mo)}$	$^2J_{P183W}$	$\delta_{(P-W)}$	$^1J_{P183W}$	$^3J_{PP}$	$\delta_{(P-W)}$	$^1J_{P183W}$	$^2J_{P183W}$	$^3J_{PP}$
$PMePh_2$	7.7	-12.1	95	23.0	267	23.5	2.1	234	51	28
PMe_2Ph	-2.3	-19.6	98	17.8	271	24.4	-1.0	236	49	28
PMe_3	-10.5	-27.4	~97	10.9	272	24.5	-6.8	236	51	28
1/2 dppm[f]	15.8	2.49	—	35.35	406	—	18.14	—	44	

[a] Chemical shift referenced to 85% H_3PO_4.

[b] The chemical shift unit is in ppm and the coupling constant is in Hz.

[c] benzene-d_6 solvent

[d] $CDCl_3$ solvent

[f] Spectrum of $MoWCl_4(dppm)_2$ is obtained in CD_2Cl_2 solvent at –40 •C.

[e] These data are consistent with the literature reports (references 110, 111, 112)

tungsten. In the case of D_{2d} heterobimetallic series, the chemical shift difference between the phosphorus ligands on the two metals increases slightly with an increase of the phosphine basicity, suggesting that the electron-donating abilities support an effective charge separation within the heterobimetallic core.

The difference in electron density on the two metal atoms of the heterobimetallic core also results in chemical shift differences in ^{1}H NMR spectra of $MoWCl_4(PR_3)_4$. Figures 6.7, 6.8, and 6.9 for PR_3 = $PMePh_2$, PMe_2Ph, PMe_3, respectively, reveal two separate methyl resonances associated with two types of protons on the molybdenum site vs the tungsten site. The downfield resonances are attributed to the methyl groups of the phosphines bound to the tungsten and the upfield resonances are the resonances for the methyl groups of the phosphines bound to molybdenum. This trend is consistent with that observed for the ^{31}P chemical shifts of these complexes.

The different substituent groups on phosphine ligands exhibit some interesting features. A broad unresolved singlet was obtained for the methyl groups on $MoWCl_4(PMePh_2)_4$ and a triplet pattern for those on $MoWCl_4(PMe_2Ph)_4$ and $MoWCl_4(PMe_3)_4$. While the methyl resonance on $MoWCl_4(PMe_3)_4$ appears as a semi-quartet at 121.4MHz (recorded at Varian VXR-300), two resolved triplets can be observed when the magnetic field is increased to 202.4 MHz (recorded at Varian VXR-500); this result is shown in Figure 6.10. In contrast, the resonances of the ^{1}H NMR spectrum for $MoWCl_4(dppm)_2$ complex appear to be complex multiplets (Figure 6.11). It should be noted that the protons on the bridging methylene position are affected by the diamagnetic anisotropy of the quadruple bond and the ^{1}H NMR chemical differences for a series of $MoWCl_4(LL)_2$ have been used to estimate the value for diamagnetic anisotropy.[112,189]

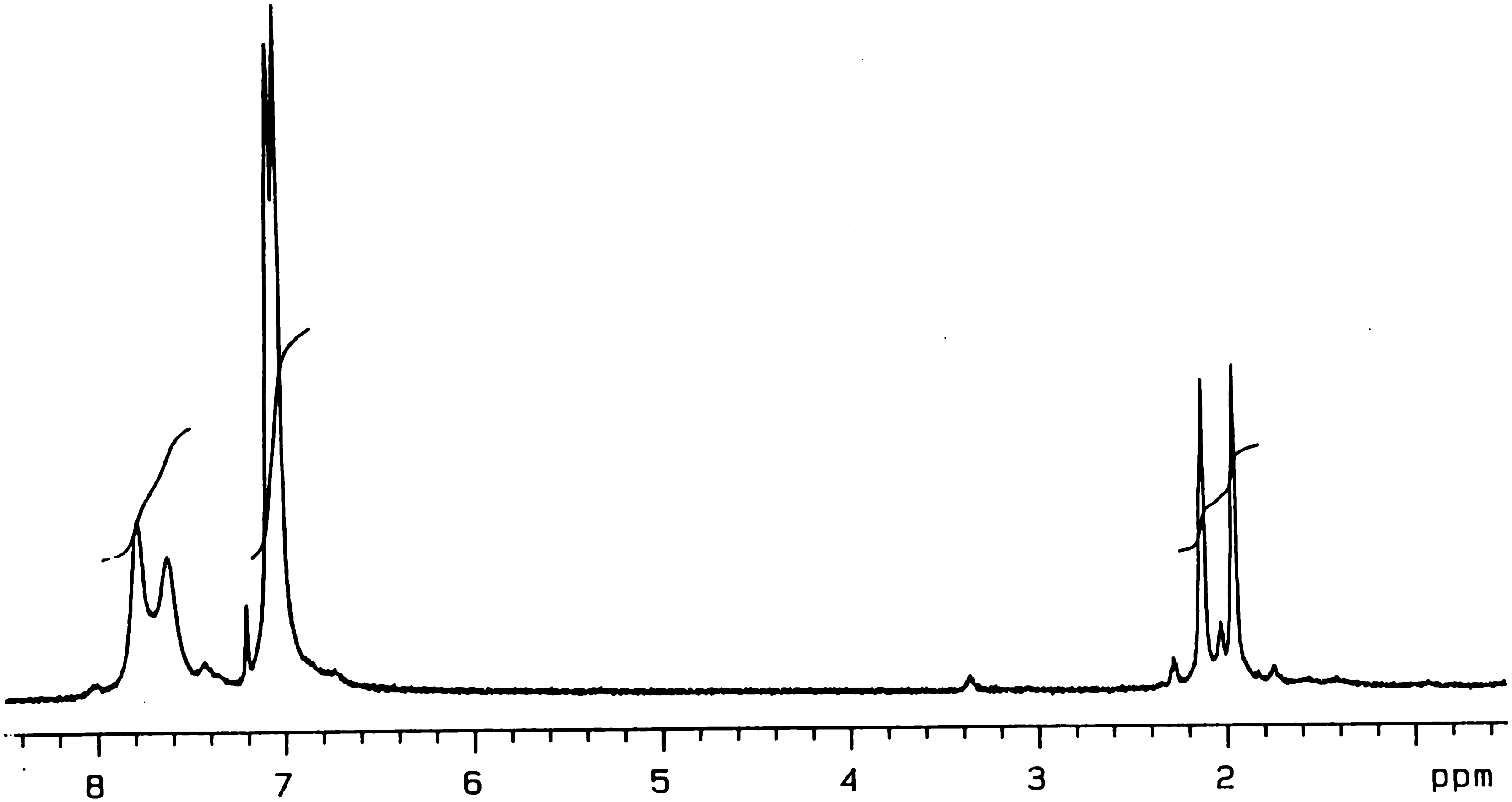

Figure 6.7 ^{1}H NMR spectrum of $MoWCl_4(PMePh_2)_4$ at 300 MHz in benzene-d_6 at room temperature.

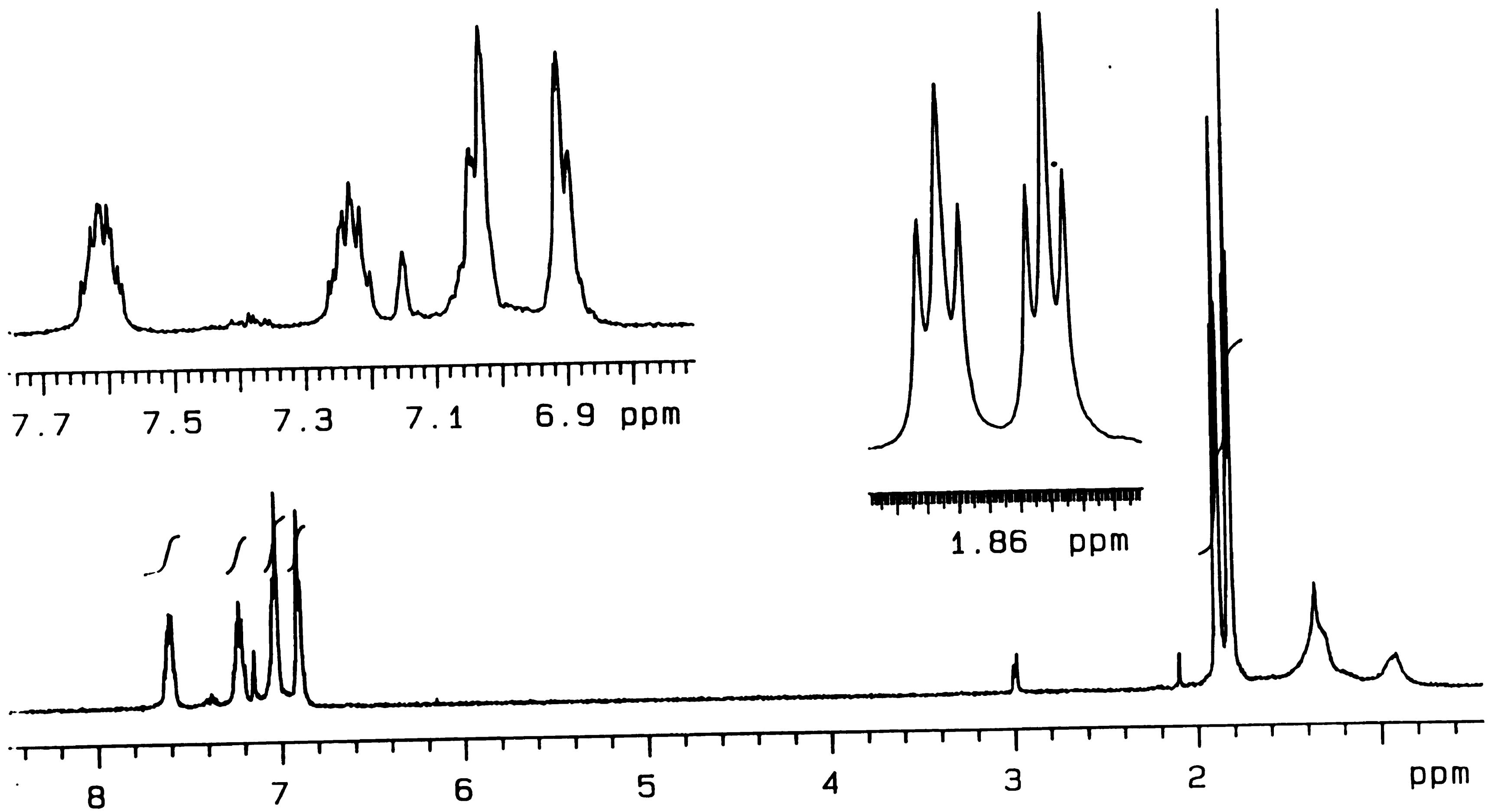

Figure 6.8 ^{1}H NMR spectrum of MoWCl$_4$(PMe$_2$Ph)$_4$ at 300 MHz in benzene-d$_6$ at room temperature.

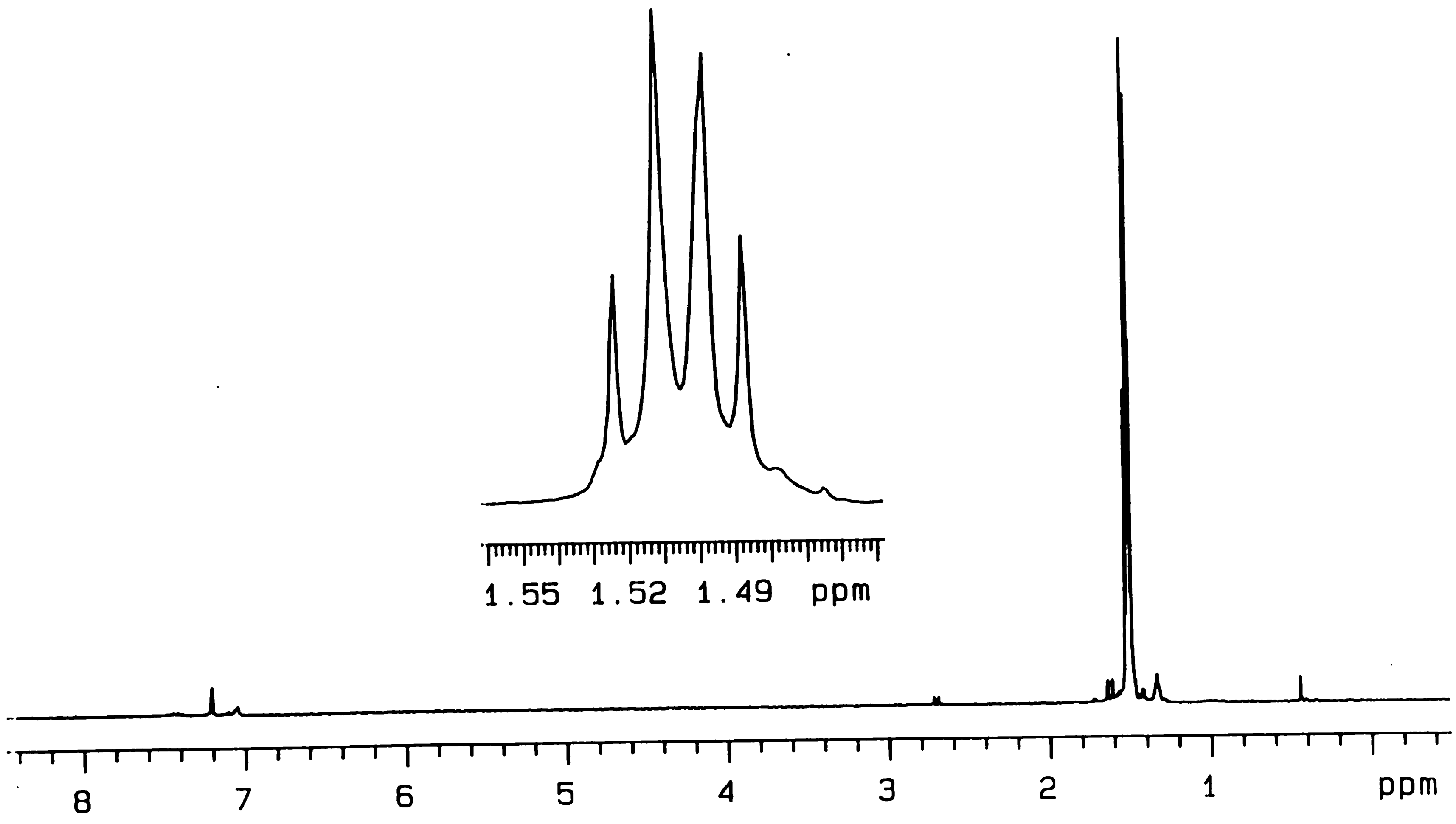

Figure 6.9 ^1H NMR spectrum of $MoWCl_4(PMe_3)_4$ at 300 MHz in benzene-d_6 at room temperature.

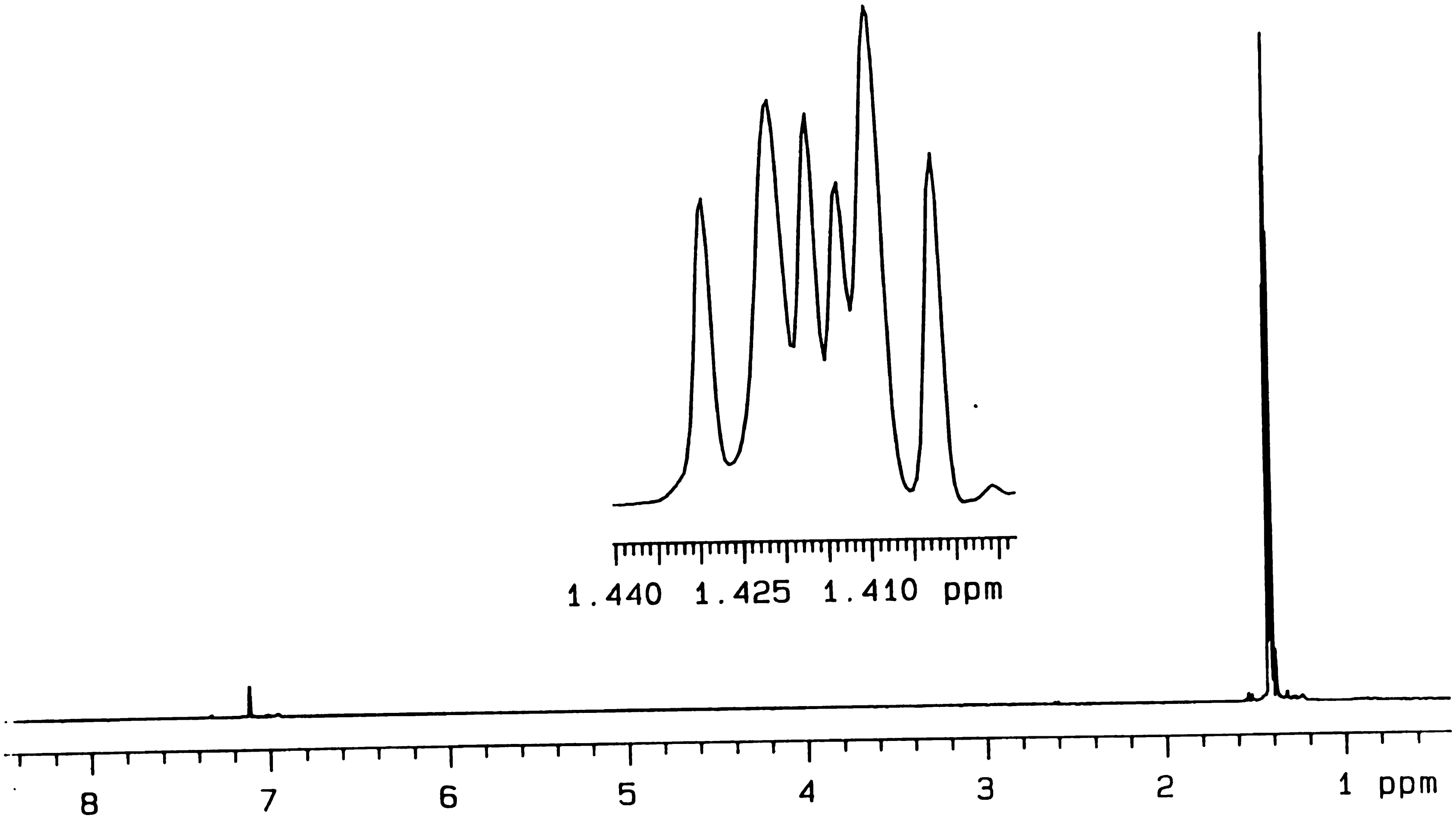

Figure 6.10 ^1H NMR spectrum of $MoWCl_4(PMe_3)_4$ at 500 MHz in benzene-d6 at room temperature.

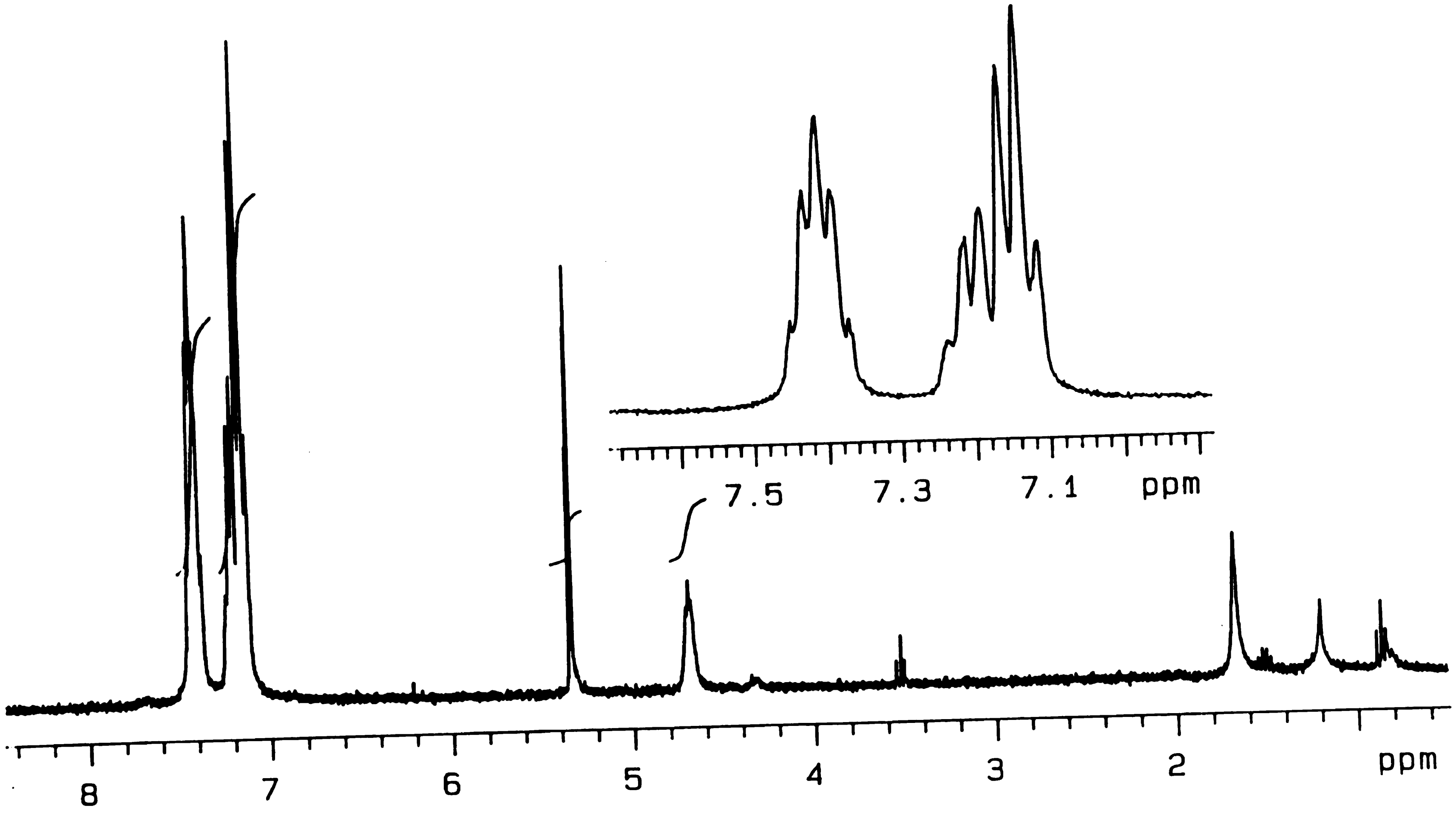

Figure 6.11 ^{1}H NMR spectrum of $MoWCl_4(dppm)_2$ obtained at 300 MHz in CD_2Cl_2 at –40 °C.

B. Electronic Absorption Spectroscopy

The visible absorption spectra of $MoWCl_4(PR_3)_4$ ($PR_3 = PMePh_2$, PMe_2Ph, PMe_3) complexes are shown in Figure 6.12. The assignment of their electronic transitions is consistent with the metal-localized transitions of their Mo_2 and W_2 homologs. The $^1(\delta^2 \rightarrow \delta\delta^*)$ transition for $MoWCl_4(PR_3)_4$ lies between the energies of the Mo_2 and W_2 congeners, but it is closer to the W_2 values (see Figure 6.13). The energies of $^1(\delta^2 \rightarrow \delta\delta^*)$ transitions of the $MoWCl_4(PR_3)_4$ complexes blue-shift with increasing basicity of the phosphine ligands, $PMePh_2 < PMe_2Ph < PMe_3$ (Figure 6.12).[190] Such a shift is expected and it can be attributed to an increase in the electron density at the metals and in the Mo–W bond, in agreement with the NMR results above.

C. Luminescence Spectroscopic Studies

Solids and benzene solutions of $MoWCl_4(PR_3)_4$ complexes exhibit intense red luminescence both at room and low temperatures upon excitation of the $^1(\delta^2 \rightarrow \delta\delta^*)$ transition. The emission spectra for this series of compounds in benzene at room temperature are shown in Figures 6.14, 6.15 and 6.16. In all cases, electronic absorption and emission spectra are essentially mirror images with a small Stoke shift. This implies that the emission arises from an excited state complex geometrically similar to the ground state structure. Figures 6.14, 6.15 and 6.16 also display the excitation profiles of $MoWCl_4(PR_3)_4$ obtained by monitoring the $^1(\delta\delta^* \rightarrow \delta^2)$ emission. The transitions are energetically coincident with absorptions in their ground state spectra, indicating that $MoWCl_4(PR_3)_4$ complexes fluoresce directly from the lowest-lying singlet $^1\delta\delta^*$ excited state in which D_{2d} symmetry is preserved; chemically distorted excited states do not

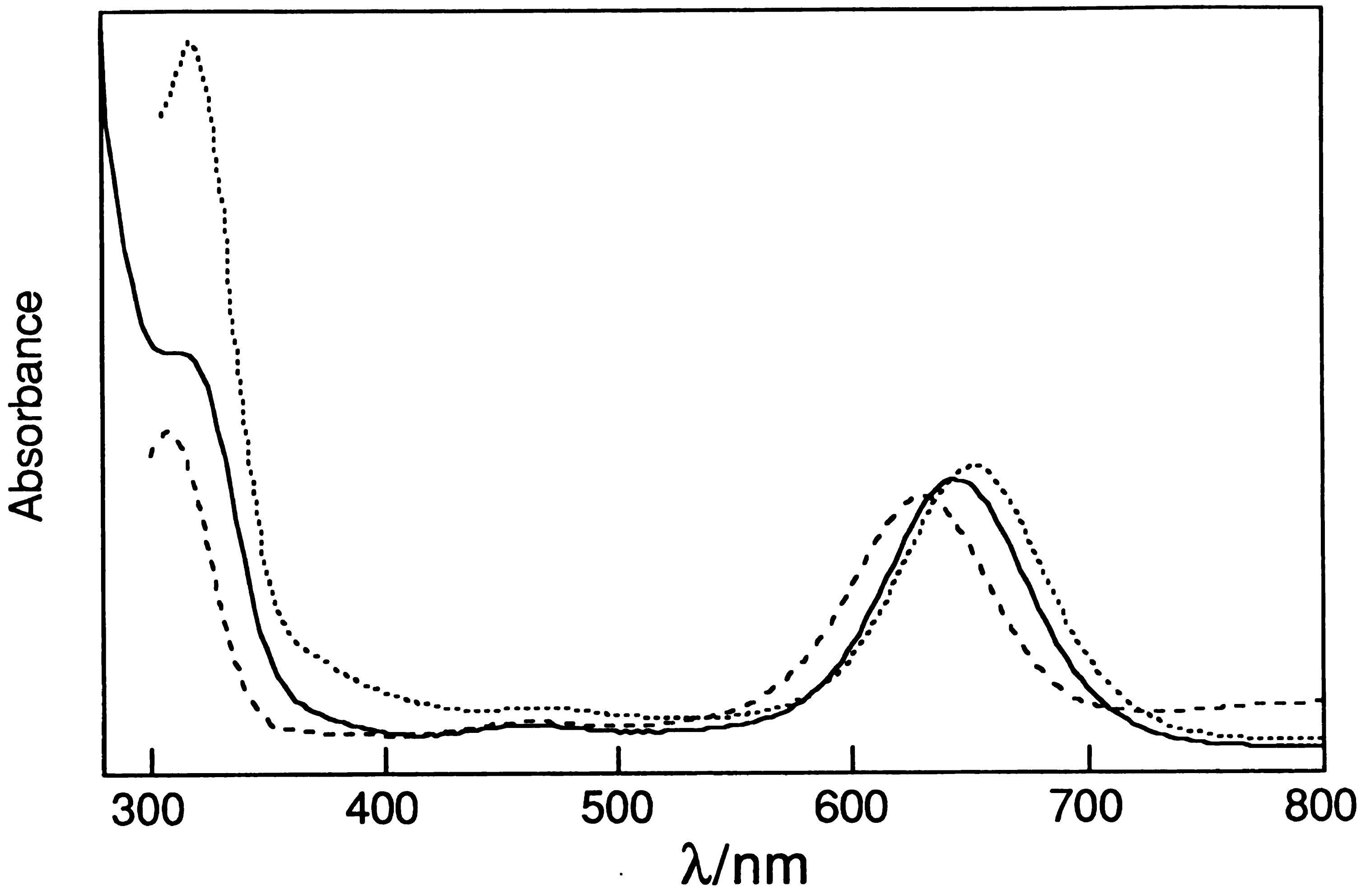

Figure 6.12 Electronic absorption spectra of (a) $MoWCl_4(PMe_3)_4$(– – –) (b) $MoWCl_4(PMe_2Ph)_4$ (——) (c) $MoWCl_4(PMePh_2)_4$ (. . . .) in benzene solution at room temperature.

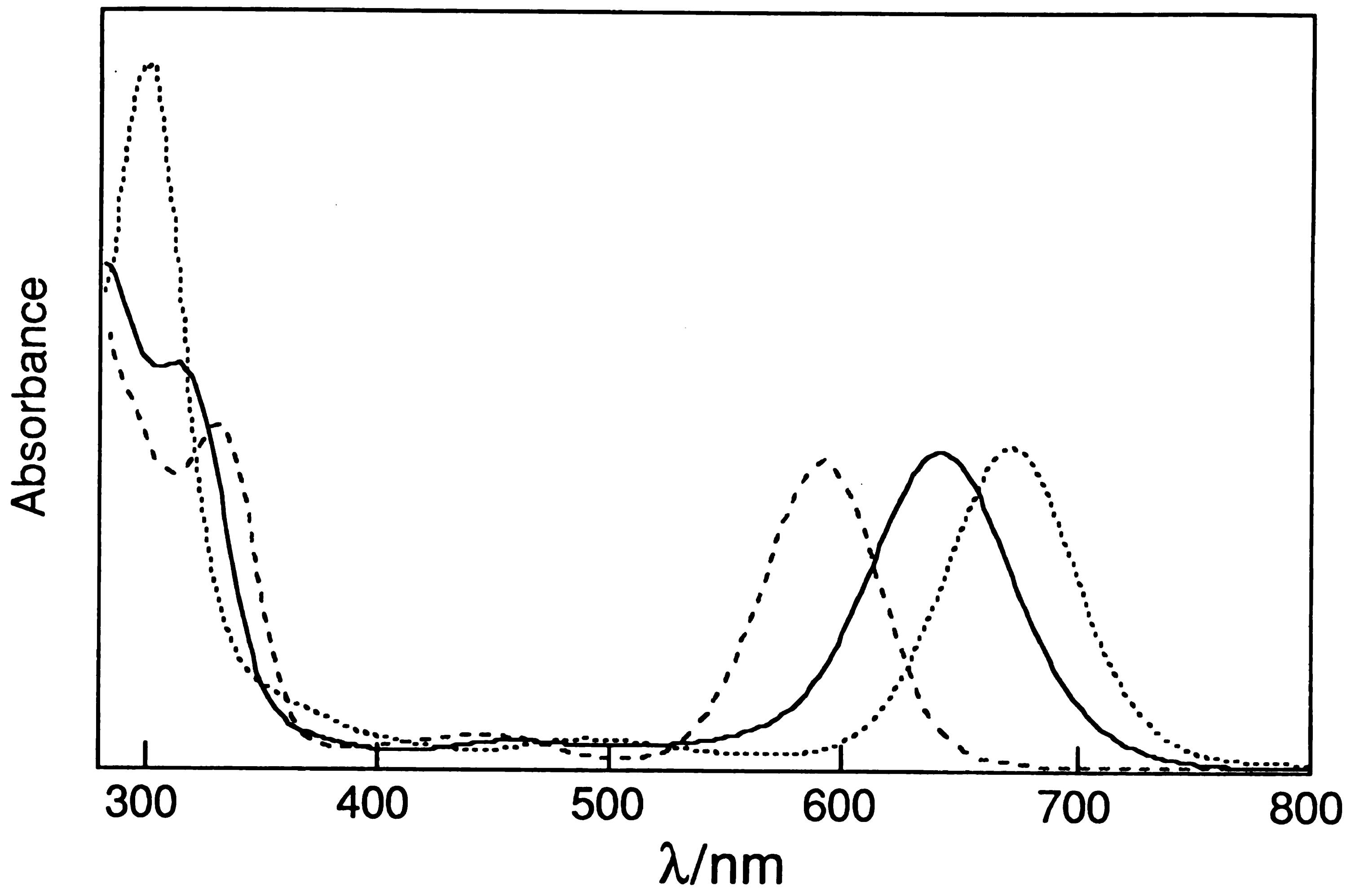

Figure 6.13 Electronic absorption spectra of (a) $Mo_2Cl_4(PMe_2Ph)_4$ (– – –) (b) $MoWCl_4(PMe_2Ph)_4$ (—) (c) $W_2Cl_4(PMe_2Ph)_4$ (....) in benzene solution at room temperature.

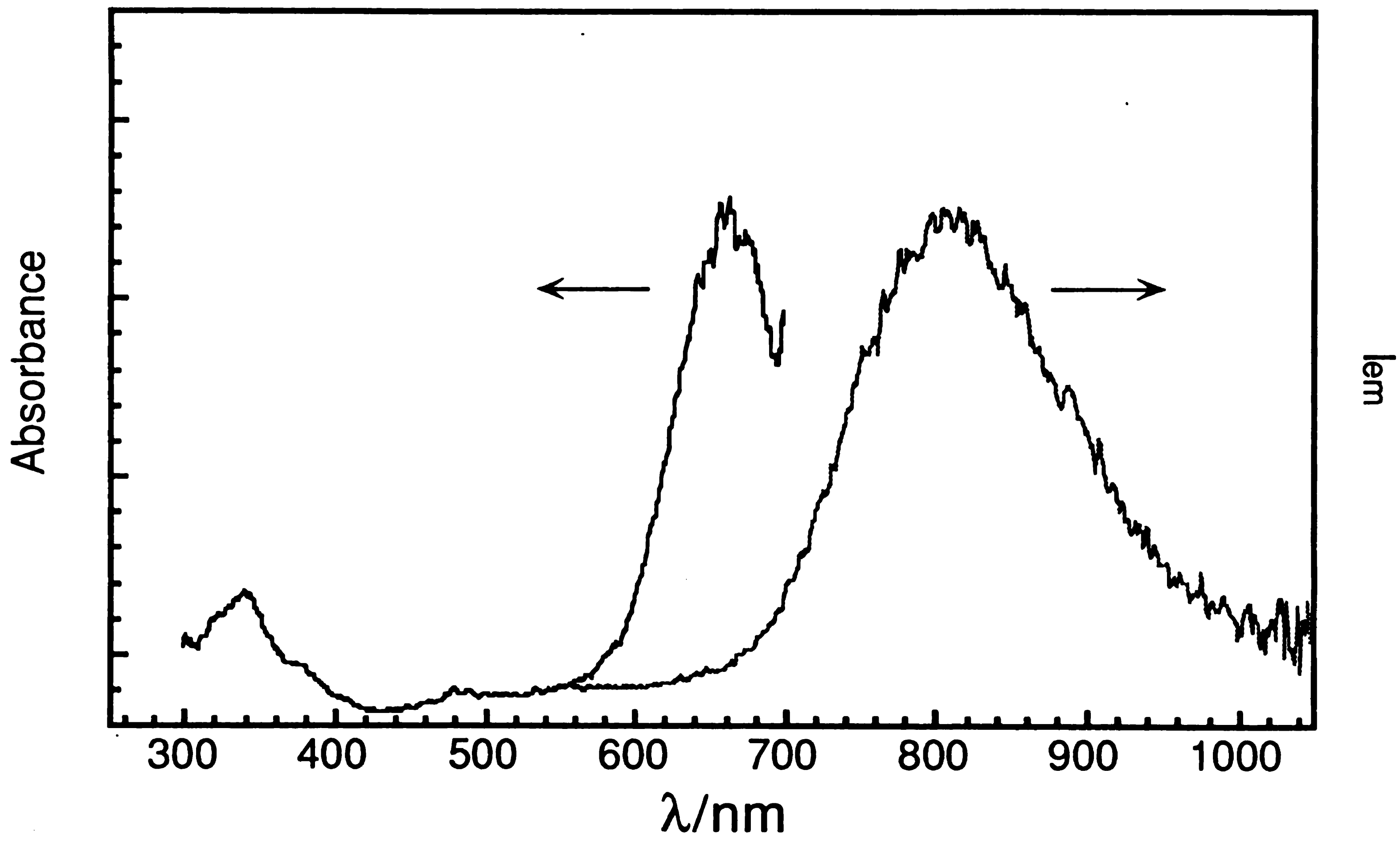

Figure 6.14 Absorption and emission spectra of $\delta^2 \leftrightarrow \delta\delta^*$ transitions of $MoWCl_4(PMePh_2)_4$ in benzene solution at room temperature.

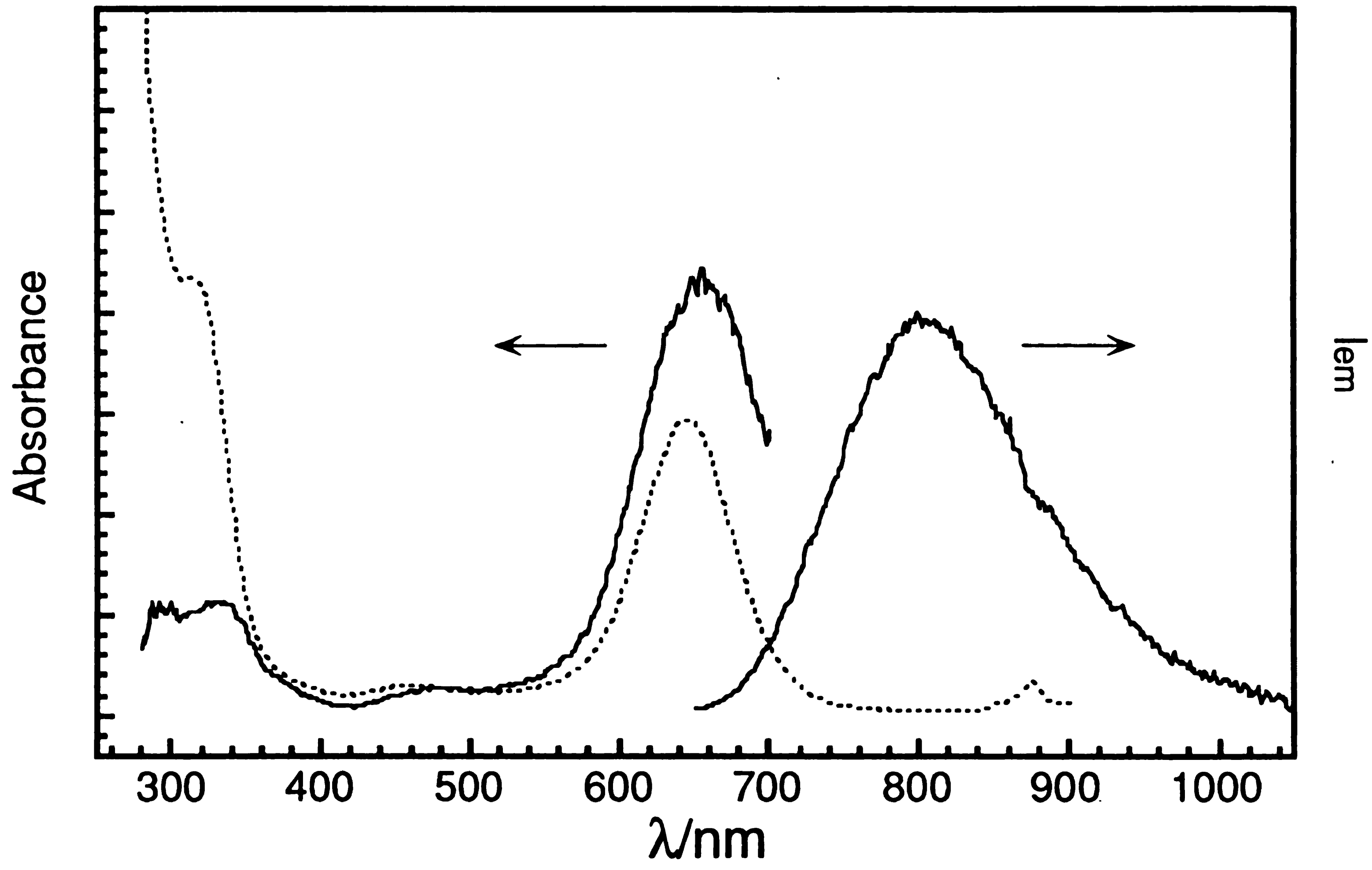

Figure 6.15 Excitation, absorption (....) and emission spectra of $\delta^2 \leftrightarrow \delta\delta^*$ transitions of $MoWCl_4(PMe_2Ph)_4$ in benzene solution at room temperature.

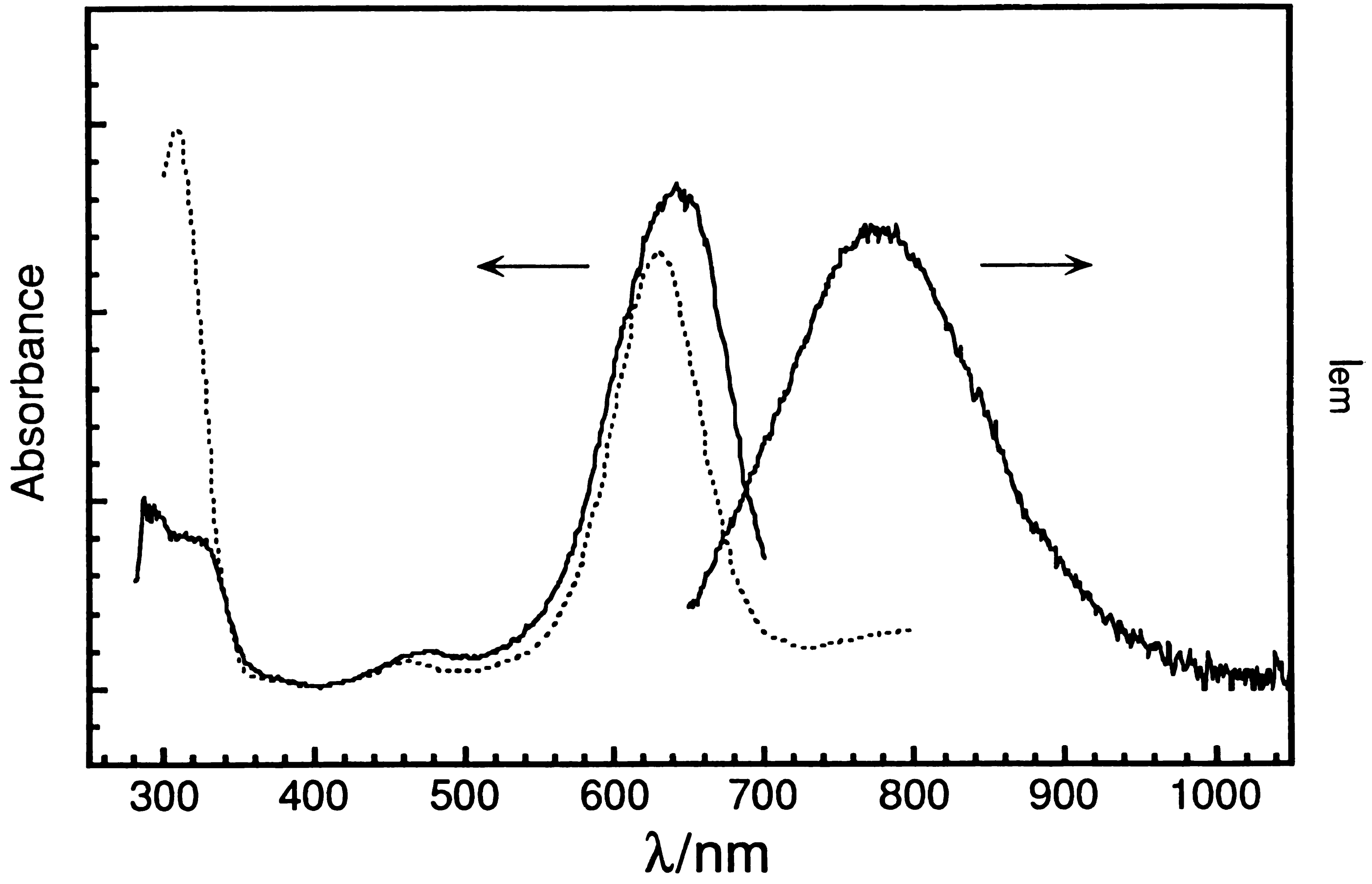

Figure 6.16 Excitation, absorption (....) and emission spectra of $\delta^2 \leftrightarrow \delta\delta^*$ transitions of $MoWCl_4(PMe_3)_4$ in benzene solution at room temperature.

appear to contribute to the emission. Whereas the absorption spectra of D_{2d} complexes are solvent insensitive, their emission spectra show significant perturbations with solvent. This has been observed previously for the homobimetallic species and the observation is consistent with the charge seprarted character of a zwitterionic excited states. The emission profile also exhibits a pronounced temperature dependence as illustarted in Figure 6.17 for solid $MoWCl_4(PMePh_2)_4$ over a 77 - 300 K temperature range. The emission bandwidth decreases with increasing temperature; surprisingly in view of the emission spectra of the homobimetallics vibrational fine structure is not resolved even at low temperature.

Lifetimes of $MoWCl_4(PR_3)_4$ complexes in benzene and in the solid state were measured by time-correlated photon counting spectroscopy. The emission signals show a biexponential decay. The shorter lifetime component arises from the $^1\delta\delta^*$ excited state while the origin of the other component remains unknown. Table 6.2 lists the luminescence maxima and the lifetimes of $MoWCl_4(PR_3)_4$ complexes, along with a comparison to the emission data of their homonuclear counterparts. $MoWCl_4(PR_3)_4$ complexes exhibit typical $^1\delta\delta^*$ excited state lifetimes with values that are closer to the W_2 congeners. An exceptionally long lifetime is observed for $MoWCl_4(PMe_3)_4$, but this observation is consistent with the lifetime for D_{2d} phosphine compunds. It has been postulated that the lifetime is lengthened by the reduced steric of the smaller phosphine PMe_3 ligand,[191] or owing to the absence of additional nonradiative decay pathways[97] arising from the existence of long-lived transient species.[192] Absolute emission quantum yields for $Mo_2Cl_4(PMePh_2)_4$, $MoWCl_4(PMePh_2)_4$, and $W_2Cl_4(PMePh_2)_4$ complexes are 0.011, 0.036 and 0.044, respectively; this trend is consistent with an increasing emission lifetime along this series.

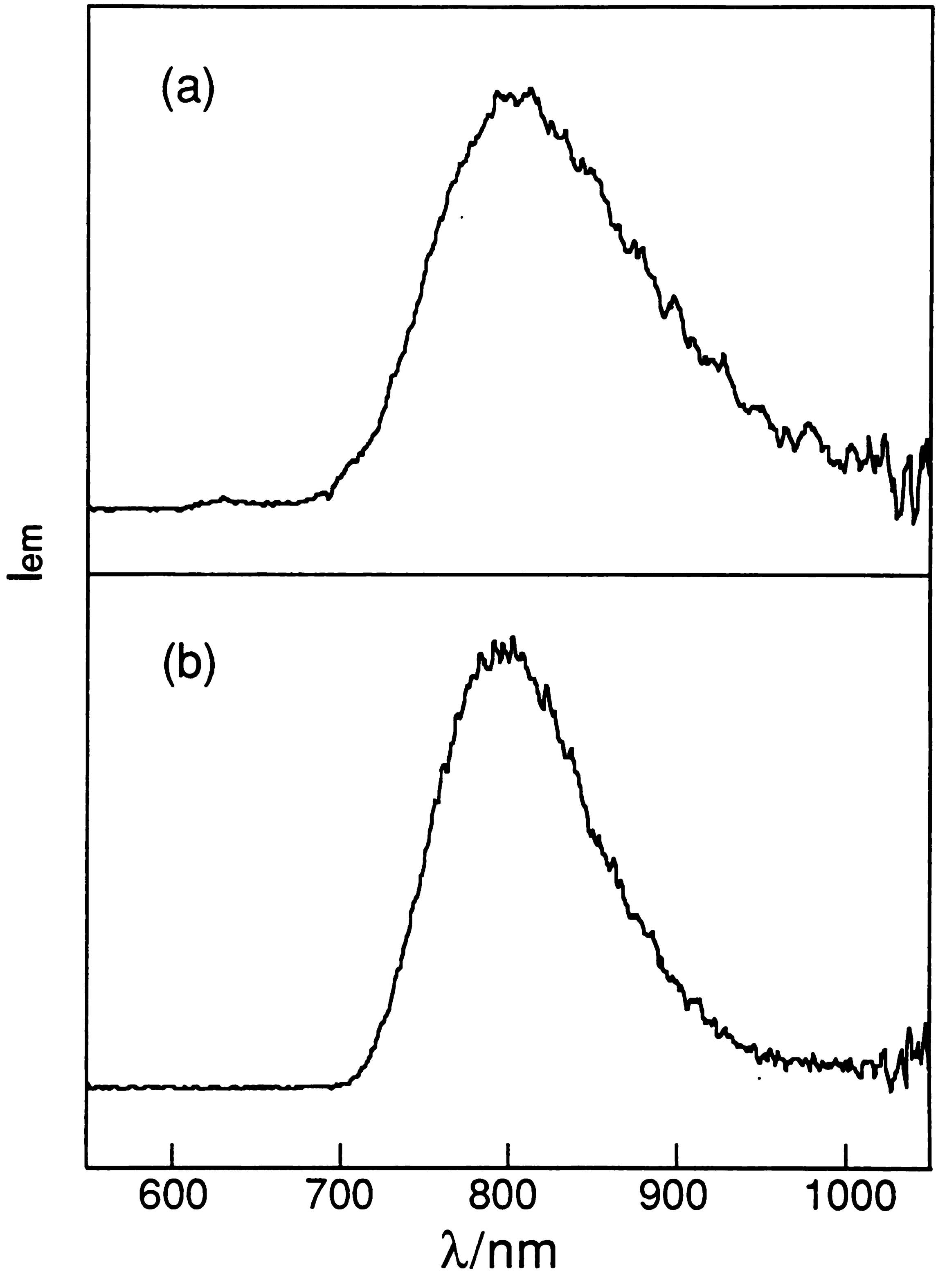

Figure 6.17 Emission spectra of $\delta\delta^* \rightarrow \delta^2$ transitions of $MoWCl_4(PMePh_2)_4$ in solid state (a) at room temperature and (b) at 77 K.

Table 6.2 Luminesence Lifetimes and Emissive Quantum Yields of $\delta\delta^*$ Excited State of $M_2Cl_4(PR_3)_4$ ($M_2 = Mo_2$ MoW, W_2) Complexes.

$M_2Cl_4(PR_3)_4$	τ_{em} (ϕ_{em})[a]		
	Mo_2	MoW	W_2
$PMePh_2$	11.4 ns (0.011)	54 ns (0.036)[a]	65 ns (0.044)
PMe_2Ph	16.4 ns (0.036)[a]	38 ns	43 ns
PMe_3	135 ns (0.259)[b]	59 ns	50 ns

[a] Emission quantum yield was mearured in dilute benzene solution of the $M_2Cl_4(PR_3)_4$ (absorbance = 0.2) as determined by using a 2-methylpentane solution of $Mo_2Cl_4(PMe_3)_4$ at $\lambda_{em,max}$ = 585 nm at 300K.

[b] ref. 117

The D_{2h} $MoWCl_4(dppm)_2$ complexes exhibits no appreciable emission in benzene solution at room temperature, The same is true for the Mo_2 and W_2 homologs. This is in contrast to the luminescence previously observed for D_2 staggered complexes of $Mo_2Cl_4(dppe)_2$ (dppe = bis(diphenylphosphino)ethane) and $Mo_2Cl_4(dmpe)_2$ (dmpe = bis(dimethylphosphino)ethane) (torsion angle χ = 30° and 40°, respectively).[114] The trend of decreasing luminescence along the series of eclipsed $D_{2d} > D_2 > D_{2h}$ may be explained by the lifting of the π_{xz} and π_{yz} orbital degenracy with rotation. The increase in the π/π^* splitting with increasing torsion angle results in the decreased energy gaps between π and δ states. Thus the presence of additional nonradiative decay pathways may arise from the proximity of the $^1(\delta\delta^*)$ excited state to π based states of the metal-metal bond.

III. Conclusion

The NMR and electronic absorption studies reveal the presence of a ground state of $^{(\delta-)}$Mo—W$^{(\delta+)}$ with a partial dipole on each metal. Luminescence spectroscopic studies show that the geometry of the excited state is preserved. Based on this, we believe that the $Mo\overset{4}{—}W$ bimetallic compounds should have structurally undistorted Mo^{I}–W^{III} excited states that can be accessed from the $^1(\delta\delta^*)$ excited state. This is in contrast to the homobimetallics which need to eneter a charge-separated excited state from higher energy excited state (see Figure 4.11). In these cases charge transfer within the bimetallic core does not appear to be solely sufficient to promote rearrangement because the structurally distorted transient intermediate is not observed to form upon $\delta\delta^*$ excitation, but rather is observed when energy metal localized transitions (e.g., $\delta \rightarrow \pi^*$, $\pi \rightarrow \delta^*$) immediately to higher energy of $\delta \rightarrow \delta^*$ are excited. These states not only possess charge transfer character, but their population leads to diminished metal-metal π

bonding relative to that in the ground state molecule. This feature is needed to enhance formation of a bioctahedral intermediate because interactions of the metal d_{yz} (or d_{xz}) orbitals with those of ligands in the equatorial plane of an edge-sharing bioctahedron occur at the expense of M—M π interactions. Because a intramolecularly distorted intermediate is not needed to stabilize charge separation within the bimetallic core of homobimetallics, the excited states of these complexes may be more potent photoreductants of substrates from the $^1(\delta\delta^*)$.

If photochemistry is to occur from higher energy excited states, then we expect the photoreactivity to parallel that observed in Chapters IV and V. We come to this conclusion on the basis of the photophysical and spectroscopic properties of $\mathrm{Mo}\overset{4}{-}\mathrm{W}$ species, which are intermediate to those for the $\mathrm{Mo}\overset{4}{-}\mathrm{Mo}$ and $\mathrm{W}\overset{4}{-}\mathrm{W}$ analogues. Consequently, the D_{2d} systems would be expected to exhibit LMCT photoreactivity whereas the D_{2h} $MoWCl_4(dppm)_2$ complexes would be expected to exhibit photoreactivity from metal-localized excited states. For this reason, the latter complexes are the more promising multielectron photoreagents.

From a practical standpoint, it has been previously shown that $MoWCl_4(dppm)_2$ reacts halocarbons thermally. Thus the photochemistry of $MoWCl_4(dppm)_2$ with YZ is best investigated at low temperatures to prevent the thermal reaction or decomposition of the photoproducts.

Finally it should be noted that asymmetry about the bimetallic core may also be induced by the ligand coordination sphere. Two ground state mixed-valence compounds are currently known, $Mo_2(OPri)_4(dmpe)_2$[193] and $Mo_2(CH_2SiMe_3)_2[(CH_2)_2SiMe_2](PMe_3)_3$.[194] The former contains a $\mathrm{Mo}^{0}\mathrm{Mo}^{IV}$ bimetallic core and the latter contains a $\mathrm{Mo}^{I}\mathrm{Mo}^{III}$ core formed from a dative component of quadruple bond, $\mathrm{Mo}^{I}\overset{\rightharpoonup}{\equiv}\mathrm{Mo}^{III}$. It might be interesting to investigate the photophysical and photochemical properties of these compounds in a comparative study to the Mo—W systems.

LIST OF REFERENCES

1. Parmon, V. N.; Zamareav, K. I. In *Photocatalysis: Fundamentals and Applications*; Serpone, N.; Pelizzetti, E. Eds.; Wiley-Interscience: New York, 1989, pp. 565.

2. (a) *Photochemical Energy Conversion;* Norris, J. R., Jr.; Meisel, D., Eds.; Elsevier: New York, 1989. (b) *Energy Resources through Photochemistry and Catalysis;* Grätzel M., Ed.; Academic Press: New York, 1983. (c) *Photochemical Conversion and Storage of Solar Energy*; Connolly, J. S. Ed.; Academic Press: New York, 1981.

3. (a) Gust, D.; Moore, T. A.; Moore, A. L. *Acc. Chem. Res.* **1993**, *26*, 198. (b) Gust, D.; Moore, T. A.; Moore, A. L. *Science* **1990**, *248,* 199. (c) Gust, D.; Moore, T. A. *Science* **1989**, *244,* 35.

4. Bard, A. J.; Fox, M. A. *Acc. Chem. Res.* **1995**, *28*, 141.

5. Meyer, T. J. *Acc. Chem. Res.* **1989**, *22*, 163.

6. Kurreck, H.; Huber, M. *Angew. Chem. Int. Ed. Engl.* **1995**, *34,* 849.

7. *Principle of Biochemisty;* Lehninger, Nelson, D. L.; Cox, M. M. Eds.; 2nd ed., Worth Publisher: USA, 1993.

8. (a) *Manganese Redox Enzymes*; Pecararo, V., Ed.; VCH: New York, 1992. (b) Brudvig, G. W.; Thorp, H. H.; Crabtree, R. H. *Acc. Chem, Res.* **1991**, *24*, 311. (c) Wieghardt, K. *Angew. Chem. Int. Ed. Engl.* **1989**, *28,* 1153.

9. *Metalloproteins: Chemical Properties and Biological Effects*; Otsuka, S.; Yamanaka, T. Eds. Elsevier, Amsterdam, 1988.

10. *Molybdenum and Molybdenum Containing Enzymes*; Coughlan, M. Ed.; Pergamon Press: London, U.K. 1980.

11. Kroneck, P. M. H.; Beurle, J.; Schumacher, W. In *Metal Ions in Biological Systems;* Sigel, H.; Sigel, A. Eds.; Marcel Dekker: New York. 1992, Vol. 28, p.455.

12. (a) Tan, J.; Cowan, J. A. *Biochemistry* **1991**, *30*, 8910. (b) Lui, S. M.; Soriano, A.; Cowan, J. A. *J. Am. Chem. Soc.* **1993**, *115*, 10483. (c) Lui, S. M.; Liang, W.; Soriano, A.; Cowan, J. A. *J. Am. Chem. Soc.* **1994**, *116*, 4531.

13. Adams, M. W. W.; Mortenson, L. E. In *Molybdnum Enzymes*; Spiro, T. G., Ed.; Wiley-Interscience: New York, 1985, pp. 519.

14. (a) Cammack, R.; Hucklesby, D.; Hewitt, E. J. *Biochem. J.* **1978**, *171*, 519. (b) Moura, I.; Lina, A. R.; Mourta, J. J. G.; Xavier, A. V.; Fauque, G.; Peck, H. D.; LeGall, J. *J. Biochem. Biophys. Res. Commun.* **1986**, *141*, 1032.

15. (a) Wikström, M.; Krab, K.; Saraste, M. *Cytochrome Oxidase: A Synthesis*; Academic Press: London, 1981. (b) Babcock, G. T.; Wikström, M. *Nature* **1992**, *356*, 301.

16. (a) *Copper Proteins and Copper Enzymes*; Lontie, R., Ed.; CRC Press: Boca Raton, FL. USA 1984. Vol. III. (b) Reinhammar, B.; Malmström, B. G. In *Copper Proteins*, Spiro, T. G., Ed.; Wiley-Interscience: New York, 1981, Chapter 3, pp. 109. (c) *The Biochemistry of Copper Enzymes*; Peisach, J.; Blumberg, W. E., Eds.; Academic Press: New York, 1966.

17. (a) Thorneley, R. N. F.; Ashby, G. A.; Fisher, K.; Lowe, D. J. In *Molybdnum Enzymes, Cofactors and Model Systems*; Stiefel, E.; Coucouvanis, D.; Newton, Eds.; *ACS Symp. Ser.* **1993**, *535*, 290. (b) Thorneley, R. N. F.; Lowe, D. J. In *Molybdnum Enzymes*; Spiro, T. G., Ed.; Wiley-Interscience: New York, 1985, pp. 221.

18. (a) Burgess, B. K. *Chem. Rev.* **1990**, *90*, 1377. (b) Orme-Johnson, W. *Annu. Rev. Biophys. Biophys. Chem.* **1985**, *14*, 419. (c) Stiefel, E. I.; Thomann, H.; Jin, H.; Bare, R. E.; Morgan, T. V.; Burgmayer, S. J. N.; Coyle, C. L. In *Metal Clusters in Proteins*; Que, Jr., L., Ed.; *ACS Symp. Ser.* **1988**, *372*, 372. (d) Burris, R. H. *J. Bio. Chem.* **1991**, *266*, 9339. (e) Smith, B. E.; Eady, R. R. *Eur. J. Biochem.* **1992**, *205*, 1.

19. (a) Adams, M. W. W. *Biochem. Biophys. Acta* **1990**, *1020*, 115. (b) *The Bioinorganic Chemistry of Nickel*; Lancaster; J. R., Ed.; VCH: New York, 1988. (c) Cammack, R.; Fernandez, V. M.; Schneider, K. *Biochem. Biophys. Acta* **1990**, *1020*, 167. (d) Moura, J. J. G.; Teixeira, M.; Mourta, I.; LeGall, J. *Biochem. Biophys. Acta* **1990**, *1020*, 191.

20. Collman, J. P.; Wagenknecht, P. S.; Hutchison, J. E. *Angew. Chem. Int. Ed. Engl.* **1994**, *33*, 1537.

21. Pessiki, P. J.; Khangulov, S. V.; Ho, D. M.; Dismukes, G. C. *J. Am. Chem. Soc.* **1994**, *116*, 891.

22. Ram, M. S.; Jones, L. M.; Ward, H. J.; Wong, Y.-H.; Johnson, C. S.; Surbramanian, P.; Hupp, J. T. *Inorg. Chem.* **1991**, *30*, 2928.

23. (a) Knor, G.; Vogler, A. *Inorg. Chem.* **1994**, *33*, 314. (b) Vogler, A.; Paukner, A.; Kunkely, H. *Coord. Chem. Rev.* **1990**, *97*, 285. (c) Vogler, A.; Nikol, H. *Pure Appl. Chem.* **1992**, *64*, 1311. (d) Vogler, A.; Osman, A. H.; Kunkely, H. *Coord. Chem. Rev.* **1985**, *64*, 159.

24. Seok, W. K.; Meyer, T. J. *J. Am. Chem. Soc.* **1988**, *110*, 7358.

25. (a) Steiger, B.; Anson, F. C. *Inorg. Chem.* **1994**, *33*, 5767. (b) Steiger, B.; Shi, C.; Anson, F. C. *Inorg. Chem.* **1993**, *332*, 2107. (c) Shi, C.; Anson, F. C. *J. Am. Chem. Soc.* **1991**, *113*, 9564.

26. Kutal, C. *J. Chem. Ed.* **1983**, *60*, 882.

27. (a) O'Toole, T. R.; Sullivan, P. B.; Meyer, T. J. *J. Am. Chem. Soc.* **1989**, *111*, 5699. (b) Surridge, N. A.; Hupp, J. T.; Danielson, E.; McClanahan, S. F.; Gould, S.; Meyer, T. J. *J. Phys. Chem.* **1989**, *93*, 304. (c) Leasure, R. M.; Moss, J. A.; Meyer, T. J. *Inorg. Chem.* **1994**, *33*, 1247.

28. (a) Worl, L. A.; Strouse, G. F.; Younathan, J. N. *J. Am. Chem. Soc.* **1990**, *112*, 7571. (b) Baxter, S. M.; Jones, Jr., W. E.; Danielson, E. *Coord. Chem. Rev.* **1991**, *111*, 47.

29. (a) Nishikata, Y.; Morikawa, A.; Kakimoto, M.; Imai, Y.; Hirata, Y.; Nishiyama, K.; Fujihira, M. *J. Chem. Soc. Chem. Commun.* **1989**, 1772. (b) Sato, H.; Kawasaki, M.; Kasatani, K.; Higuchi, Y.; Azuma, T.; Nishikata, Y. *J. Phys. Chem.* **1988**, *92*, 754. (c) Fujihira, M.; Nishiyama, K.; Yamada, H. *Thin Solid Films* **1985**, *132*, 77.

30. Moebius, D. *Acc. Chem. Res.* **1981**, *14*, 63.

31. (a) Shafirovich, V. Y.; Shilov, A. E. *Isr. J. Chem.* **1988**, *38*, 149. (b) Zamaraev, K. I.; Lymar, S. V.; Khramov, M. I.; Parmon, V. N. *Pure Appl. Chem.* **1988**, *60*, 1039.

32. Whitten, D. G. *Acc. Chem. Res.* **1980**, *13*, 83.

33. (a) Gosztola, D.; Yamada, H.; Wasielewski, M. R. *J. Am. Chem. Soc.* **1995**, *117*, 2041. (b) Wasielewski, M. R. *Chem. Rev.* **1992**, *92*, 435. (c) Wasielewski, M. R.; Minsek, D. W.; Niemczyk, M. P.; Svec, W. A.; Yang, N. C. *J. Am. Chem. Soc.* **1990**, *112*, 2823. (d) Wasielewski, M. R. In *Photoinduced Electron Transfer*; Fox, M. A.; Chanon, M. Eds.; Elservier: Amsterdam, 1988.; Part A, p161.

34. Balzani, V.; Scandola, F. *Supramolecular Photochemistry*; Ellis Horwood: England, 1991.

35. (a) Fox, M. A. *Nature* **1992**, *355*, 500. (b) Slama-Schwok, A.; Ottolenghi, M.; Avnir, D. *Nature* **1992**, *355*, 240.

36. *Photoinduced Electron Transfer*; Fox, M. A.; Chanon, M. Eds.; Elservier: Amsterdam, 1988; Parts A-D.

37. (a) Balzani, V.; Campagna, S.; Denti, G.; Juris, A.; Serroni, S.; Venturi, M. *Coord. Chem. Rev.* **1994**, *132*, 1-13. (b) Balzani, V.; Scandola, F. *Supramolecular Photochemistry*; Ellis Horwood: England, 1991. Charpter 12, pp355-394.

38. *Photochemistry of Polypyridine and Porphyrin Complexes*; Kalyanasundaram, K. Ed. Academic Press: London, 1992.

39. *Electron Transfer in Biology and the Solid State*; Johnson, M. K.; King, R. B.; Kurtz, D. M., Jr.; Kutal, C.; Norton, M. L.; Scott, R. A. Eds.; Advances in Chemistry 226; Ameriacn Chemical Society: Washington, DC, 1990.

40. *Electron Transfer in Inorganic, Organic, and Biological Systerms*; Bolton, J., Mataga, N.; McLendon, G. Eds.; Advances in Chemistry 228; American Chemical Society: Washington, DC, 1992.

41. *Photocatalysis: Fundamentals and Applications*; Serpone, N.; Pelizzetti, E. Eds.; Wiley-Interscience: New York, 1989.

42. *Homogeneous and Heterogeneous Photocatalysis*; Sperpone, N.; Pelizzetti, E. Eds.; NATO ASI series C: Mathematical and Physical Sciences - Vol. 174; D. Reidel, Dordrecht, The Netherlands, 1986.

43. *Photoelectrochemistry, Photocatalysis and Photoreactors: Fundamentals and Developments;* Schiavello, M. Ed.; NATO ASI series C: Mathematical and Physical Sciences - Vol. 146; D. Reidel, Dordrecht, The Netherlands, 1984.

44. Fox, M. A.; Dulay, M. T. *Chem. Rev.* **1993**, *93*, 341.

45. Hagteldt, A.; Grätzel, M. *Chem. Rev.* **1995**, *95*, 49.

46. Linsebigler, A. L.; Lu, G.; Yates, J. T. Jr. *Chem. Rev.* **1995**, *95*, 735.

47. Hoffmann, M. R.; Martin, S. T.; Choi, W.; Bahnemann, D. W. *Chem. Rev.* **1995**, *95*, 69.

48. Hirano, K.; Inoue, K.; Yatsu, T. *J. Photochem. Photobiol A: Chem.* **1992**, *64*, 255.

49. Inoue, I.; Fujishima, A.; Konishi, S.; Honda, K. *Nature*, **1979**, *277*, 637.

50. Ishitani, O.; Inoue, C.; Suzuki, Y.; Ibusuki, T. *J. Photochem. Photobiol A: Chem.* **1993**, *72*, 269.

51. (a) Tennakone, K. *Sol. Engergy. Mater.* **1984**, *10*, 235. (b) Rophael, W. M.; Malati, M. A. *J. Chem. Soc. Chem. Commun.* **1987**, 1418.

52. (a) Sclafani, A.; Mozzanega, M.-N.; Pichat, P. *J. Photochem. Photobiol. A: Chem.* **1991**, *59*, 181. (b) Gopidas, K. R.; Bohorquez, M.; Kamat, P. V. *J. Phys. Chem.* **1990**, *94*, 6435. (c) Spanhel, L.; Weller, H.; Henglein, A. *J. Am. Chem. Soc.* **1987**, *109*, 6632.

53. (a) Patrick, B.; Kamat, P. V. *J. Phys. Chem.* **1992**, *96*, 1423. (b) Kamat, P. V. *J. Phys. Chem.* **1989**, *93*, 859. (c) Kamat, P. V.; Fox, M. A. *Chem. Phys. Lett.* **1983**, *102*, 379.

54. (a) McEvoy, A. J.; Grätzel, M. *Sol. Energy Mater. Sol. Cells* **1994**, *32*, 221. (b) Nazeruddin, M. K.; Kay, A.; Rodicio, I.; Humphry-Baker, R.; Muller, E.; Liska, P.; Vlachopoulos, N.; Grätzel, M. *J. Am. Chem. Soc.* **1993**, *115*, 6382. (c) Vlachopoulos, N.; Liska, P.; Augustynski, J.; Grätzel, M. *J. Am. Chem. Soc.* **1988**, *110*, 1216. (d) Desilvestro, J.; Grätzel, M.; Kavan, L.; Moser, J.; Augustynski, J. *J. Am. Chem. Soc.* **1985**, *107*, 2988.

55. Eichberger, R.; Willig, F. *Chem. Phys.* **1990**, *141*, 159.

56. (a) Butler, E. C.; Davis, A. P. *J. Photochem. Photobiol. A: Chem.* **1993**, *70*, 273. (b) Gratzel, M.; Howe, R. F. *J. Phys. Chem.* **1990**, *94*, 2566. (c) Herrmann, J.-M.; Disdier, J.; Pichat, P. *Chem. Phys. Lett.* **1984**, *108*, 618. (d) Fujihira, M.; Satoh, Y.; Osa, T. *Bull. Chem. Soc. Jpn.* **1982**, *55*, 666.

57. Yamase, T. *Polyhedron* **1986**, *5*, 1267.

58. Fox, M. A.; Cardona, P.; Gaillard, E. *J. Am. Chem. Soc.* **1987**, *109*, 6347.

59. (a) Papaconstantinou, E. *Chem. Soc. Rev* **1989**, *18,* 1. (b) Papaconstantinou, E.; Argitis, P.; Dimoticali, D.; Hiskia, A. In *Homogeneous and Heterogeneous Photocatalysis*; Sperpone, N.; Pelizzetti, E. Eds.; NATO ASI series C: Mathematical and Physical Sciences - Vol. 174; D. Reidel: Dordrecht, The Netherlands, 1986, p 415. (c) Argitis, P.; Papaconstantinou, E. *Inorg. Chem.* **1986**, *25,* 4386. (d) Ioannidis, A; Papaconstantinou, E. *Inorg. Chem.* **1985**, *24,* 439. (e) Dimoticali, D.; Papaconstantinou, E. *Inorg. Chim. Acta* **1984**, *87,* 177.

60. (a) Renneke, R. F.; Kadkhodayan, M.; Pasquali, M.; Hill, C. L. *J. Am. Chem. Soc.* **1991**, *113*, 8357. (b) Chambers, R. C.; Hill, C. L. *Inorg. Chem.* **1989**, *28,* 2509. (c) Hill, C. L.; Brown, R. B., Jr. *J. Am. Chem. Soc.* **1986**, *108*, 536.

61. Nomiya, K.; Sugie, Y.; Miyazaki, T.; Miwa, M. *Polyhedron* **1986**, *5*, 1267.

62. Hiskia, A.; Papaconstantinou, E. *Inorg. Chem.* **1992**, *31,* 163.

63. *Photosensitive Metal-Organic Systems*; Kutal, C.; Serpone, N., Eds.; Advances in Chemistry Series 238; American Chemical Society: Washington, DC, 1993.

64. Horváth, O.; Stevenson, K. L. *Charge Transfer Photochemistry of Coordination Compounds*; VCH Publisher: New York, 1993.

65. Roundhill, D. M. *Photochemistry and Photophysics of Metal Complexes*; Plenum Press: New York, 1994.

66. Meyer, T. J.; Caspar, J. V. *Chem. Rev.* **1985**, *85*, 187.

67. (a) Geoffroy, G. L.; Wrighton, M. S. *Organometallic Photochemistry*; Academic Press: New York, 1979. (b) Wrighton, M. S.; Graff, J. L.; Luong, J. C.; Reichel, C. L.; Robbins, J. L. In *Reactivity of Metal-Metal Bonds*; Chrisholm, M. H., Ed.; ACS Symposium Series No. 155; American Chemical Society: Washington, DC, 1981; pp 85.

68. Yasufuku, K.; Hiraga, N.; Ichimura, K.; Kobayashi, T. In *Photochemistry and Photophysics of Coordination Compounds*; Yersin, H.; Vogler, A. Eds.; Springer-Verlag: New York, 1987, p 271

69. Wegman, R. W.; Olsen, R. J.; Gard D. R.; Faulkner, L. R.; Brown, T. L. *J. Am. Chem. Soc.* **1981**, *103*, 6089.

70. Reinking, M. K.; Kullberg, M. L.; Culter, A. R.; Kubiak, C. P. *J. Am. Chem. Soc.* **1985**, *107,* 3517.

71. Roundhill, D. M.; Gray, H. B.; Che, C.-M. *Acc. Chem. Res.* **1989**, *22*, 55.

72. (a) Smith, D. C.; Gray, H. B. *Coord. Chem. Rev.* **1990**, *100*, 169. (b) Smith, D. C.; Gray, H. B. In *The Challenge of d and f Electrons*; Salahub, D. R.; Zerner, M. C., Eds.; ACS symposium Series 394; American Chemical Society; Washington, DC, 1989; pp356.

73. Marshall, J. L.; Stiegman, A. E.; Gray, H. B. *ACS Symp. Sec.* **1986**, *307*, 166, and references therein.

74. Che, C.-M.; Lee, W.-M.; Cho, K.-C.; Harvey, P. D.; Gray, H. B. *J. Phys. Chem.* **1989**, *93*, 3095.

75. (a) Li, D.; Che, C.-M.; Kwong, H.-L. *J. Dalton Trans.* **1992**, 3325. (b) Che, C.-M.; Kwong, H.-L.; Yam, V. W.-W.; Cho, K.-C. *J. Chem. Soc. Chem. Commun.* **1989**, 885.

76. Yip, H.-K.; Che, C.-M.; Peng, S.-M. *J. Chem. Soc. Chem. Commun.* **1991**, 1626.

77. Che, C.-M.; Butler, L. G.; Gray, H. B. *J. Am. Chem. Soc.* **1981**, *103*, 7796.

78. (a) Roundhill, D. M. *J. Am. Chem. Soc.* **1985**, *107*, 4354. (b) Roundhill, D. M.; Atherton, S. J.; Shen, Z.-P. *J. Am. Chem. Soc.* **1987**, *109*, 6076.

79. (a) Julliard, M.; Chanon, M. *Chem. Rev.* **1983**, *83*, 425. (b) Kavarnos, G. J.; Turro, N. J. *Chem. Rev.* **1986**, *86*, 401.

80. Lever, A. B. P. *Inorganic Electronic Spectroscopy*; Elsevier: Amsterdam, 1985.

81. Creutz, C.; Taube, H. *J. Am. Chem. Soc.* **1969**, *91*, 3988.

82. Taube, H. *Angew. Chem., Int. Ed. Engl.* **1984**, *23*, 329.

83. (a) Wu, Y.; Cohran, C.; Bocarsly, A. B. *Inorg. Chim. Acta.* **1994**, *226*, 251. (b) Pfennig, B. W.; Bocarsly, A. B. *Coord. Chem. Rev.* **1991**, *111*, 91. (c) Zhou, M.; Pfennig, B. W.; Steiger, J.; VanEngen, D.; Bocarsly, A. B. *Inorg. Chem.* **1990**, *29*, 2456.

84. Cotton, F. A.; Walton, R. A. *Multiple Bonds Between Metal Atoms*; 2nd ed.; Clarendon Press: Oxford, 1993.

85. Trogler, W. C.; Gray, H. B. *Nouv. J. Chim.* **1977**, *1*, 475.

86. Trogler, W. C.; Gray, H. B. *Acc. Chem. Res.* **1978**, *11*, 232.

87. Winkler, J. R.; Nocera, D. G.; Netzel, T. L. *J. Am. Chem. Soc.* **1986**, *108*, 4451.

88. Nocera, D. G.; Gray, H. B. *Inorg. Chem.* **1984**, *23*, 3686.

89. Merer, A. J.; Mulliken, R. S. *Chem. Rev.* **1969**, *69*, 639.

90. Salem, L.; Rowland, C. *Angew. Chem. Int. Ed. Engl.* **1972**, *11*, 92.

91. Michl, J. *J. Mol. Photochem.* **1972**, *4*, 257.

92. Dauben, W. G.; Salem, L.; Turro, N. J. *Acc. Chem. Res.* **1975**, *8*, 41.

93. Hay, P. J. *J. Am. Chem. Soc.* **1982**, *104*, 7007.

94. Engebretson, D. S.; Zaleski, J. M.; Leroi, G. E.; Nocera, D. G. *Science* **1994**, *265*, 759.

95. (a) Cotton, F. A.; Eglin, J. L.; Hong, B.; James, C. A. *J. Am. Chem. Soc.* **1992**, *114*, 4915. (b) Cotton, F. A.; Eglin, J. L.; Hong, B.; James, C. A. *Inorg. Chem.* **1993**, *32*, 2104.

96. Hopkins, M. D.; Gray, H. B.; Miskowski, V. M. *Polyhedron* **1987**, 6, 705.

97. Zietlow, T. C.; Hopkins, M. D.; Gray, H. B. *J. Solid State Chem.* **1985**, *57*, 112.

98. Brencic, J. V.; Cotton, F. A. *Inorg. Chem.* **1969**, *8*, 7.

99. (a) Brencic, J. V.; Cotton, F. A. *Inorg. Chem.* **1970**, *9*, 346.(b) San Filippo, J. Jr.; Sniadoch, H. J. *Inorg. Synth.* **1979**, *19*, 128.

100. Brignole, A. B.; Cotton, F. A. *Inorg. Synth.* **1972**, *13*, 81.

101. Lucas, H. J.; Kennedy, E. R.; Formo, M. W. *Org. Synth.* **1955**, *3*, 482.

102. Santure, D. J.; Sattelberger, A. P. *Inorg. Synth.* **1989**, *26*, 221.

103. Gordon, A. J.; Ford, R. A. *The Chemist's Companion: A Handbook of Practical Data, Techniques, and References* Wiley-Interscience: New York, 1972, pp. 429.

104. San Filippo, J. Jr.; *Inorg. Chem.* **1972**, *11*, 3140.

105. Best, S. A.; Smith, T. J.; Walton, R. A. *Inorg. Chem.* **1978**, *17*, 99.

106. Schrock, R. R.; Sturgeoff, L. G.; Sharp, P. R. *Inorg. Chem.* **1983**, *22*, 2801.

107. (a) Luck, R. L.; Morris, R. H.; Sawyer, J. F. *Organometallic* **1984**, *3*, 247. (b) Luck, R. L.; Morris, R. H. *J. Organometallic Chem.* **1983**, *255*, 221. (c) Azizian, H.; Luck, R. L.; Morris, R. H.; Wong, H. *J. Organometallic Chem.* **1982**, *238*, C24.

108. Cotton, F. A.; Luck, R. L.; Morris, R. H. *Organometallic* **1989**, *8*, 1282.

109. (a) Butcher, A. V.; Chatt, J.; Leigh, G. J.; Richards, R. L. *J. Chem. Soc. Dalton Trans.* **1972**, 1064. (b) Dilworth, J. R.; Richards, R. L. *Inorg. Synth.* **1980**, *20*, 124.

110. (a) Luck, R. L.; Morris, R. H.; Sawyer, J. F. *Inorg. Chem.* **1987**, *26*, 2422. (b) Morris, R. H. *Polyherdron* **1987**, *6*, 793. (c) Luck, R.; Morris, R. H. *J. Am. Chem. Soc.* **1984**, *106*, 7978.

111. Cotton, F. A.; Falvello, L. R.; James, C. A.; Luck, R. L. *Inorg. Chem.* **1990**, *29*, 4759.

112. Cotton, F. A.; James, C. A. *Inorg. Chem.* **1992**, *31*, 5298.

113. Canich, J. M.; Cotton, F. A.; Dunbar, K. R.; Falvello, L. R. *Inorg. Chem.* **1988**, *27*, 804.

114. Chang, I-J. Ph. D. Dissertation, Michigan State University, 1989.

115. (a) Gordon, A. J.; Ford, R. A. *The Chemist's Companion: A Handbook of Practical Data, Techniques, and References;* Wiley-Interscience: New York, 1972, pp. 362. (b) Calvert, J. G.; Pitts, J. N. *Photochemistry*; Wiley-Interscience: New York, 1966.

116. Newsham, M. D. Ph. D. Dissertation, Michigan State University, 1988.

117. Hopkins, M. D.; Gray, H. B. *J. Am. Chem. Soc.* **1984**, *106*, 2468.

118. Demas, N. J.; Crosby, G. A. *J. Phys. Chem.* **1971**, *75*, 991.

119. Bowman, L. E.; Berglund, K. A.; Nocera, D. G. *Rev. Sci. Inst.* **1993**, *64*, 338.

120. Zaleski, J. M.; Chang, C. K.; Nocera, D. G. *J. Phys. Chem.* **1993**, *97*, 13206.

121. Frenz, B. A. In *Computing in Crystallography;* Schenk, H.; Olthof-Hazelkamp, R.; van Konigsveld, H.; Bassi, G. C., Eds.; Delft: Holland; 1978; p 64.

122. Zachariasen, W. H. *Acta Crystallogr.* **1963**, *16*, 1139.

123. Sheldrick, G. M. In '*Crystallographic Computing 3*', Sheldrick, G. M.; Kruger, C.; Goddard, R., Eds. Oxford University Press: 1985, pp. 175.

124. Cromer, D. T.; Waber, J. T. *International Tables for X-Ray Crystallography*; Kynoch Press: Birmingham, England, 1974; Vol IV, Table 2.2B.

125. Ibers, J. A.; Hamilton, W. C. *Acta Crystallogr.* **1964**, *17*, 781.

126. Cromer, D. T.; Waber, J. T. *International Tables for X-Ray Crystallography*; Kynoch Press: Birmingham, England, 1974; Vol IV, Table 2.3.1.

127. Cruickshank, D. W. J. *Acta Crystallogr.* **1949**, *2*, 154.

128. Erwin, D. K.; Geofferoy, G. L.; Gray, H. B.; Hammond, G. S.; Soloman, E. I.; Trogler, W. C.; Zagars, A. A. *J. Am. Chem. Soc.* **1977**, *99*, 3620.

129. Chang, I-J.; Nocera, D. G. *J. Am. Chem. Soc.* **1987**, *109*, 4901.

130. Trogler, W. C.; Erwin, D. K.; Geofferoy, G. L.; Gray, H. B. *J. Am. Chem. Soc.* **1978**, *100*, 1160.

131. Partigianoni, C. M.; Chang, I-J.; Nocera, D. G. *Coord. Chem. Rev.* **1990**, *97*, 105.

132. The reduction potential of an excited state was calculated from $E_{1/2}(Mo_2[O_2P(OC_6H_5)_2]^{4+/*}) = E_{1/2}(Mo_2[O_2P(OC_6H_5)_2]^{4+/0}) - E_{0-0}$ $(E_{1/2}(Mo_2[O_2P(OC_6H_5)_2]^{4*})$ where the electronic origin, E_{0-0} was estimated from the emission spectrum to be 2.17 eV.

133. Chang, I-J.; Nocera, D. G. *Inorg. Chem.* **1989**, *28*, 4309.

134. Fanwick, P. E.; Martin, D. S.; Webb, T. R.; Robbins, G. A.; Newman, R. A. *Inorg. Chem.* **1978**, *17*, 2723.

135. Hsu. T.-L. C.; Chang, I-J.; Ward, D. L.; Nocera, D. G. *Inorg. Chem.* **1994**, *33*, 2932.

136. Cotton, F. A.; Frenz, B. A.; Pedersen, E.; Webb, T. R. *Inorg. Chem.* **1975**, *14*, 391.

137. Cotton, F. A.; Walton, R. A. *Multiple Bonds Between Metal Atoms*, 2nd ed.; Oxford: New York, 1993; Chapter 10, p 632.

138. Heller, S. R.; Milne, G. W. A. *EPA/NIH Mass Spectral Data Base*; U.S. Department of Commerce/National Bureau of Standards, 1978; Vol I.

139. Uyeta, M.; Taue, S.; Chikasawa, K.; Mazaki, M. *Nature* **1976**, *264*, 583.

140. (a) Bakac, A.; Espenson, J. H. *J. Am. Chem. Soc.* **1986**, *108*, 713. (b) Andrieux, C. P.; Gallardo, I.; Savéant, J.-M.; Su, K.-B. *J. Am. Chem. Soc.* **1986**, *108*, 638. (c) Lexa, D.; Savéant, J.-M.; Schafer, H. J.; Su, K.-B.; Vering, B.; Wang, D. L. *J. Am. Chem. Soc.* **1990**, *112*, 6162. (d) Andrieux, C. P.; Le Gorande, A.; Savéant, J.-M. *J. Am. Chem. Soc.* **1992**, *114*, 6892. (e) Savéant, J.-M. *J. Am. Chem. Soc.* **1992**, *114*, 10595.

141. (a) Savéant, J.-M. *J. Am. Chem. Soc.* **1987**, *109*, 6788. (b) Lexa, D.; Savéant, J.-M.; Su, K.-B.; Wang, D. L. *J. Am. Chem. Soc.* **1988**, *110*, 7617. (c) Savéant, J.-M. *Adv. Phys. Org. Chem.* **1990**, *26*, 1.

142. Morrow, J. R.; Trogler, W. C. *Inorg. Chem.* **1989**, *28*, 615.

143. Private communication with Professor Peter Wagner.

144. Casanova, J.; Eberson, L. in *The Chemistry of the Carbon-halogen Bond*; Patai, S., Ed.; Wiley-Interscience: New York, 1973; Chapter 15.

145. von Stackelberg, M.; Stracke, W. *Z. Electrochem.* **1949**, *53*, 118.

146. (a) Bunnett, J. F. *Acc. Chem. Res.* **1992**, *25*, 2. (b) Bolton, R.; Moore, C.; Sandall, J. P. B. *J. Chem. Soc., Perkin Trans.* **1982**, *2*, 1593. (c) Bard, R. R.; Bunnett J. F.; Traber, R. P. *J. Org. Chem.* **1979**, *44*, 4918.

147. Jura, W. H.; Gaul, R. J. *J. Am. Chem. Soc.* **1958**, *80*, 5402.

148. Nocera, D. G. *J. Cluster Sci.* **1994**, *5*, 185.

149. Cotton, F. A.; Diebold, M. P.; O'Connor, C. J.; Powell, G. L. *J. Am. Chem. Soc.* **1985**, *107*, 7438.

150. Canich, J. A. M.; Cotton, F. A.; Daniels, L. M.; Lewis, D. B. *Inorg. Chem.* **1987**, *26*, 4046.

151. (a) Agaskar, P. A.; Cotton, F. A.; Dunbar, K. R.; Falvello, L. R.; O'Connor, C. J. *Inorg. Chem.* **1987**, *26*, 4051. (b) Cotton, F. A.; Daniels, L. M.; Dunbar, K. R.; Falvello, L. R.; O'Connor, C. J.; Price, A. C. *Inorg. Chem.* **1991**, *30*, 2509.

152. Fanwick, P. E.; Harwood, W. S.; Walton, R. A. *Inorg. Chem.* **1987**, *26*, 242.

153. Cotton, F. A.; James, C. A.; Luck, R. L. *Inorg. Chem.* **1991**, *30,* 4370.

154. (a) Cotton, F. A. *Polyhedron* **1987**, *6,* 667. (b) Cotton, F. A.; Hong, B.; Shang, M. *Inorg. Chem.* **1993**, *32*, 3620. (c) Cotton, F. A.; Eglin, J. L.; James, C. A. *Inorg. Chem.* **1993**, *32*, 687.

155. Poli, R.; Torralba, R. C. *Inorg. Chim. Acta* **1993**, *212*, 123 and references therein.

156. Nocera, D. G. *Acc. Chem. Res.* **1995**, *28*, 209.

157. Partigianoni, C. M.; Nocera, D. G. *Inorg. Chem.* **1990**, *29*, 2033.

158. For example: (a) Lindsay, E.; Aramice, Y. S.; Langford, C. H. *Inorg. Chem.* **1994**, *33,* 944. (b) Sandrini, D.; Maestri, M.; Balzani, V.; Chassot, L.; von Zelewsky, A. *J. Am. Chem. Soc.* **1987**, *109*, 7720. (c) Horvath, D.; Stevenson, K. L. *Charge Transfer Photochemistry of Coordination Compounds* VCH publishers: New York 1993.

159. Benson, S. W. *Chem. Rev.* **1978**, *78,* 23.

160. Block, E. In *Reactions of Organosulfur Compounds*; Blomquist, A. T.; Wasserman, H. H., Eds.; Organic Chemistry, Vol. 37; Academic Press: New York, 1978; pp 175.

161. Heiba, E. I.; Dessau, R. M. *J. Org. Chem.* **1967**, *32*, 3837.

162. Hopkins, M. D.; Miskowski, V. M.; Gray, H. B. *J. Am. Chem. Soc.* **1988**, *110*, 1787.

163. Agaskar, P. A.; Cotton, F. A.; Fraser, I. F.; Manojlovic-Muir, L.; Muir, K. W.; Peacock, R. D. *Inorg. Chem.* **1986**, *25*, 2511.

164. Hsu, T.-L. C.; Helvoigt, S. A.; Partigianoni, C. M.; Turró, C.; Nocera, D. G. *Inorg. Chem.* **1995**, *accepted for publication.*

165. Fife, D. J.; Morse, K. W.; Moore, W. M. *J. Photochem.* **1984**, *24*, 249.

166. Cotton, F. A.; Falvello, L. R.; Harwood, W. S.; Powell, G. L.; Walton, R. A. *Inorg. Chem.* **1986**, *25*, 3949.

167. Cotton, F. A.; Eglin, J. L.; James, C. A. *Inorg. Chem.* **1992**, *31*, 5308.

168. Chakravarty, A. R.; Cotton, F. A.; Diebold, M. P.; Lewis, D. B.; Roth, W. J. *J. Am. Chem. Soc.* **1986**, *108*, 971.

169. Shaik, S.; Hoffman, R.; Fisel, R.; Summerville, R. H. *J. Am. Chem. Soc.* **1980**, *102*, 4555.

170. Collman, J. P.; Hegedus, L. S.; Norton, J. R.; Finke, R. G. *Principles and Applications of Organotransition Metal Chemistry*; University Science: Mill Valley, CA, 1987; p177.

171. Partigianoni, C. M.; Turró, C.; Hsu, T.-L. C.; Chang, I-J.; Nocera, D. G. In *Photosensitive Metal-Organic Systems*; Kutal, C., Serpone, N., Eds.; Advances in Chemistry Series 238; American Chemical Society: Washington, DC, 1993; pp 147.

172. Roundhill, D. M.; Atherton, S. J. *Inorg. Chem.* **1986**, *25*, 4071.

173. (a) Poli, R.; Torralba, R. C. *Inorg. Chim. Acta* **1993**, *212*, 123. (b) Cotton, F.A.; Poli, R. *Inorg. Chem.* **1987**, *26*, 3310. (c) Rothfuss, H.; Barry, J. T.; Huffman, J. C.; Caulton, K. G.; Chisholm, M. H. *Inorg. Chem.* **1993**, *32*, 4573. (d) Poli, R.; Gordon, J. C. *J. Am. Chem. Soc.* **1992**, *114* , 6723. (e) Chacon, S. T.; Chisholm, M. H.; Streib, W. E.; Van Der Sluys, W. G. *Inorg. Chem.* **1989**, *28*, 5. (f) Cotton, F. A.; Luck, R. L. *Inorg. Chem.* **1989**, *28* , 182.

174. Glickman, H. D.; Hamer, A. D.; Smith, T. J.; Walton, R. A. *Inorg. Chem.* **1976**, *28*, 2205.

175. Brant, P.; Salmon, D. J.; Walton, R. A. *J. Am. Chem. Soc.* **1978**, *100*, 4424.

176. Zietlow, T. C.; Klendworth, D. D.; Nimry, T.; Salmon, D. J.; Walton, R. A. *Inorg. Chem.* **1981**, *20*, 947.

177. Cotton, F.A.; Mandal, S. K. *Inorg. Chem.* **1992**, *31*, 1267.

178. Over, D. E.; Critchlow, S. C.; Mayer, J. M. *Inorg. Chem.* **1992**, *31*, 4643.

179. Barry, J. T.; Chacon, S. T.; Chisholm, M. H.; DiStasi, V. F.; Huffman, J. C.; Streib, W. E.; Van Der Sluys, W. G. *Inorg. Chem.* **1993**, *32*, 2322

180. Cotton, F. A.; Walton, R. A. *Multiple Bonds between Metal Atoms*, Clarendon Press, Oxford, 2nd ed., 1993, Ch. 10, p.742.

181. Cotton, F. A.; Dikarev, E. V. *Inorg. Chem.* **1995**, *34*, 3809.

182. *EPA/NIH Mass Spectral Data Base*, Heller, S. R.; Milne, G. W. A. Eds., U.S. Department of Commerce/National Bureau of Standards, Washington, DC, 1978, Vol. I.

183. Hsu, T.-L. C.; Helvoigt, S. A.; Engebretson, D. S.; Nocera., D. G. *Inorg. Chim. Acta, special issue in honor of Fred Basolo, accepted for publication.*

184. Zhang, X.; Kozik, M.; Sutin, N.; Winkler, J. R. In *Electron Transfer in Inorganic, Organic, and Biological Systems*; Bolton, J. R.; Mataga, N.; McLendon, G. Eds., Advances in Chemistry Series No. 228, American Chemical Society, Washington, DC, 1991, Ch. 16, p.247.

185. (a) Kober, E. M.; Caspar, J. V.; Lumpkin, R. S.; Meyer, T. J. *J. Phys. Chem.* **1986**, *90*, 3722. (b) Bixon, M.; Jortner, J.; Cortes, J.; Heitele, H.; Michel-Beyerle, M. E. *J. Phys. Chem.* **1994**, *98*, 7289.

186. (a) Cotton, F. A.; Hubbard, J. L.; Lichtenberger, D. L.; Shim, I. S. *J. Am. Chem. Soc.* **1982**, *104*, 679. (b) Ziegler, T. *J. Am. Chem. Soc.* **1984**, *106*, 5901.

187. Cotton, F. A.; Feng, X. *J. Am. Chem. Soc.* **1993**, *115*, 1074.

188. Miskowski, V. M.; Gray, H. B.; Hopkins, M. D. *Inorg. Chem.* **1992**, *31*, 2085.

189. Chen, J. D.; Cotton, F. A.; Falvello, L. R. *J. Am. Chem. Soc.* **1990**, *112*, 1076

190. Cotton, F. A.; Daniels, L. M.; Powell, G. L.; Kahaian, A. J.; Smith, T. J.; Vogel, E. F. *Inorg. Chim. Acta* **1988**, *144*, 109.

191. (a) Partigianoni, C. M., Ph. D. Dissertation, Michigan State University, 1991. (b) Turró, C., Ph. D. Dissertation, Michigan State University, 1992.

192. Miskowski, V. M.; Gray, H. B.; Hopkins, M. D. *Inorg. Chem.* **1992**, *31*, 2085-2091. ref 22.

193. Chisholm, M. H.; Huffman, J. C.; Van Der Sluys, W. G. *J. Am. Chem. Soc.* **1987**, *109*, 2514.

194. Andersen, R. A.; Jones, R. A.; Wilkinson, G. *J. Chem. Soc., Dalton Trans.* **1978**, 446.